



CRRES Combined Radiation and Release Effects Satellite Program

Compiled by
B.L. Giles, M.A. McCook,
M.W. McCook, and G.P. Miller



CRRES Combined Radiation and Release Effects Satellite Program

Compiled by
B.L. Giles
Marshall Space Flight Center • MSFC, Alabama

and

M.A. McCook, M.W. McCook, and G.P. Miller
Department of Chemistry
The University of Alabama in Huntsville
Huntsville, Alabama

National Aeronautics and Space Administration
Marshall Space Flight Center • MSFC, Alabama 35812

June 1995

ACKNOWLEDGMENTS

This publication is dedicated to:

Dr. Stanley D. Shawhan and to Dr. David Lukens Reasoner

who both left this Earth during the CRRES Program, and without whom the Program would not have survived or succeeded.

Special appreciation goes to Richard Howard, Program Manager, Code SS, NASA Headquarters, for his neverending support and contributions during and in the completion of the CRRES Program. Special thanks go to the staff of the Wallops Executive Support Corporation, Wallops Island, VA (especially Ms. Nadine B. Estes) and to the staff of the NASA Library, Wallops Flight Facility, VA (especially to Ms. Bobbi Eddy).

TABLE OF CONTENTS

LIST OF PRINCIPAL INVESTIGATORS.....	vi
INTRODUCTION	1
ACTUAL RELEASE AND LAUNCH SEQUENCE	3
PEGSAT	4
EXPERIMENT - PEGSAT/PEGASUS 001A.....	4
KWAJALEIN CAMPAIGN	6
EXPERIMENTS AA-5, AA-6.....	6
CRRES SATELLITE EXPERIMENTS.....	8
EXPERIMENTS G-13, G-14	8
EXPERIMENT G-13.....	8
EXPERIMENT G-14.....	9
EXPERIMENTS G-1, G-2, G-3, G-4.....	15
EXPERIMENT G-2	15
Releases G-2, G-3 and G-4.....	16
EXPERIMENT G-7	19
RELEASES G-5, G-6, and G-7.....	20
EXPERIMENT G-3	25
EXPERIMENT G-4	26
G-4 TRIANGULATION AND ITS RELATIONSHIP TO G-2 AND G-3	26
EXPERIMENT G-5	37
EXPERIMENT G-10.....	38
EXPERIMENT G-6	40
EXPERIMENT G-8	46
RELEASE G-8 OBSERVATIONS	47
EXPERIMENT G-1	48
EXPERIMENT G-9	49
EXPERIMENTS G 11, G-12	51
EXPERIMENT G-11a.....	52
EXPERIMENT G-11b	53
EXPERIMENT G-12.....	54
EL COQUI SOUNDING ROCKET CAMPAIGN.....	55
EXPERIMENT AA-3 A.....	55
EXPERIMENT AA-4.....	61
EXPERIMENT AA-3 B.....	82
EXPERIMENT AA-1.....	98
EXPERIMENT A-7.....	104
EXPERIMENT AA-2.....	109
APPENDIX A. RUSSIAN STATIONS	129
APPENDIX B. INSTRUMENTATION	133
APPENDIX C. THEORY AND COMPUTATIONS.....	139
APPENDIX D. CRRES PUBLICATIONS BY MAIN AUTHOR	151

LIST OF PRINCIPAL INVESTIGATORS

Dr. Roger Anderson
Dept. of Physics & Astronomy
615 Van Allen Hall
University of Iowa
Iowa City, Iowa 52242
319-335-1924

Dr. Paul Bernhardt
Code 4780
Naval Research Lab
4555 Overlook Ave., SW
Washington, DC 20375
202-767-0631

Dr. Frank Djuth
Geospace Research, Inc.
550 North Continental
Blvd. Suite 110
El Segundo, CA 90245
310-322-1160

Dr. Adam Drobot
Plasma Physics Division
SAIC 1710 Goodridge Dr.
McLean, VA 22102
703-734-5840

Dr. Lewis Duncan
University of Tulsa
600 South College
M203 Keplin Hall
Tulsa, OK 74104
918-631-2288

Dr. Gerhard Haerendel
Max-Planck Institute
Extra-Terr Physik
8046 Garching
Germany
49-89-329-9516

Dr. Robert Hoffman
Code 696
Goddard Space Flight Center
Greenbelt, MD 20771
301-286-7386

Dr. Joseph Huba
Code 4780
Naval Research Lab.
4555 Overlook Ave., SW
Washington, D.C. 20375
202-767-3630

Dr. Steven Mende
Lockheed Palo Alto
3251 Hanover Street
Palo Alto, CA 94304
415-424-3282

Dr. Michael Mendillo
Dept. of Astronomy
Boston University
705 Commonwealth Ave.
Boston, MA 02215
617-353-2629

Dr. William Peterson
Lockheed Palo Alto
3251 Hanover Street
Palo Alto, CA 94304
415-424-3269

Dr. Morris Pongratz
EES-DOT MSD446
Los Alamos Nat'l Laboratory
Los Alamos, NM 87545
505-667-4740

Dr. David Simons
EES-7 MS-D466
Los Alamos Nat'l Laboratory
Los Alamos, NM 87545
505-667-5930

Dr. Edward Szuszcwicz
Plasma Physics Division
SAIC 1710 Goodridge Dr.
McLean, VA 22102
703-734-5516

Dr. Arnoldo Valenzuela
Max-Planck Institute
Extra-Terr Physik
8046 Garching, Germany
49-89-329-9513

Dr. Edward Weber
AFFL Hanscom AFB
Bedford, MA 01791
617-377-3121

Dr. Eugene Wescott
Geophysical Institute
University of Alaska
Fairbanks, AK 99701
907-474-7576

INTRODUCTION

In an area of space surrounding the Earth, matter exists in an ionized state and the Earth's magnetic field exerts a large degree of control. This space is called the Earthspace and the ionized material is a plasma. A plasma is unique because it consists of charged particles that can interact through long-range electromagnetic forces and can carry electric currents over long distances. The source of energy to Earthspace is the Sun. Solar ultraviolet is a source of ionizing radiation while the solar wind provides both energy and particles. The lower altitude region of this space is called the ionosphere, and at higher altitudes is found the magnetosphere. In one view, the magnetosphere can be pictured as a large-scale generator driven by the action of the high-speed electrically conducting solar wind moving through the Earth's magnetic field.

The various regions of the magnetosphere-ionosphere system are coupled by flows of electric particle beams, and electromagnetic waves. This coupling gives rise to processes that affect both technical and non-technical aspects of life on Earth. An obvious manifestation of Earthspace processes is the aurora, which represents a significant input of energy into the ionosphere in polar regions. The ionosphere is actually the sink for excess energy in the magnetosphere and becomes highly structured and variable during periods of intense geomagnetic activity. The structuring in the ionosphere affects high-frequency radio communications, causes scintillations of satellite-Earth signals, and the large currents driven in the ionosphere by the magnetospheric dynamo actually couple into large-scale systems such as power grids and pipelines with destructive effects.

The magnetosphere is a reservoir of the high-energy radiation belts which the Chemical Release and Radiation Effects Satellite (CRRES) was designed in part to study. This document pertains to the NASA chemical release portion of the CRRES Program. The experiments were designed to produce a controlled and known input to the space environment and the effects were measured with arrays of diagnostic instruments.

The CRRES satellite was a dual-mission spacecraft with a NASA mission to perform active chemical-release experiments. These may be broadly grouped into categories of tracer, modification, and simulation experiments. Tracer experiments inject relatively small amounts of material which can be detected by remote sensing. Larger amounts of material can be used to modify or perturb the environment in a controlled manner, and the system response to this perturbation is studied. The simulation function is designed to mimic a natural process. As an example, the active magnetospheric particle tracer experiment (AMPTE) spacecraft released a cloud of barium vapor in the solar wind which thus simulated a comet.

The CRRES Program began in 1983 as a joint NASA/USAF endeavor that was the result of the combination of two separate programs, NASA's Chemical Release Module (CREM) Program and the USAF Space Radiation Program. Originally designed for a Space Shuttle launch, the CRRES spacecraft was modified for launch on an Atlas Centaur following the Challenger accident. A result of the change in launch vehicles was that half of the original chemical canisters had to be removed (in order to reduce the weight of the spacecraft). The CRRES chemical release portion of the program was then restructured to accommodate as much of the off-loaded science as possible. This resulted in a program consisting of chemical releases from two satellites (CRRES and PEGSAT) and two sounding rocket chemical release campaigns (Kwajalein Atoll in the Marshall Islands and El Coqui in Tortugero, Puerto Rico).

Atlas Centaur 69 successfully launched the CRRES satellite on July 25, 1990, and had a successful lifetime of thirteen months, having released all canisters as planned. The elements of the CRRES Program which had been off-loaded from the original CRRES mission were successfully launched over three scheduled periods ending in July 1992. Advances in scientific understanding resulting from these experiments require the synthesis of large pools of data collected by many diverse diagnostic instruments. The preliminary results are very encouraging, but this process must by

necessity continue for a considerable period of time. It is hoped that this process will be aided and assisted by the information presented in this document of the initial results.

NOTE: This technical summary is arranged chronologically as much as possible to provide the most fluency in describing events. Experiment numbers were used for the sake of identification. However, seasonal variations, altitude necessities, and satellite and radar positions determined the chronological order of events.

ACTUAL RELEASE AND LAUNCH SEQUENCE

RELEASE	DATE	TIME	LATITUDE	LONGITUDE	ALTITUDE (km)
PEGSAT	04/5/90	19:10:00			
AA-S	08/11/90	08:08:17	11.0 N	166.9E	375
AA-6	08/15/90	08:24:00	10.9 N	167.1E	428
G-13	09/10/90	06:10:25	17.5 S	198.9 E	517
G-14	09/14/90	08:47:10	18.1 S	161.6E	593
G-02	01/13/91	02:17:00	16.9 N	103.1 W	6180
G-07	01/13/91	07:05:00	8.0 N	86.7 W	33403
G-03	01/15/91	04:11:00	17.9 N	97.5 W	15053
G-04	01/16/91	06:25:00	0.7 S	53.8 W	23977
G-05	01/18/91	05:20:00	6.6 N	62.8 W	33337
G-10	01/20/91	05:30:00	8.9 N	75.6 W	33179
G-06	02/12/91	04:15:00	4.9 N	76.1 W	32249
G-08	02/17/91	03:30:00	0.4 N	58.1 W	33553
G-01	07/13/91	08:35:25	17.8 N	62.9 W	495
G-09	07/19/91	08:37:07	17.4 N	62.8 W	441
G-11a	07/22/91	08:38:24	16.8 N	60.3 W	411
G-11b	07/25/91	08:37:11	17.3 N	69.5 W	478
G-12	08/12/91	09:31:20	9.1 N	63.5 W	507
AA-3A	05/25/92	19:52:00			250
AA-4	05/30/92	04:13:50	18.97 N	66.6 W	285
AA-3B	06/06/92	08:37:31			173-230 (4)
AA-1	07/2/92	05:01:15			~250 (3)
AA-7	07/04/92	04:58:00			~250 (3)
AA-2	07/12/92	05:02:00			~250 (3)

PEGSAT

EXPERIMENT - PEGSAT/PEGASUS 001A

Principal Investigator: R. A. Hoffman, Goddard Space Flight Center

Collaborative Investigators: E. Wescott, H. Stenbaek-Nielsen, D. Simons, M. Pongratz, P. Bernhardt, A. Valenzuela, G. Haerendel S. Mende, D. Rees, D. Slater

Launch Site: Vandenberg, AFB
Launcher: Pegasus Rocket on B-52 Aircraft/Pegsat Satellite
Launch Date: 5 April 1990
Time: 1910 GMT
Weight of Pegsat Satellite: 178 kg
Chemicals: 5.6 kg barium, 0.2 kg strontium

POINT OF CONTACT:

R. A. Hoffman
Code 696
Goddard Space Flight Center
Greenbelt, MD 20771

SPAN - DE696::U6RAH
PHONE (301) 286-7386
FAX - (301) 286-1648

SATELLITE ORBIT:

	APOGEE	PERIGEE	PERIOD	INCLINATION
Initial	680 km	495 km	96.424 min	94.2 min
(current)	599 km	438 km	94.995 min	94.1 min

OBJECTIVE:

In 1988 NASA became aware of a scheduled test launch of the first Pegasus rocket (rocket: Orbital Sciences Corporation, launch vehicle: Hercules Aircraft Company) and realized that it could carry a simple chemical release payload into an orbit similar to the one used in the CAMEO releases (Heppner et al., 1981). The idea was to release barium above an active auroral arc and monitor the ion acceleration processes occurring there by observing the motion of the barium ions created when the released barium photoionized. A simple battery operated spacecraft and transportable ground control communications van were designed and rapidly built. The operating concept was simple. Releases would be made when ground observers determined that an active aurora was occurring when the spacecraft flew over it. The same observers would then optically track the barium ions.

The lighting conditions necessary for photoionization of the barium at high altitudes on auroral field lines and optical detection of aurora occur regularly over the northern polar cap in winter. The lighting conditions determined the orbital plane of the PEGSAT satellite. Northern Canada was selected for the location of the releases because of the availability of observation sites widely separated in longitude with regularly scheduled airline service. The Orbit of DE-1 was such that it would pass over the proposed release site about two hours after one (of about 4 or 5) potential release opportunity every two days. We noted that if barium ions were only modestly accelerated above the aurora, or if there was a latitude dependence to the acceleration, that DE-1 would be in a position to detect barium ions that had only experienced a modest acceleration.

RELEASE CONDITIONS:

RELEASE 1: Occurred above aurora based on visual observations from camera sites. Double arcs were reported active before release, but fading by time of release.

RELEASE 2: Slightly north of the northern-most auroral arc. Active aurora.

TYPE AND DESCRIPTION OF DATA: 1) ICCD, all sky. 2) ICCD, narrow field. 3) IPD, narrow field. 4) ISIT, narrow field.

RESULTS: No barium ions were detected on DE-1 in support of the PEGSAT releases. The April 16 release occurred at east longitude 244°. DE-1 next crossed 70° invariant latitude at a magnetic local time of 19:12 and a latitude of 8,800 km 15 minutes later. The east longitude of the DE-1 subsatellite point on this crossing was 216°, 25° westward of the release point. The barium ions would have to travel 8,000 km vertically and over 25° westward from their point of release to be detected by the ion mass spectrometer on DE-1. It is not inconceivable for released ions to be energized enough to travel these distances. However, it is difficult to imagine the geophysical conditions that could lead to the required westward drift in the time between release and the DE-1 arrival at 70° degrees invariant latitude. The actual geophysical conditions were quiet and barium ions were tracked successfully for about 30 minutes to altitudes above 8,000 km. On April 25 the DE-1 orbital track was even less favorable for monitoring the release. The release took place at 254° east longitude. The ground track of the DE-1 satellite repeated approximately every two days. DE-1 crossed 70° invariant latitude in the northern hemisphere night, seven times every two days. The approximate east longitude and times of the crossings of 70°, north, night point were (162°, 09:00), (61°, 15:45), (319°, 22:15), (215°, 05:15 April 26), (112°, 12:30, April 26), (10°, 19:00, April 26), and (268°, 01:45, April 27).

PEGSAT STATIONS AND DATA COLLECTED:

CHURCHILL

Canister A: Skies clouded over--no data

Canister B: Skies cloudy; however, some autmax data are available from 0510-0515 UT.

FT. SMITH

Canister A: Clear skies. Data until 0556:25

Canister B: Clear skies.

HAY RIVER

Canister A: Auroral pictures only on 35 mm SLR camera.

Canister B: Site not staffed.

LYNN LAKE

Canister A: Clear skies. Power loss from 0546:30 to about 0554.

Quality of data good.

Canister B: Cloudy. No useful data.

Mt. LOCKE

Canister A: Data available not usable.

STONY RAPIDS

Canister A: Clear skies.

Canister B: Clear skies.

TABLE Mt.

Canister A: Images from 0455:35 through 0502:31.

KWAJALEIN CAMPAIGN

EXPERIMENTS AA-5, AA-6

Title: Release to Induce Plasma Instabilities at the Equator

Principal Investigator: Michael M. Mendillo, Boston University

Collaborative Investigators: R. Tsunoda, D. Hunton, P.A. Bernhardt, M. Kelley, W. Swartz, and J. Huba

Location: Kwajalein Atoll, Marshall Islands

Altitude: CRRES - 1 375 km
CRRES - 2 427 km

Time: CRRES - 1 08:17:00
CRRES - 2 08:34:00

Dates: CRRES - 1 08/11/90
CRRES - 2 08/15/90

Chemicals: 35 kg sulfur hexafluoride

OBJECTIVE:

The ionosphere near the equator, where the magnetic field is horizontal, suffers from naturally occurring perturbations known as Spread-F. The normally smooth ionosphere becomes structured and radio wave signals are distorted. These rocket experiments released sulfur hexafluoride, which created a "bubble" at the bottom of the ionosphere, in an attempt to trigger artificial Spread-F. These missions thus allowed study of the growth and decay of this effect with a controlled experiment. In each experiment one rocket was used to deploy the ionospheric depletion chemical, followed by a second rocket's carrying instrument to diagnose the release effects.

ALTAIR RADAR

STATION LEADER:

Michael M. Mendillo
Boston University
Boston, MA 02215

PHONE (617) 353-5990

TYPE AND DESCRIPTION OF DATA:

Steerable UHF/VHF incoherent scatter radar; calibrated electron densities, plasma drift velocities, and electron and ion temperatures, as functions of time, range, azimuth, and elevation.

LOCATION: 9.39 N, 167.48 E, 4.3 DIP

FIELD(S) OF VIEW: Data taken to 1600 km range.

TIME PERIODS OF DATA: 7 July-22 August 1990

Drifts: 25 nights of eastward, westward, northward, vertical plasma drift measurements, 6-10 UT.

Scans: 22 nights of elevation and azimuth scans.

SAMPLING RATES: 300 μ sec pulse used predominantly with 10 second integration.

ASSESSMENT OF DATA QUALITY: Reliable densities to ~1000 km altitude, VHF data only available on night of CRRES - 1 launch (11 Aug.) 08:17-09:53 UT.

INITIAL FINDINGS: Small-scale irregularity plumes observed near positions of drifted, release clouds, suggesting artificial initiation of ESF events.

ADDITIONAL RESEARCH: 17 nights of spread-F activity were observed by the radar scans.

CUPRI RADAR

STATION LEADER:

Wesley E. Swartz
Engineering Theory Center
Cornell University Ithaca, NY 14863

SPAN - wes@magneto.ee.cornell.edu
PHONE (607) 255-7120

TYPE AND DESCRIPTION OF DATA: Pulsed Radar SN, Doppler Spectra, Interferometry as functions of range and time.

FIELD(S) OF VIEW: 100-900 km Altitude: Zenith, 5° W of 5° E of Zenith

TIME PERIODS OF DATA: 11 Aug. 1990 06:10-18:15 UT, 15 Aug. 1990 06:30-12:00 UT

SAMPLING RATES: 60 μ s range gating, 10 ms IFF, typical integration time 1 m (off-line)

ASSESSMENT OF DATA QUALITY (CLOUD COVER; LIGHT CONTAMINATION): Data collection during period of strong SFY noise (i.e., galactic center overhead during observation time)

INITIAL FINDINGS: No F-region echoes on 11 Aug. Two faint scattering regions on 15 Aug. at 9:30 and 11:00 UT from 300-600 km and 300-400 km, respectively.

ADDITIONAL RESEARCH: More than 20 days of excellent natural ionospheric data were obtained.

OPTICAL AND SATELLITE RADIO BEACON OBSERVATIONS

TYPE AND DESCRIPTION OF DATA: All-sky images from Wake Island, Kosrae (FSM) and airborne observatory above Kwajalein. Total electron content and VHF scintillations from Wake and Kosrae.

FIELD(S) OF VIEW: Optical - all sky; TEC at fixed points

TIME PERIODS OF DATA: 7 Jul.-22 Aug. 1990

SAMPLING RATES: Images every 1 to 10 minutes; TEC continuous (except for data gaps due to power outages).

ASSESSMENT OF DATA QUALITY: Excellent optical data; good SRB data.

INITIAL FINDINGS: No optical signatures of AA-5 release.
Excellent optical coverage of AA-6 release.

ADDITIONAL RESEARCH: More than 20 days of excellent natural ionospheric data were obtained.

CRRES SATELLITE EXPERIMENTS

EXPERIMENTS G-13, G-14

Principal Investigator: G. M. Wescott

Collaborative Investigators: D. Papadopolous, R. Smith, G. Haerendel, A. Valenzuela, H.C. Stenbaek-Nielsen, M. Kelley, R. Anderson

Location: South Pacific in the vicinity of Fiji and American Samoa

Time of Day: Dusk

Altitude: CRRES/GTO Near Perigee

OBJECTIVE:

The objective of these releases was to investigate the critical ionization velocity phenomenon, first proposed by Alfvén to explain mass differentiation in planetary formation, or why the inner planets are made of heavy material and the outer planets are mostly hydrogen. The critical ionization velocity model states that if the relative velocity of a neutral species and a magnetized plasma is large enough, ionization of the neutral gas will take place even though the gas is so thin that the particles are not directly colliding. Barium, calcium, and strontium will be released in these experiments, for these materials have a range of critical ionization velocities and allow study of the effect over a wide range of this parameter.

EXPERIMENT G-13

10 September 1991

06:10:25 UT

TITLE: Critical Ionization Velocity (C IV I)

POINT OF CONTACT:

E. Wescott
Geophysical Institute
University of Alaska
Fairbanks, AK 99701

SPAN- UAFGI::ROCKET
PHONE (907) 474-7576
FAX - (907) 474-7290

EXPERIMENT ELEMENTS:

Coordinates of Release: 17.5S 198.9E 517 km
Canister Type: Large
Chemicals: 13A TI 4254 gms B 1920 gms SR 3784 gms
 13B TI 4554 gms B 2055 gms BA 5408 gms
Delay: 13A: None. 13B: 2.5 sec

STATIONS COVERING THE RELEASE:

Aircraft - C135-131 Aeromet, Inc. Learjet

EXPERIMENT G-14

10 September 1991

08:47:10 UT

TITLE: Critical Ionization Velocity (C IV II)

POINT OF CONTACT:

E. Wescott
Geophysical Institute
University of Alaska
Fairbanks, AK 99701

SPAN - UAFGI::ROCKET
PHONE (907)474-7576
FAX - (907) 474-7290

EXPERIMENTAL ELEMENTS:

Coordinates of Release: 18.1S 161.6E 593 km
Canister Type: Large
Chemicals: 14A Ti 5214 gms B 2353 gms CA 1891 gms
14B Ti 4554 gms B 2056 gms BA 5409 gms
Delay: 14A: None. 14B: 2.5 sec

STATIONS COVERING THE RELEASE: Aircraft - C135- 131 Aeromet, Inc. Learjet

INTRODUCTION:

In the past decade, the hypothesis of critical ionization proposed by Alfven (1954) has been tested in free space in several sounding rocket experiments (Haerendel, 1982; Simons et al., 1984; Wescott et al., 1986a,b; Stenbaek-Nielsen et al., 1990a,b; Wescott et al., 1990; Torbert, 1990). These experiments used high explosive shaped charges to produce directed jets of super critical velocity Ba or Sr vapor. The angular distribution of the fast jet is a Gaussian with a full width, half amplitude of 13.2° . CRRES offered the possibility of performing critical ionization velocity (CIV) experiments with a different velocity distribution centered on the orbital velocity of about 10 km/s. There were 4 canisters (2 Ba and 1 Sr and 1 Ca) devoted to the critical velocity experiments G13 and G14. The critical velocities of these elements are 2.7, 3.5, and 5.4 km/s. The Ba and Ca burning temperature was 2750 K, and the Sr 2650 K. The metallic vapor and TiB₂ was released through a nozzle in less than a second, and expanded nearly spherically. We have assumed 40% efficiency of vaporization based on observations of rocket test results, (Huba et al., 1992). Recent reviews of experimental and theoretical studies have been published by Newell (1985), Lai et al. (1989), Lai and Murad (1989), Torbert (1990), and Brenning (1992). Of the shaped charge experiments only the "Porcupine" experiment (Haerendel, 1982), and CRIT II (Stenbaek-Nielsen et al., 1990) produced significant ionization attributed to the CIV process. Both were conducted in high electron background densities ($>5 \times 10^5 \text{ cm}^{-3}$). So we decided to do the CRRES CIV releases in high electron densities, in darkness well below the solar UV terminator, on field lines such that any ions created in the darkness travel up the field into the sunlight. These release conditions and the satellite orbit dictated releases near perigee in the south Pacific area.

DESCRIPTION OF EXPERIMENTS:

The first experiment, G13, was carried out on Sept. 10, 1990, east of American Samoa. The second experiment, G14, was carried out on Sept. 14, west of New Caledonia. Table 1 gives the pertinent parameters.

TABLE 1

	G13		G14	
	Sr	Ba	Ca	Ba
Date	Sept. 10, 1990		Sept. 14, 1990	
Time UT	06:10:22.5	06:10:25	08:47:10	08:47:12.5
Lat.(°)	-17.54	-17.58	-18.07	-8.08
Long.(°E)	198.85	199.07	161.55	161.754
Alt. (km)	516.8	513.6	592.5	596.4
Solar screening ht	-15.38	-21.92	-24.5	-30.8
Dip angle of B(°)	33.6	33.3	44.3	44.3
Angle, B to sun dir.	113.97	113.97	117.31	117.31
Angle, B to velocity	79.89	79.89	77.96	77.96
Pitch angle(°)	79.83	79.73	7.9	77.80
Vpar(km/s)	1.67	1.68	1.97	1.98
Vperp (km/s)	9.31	9.31	9.20	9.18
Moles @ 40% eff.	17.28	17.33	18.08	17.33
Atoms (x10 ²⁵)	1.04	0.949	1.14	0.949
n(e) (x10 ⁶ cm ⁻³)	3.5	3.4	1.6	1.5
n(O) (x10 ⁷ cm ⁻³)	4.89	5.11	2.47	2.35
n(He) (x10 ⁶ cm ⁻³)	2.10	2.13	1.89	1.86
TeXo (K)	923	923	1134	1134
mean free path (km)	131	126	260	273
B (nT)	30530	30557	34937	34852
Gyro freq.(Hz)	5.33	3.41	13.33	3.89
Gyro radius (m)	243	435	110	376
Learjet Position, Lat. (N)		-19.353	-22.390	
at release Long. (E)	195.047	199.211		
Alt. (km)	12.034	12.072		
C-135 Position, Lat. (N)	-21.530	-20.056		
at release Long. (E)	199.490	157.324		
Alt. (km)	10.060	9.449		

RESULTS:

In each experiment the releases were recorded with low light level imagers mounted in two aircraft flown on paths about 500 km apart. IPD systems were fitted with 30 Å FWHM Ba ion filters at 4554 Å, while ICCD cameras were initially operated in white light and later operated with either 30 Å FWHM Sr ion line filters at 4077.71 Å or with 70 Å WHM Ca ion filters centered between the doublet 3968.47 Å and 3933.67 Å. We used the stars present in the images for triangulation of release phenomena and for calibration of the images to determine ion inventories.

As each release occurred, we observed the expected momentary bright flash as the hot gas exited the canister at about 2750 K and then saw the expanding spherical shell following the satellite trajectory continue to glow in the dark for about 15 seconds.

We fitted the observed distribution of Ba luminosity with an assumed Gaussian function:

$$f(v) = \exp[-(v-v_0)/v_t]^2,$$

where v is the radial velocity, $v_0 = 1.33$ km/s and $v_0/v_t = 4.5$. The shells expanded at rates proportional to the inverse square root of their atomic weights: 1.33, 1.62, and 2.4 km/s for Ba, Sr,

and Ca, respectively. The G13 Ba release was outside the Sr gas shell, but the G14 Ba release occurred within the peak density of the Ca shell.

After about 30 s, ions of each released neutral element were observed to appear above the solar terminator traversing up the magnetic field lines, proving that some ionization process or processes had produced ions in the absence of solar UV radiation. Ions from a non-solar UV source were being produced for at least 45 s, or a distance along the orbit of about 300 km.

Another important result, seen on all the releases, is that for a few s after release we observed a "fast jet," ions with higher velocities than those created later along the satellite track. Similar populations of fast ions near the release field line were seen on later CRRES experiments where the release took place in full sunlight.

ION INVENTORIES:

All imagers except the ISIT were intensity calibrated based on the signal in individual stars present in the respective images. The expected flux for all of the stars in a catalog of high resolution stellar spectra (Jacoby et al., 1984) was calculated by integrating each spectrum folded with the filter transmission function. The emission rates specific for these releases, taking into account the Doppler brightening due to the gyro motion and the velocity along B were: Ba II, 4554 Å: 1.78 and 1.59 (photons/ion/s) for G13 and G14, respectively, Sr II, 4078 Å: 0.82 (photons/ion/s); and Ca II, 3933.66 Å plus 3968.47 Å: 0.376 (photons/ion/s).

The most significant measurement of the ion yield was obtained by computing the position to the satellite from the aircraft situated perpendicular to the satellite motion at 2 s increments along the track, superposing magnetic field lines on the ion images, and then doing an ion inventory between adjacent field lines. There is much more total ionization for G14 than G13, but both show much the same time behavior: a rapid rise to a peak, followed by a decay to nearly a constant rate, then a decrease at the edge of the frame. The fall off after the peak is exponential with characteristic lengths of 47 km and 62.1 + 5.9 km for G13 and G14. Table 2 gives the total ion inventories and the estimated C IV yields.

TABLE 2

C IV yield, % of N_{total}

G13:

$$N_{(\text{Sr}^+)} = 8.39 \times 10^{21} \text{ at } 1 \text{ m } 51 \text{ s}$$

$$N_{(\text{Sr}^+)}/N_{\text{total Sr}} = 0.02\%$$

$$N_{(\text{Ba}^+)} = 9.63 \times 10^{21} \text{ at } 2 \text{ m } 30 \text{ s}^* \quad 0.014\%$$

$$N_{(\text{Ba}^+)}/N_{\text{total Ba}} = 0.15\%^*$$

$$N_{(\text{Ca}^+)} = 3.09 \times 10^{22} \text{ at } 2 \text{ m}$$

$$N_{(\text{Ca}^+)}/N_{\text{total Ca}} = 0.27\%$$

G14:

$$N_{(\text{Ba}^+)} = 1.75 \times 10^{23} \text{ average } 3 \text{ m } 28 \text{ s to } 4 \text{ m } 28 \text{ s}^*$$

$$N_{(\text{Ba}^+)}/N_{\text{total Ba}} = 1.84\% \text{ }^* 0.40\%$$

* These are minimum values since the image cuts off at the right, and obviously ionization was continuing at a nearly level rate up to the edge of the frame. We estimate that about 2% of the observed ions in C IV II Ba experiment had not risen above the terminator at the time of the inventory.

COMPUTATIONS:

Using the observed nearly uniform spherical expansion of the Ba neutral shell of G14 and the Gaussian function of radial velocity, we derived the pitch angle-velocity distribution. We assumed that the neutral atoms ionize at once with little change to pitch angle and velocity, to calculate a linear density along B at any time of interest. For the collisionless case we used scaled numbers of test particles injected into the B field at all the pitch angles and velocities, and calculated the position along B vs. time of all the particles, including gravity and gradient of B forces. The actual density distribution in three dimensions will depend on the rate of ionization, the radial expansion and the velocity along the satellite trajectory. However the linear density along the release point field line gives a good approximation of the distribution at later times.

The elastic momentum loss collisions are modeled by two Monte Carlo computer codes using 31,500 test particles, 50 per each pitch angle-velocity bin. We used a Ba(II) + O(I) collision cross section derived by Clodius at LANL (private communication, 1991). The density of O atoms along the helical trajectory was calculated using MSIS (Hedin, 1987).

Figure 5 combines the observed brightness (normalized) with the theoretical density distribution from the Monte Carlo modeling along the +2.5 s field line at four times from 150 s to 240 s after release. The figure shows the observed distribution and that computed with no losses and with collisions using the LANL cross sections. It is clear that the observed distribution is not as far along B as the collision-free curve. The observed data fit fairly well with the collisions curve except for the observed high velocity wing shown in Figure 5.

Using the radial velocity function, we have derived the neutral density as a function of time. The peak neutral density, decreases as t^{-3} , at one s is 8.45×10^8 atoms cm^{-3} and equals the ambient density at 3.5 s. We expect that there was a snow plow effect for the first several seconds which moved some of the ambient atmosphere away from the expanding gas.

SOURCES OF NON-SUNLIT IONIZATION:

The C IV ionization process is much more complicated than originally proposed by Alfven (1954). Ambient electrons collide with the streaming neutrals creating new ionization. The newly ionized neutrals participate in one or more plasma instabilities, heating electrons to energies in excess of the ionization potential. The hot electrons then collide with neutral atoms (Ba, Sr, or Ca) creating new ions and new free electrons, inducing a self supporting discharge. Lai and Murad (1992) have discussed inequality conditions for C IV experiments. One measure is called Townsend's condition (Townsend, 1915): on average each new electron must remain long enough within the neutral cloud to have another ionizing collision before exiting along B. For the CRRES Ba releases, using 10 eV electrons, whose cross section for ionizing collisions is $\sigma = 1.2 \times 10^{-15} \text{ cm}^2$ the classical Townsend condition is met for about 0.6 s. The C IV ionization is expected to rise to a peak and then fall off as the cloud becomes too diffuse to support the discharge. However, Newell and Torbert (1985) and Torbert et al. (1992) have shown from several rocket shaped charge experiments that the calculated Townsend's condition may be irrelevant, because for causes unknown the hot electrons are observed to be contained in the interaction region for longer times, and do not escape from the cloud as predicted.

Aside from the critical velocity ionization process, there are at least four other possible sources of ionization of the neutral streaming gas: collisions with ambient atmospheric atoms and molecules (stripping); charge exchange collisions with ambient ions, associative ionization and; initial thermal ionization. Torbert and Liou (1991) have shown that the ionization from processes which depend upon collisions with the ambient neutral or ion background must be essentially constant. Observation of the ionization rate vs. time down the satellite track allows the identification of C IV vs. other processes.

For stripping to occur by Ba colliding with O, the most numerous ambient constituent, the minimum rest frame velocity is 8.4 km/s, for Sr it is 9.0 and for Ca it is 10.2 km/s. For G13 and G14 stripping

is possible for a fraction of all three species: 77% for Ba, 67% for Sr and 40% for Ca. The rate of stripping ionization is $n(O)xsV$. Based largely on theoretical considerations, we estimate that the cross section for stripping Ba is $3.5 \times 10^{-19} \text{ cm}^2$, and the ionization rate is:
 $1.7 \times 10^{-4} \text{ s}^{-1}$

Charge exchange ionization e.g., $\text{Ba} + \text{O}^+ \rightarrow \text{Ba}^+ + \text{O}$, is probably responsible for more ionization than any of these processes. Swenson et al. (1991) have pointed out that the cross section for charge exchange ionization which has been measured for O^+ colliding with Ca (Rutherford et al., 1972) is about $1 \times 10^{-14} \text{ cm}^2$ at the velocity of CRRES. The cross sections for O^+ colliding with Sr and O^+ Ba have not been measured, but they suggest on theoretical considerations, that Ba and Sr have only slightly smaller cross sections than Ca. Using the Ca- O^+ cross section measured by Rutherford et al. (1972), and the electron density $1.6 \times 10^6/\text{cm}^3$, the charge exchange ionization rate should be: $1.5 \times 10^{-2} \text{ s}^{-1}$. If ionization proceeded at that rate for 10 s, it would amount to 14% of the neutral Ca, but from Table 2 only 0.27% was observed over 45 s.

If the published and estimated cross sections for charge exchange are to be believed, Ca^+ should have been the most abundant ion observed. If the G14 Ba ionization was anomalously large because it was released in the Ca maximum then perhaps we should only consider the C IV I Ba in this respect. There was more Ca^+ in G14 than Ba^+ in G13 (0.27% vs. 0.15%). However all the observed ionization is less than one would predict from charge exchange alone.

Lai et al. (1989, 1992) have suggested associative ionization as an important process in creating Ba^+ ions. They propose that:



proceeds with a cross section comparable with charge exchange. They further speculate that when the BaO^+ ions reach sunlight that they can dissociate by absorption of solar UV (principally Lyman- α) by two schemes producing Ba^+ which is indistinguishable from ions produced by C IV or other processes. This is an interesting suggestion, but none of the cross sections involved have been measured so it is impossible for us to evaluate. However we do not discern a sharp increase in 4554-brightness above the Lyman screening height at about 100 km, or about 200 km along B above the terminator.

The ionization due to the temperature of the barium thermite reaction and release is not well known by any direct measurement. Using the Saha equation, Stokes (personal communication, 1990) has calculated that the temperature of the B + Ti thermite reaction would produce 10^{-4} fraction of ions in the first few msec after release. These would be very close to the release point as the adiabatic temperature falls very rapidly. This fraction is probably too high, as we have never seen this many ions concentrated near the release field line. However they may contribute to the "fast Jet."

CONCLUSIONS:

These C IV experiments were carried out at super-critical velocities and at injection angles about 78° to B well below the solar UV horizon. The expanding neutral spherical shells were observed optically while they were below the sunlight terminator. From the Star of Condor, Crit I and Crit II C IV releases, in situ detectors measured large numbers of hot electrons as the gas streamed by (Torbert and Newell, 1986; Torbert, 1990). Collisions of these electrons with the neutral atoms are expected to be the source of the C IV ionization. Newell and Torbert (1985) point out that some of the electron energy goes into excitation rather than ionization, which is probably the source of the emissions that we observed from the expanding gas shells. Ions of all three elements were observed with low light level imagers streaming up the field lines into the sunlight about 30 s after the releases. The velocity along B was much less than expected from collisionless single particle trajectories. Momentum loss collisions of Ba^+ with O atoms are sufficient to explain most of the difference using the velocity dependent collision cross section derived by Clodius (Personal Communication, 1991). However inelastic and coulomb collisions may also play a part in the energy loss. There may also be a very small parallel electric field along B which could retard the ions, but we have no independent evidence for such a field.

The ionization process or processes continued for at least 45 s along the satellite trajectory. Using data from the aircraft situated perpendicular to the releases, we have measured the ion production vs. time for the Ba releases of G13 and G14. The ion inventory summarized in Table 2 ranges from 0.02% to 1.84%. The classical Townsend's criteria is met for the Ba releases for only about 0.6 s. However Torbert (1985) and Torbert et al. (1992) have shown from several rocket shaped charge experiments that the calculated Townsend's condition may be irrelevant because for causes unknown the hot electrons are contained in the interaction region for a longer time, and do not escape from the cloud. We would expect that the CIV process would build up to a peak, and then decay exponentially as the neutral cloud becomes diffuse and can no longer support the process. This sort of time behavior for Ba⁺ was found. The ionization rate decays to a plateau at about 26 s. The decay after the peak value is exponential. For G13 the characteristic length is 47 km, and for G14, 62.1–5.9 km. The characteristic length for the rise is more uncertain due to the 2-s increments, but our best estimate is 3 and 10 km, respectively. The later decays are due to the field lines intersecting the edge of the image. We interpret measurements of the ion production vs. distance along the center of mass track of the neutral cloud as a means to separate C IV ions from ions due to charge exchange, stripping and associative ionization. Our interpretation is as follows:

Torbert and Liou (1991) have shown that the ionization from processes such as charge exchange, stripping or associative ionization, which depend upon collisions with the ambient neutral or ion background must be essentially constant with time or distance along the neutral cloud track. We interpret the plateau as the constant production from charge exchange, stripping and associative ionization. When we subtract this constant amount from the early time production, we interpret the remainder as the C IV ionization. The estimated C IV Ba ionization yield is then 0.014% and 0.40% for G13 and G14, respectively.

The most significant result was the difference in the total ion and C IV yield of Ba ions between G13 and G14. In G14 the electron and O densities were smaller by a factor of 2, while the ion yield was about 13 times larger. One possible explanation for the difference in the Ba ionization rates may be found in the relative positions in which the release occurred with respect to the preceding Sr and Ca releases. The G13 Ba release was outside the peak of the Gaussian shell in a Sr density of $1.3 \times 10^5 \text{ cm}^{-3}$, but the G14 Ba release would have occurred at the peak of the Ca shell in a Ca density of $1.0 \times 10^7 \text{ cm}^{-3}$. The Ca⁺ density is more difficult to estimate, but the G14 Ba encountered an environment of hot electrons from the Ca ionization processes. Since the Ca shell is expanding faster than the Ba shell, the Ca will always be ahead of the Ba, thus altering the environment. The Sr shell will begin to overlap portions of the Ba shell after about 1 s, but the peaks will not reach the maximum overlap until 6.5 s. So we interpret the G13 Ba release as "normal" and the G14 "anomalous" because of the disturbance to the ambient background by the ionizing Ca. Since the greater ionization was created for as much as 45 s, the effect was efficient in boosting ionization from other processes as well as C IV.

Current theory does not adequately explain our results. In particular, the Porcupine experiment where the neutral Ba was injected at 30° to B produced about 20% C IV ionization compared to the 0.014% to 0.40% in these experiments. It would seem that the Porcupine experiment should be duplicated with adequate diagnostics similar to the CRIT II experiment.

EXPERIMENTS G-1, G-2, G-3, G-4

Title: Diamagnetic Cavity, Unstable Velocity Distributions, Plasma

Principal Investigators: R. A. Hoffman (G-1,G-2,G-3) and S. B. Mende (G-4)

Collaborative Investigators: M. Pongratz, D. Papadopoluos, R. Smith, R. Anderson, D. Young, H. Singer, E. Szuszczewicz, J. P. Heppner, E. M. Wescott, H. C. Stenbaek Nielsen, G. Haerendel, A. Valenzuela, P. A. Bernhardt, J. D. Huba.

Location: Over North America

Time: Sunlit Releases, Ground in Darkness

Altitude: B=15000 gammas (1500-3000 km), 5000 gammas (5000-6000 km)
1000 gammas (14000-16000 km), 200 gammas (123000 km)

OBJECTIVE:

As a result of natural processes, plasma clouds are often injected into the magnetosphere. These chemical releases can be used to study many aspects of such injections. When a dense plasma is injected into the inner magnetosphere, it is expected to take up the motion of the ambient plasma. However, it has been observed in previous releases at moderate altitudes that the cloud preserved its momentum for some time following the release and that parts of the cloud "peeled off" from the main cloud presumably due to the action of an instability. As one moves outward into the magnetosphere, the mirror force becomes less dominant and the initial conditions following a release are dominated by the formation of a diamagnetic cavity since the initial plasma pressure from the injected Ba ions is greater than the magnetic field energy density. A previous high altitude release (31,300 km.) showed this to be the case initially, but at later times there was evidence for acceleration of the Ba plasma to velocities corresponding to 60,000 K. This effect is not explained.

This series of experiments is therefore designed to inject plasma clouds into the magnetosphere under widely varying conditions of magnetic field strength and ambient plasma density. In this way the coupling of injected clouds to the ambient plasma and magnetic field, the formation of striations due to instabilities, and possible heating and acceleration of the injected Ba plasma can be studied over a wide range of magnetospheric parameters. Adding to the scientific yield, would be the availability of measurements for the DOD/SPACERAD instruments. These instruments can monitor plasma parameters, electric and magnetic fields, and waves; before, during, and after the releases.

EXPERIMENT G-2

13 January 1991

02:17:03 UT

POINT OF CONTACT: Robert Hoffman
GSFC CODE 696
Greenbelt, MD 20771

SPAN - DE696::U6RAH
PHONE (301) 286-7386
FAX - (301) 286-9240

EXPERIMENTAL ELEMENTS:

Coordinates of Release: 16.9N 103.1W 6180 km
Canister Type: Small
Chemicals: TI 1269 gms B 572 gms BA 1468 gms SR 19 gms
Delay: None

Model Calculations:

Ted Fritz

SPAN - ESSDP1::FRITZ

LANL
MS - D438
Los Alamos, NM 87545

PHONE (505) 667-9234
FAX - (505) 665-3332

STATIONS COVERING THE RELEASE:

Caribbean -	Bonaire, NA. St. Croix, USVI
North America -	Los Alamos, NM White Sands, NM Rosemary Hills, FL
South America -	Cerro Tololo, Chile

Releases G-2, G-3 and G-4

The series of barium chemical releases G-1 - G-4 was designed to inject plasma clouds into the magnetosphere under widely varying conditions of ambient magnetic field strength and plasma density. Through this process the coupling of the dense injected ion clouds to the ambient plasma and magnetic field, the formation of striations on the edges of the clouds due to instabilities, the generation of plasma waves, and possible heating and acceleration of the injected barium plasma could be studied over a wide range of magnetospheric parameters. It was the intent to use the available in-situ measurements by instruments on the CRRES spacecraft to monitor plasma parameters, electric and magnetic fields and waves before, during and after the releases.

Releases G-2, G-3 and G-4 were performed for these purposes. The following table gives the release conditions.

RELEASE #	MAGNETIC FIELD	PLASMA DENSITY
G-2	5,000 nT	>2,000/cm ³
G-3	1,000 nT	300-400/cm ³
G-4	250 nT	150/cm ³

When a dense plasma is injected into a magnetic field, the initial conditions of the system following the injection can be dominated by the relative energy densities of the plasma versus the magnetic field.

At low altitudes, the $\mu\nabla B$ mirror force is large, the injected ions become quickly magnetized and move with the ambient plasma. However, at high altitudes where B is small, this force becomes small and the initial conditions can be dominated by the formation of a diamagnetic cavity when the dynamic pressure from the expanding barium ion cloud greatly exceeds the magnetic field energy density. The maximum cavity radius R may be estimated by solving the pressure balance equation $MV^2/2 = (B^2/2\mu_0)(4\pi R^3/3)$, where M is the mass of the ions released, V the expansion speed, B the unperturbed strength of the magnetic field, and μ_0 the permeability constant. At this point the diamagnetic cavity is expected to collapse. By knowing the expansion speed of the barium and the amount of barium released, the size of the diamagnetic cavity as a function of time can be calculated, and thus its energy density. By measuring the time until collapse, the validity of the pressure balance equation can be determined over a wide range of parameters [Huba et al., 1992].

The size of this diamagnetic cavity to the time of collapse was measured for these releases by the magnetometer on the CRRES satellite. Singer [1992] has compared the observed times with times the magnetic cavities would reach pressure balance with the ambient magnetic field, which scales as $(M/B^2)^{1/3}$, and would then collapse. The results are plotted in Figure 1, which shows excellent agreement between the measured times for the five releases with the calculation (solid line). The background magnetic field was totally excluded for the two large G-8 and G-10 releases. The other high-altitude barium releases produced less-pronounced cavities [Bernhardt, 1992]. The results of this set of releases are especially valuable in the planning of future chemical releases, since they provide guidelines for the size of a release to avoid significant cavity formation.

While the G2 and G3 releases occurred in the plasmasphere, the G4 release apparently occurred in the plasmopause instead, where the density was considerably lower than expected and had a steep

gradient. Thus, any effects of ambient plasma density on the formation of the diamagnetic cavity have been made more complicated to ascertain. Preliminary theoretical and computational analyses of these same releases have been performed by Huba et al. [1992] and compared with the observations from the satellite and with high resolution optical images taken from New Mexico. They focused on the evolution of the diamagnetic cavity, and also on the structuring of the density and magnetic field during the expansion phase of the releases. Two sets of simulation studies were performed, the first based upon a two-dimensional ideal MHD code which estimates the time and length scales associated with the formation and collapse of the diamagnetic cavity. The second set used a non-ideal MHD code, which included a Hall term responsible for instability, structuring of the surface of the diamagnetic cavity, and jetting of ions through irregularities in the surface of the expanding plasma. For the G4 and G10 releases they obtained rapidly developing structures, and also found that the diamagnetic cavity size is reduced because of the structure. On the other hand, the structuring allows the formation of plasma blobs which free stream across the magnetic field, so the barium plasma propagates to larger distances transverse to the magnetic field than for the case of no structuring. Structuring was observed in the G4 release, but considerably later than the calculations indicate. The simulation showed that the recovery of the magnetic field at the edge of the cavity was accompanied by a series of undulations in the field due to irregularities. The CRRES passive plasma sounder recorded a burst of low-frequency (10-100 Hz) noise each time the satellite crossed the boundary of a diamagnetic cavity. After the diamagnetic collapse, residual field-aligned irregularities could be observed with ground-based cameras [Bernhardt, 1992].

A new aspect of irregularity formation on the surface of the barium ion cloud was studied using data from the G-2 release. This release showed evidence of curved irregularities not aligned with the ambient magnetic field but conformed to the contour of the expanding barium cloud shell. A high resolution telescope filtered at the 455.4 nm barium ion line recorded irregularities 25 sec after the release (Fig. 2) [Bernhardt et al., 1993]. These newly discovered curved structures have been explained by Bernhardt et al. [1993] by a process called cycloid bunching, which does not require plasma instability. This phenomenon occurs when plasma is created by photoionization of a neutral cloud injected at high velocity perpendicular to the magnetic field. If the injection velocity is much larger than the expansion speed of the cloud, the ion trail will form a cycloid that has irregularities spaced by the product of the perpendicular injection speed and the ion gyroperiod (Fig. 3).

At the cusps of the cycloid, the density of the ions is larger giving the appearance of curved structures on the surface of the cloud. The authors solved the three-dimensional Vlasov equation to demonstrate that cycloid bunching plays an important role in this striation formation. The CRRES search coil magnetometer and the passive plasma sounder recorded the spectrum of plasma waves for the G-2 to G-4 releases. A low-frequency burst of electromagnetic radiation was observed as the leading edges of all the expanding ion clouds passed over the CRRES spacecraft.

Fig. 1. Comparison of measured time for the diamagnetic cavity to reach pressure balance with the ambient magnetic field (points) with theory (line). (from Singer, 1992)

Fig. 2. Linear scan across the curved irregularities from an image from an intensified CCD camera operated at the White Sands Missile Range, New Mexico. The scan along the satellite trajectory shows 10-km separation in irregularities. (from Bernhardt et al., 1993)

Fig. 3. Diagram of the cycloid produced by photoionization of a moving, localized source of neutral barium. The ions follow spiral paths along the ambient magnetic field. Equidistant points on the straight-line source map to points that are bunched near the cusps of the cycloid where the ion density maxima are found. (from Bernhardt et al., 1993).

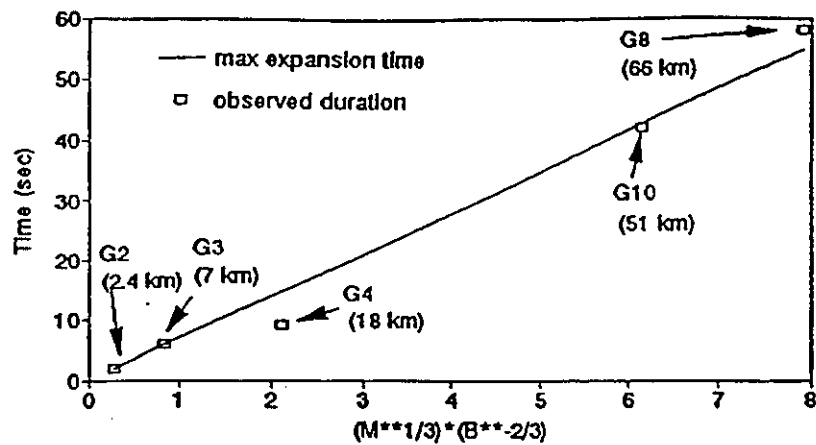


Fig. 1.

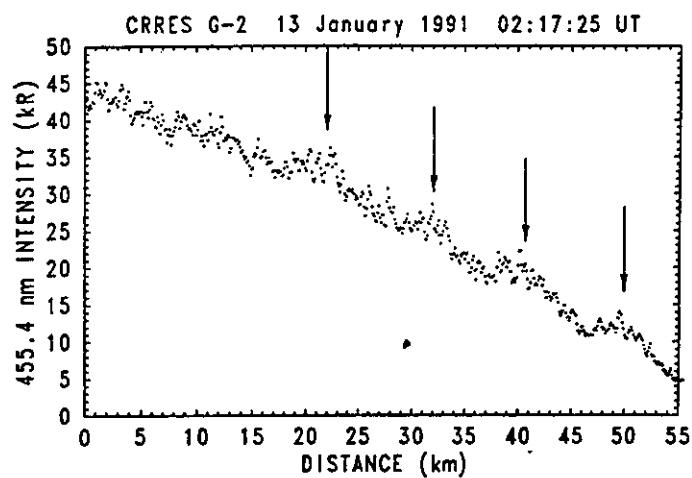


Fig. 2.

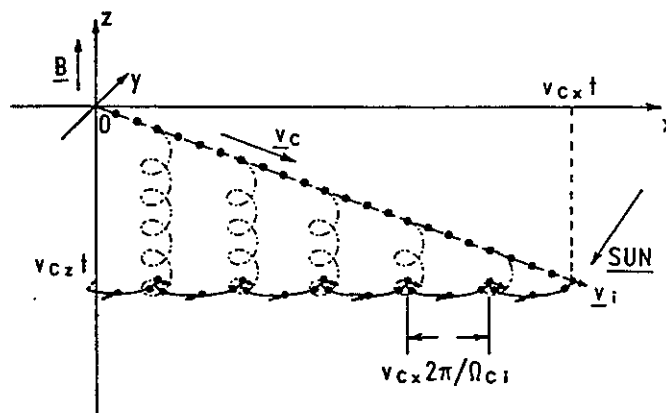


Fig. 3

EXPERIMENT G-7

13 January 1991

07:05:00 UT

Title: Ion Tracing and Acceleration

Principal Investigator: W. K. Peterson

Collaborative Investigators: G. Haerendel, A. Valenzuela, R. Rairden, E. Wescott, B. Candey, M. Pongratz

Location: Magnetosphere

Altitude: 33403 km

Chemicals: 20 kg Lithium (2 large canisters)

OBJECTIVE:

This experiment was proposed to utilize two additional Lithium canisters to be carried on the CRRES/GTO using two spare large canisters that were left after the allocation of canisters to the existing experiments was made. Originally, this experiment planned to use the GTO Lithium and Barium releases to trace ion transport and acceleration through the magnetosphere. Detection of the ions would be with mass spectrometers on board existing satellites. Due to delays there were not suitable satellites (ISEE, DE) still operating when the main group of CRRES/GTO releases were completed. Therefore, this experiment waited until components of the ISTP mission are in place and choosing an optimum location for the release based on the position of the CRRES/GTO and other satellites with mass spectrometers. This experiment offered a unique opportunity to study the transport and possible acceleration of ions from a point release, and were complementary to the goals of the ISTP Program with regard to study of the sources of plasma within the magnetosphere.

POINT OF CONTACT:

W. Peterson	SPAN- LOCKHD::PETE
3251 Hanover St.	LPARLPHONE (415) 424-
Palo Alto, CA 94304	FAX -(415) 424

EXPERIMENT ELEMENTS:

Coordinates of Release: 8.0N 86.7W 33403 km

Type of Canister: Large

Chemicals: 7A TI 5768 gms B 2603 gms LI 457 gms EU 299 gms
7B TI 5768 gms B 2603 gms LI 457 gms EU 299 gms

Delay: None

Model Calculations:

Ted Fritz	SPAN - ESSDPI::FRITZ
LANL MS-D438	PHONE (505) 667-9234
Los Alamos, NM 87545	FAX - (505) 665-3332

STATIONS COVERING THE RELEASE:

Aircraft - Argentine B-707, C135-127

Caribbean - St. Croix, USVI

North America - Los Alamos, NM; Rosemary Hills, FL; White Sands, NM

Satellite - Akebono, CRRES, Dynamics Explorer-1

South America - Cerro Tololo, Chile El Leoncito, Argentina

RELEASES G-5, G6, and G-7

The G-5, G-6, and G-7 investigations all involved release of two large LiI canisters near (± 1.5 hours) local midnight at high altitude ($r/Re > 5.5$). The objective of the G-7 release was the direct observation of released lithium by *in-situ* ion mass spectrometers to provide new insight into ion transport and acceleration processes acting in the magnetosphere. The primary objective of the G-5 release was to see if the increase in local plasma density associated with the release would create an artificial aurora as predicted by Kennel and Petschek (1966). The primary objective of the G-6 release was to see if the increase in local plasma density associated with the release would create ion cyclotron waves that caused ion precipitation as predicted by Kennel and Petschek (1966).

There were extensive optical observing (including aircraft) and geophysical condition restraints on the G-5 and G-6 releases. The physical constraints the G-5 and G-6 releases required CRRES apogee to be over eastern North America, and that there be indications from real time monitors of geophysical conditions that the particle energy density near synchronous orbit was increasing. The physical, as opposed to the geophysical, constraints on the G-5 and G-6 release allowed for approximately one release opportunity every 2 days for about 12 days in January and February of 1991. Obviously there were only a few selected time intervals where the relative positions of the DE-1, Akebono, and CRRES satellites were suitable for the G-7 release. Because the geophysical condition constraints on the G-5 and G-6 releases were so restrictive, it was decided to field the aircraft and ground observers and prepare for a release at each opportunity.

We used software developed especially for the CRRES program to determine the relative positions of the DE-1, CRRES, and Akebono satellites during each of the release opportunities for the G-5 and G-6 experiment. It was found that the position of the DE-1 spacecraft was most acceptable for the release opportunity on January 13, 1991.

Figure 1 shows the relative position of the CRRES and DE-1 satellites on January 13. Also shown are the positions of the DE-1 and CRRES orbital tracks from 07:00 to 08:00 (CRRES) and 08:00 to 11:00 (DE-1) on January 13, 1991, viewed in geographic coordinates from the dawn side (top left) and nightside (top right). The orbital tracks are given in invariant latitude and magnetic local time coordinates for the same time periods in the lower right panel. Magnetic field lines calculated using the Magsat magnetic field model are shown in the top two figures. The position of DE-1 at 08:00 is indicated by a large circle and the position of CRRES at 07:00 is indicated by a + sign.

The G-7 release was made at 07:05 universal time when CRRES was just past apogee and moving toward the dawn side of the magnetosphere. The natural motion of the magnetic field line transports cold ions downward toward the plane of the DE-1 orbit. DE-1 crossed the invariant latitude of the release (67.7 degrees) at 09:40 UT. The photoionization time for lithium is on the order of 1 hour. During the hour required for the bulk of the lithium to photoionize, the cloud of neutral lithium expands across and along magnetic field lines. Once photoionized, lithium ions move along magnetic field lines. At the time of the release the CRRES satellite was at an altitude of -33,000 km. Depending on the additional energy acquired from plasma wave heating or other acceleration processes lithium ions could have reached the location of DE-1 from -08:40 when DE-1 was at 62.5 degrees invariant latitude and -20,000 km altitude to -10:40 (72 degrees invariant latitude and -22,000 km altitude). Data were acquired on DE-1 during this interval in a special mode designed to maximize the sensitivity for detecting $^7\text{Li}^+$.

It was not possible to recover the data acquired on January 13 from the tape recorder on DE-1. The satellite was near the end of its life. DE-1 was launched in 1981 with two tape recorders. It was planned to terminate DE-1 operations in March 1991, shortly after the CRRES releases. One of the tape recorders failed earlier in the mission. During November 1990, the spacecraft stopped accepting commands, presumably because of the degradation in satellite thermal control that resulted in an operating environment at and above the nominal service temperatures. Spacecraft operations were suspended until December 1990, when DE-1 cooled because of the changing solar aspect angle and the reduced power dissipation associated with suspended operations. The data on the tape recorder acquired on November 17th, when commands were first not accepted, were recovered on December

17th, when commanding was restored. Limited operations using the tape recorder were resumed in January 1991. Data were acquired on the tape recorder and transmitted to the ground from 16:03 to 16:19 on January 4, from 11:39 to 13:41 on January 8, and from 08:24 to 08:40 on January 11. The spacecraft stopped accepting commands again shortly after 11:00 on January 13th during the period data were being acquired in support of the G-7 release. Presumably the power dissipated by the tape recorder and limited instrument complement operating at the time raised the satellite temperature to the point where the spacecraft would not accept commands. When the spacecraft cooled and again began accepting commands in February, the remaining tape recorder had failed. Limited data, in a mode not useful for chemical releases, were acquired from DE-1 using a real-time data link between February 14 and 18. Repeated and creative attempts to recover the data from the January 13th release on the tape recorders were made until the DE-1 operations center was physically dismantled in April 1991.

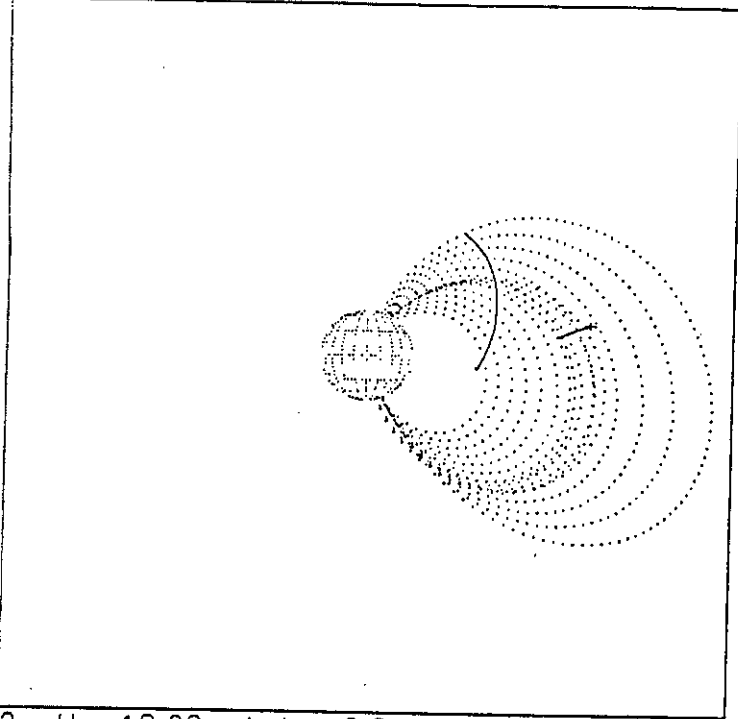
A special mode, designed to maximize the sensitivity of the SMS instrument to lithium ions was developed and up-linked to the Akebono satellite. However, no useful data were acquired by the Akebono satellite in support of the G-7 release. The on board RAM memory chip in the SMS instrument on Akebono experienced an upset event on January 10, shortly after the regularly scheduled RAM check procedure. The problem with SMS operations was not recognized until January 16 shortly after the next scheduled RAM check. The limited instrument health and safety monitoring is integral to the operation of the Akebono satellite. Useful Akebono data were also not acquired on January 18 in support of the G-lithium release. Normal operations had not yet been re-established after the identification of the SMS instrument RAM problem noted above.

Some Akebono data were acquired in a mode sensitive to lithium on February 12 after the G-6 release. The G-6 release occurred at 04:15 UT at an altitude of 32,200 km, invariant latitude of 67 degrees and magnetic local time of 22:54. The Akebono orbit has an inclination of 75°. Early 1991 had perigee on the morning side of the Earth (~500 km) and apogee on the evening side (~10,000 km). Data from the Akebono apogee passes on February 12 were acquired at Showa Station in the Antarctic and physically transported to Japan by ship, although not immediately usable. In November 1992, attempts were still made to recover data from the tapes shipped from the Antarctic. The data intervals noted above for which data are available, included two perigee passes. Akebono crossed 67 degrees invariant latitude at ~14:23 and 17:39 at altitudes and magnetic local times of 980 and 926 km and 7:48 and 6:39, respectively. The data from the two perigee passes showed an increased counting rate in the mass range centered on $m/q=7$. In addition to ${}^7\text{Li}^+$, ${}^{14}\text{N}^{++}$ can contribute to the low altitude signal detected by the SMS instrument. To determine the extent of the ${}^{14}\text{N}^{++}$ contribution data acquired on February 27 and March 13, days with moderately disturbed geomagnetic conditions, similar to those found on February 12 were examined in detail.

Figure 2 shows the mass spectra obtained by the SMS instrument on Akebono on March 13, 1991. These data show the clear indication of a flux of N^{++} ions with an intensity - V130 that of O^+ ions. Previous reports of N^{++} ions have been episodic (Chappell et al., 1982) and indicated a range of N^{++} fluxes considerably lower than those shown in Figure 2. Clearly a systematic investigation of the magnitude and variation of N^{++} fluxes is called for. Such studies are underway or planned (A.W. Yau and B.L. Giles, private communication, 1992).

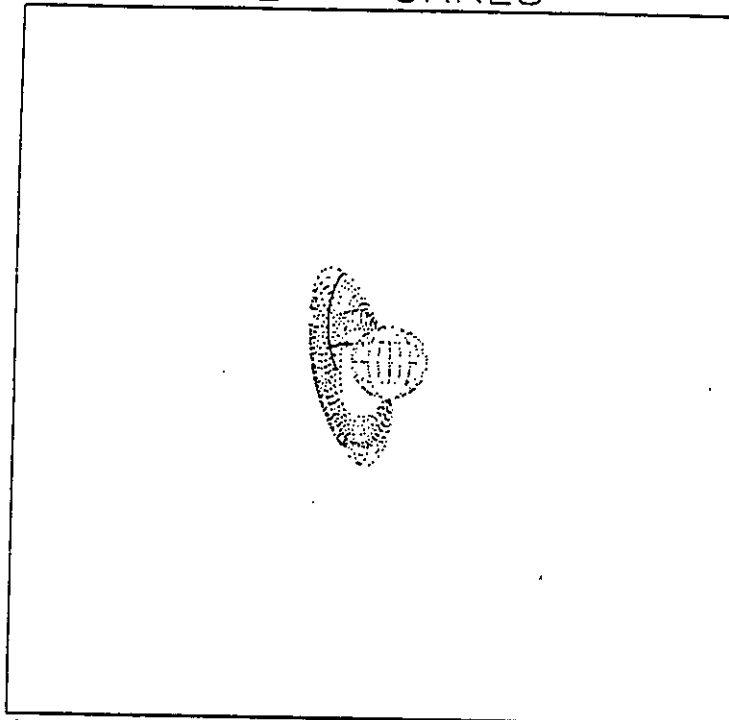
In summary, no lithium was detected from the DE-1 or Akebono space based ion mass spectrometers from the G-5, G-6, and G-7 releases. The lack of detection was the result of problems associated with satellite systems at the end of their useful life (Dynamics Explorer) and operational limitations associated with low cost satellite operations and telemetry acquisition systems. It must be pointed out, however, that the probability of detection of lithium ions in the dusk side magnetosphere was minimal at best, for after the release they would have had to have acquired energies of several keV.

DE - CRRES



2 Hr: 18:00 Lat: 0.0 Alt: 10.0
DE - CRRES

DE - CRRES



1 Hr: 12:00 Lat: 0.0 Alt: 8.0

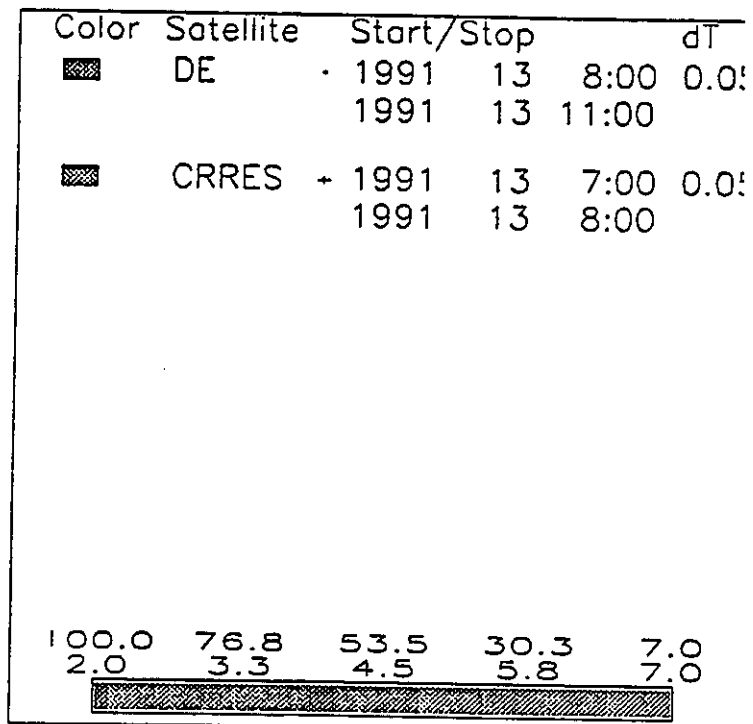
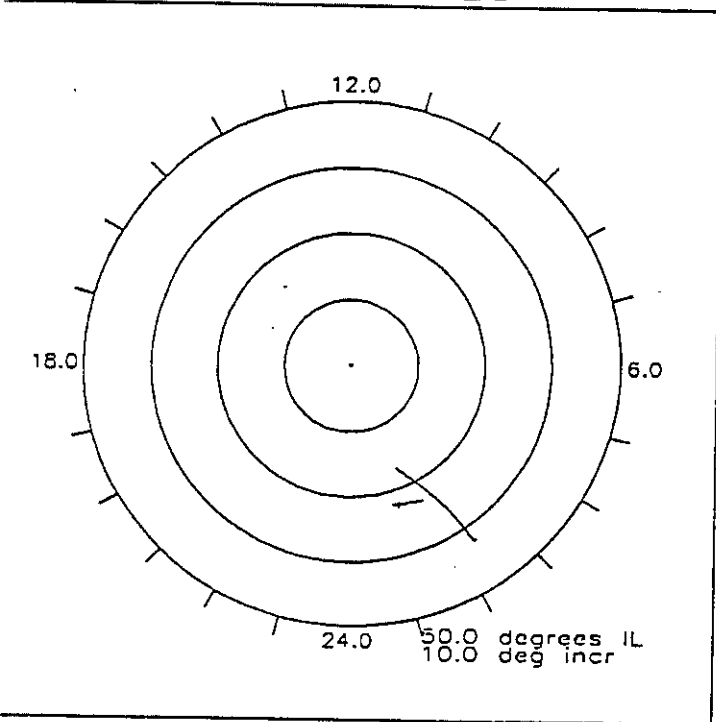


Figure 1

~9400 km
 10 MLT
 76° inw
 k_p 3°

Mar 13, 1990 EXOS-D SMS

$$N^+/O^+ \approx 0.15$$

$$\Delta m/m \approx 0.06$$

2319:12-2320:16

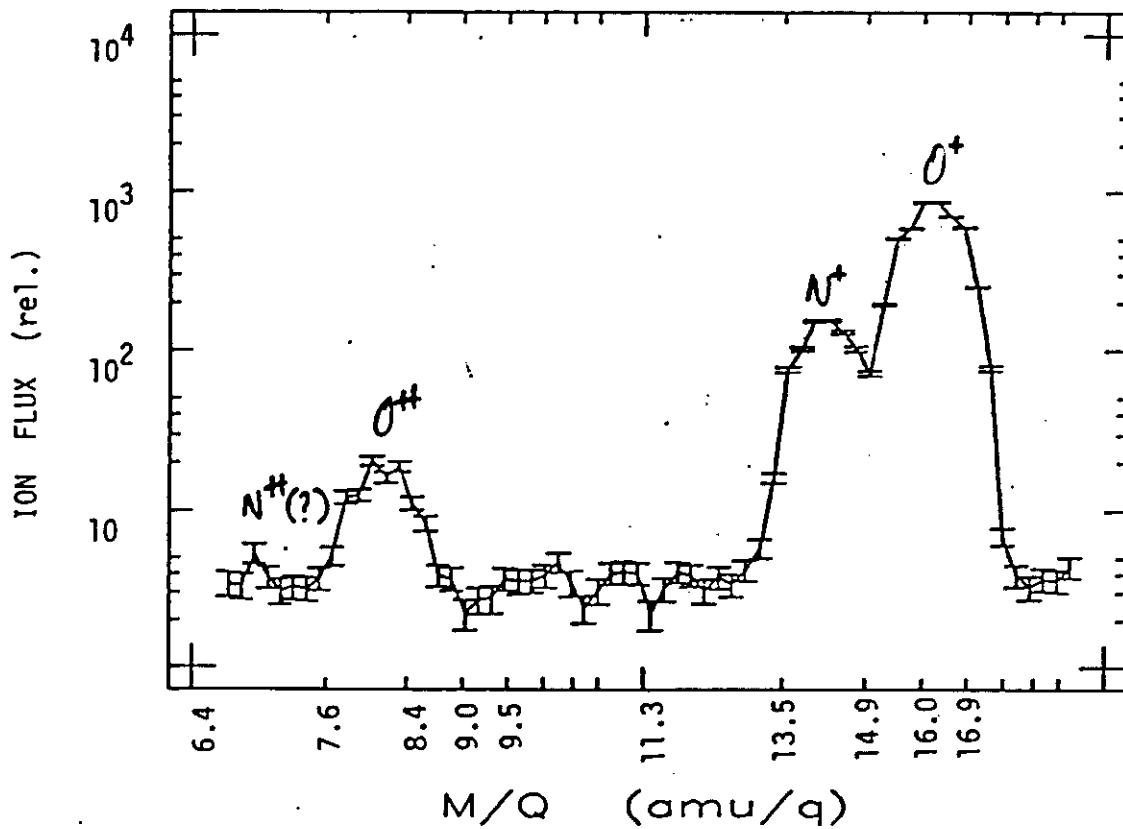


Figure 2.

FEBRUARY 18, 1991

SATELLITES:

DE-1
CRRES
DMSP-F8
DMSP-F9
DMSP-F10

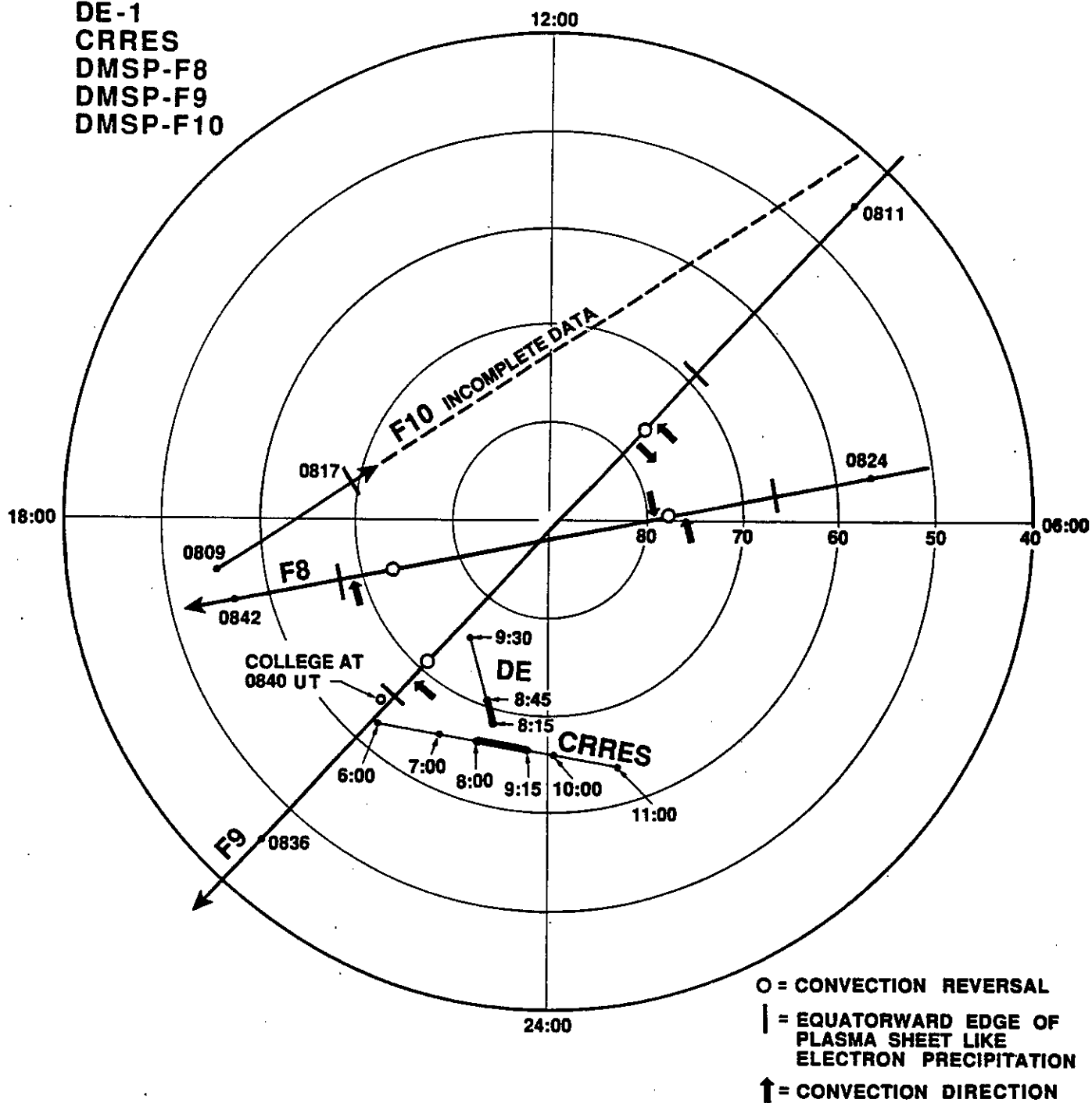


Figure Ala

EXPERIMENT G-3

15 January 1991 04:11:00 UT

Title: Diamagnetic Cavity, Unstable Velocity Distributions, Plasma Coupling

Principal Investigator: R. Hoffman

Collaborative Investigators: M. Pongratz, D. Papadopoluos, R. Smith, R. Anderson, D. Young, H. Singer, E. Szuszczewicz, E. M. Wescott, H. C. Stenbaek-Nielsen, G. Haerendel, A. Valenzuela

Location: Over North America

Time: Sunlit Releases, Ground in Darkness

POINT OF CONTACT:

Robert Hoffman	SPAN - DE696::U6RAH
GSFC Code 696	PHONE (301) 286-7386
Greenbelt, MD 20771	FAX (301) 286-9240

EXPERIMENTAL ELEMENTS:

Coordinates of Release: 17.9N 97.5W 15053 km
Canister Type: Small
Chemical: TI 1270 gms B 574 gms BA 1471 gms SR 19 gms
Delay: None

Model Calculations:

Ted Fritz	SPAN - ESSDP1::FRITZ
LANL	PHONE (505) 667-9234
MS - D438	FAX - (505) 665-3332
Los Alamos, NM 87545	

STATIONS COVERING THE RELEASE:

Caribbean - Bonaire, NA St. Croix, USVI
North America - Boston, MA; Greenbelt, MD; Los Alamos, NM; Richmond Hill, GA
Rosemary Hills, FL White Sands, NM
South America - Cerro Tololo, Chile El Leoncito, Argentina

EXPERIMENT G-4

16 January 1991

06:25:00 UT

Title: Diamagnetic Cavity, Plasma Coupling Principal Investigator: Collaborative Investigators:

Principal Investigator: S. B. Mende

Collaborative Investigators: M. B. Pongratz, D. Papadopolous, R. Smith, R. Anderson, Young, H. Singer, E. Szuszczewicz, E. Wescott, H. C. Stenbaek-Nielsen, G. Haerendel, A. Valenzuela, P. A. Bernhardt, J. D. Huba

Location: 0.7 degrees S, 53.8 degrees W

Time: 06:25:00 UT

EXPERIMENT ELEMENTS:

Coordinates of Release: 0.7S 53.8W 23977 km

Canister Type: Small

Chemicals: TI 1271 gms, B 574 gms, BA 1471 gms, SR 19 gms

Delay: None

Model Calculations:

Ted Fritz

LANL

MS-D438

Los Alamos, NM 87545

SPAN - ESSDP 1 ::FRITZ

PHONE (505-6679234)

FAX (505) 665-3332

POINT OF CONTACT:

Robert Hoffman

GSFC CODE 696

Greenbelt, MD 20771

SPAN - DE696::U6RAH

PHONE (301) 286-7386

FAX (301) 286-9240

STATION COVERING THE RELEASE:

Caribbean -

North America -

South America -

St. Croix, USVI Arecibo, PR

Boston, MA; Long Key, FL; Los Alamos, NM; White Sands, NM

Cerro Tololo, Chile El Leoncito, Argentina

G-4 TRIANGULATION AND ITS RELATIONSHIP TO G-2 AND G-3

From 13 to 16 January, 1991, a series of 3 small barium canisters were released by the CRRES spacecraft at different altitudes. The objectives of this series of releases were to study diamagnetic cavity formation, unstable velocity distribution and coupling of the cavity to the ambient plasma. Table 1 shows the dates, times, geographic coordinates and altitudes of the three releases.

TABLE 1

Name	Date	Time	Latitude	Longitude	Altitude
G-2 13	Jan. 1991	0217:03 UT	16.9°	-103.1°	6,180 km
G-3 15	Jan. 1991	0411:00 UT	17.9°	-97.5°	15,063 km
G-4 16	Jan. 1991	0625:00 UT	-0.7°	-53.8°	23,977 km

While this report describes the results of the G-4 triangulation, the relationship between this release and the other two in Table 1 is important for understanding the coupling of the cavity to the ambient plasma. Therefore, this report also contains a comparison of the G-4 releases with the other releases in the series.

Several ground stations participated in the G-4 release. However, not all stations provide favorable baselines for triangulation of the cloud. The plasma cloud that forms in a barium release of this type striates along the magnetic field, which is approximately perpendicular to the equator in geographic coordinates. Newly formed barium ions are relatively free to move along the magnetic field but motion perpendicular to the magnetic field direction is controlled by the coupling of the plasma cloud to the ambient plasma. Understanding this coupling is a major objective of this series of Barium releases, so it is desirable to obtain the motion of the cloud perpendicular to the magnetic field (through triangulation from two different ground stations). This favors ground stations with large east-west ground baselines, and not baselines with primarily north-south baselines.

Triangulation of the G-4 release was initially completed using Arecibo (PR) and Long Key (LK) data. However, these stations were only $\sim 14^\circ$ apart in longitude. Triangulation errors due to the small longitude spread and distance of the release (~ 4 RE altitude) were relatively large (0.03 RE). To improve the triangulation, we chose to use a larger baseline consisting of Breezy Point (Los Alamos, NM) and (PR) ground stations. These stations have the advantage of separation by almost 40° in longitude and, because the PR data is in video tape form, essentially all images from Breezy Point can be paired with an PR image. The drawback of this baseline is that after the first minute, the Breezy Point data does not have a time code. However, extremely accurate timing (\sim seconds) was not necessary since observable changes in the cloud position occurred over time intervals closer to 30 seconds. The station leader for Breezy Point reviewed the data and using simultaneous video images taken at the same location, was able to reconstruct the time sequence of the Breezy Point images.

We triangulated the first 7 minutes of data from the two ground stations. After this, multiple striations and fading of the cloud caused it to be nearly lost from the Breezy Point images despite the fact that the cloud was tracked for over 45 minutes at Arecibo. Although this appears to be a short amount of time, it was sufficient to obtain a very good history of the cloud motion and deduce details of the coupling of the cloud to the ambient plasma.

As with the G-2 release, the triangulation was done using the "CRRESTR2" program in the CRRES directory on the Lockheed VICOM computer. The following is a list of the image pairs with some brief comments. The image data files can be found in the CRRES directory in the format below as well as the data files containing the triangulated points.

BP021758 - BP = Breezy Point, 021758 = the center time of the image in hhmmss

Images	Triangulated	comments
Breezy Point Arecibo	data filename	
BP062501 AR062502	crrestr0625a1.pt	Just after release
BP062532 AR062529	crrestr0625a2.pt,	
BP062558 AR062557	crrest10625a3.pt	
BP062631 AR062629	crrestr0626c1.pt	
BP062657 AR062656	crrestr0626c2.pt	
BP062727 AR062727	crrestr0627c.pt	
BP062806 AR062806	crrestr0628c1.pt	
BP062858 AR062858	crrestr0628c2.pt	
BP062937 AR062940	crrestr0629c1.pt	
BP063029 AR063028	crrestr0630c1.pt	
BP063134a AR063433a	crrestr0631c1.pt	
BP063252 AR063252	crrestr0632c1.pt	

A typical triangulated data file contains triangulated points at a different positions along the ionized cloud. Since the Arecibo camera was filtered for the barium ion line it may not show the neutral cloud. In the first minute, the Breezy Point data do not show a separation of the cloud and trail.

Triangulation Procedure

Triangulation was performed using the triangulation computer codes developed for the AMPTE barium releases [Mende et al., 1989]. Arecibo images were digitized from video tape at the Lockheed Palo Alto Research Laboratory image data analysis facility. Breezy Point images were digitized from 35 mm film by Mary Miller at GSFC. These digitized images were copied onto the Lockheed VICOM computer. Using a star catalog on the VICOM computer with the position of stars down to 9th magnitude, the star field in the image was matched and positions of the stars were overlaid onto the video image to verify that the conversion from video image pixel location to right ascension and declination was accurate. Once this was accomplished, two stars (relatively far from one another) were selected as reference stars for the triangulation. The triangulation program used these two stars to assign right ascension and declination values to arbitrary pixel locations on the image by linear interpolation. After reference stars for an image pair were selected, triangulation was performed using software designed to determine the geographic coordinates of a location on the cloud. An example of a triangulated point on one of the G4 release image pairs that illustrates the procedure is shown in Figure 1. The upper panel of that figure shows the Arecibo image at 0631:33 UT (6 min., 33 s after release) while the lower panel shows the Breezy Point image at the same time.

To triangulate the point on the image, the operator selects a point on the first image (shown by the cross in the upper panel of Figure 1), then, using an assumed cloud distance, the computer swaps images on the video display and draws a line centered on the assumed cloud distance (initially, this is chosen to be the spacecraft distance) and with length equal to 0.2 RE on the second image. An example of the line is shown in the lower panel in Figure 1. This line is centered on an assumed distance of 4.61 RE. The operator now chooses the location on the second image along the line that appears to correspond best with the point chosen in the first image. In the example in the lower panel of Figure 1, this point would be where the line drawn by the computer and the white cloud intersect. Once selected, the geographic coordinates of the triangulated point are stored in a data file. The process is repeated until several points along the cloud are triangulated.

The fact that the line drawn by the computer and the cloud are nearly perpendicular is simply the result of the fact that the baseline is nearly east-west while the cloud striates along the nearly north-south magnetic field. For north-south baselines, the angle between the line and the cloud would be much smaller and would result in significant uncertainty in the triangulated position.

Because of the large distance between the observer and release point, the uncertainty in the measurements was relatively large for the G-4 triangulation. The error was reduced somewhat by using a large baseline (one of the largest available) than the other releases (discussed below). The error in the triangulated measurement appears to be about 0.008 RE based on the scatter in the points used to define the center of the cloud and on the computed distance between adjacent pixels on the image.

To illustrate the improvement in the triangulation procedure when the cloud distance is much smaller, Figure 2 shows a pair of images taken approximately 1 minute after the G-2 release. The upper panel of Figure 2 shows the digitized image from Rosemary Hills (FL) while the lower panel shows the digitized image from Breezy Point. The baseline is somewhat smaller but still comparable to the baseline used in the G-4 triangulation and the identical camera system was used at Breezy Point for both the G-2 and G-4 releases. The cross in the upper panel in Figure 2 shows a selected position on the Rosemary Hills image while the lower panel shows the 0.2 RE long line centered on the assumed distance (in this case, 1.97 RE). Comparing the lower panels of Figures 1 and 2, it is clear that the uncertainty in the cloud position due to the finite size of a pixel on the image is much smaller for the G-2 release near the Earth compared to the G-4 release almost 2.5 times further away.

ANALYSIS OF TRIANGULATION RESULTS

Early chemical releases at high altitudes showed that the cloud striates along the local magnetic field [e.g., Mende et al., 1973]. We use this fact as a consistency check on the triangulated data and also to simplify the determination of the motion of the cloud with respect to the background plasma

As a consistency check, the triangulated positions along the cloud should line up along the local magnetic field. To test this, we use the model magnetic field contained in the CRRES spacecraft ephemeris. Differences between the triangulated magnetic field direction and the model direction indicate that either the triangulation is in error or the model magnetic field is not correct. In fact, the differences between the two directions for all three releases were quite small. Table 2 shows the angle between the triangulated magnetic field direction (B_{tri}) and the model magnetic field direction (B_{mod}) obtained by taking the dot product of the two vectors. The only large angle is the first triangulated direction in the G4 release and is the result of the fact that the cloud dimensions were quite small and prone to large error in the triangulated direction. Otherwise, the triangulated and model magnetic field direction agree to within 5 to 10°.

Table 2.

G-2 Release hmmss	13-Jan-1991 $B_{tri} \cdot B_{mod}$	G-3 Release hmmss	15-Jan-1991 $B_{tri} \cdot B_{mod}$	G-4 Release hmmss	16-Jan-1991 $B_{tri} \cdot B_{mod}$
21700	(release)	41100	(release)	62500	(release)
21759	4.7	41200	1.9	62557	30.4
21935	1.6	41231	0.6	62629	14.5
22011	1.3	41300	1.1	62656	5.6
22048	1.0	41331	5.3	62727	5.7
22125	2.2	41400	3.7	62806	6.4
22233	3.3	41500	0.9	62858	10.7
22339	1.8	41600	3.0	62940	8.7
22407	2.3	41900	4.8	63028	6.8
22453	2.6	42000	4.4	63133	10.1
22703	8.8	42100	7.0	63252	7.0
		42202	9.4		
		42303	10.4		
		42400	9.0		
		42505	12.1		
		42600	9.9		

We also used the fact that the cloud striates along the magnetic field, to simplify the determination of the motion of the cloud. To do this, we noted collectively that the ions in the cloud had two motions, perpendicular and parallel to the ambient magnetic field. The parallel motion presented somewhat of a problem. The fields of view of the cameras that photographed the clouds were typically small (few degrees). When the angle the cloud subtends becomes greater than the field of view of a given camera, only a portion of the cloud can be tracked. Therefore, different stations tracked different parts of the cloud. This problem is illustrated in Figure 1, where it is evident that the cloud in the Breezy Point image (lower panel) is not completely contained in the field of view. By triangulating different parts of the cloud from image pair to image pair as the cameras are moved to keep some portion of the cloud in the center of the field of view, apparent motions along the magnetic field are introduced. Because of this, we could not accurately analyze the motion along the magnetic field except in the very early stages of the cloud formation and thus wanted to remove this motion from the analysis.

To remove the parallel motion, we define a coordinate system where the magnetic field is along the z-axis and the spacecraft velocity perpendicular to the magnetic field at the time of release is along the y-axis. For accuracy, we use the triangulated magnetic field direction to determine the rotation from the triangulated geographic coordinates to the B-V coordinate system although it is evident in Table 2 that

using the model field would produce similar results. Last we translate the points so that the spacecraft position at the time of the release is located at the origin. Figure 3 illustrates this coordinate system.

By rotating into the $B-V_{\perp}$ coordinate system, we de-couple the motion along the magnetic field and the motion perpendicular to the magnetic field. Also, since we relate the coordinate system to fixed locations and directions, we can compare the triangulated position from image pair to image pair without biasing the comparison. Since we cannot accurately describe the motion along the magnetic field, we will consider only the projection of the triangulated points into the $x'''-y'''$ plane.

Figures 4, 5, and 6 show the projected position of the triangulated points for the three releases into the $x'''-y'''$ plane. For the G-2 release, we also had the opportunity to triangulate the neutral cloud for the first few minutes of the release. As expected, the neutral cloud for the G-2 release (Figure 4) simply moved in the $x'''-y'''$ approximately in the direction of the spacecraft velocity vector at the time of the release. Some residual motion in the x''' direction has not been explained at this time.

It is particularly interesting to compare and contrast the G-2, G-3 and G-4 results in Figures 4, 5 and 6. First, if all uncertainties in the triangulated points were equal, then the projection of the triangulated points for a given image pair should produce a small cluster in the $x'''-y'''$ plane centered on the average location of the intersection point of the magnetic field with that plane. However, all uncertainties are not equal. In the triangulation procedure, the uncertainties in the determination of the location perpendicular to the line of sight are inherently much smaller than that in the radial direction. Thus instead of a cluster of points, the projected points form short line segments approximately in the radial direction. These line segments are evident in both Figures 5 and 6.

The plasma cloud motion perpendicular to the magnetic field direction was different for all three releases. For the G-2 release, the plasma cloud simply moved a short distance from the release point and spent the remaining 10 minutes very close to it. For the G-3 release, the plasma cloud moved away from the release point at about a 45° angle for the first minute and a half, stopped, then moved in the $-V_y'''$ direction for approximately a minute and a half and finally drifted approximately in the V_x''' direction for the remaining 10 minutes. For the G-4 release, the plasma cloud moved away from the release point almost uniformly for the first 6 minutes after the release at which time it stopped. Triangulation beyond this time was not possible due to the loss of data at the Breezy Point site.



Figure 1



Figure 2

B - V_{\perp} Coordinate System

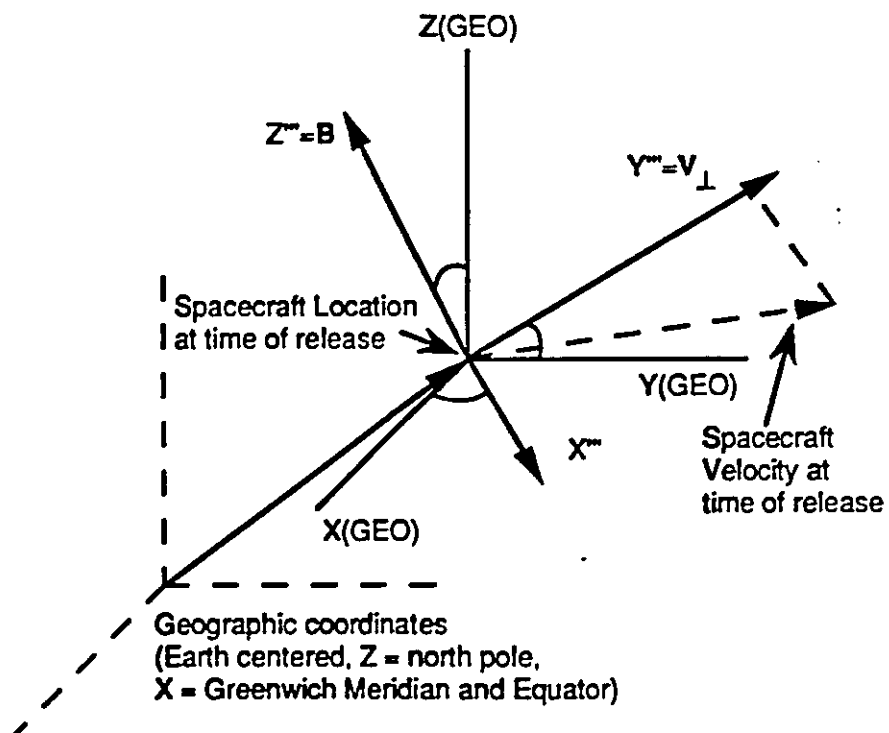


Figure 3

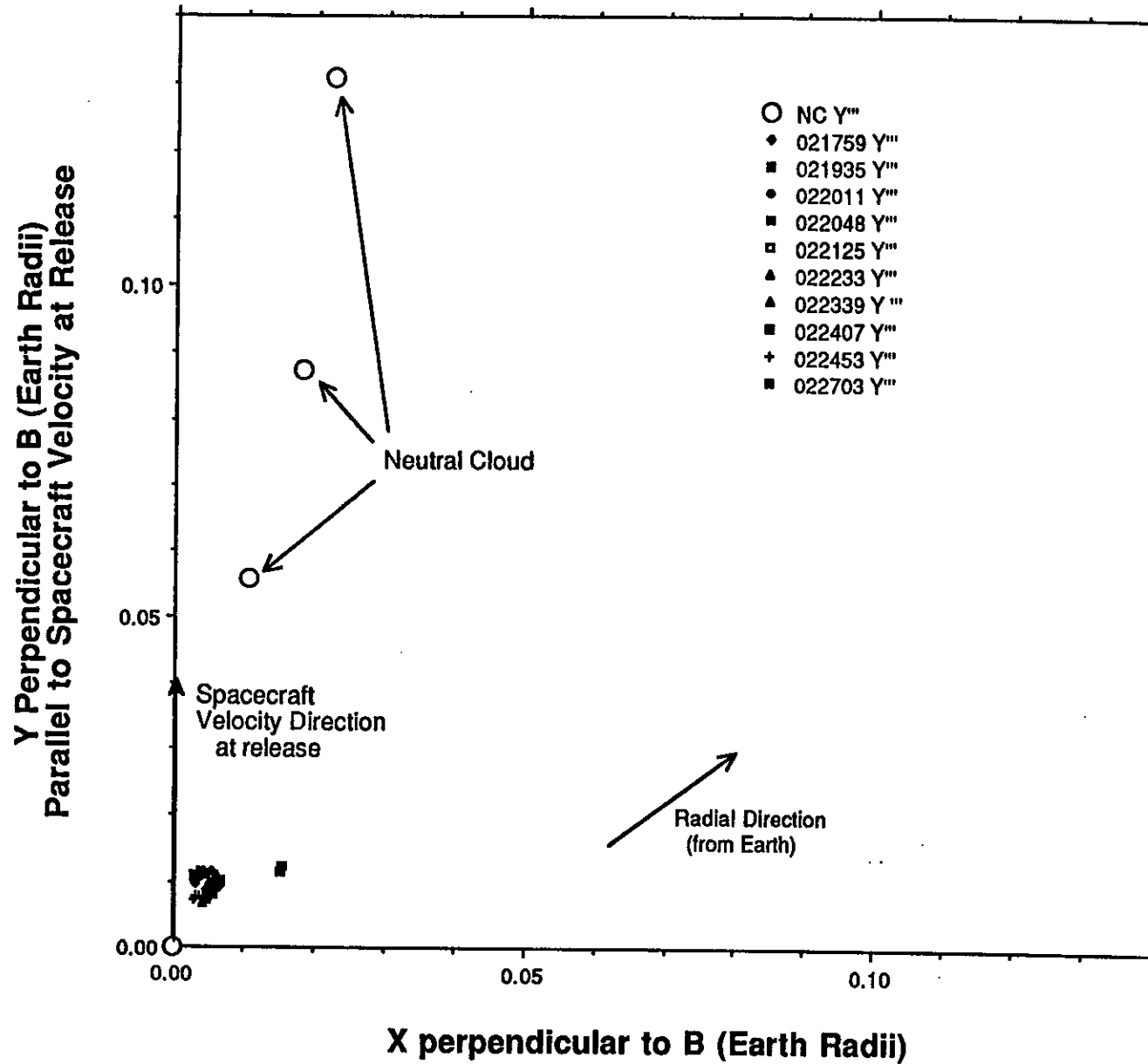


Figure 4

Data from "G-3 triang rotated to B"

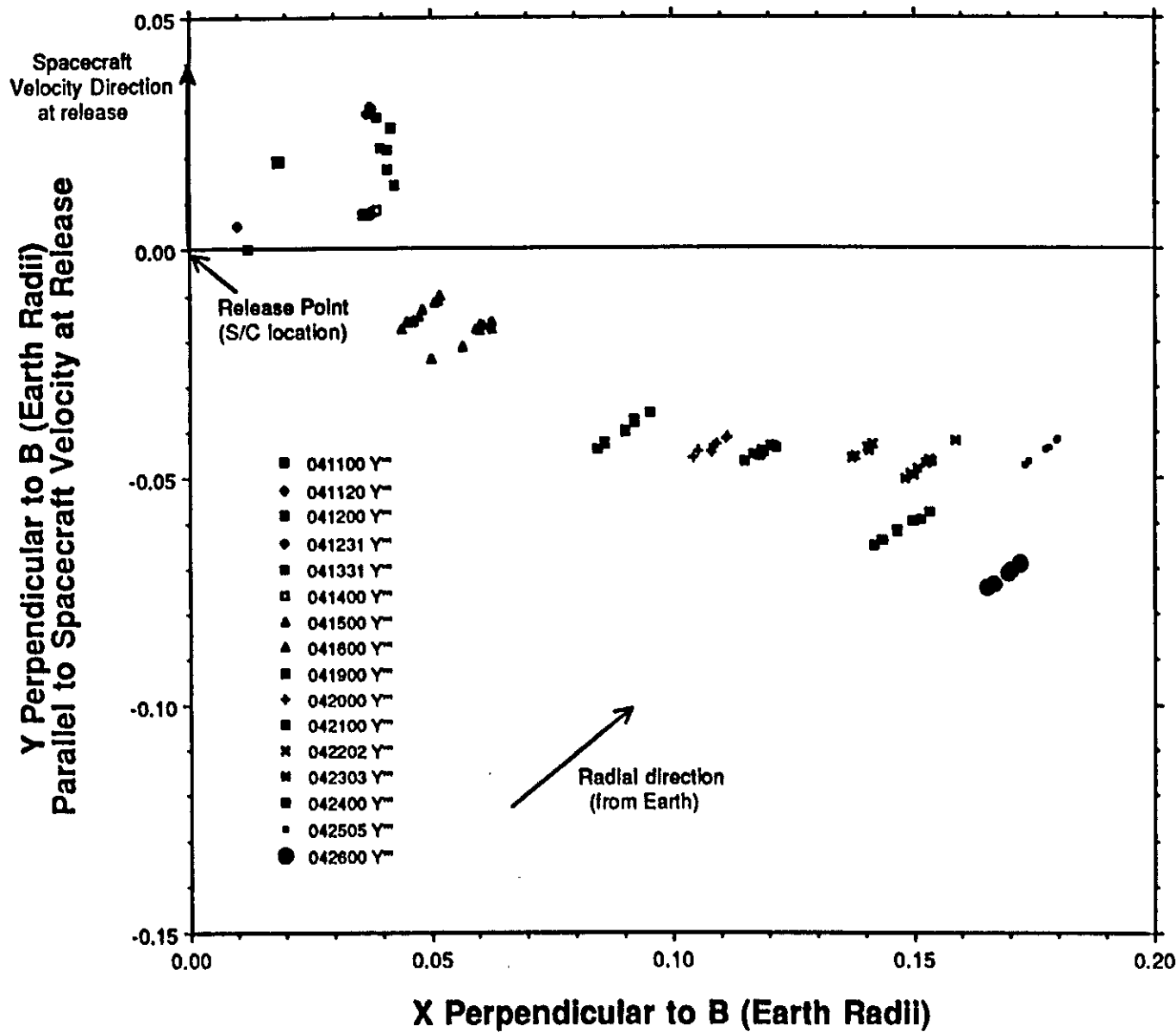


Figure 5

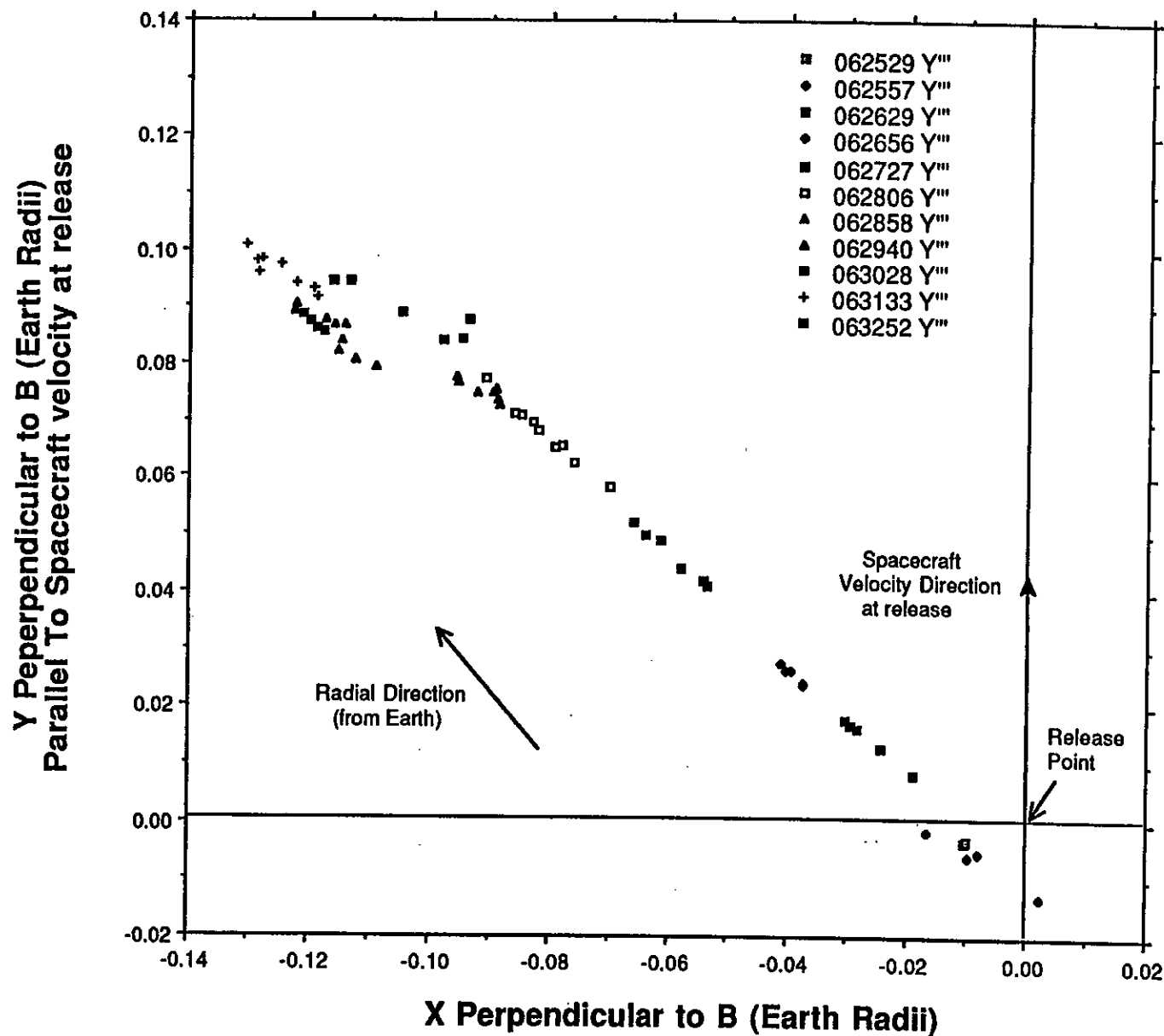


Figure 6

EXPERIMENT G-5

18 January 1991

05:20:00 UT

Title: Stimulated Electron Precipitation to Produce Auroras

Principal Investigators: P. Bernhardt, G. Haerendel

Collaborative Investigators: S. Mende, T. Fritz, W. Peterson, E. Wescott, H. Stenbaek-Nielson, D. Papadopolous, R. Smith, M. Pongratz, D. Simons, A. Valenzuela

Location: Approximately 6 Re outside plasmapause on field line accessible by Millstone Hill Radar.

Time: Post-midnight local time (0000-0200 LT)

Other Conditions: Darkness over North America; Local Plasma Density $< 1/\text{cm}^3$

Chemicals: 20 kg lithium (2 large canisters)

OBJECTIVE:

A lithium cloud was released on an $L > 6$ magnetic field line to enhance the cold plasma density in the magnetosphere. Wave particle interaction theory predicts that the electron density enhancement should precipitate trapped energetic electrons via interactions with whistler mode waves. Detection of the precipitation was attempted with optical and radar observations of the aurora at the foot of the field line where the release occurred and by in-situ wave and particle diagnostics on CRRES.

POINT OF CONTACT:

Dr. Arnoldo Valenzuela
Max Planck Institute fuer
Extraterrestrische Physik
8046 Garching, Germany

SPAN- MPE::VAL
PHONE 49-89-3299-3513 OR 3503
FAX - 49-89-3299-3569

EXPERIMENT ELEMENTS:

Coordinates of Release: 6.6N 62.8W 33337 km

Canister Type: Large

Chemicals 5A TI 5770 gms, B 2605 gms, LI 457 gms, EU 299 gms
5B TI 5770 gms, B 2605 gms, LI 457 gms, EU 299 gms

Delay: None

STATIONS COVERING THE RELEASE:

Aircraft -	Argentina B707, C135-127
Caribbean -	Bonaire, NA
North America -	Boston, MA Greenbelt, MD Long Key, FL Rosemary Hills, FL
South America -	Cerro Tololo, Chile El Leoncito, Argentina

RESULTS:

The first was not successful. Appreciable ELF wave activity was observed by the wave instrument on the CRRES satellite.

EXPERIMENT G-10

20 January 1991

05:30:00 UT

Title: Stimulate Magnetospheric Substorm

Principal Investigator: D. Simons

Collaborative Investigators: R. Hoffman, M. Pongratz, S. Mende, D. Papadopolous, A. Valenzuela, G. Haerendel, J. D. Huba, P.A. Bernhardt, E. M. Wescott, H. C. Stenbaek-Nielsen

Location: Caribbean at Points Selected for Conjugate Point Geometry

Time of Day: Dawn

OBJECTIVE:

This experiment was conceived to study the effect of cold plasma freshly injected into the plasma sheet of the Earth's magneto-tail on the onset of a magnetic substorm. The investigation is based upon a theoretical model of substorm behavior which is derived primarily from observations of phenomenological behavior before, during and after substorms. It has been observed during quiet periods, that time before and after a substorm that the magnetosphere slowly fills up with plasma primarily of ionospheric origins. The geomagnetic field expands under this particle pressure and becomes in essence blown-up like a balloon. In the Earth's magneto-tail the magnetic field is most distorted away from a dipole configuration with a region of field reversal up the center of this tail. There is a current sheet (called the plasma sheet) running up this center line to provide the necessary curl of B to support the field reversal. Geometrically it is as if the field lines have been pulled outwards and distorted to such an extent that the oppositely directed parts of the field come closer together. During or just prior to a magnetic substorm some process allows the oppositely directed magnetic fieldlines to break and jump the plasma sheet. They join together from opposite sides and snap back towards the Earth carrying plasma with them. The field relaxes back towards a dipole-like configuration and trapped particles are accelerated and dumped back into the ionosphere. The question of this investigation centers around the nature of this so called magnetic reconnection and its position as a primary driver of substorm onset or simply as a result of some other incompletely understood complex of primary drivers. It is postulated that the addition of plasma into the near-Earth plasma sheet from a barium release would lead to enhanced turbulence in the region which would provide sufficient dissipation (conductivity) to facilitate this reconnection process. By releasing barium in the midnight sector on a L-shell of 6 or greater with the satellite in the outward portion of the orbit, it will be possible to get plasma to the plasma sheet. This must occur during a quiet time well after the last substorm when the magnetosphere is filled with plasma and well distorted. If reconnection should result and a full blown substorm occur, a careful examination of the extensive optical and in-situ data provided by the CRRES program would provide an excellent opportunity to determine the precise role of reconnection in substorm onset

POINT OF CONTACT:

D. J. Simons
LANL MS - Dxxx
Group SST
Los Alamos, NM 87545

SPAN - ESSDPI::SIMONS
PHONE (505) 667-xxxx

EXPERIMENTAL ELEMENTS:

Coordinates of Release: 8.9N 75.6W 33179 km

Canister Type: Large

Chemicals: 10A TI 4584 gms B 2069 gms BA 5305 gms SR 67 gms
10B TI 4583 gms B 2069 gms BA 5305 gms LI 67 gms

Delay: 10A: None; 10B: 5 seconds

Model Calculations:

Ted Fritz

LANL

MS - D438

Los Alamos, NM 87545

SPAN- ESSDPI::FRITZ

PHONE (505) 667-9234

FAX (505) 665-3332

STATIONS COVERING THE RELEASE:

Aircraft -

Caribbean -

North America -

South America -

Argentina B707, C135-127

Arecibo, PR Bonaire, NA St. Croix, USVI

Long Key, FL Los Alamos, NM White Sands, NM

Cerro Tololo, Chile El Leoncito, Argentina

EXPERIMENT G-6

12 February 1991

04:15:00 UT

Title: Stimulation of Ion-Cyclotron Waves and Artificial Ion Precipitation

Principal Investigator: S. Mende

Collaborative Investigators: P. Bernhardt, G. Haerendel, T. Fritz, W. Peterson E. Wescott, D. Papadopolous, R. Smith, M. Pongratz, D. Simons, A. Valenzuela, R. Anderson

Location: Approximately 6 Re outside plasmopause on field line accessible to Millstone Hill Radar.

Time: Pre-Midnight Local Time Sector (2200-2400 LT)

Other Conditions: Darkness over North America, Local Plasma Density $N < 1/\text{cm}^3$

Chemicals: 20 kg lithium (2 large canisters)

OBJECTIVE:

It is expected that the pre-midnight sector will be dominated by energetic protons which precipitate to form the pre-midnight proton aurora. The injection of an artificial cloud of cold Lithium plasma will lead to the generation of ion-cyclotron waves, and these waves in turn will scatter protons into the loss cone leading to enhanced proton aurora. The enhanced precipitation will be detected by optical instruments at the foot of the field line, and the CRRES/GTO wave and particle instrumentation will aid in determining the optimum conditions for release.

POINT OF CONTACT:

Steve Mende
LPARL
3251 Hanover St.
Palo Alto, CA 94304

SPAN-LOCKHD::MENDE
PHONE (415) 424-3282
FAX (415) 424-3333

EXPERIMENT ELEMENTS

Release Coordinates: 4.9N 76.1W 32249 km

Canister Type: Large

Chemicals 6A TI 5770 gms, B 2604 gms, LI 457 gms, EU 299 gms
6B TI 5767 gms, B 2603 gms, LI 457 gms, EU 299 gms

Delay: None

Model Calculations:

Ted Fritz
LANL MS - D438
Los Alamos, NM 87545

SPAN - ESSDPI::FRITZ
PHONE (505) 667-9234
FAX (505) 665-3332

STATIONS COVERING THE RELEASE:

Aircraft - C135- 127

North America - Boston, MA Greenbelt, MD Los Alamos, NM White Sands, NM

South America - Cerro Tololo, Chile El Leoncito, Argentina

EXPERIMENT ELEMENTS:

Coordinates of Release: 4.9 N 76.1W 32249 km

Canister Type: Large

Chemicals: 6A TI 5770 gms, B 2604 gms, LI 457 gms, EU 299 gms 6B TI 5767 gms, B 2603 gms, LI 457 gms, EU 299 gms

Delay: None

RELEASE G-6 STRATEGY

The original goals of this release were to enhance ion cyclotron waves and thereby induce proton precipitation in the pre-midnight auroral oval. However, the earlier G5 release on the 18th of January failed to make a detectable electron precipitation event using whistler mode wave enhancements through cold plasma seeding. Thus it was argued that a successful repeat of the G5 release experiment would have satisfied the cold plasma induced precipitation goals of the CRRES program and the G6 release was attempted to be released in conditions which would satisfy both the G5 and G6 requirements.

The experiment released produced a large ion cloud. Since Lithium ions are invisible, there was relatively little emphasis in monitoring the cloud development optically. The important optical observations were made by the two instrumented aircraft which made observations of the aurora at the foot of the field line. If the experiment worked, the hot electrons which were measured in situ by the spacecraft should have been disturbed by the cold plasma and the waves produced inside of the cloud should have precipitated causing the artificial auroras. The airplanes were used to assure that the observations were not obscured by clouds. Operationally, the satellite control center gave the release command.

RELEASE CONDITIONS

For the successful release and detection of cold plasma injection produced precipitation, we required some very stringent release conditions.

The release conditions were as follows:

1. Lack of ambient cold plasma. Ambient plasma density as measured by the satellite should be less than 1 ~ 2. This condition was monitored by the University of Iowa experiment (R. Anderson).
2. Abundance of hot plasma mainly energetic electrons. This was monitored by the Lockheed or the AFGL experiment. The following basic considerations apply:

Synchronous altitude particles which are required to create plasma sheet precipitation can be obtained from Eather et al. [1976]. According to this, the plasma sheet precipitation is probably of the order of 1 ergs/cm²/sec precipitation energy flux. This is equivalent to about 200 Rayleighs of 4278 and perhaps kR of 557 and probably about 3 kR of white light.

This energy intensity is equivalent to $1/\pi$ times this value or in particle flux per steradian, it is 0.318 ergs/cm²/sec/sterad.

Thus, the 0.318 ergs/cm²/sec/sterad is equivalent to 2×10^{11} eV (1.6×10^{-12} ergs/eV). Table 1 summarizes the required flux levels for various particles of different energy.

TABLE 1. kR Rayleigh Local Auroral Minimum Criteria

Omnidirectional energy flux of 2.0×10^8 keV/cm²/sterad/sec

<u>Particles of energy</u>	<u>Total Particle flux</u>	<u>Flux per keV</u>
1 keV	2.03×10^8	
2 keV	1.04×10^8	$5.20 \times 10^7/\text{keV}$
5 keV	4.17×10^7	$8.53 \times 10^6/\text{keV}$
10 keV	2.03×10^7	$2.03 \times 10^6/\text{keV}$
20 keV	1.00×10^7	$5.00 \times 10^5/\text{keV}$

These fluxes are absolute minimum for release criterion. During big substorms, the particle intensities go up by factors of 10 and 20.

The release had to be initiated 30 minutes prior. The G6 release was called around 3:45 UT to take place at 4:15. The release was called on the basis of geophysical parameters which would assure that the above conditions were met.

Although for a Lithium release the weather at the ground sites was not critical, the STC operation center monitored the weather. The weather is summarized in Table 2.

3. No discrete aurora. (Absence of confusing auroral precipitation at the foot of field line.)

<u>Time</u>	<u>St. Croix</u>	<u>Arecibo</u>	<u>Bonaire</u>	<u>El Leon</u>	<u>Cerro</u>
2:11	Cld 50%	o.cast	few clouds	bad	
2:38	Clearing		OK		
3:00	Clearing		60%clear		
3:05	90%clear		60%clear	bad	good
3:36				clearing	
4:38	90%clear		not good		
<u>Time</u>	<u>Goddard</u>	<u>White Sands</u>	<u>Los Alamos</u>	<u>Lincoln Lab</u>	
2:11	90%clear	60%clear	clear		
2:38					
3:00	good	o.cast	thin clouds	clearing	
3:05	80%clear		good		
3:26					
4:38		bad	OK		

At the STC operation center, the satellite auroral electron and cold plasma density were also monitored. The cloud release was based on these parameters. These parameters were documented as a function of time in Table 3.

TABLE 3. GEOPHYSICAL PARAMETERS FOR THE G-6 RELEASE

	<u>Time</u>	<u>K index</u>	<u>Aurora 5577</u>	<u>GLf flux</u>	<u>GL anstr</u>	<u>Iowa density</u>
2/11	18:56			1.1×10^9		
	19:16					2.0
	01:56	3 -> 2				
	02:26					
	02:30			2.4×10^9 streamers decreasing	1.9×10^9	
	02:31			2.5×10^9		2.0
	02:35	3		2.1×10^9 streamers gone	1.4×10^9	2.0 strong AKR
	02:55	4		1.8×10^9	1.2×10^9	2.0 AKR
	03:00	4		2.7×10^9	1.9×10^9	2.0
			Diffuse aurora 4 kR			
	03:09			2.7×10^9	1.8×10^9	
	03:15	4		1.8×10^9	1.4×10^9	2.0
	03:30		6 kR post break op			
	03:40	4		1.1×10^9	9.3×10^9	1.5 AKR
	04:37		1.8- 3.5 kR pulsating			
	05:03					
	03 59			8.4×10^8	7.1×10^8	
	04:05			7.5×10^8	6.2×10^8	
	04:10			8.2×10^8	6.7×10^8	
	04:15			7.2×10^5	5.6×10^5	
	04:18			5.9×10^8	4.8×10^8	
	04:23			7.4×10^8	4.4×10^8	
	04:28			5.4×10^8	4.0×10^8	
	04:32		5.2×10^5	3.9×10^5		

It can be seen that the electron threshold was above the 2×10^8 keV/cm²/sterad/sec. An additional consideration for the release was the position of the satellite. In Table 4, we summarize the satellite parameters near apogee.

TABLE 4. EPHEMERIS EXTRAPOLATION FOR CRRES

Day	UT	Rev	GLAT	WLON	ALT	BTOT	BINT	GMLAT	GMLON	GMLT	L	SDANG
02/12/91	04:00:00	491	5.65	74.77	31535.	145.	157.	16.39	356.08	22:44	6.592	10.15
02/12/91	04:15:00	491	4.93	76.25	32242.	135.	147.	15.65	354.56	22:54	6.662	08.67
02/12/91	04:30:00	491	4.24	77.81	32797.	127.	140.	14.92	352.96	23:03	6.708	07.37
02/12/91	04:45:00	491	3.55	79.43	33203.	122.	135.	14.20	351.32	23:13	6.730	06.25
02/12/91	05:00:00	491	2.87	81.09	33462.	117.	131.	13.46	349.64	23:22	6.728	05.35
02/12/91	05:15:00	491	2.19	82.76	33576.	115.	129.	12.73	347.94	23:31	6.704	04.70
02/12/91	05:30:00	491	1.51	84.45	33545	113.	129.	11.98	346.25	23:41	6.658	04.32
02/12/91	05:45:00	491	0.83	86.12	33370.	113.	130.	11.22	344.57	23:50	6.589	04.25
02/12/91	06:00:00	491	0.13	87.77	33049.	115.	132.	10.44	342.93	23:59	6.500	04.50
02/12/91	06:15:00	491	-0.58	89.38	32581.	118.	136.	09.64	341.35	00:09	6.388	05.05
02/12/91	06:30:00	491	-1.31	90.92	31962.	122.	142.	08.82	339.83	00:19	6.255	05.89
02/12/91	06:45:00	491	-2.06	92.39	31189.	128.	150.	07.97	338.41	00:29	6.100	07.00
02/12/91	07:00:00	491	-2.84	93.74	30256.	137.	161.	07.09	337.10	00:40	5.923	08.34
02/12/91	07:15:00	491	-3.67	94.95	29158.	150.	175.	06.18	335.95	00:51	5.722	09.92
02/12/91	07:30:00	491	-4.54	95.98	27887.	166.	194.	05.23	334.99	01:03	5.498	11.71

For the positioning of the air plane several field models were evaluated for the time of the release The 4:15 position of the foot of the field line is shown in Table 5. Note at the time of release, the Kp was 4, therefore, it is the last line of Table 3 which is applicable. This model is based on the TtJ model. In Figure 1, we show the Millstone Hill radar convection plots. The Millstone Hill group has also inserted their prediction of the foot of the field line for 04:15 UT. The convection plot was generated from data taken at 04:05.

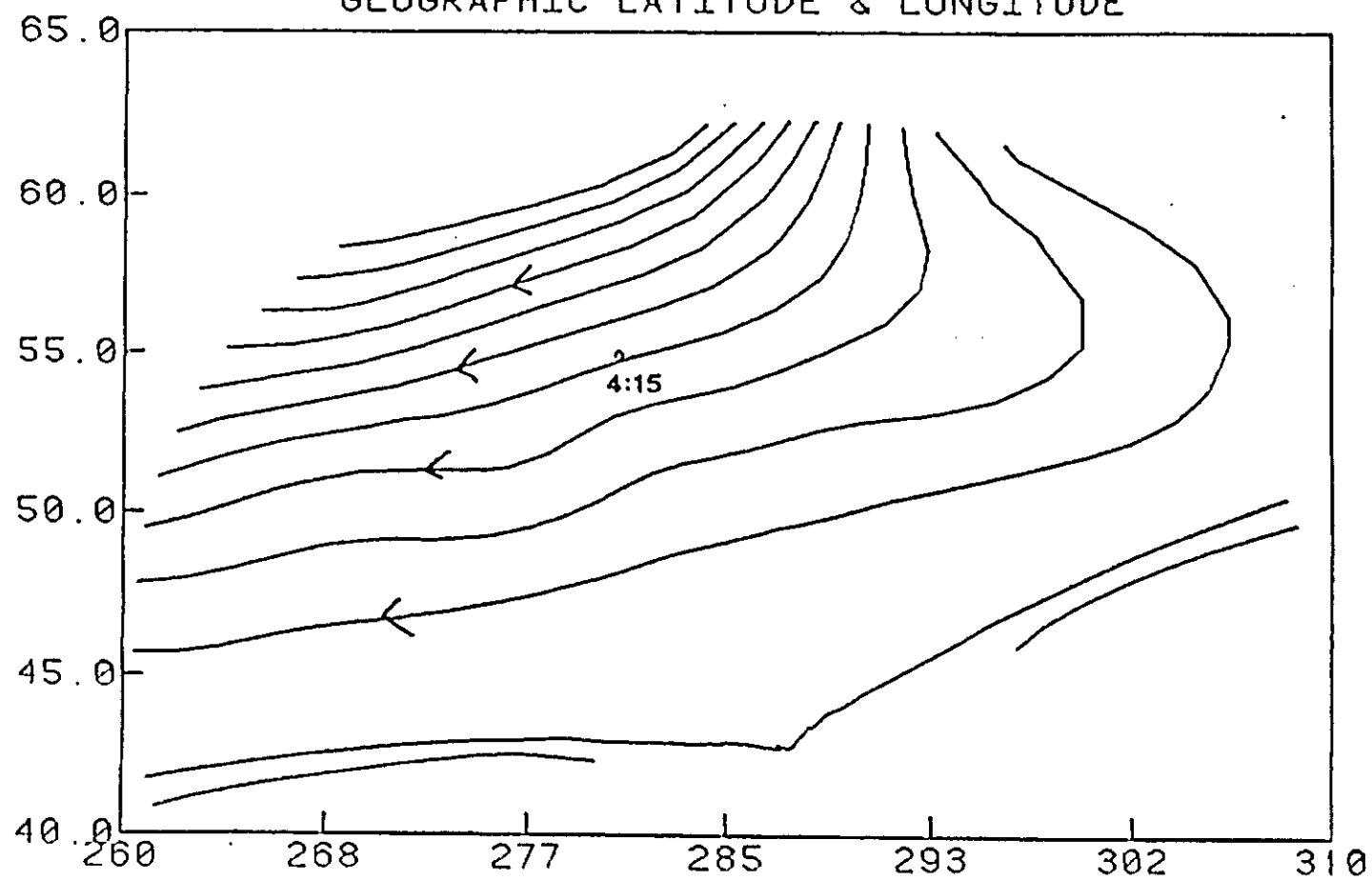
SUMMARY:

The G6 release did not accomplish its stated scientific goals and the results are inconclusive. Operationally every condition was satisfied. The ambient cold plasma density was down to 1.5 electrons per cm^3 , the energetic electrons were above the 2×10^8 keV/cm²/sterad/sec threshold. However it was very difficult to predict the situation in advance and the auroral situation over the airplanes were very confused at the time the effect should have manifested itself. A small enhancement in the aurora, which was expected to occur following the plasma injection could not be detected in the presence of the natural auroral displays which occurred. Just before calling the release at 04:37 the airplane reported auroral pulsations of 1.8–3.5 kR in strength. It was hoped that this level of aurora would not be detrimental to the observations and that it would weaken with time. This weakening did not occur. Thus the G6 release experiment could not be used to show that cold plasma releases can be responsible for increased precipitation.

TABLE 5. Satellite (Lat, Lng, Ht) 1991 2/12 4:15:0 Field Line Base (100 km Height)

KP=	0	N.LAT=	52.09	E.LONG=	-77.92
KP=	0+	N.LAT=	52.80	E.LONG=	-78.01
KP=	1-	N.LAT=	52.66	E.LONG=	-78.03
KP=	1	N.LAT=	52.52	E.LONG=	-78.08
KP=	1+	N.LAT=	52.45	E.LONG=	-77.99
KP=	2-	N.LAT=	52.36	E.LONG=	-78.07
KP=	2	N.LAT=	52.13	E.LONG=	-78.09
KP=	2+	N.LAT=	52.31	E.LONG=	-78.07
KP=	3-	N.LAT=	52.05	E.LONG=	-78.07
KP=	(3,3+)	N.LAT=	51.76	E.LONG=	-78.07
KP=	>3+	N.LAT=	51.21	E.LONG=	-78.27

CRRES G6 MILLSTONE HILL 04:05UT 02/12
GEOGRAPHIC LATITUDE & LONGITUDE



EXPERIMENT G-8

17 February 1991 03:30:00 UT

Title: Gravitational Instability, Field Equipotentiality, Ambipolar Acceleration (later changed to Triggering Aurora)

Principal Investigators: G. Haerendel/D. J. Simons

Collaborative Investigators: T. Fritz, M. B. Pongratz, G. S. Mende, E. Wescott, H. C. Stenbaek-Nielsen, A. Valenzuela

Location: Greater than 6 Re on a field line connected to plasma sheet

Time: Dawn; 03:30:00

Altitude: Near CRRES/GTO Apogee

Chemicals: 40 kg barium (2 large canisters) with 5% lithium

OBJECTIVE:

The original objective of this experiment was a study of the small-scale breakup of a plasma cloud crossing the equator at about 2000 km owing to the Rayleigh-Taylor instability (GRAD-Exp.). It was, however, realized before the campaign that the R.-T. instability would be stabilized by the centrifugal and diamagnetic forces acting on the ions as they travel along the field lines. Hence the objective of this release experiment was redefined to be a second test (after G-10) of the possibility of triggering auroral events by injection of cold plasma into the hot near-earth plasma sheet. Two effects could contribute. One is the momentum (and kinetic energy) injected with the barium plasma due to the relative motion with respect to the plasma background. Depending on the ambient convection speed the energy can be appreciable, up to 104 of the energy released in a substorm. Being confined to a narrow volume, it may at least trigger a major auroral event. The second effect rests on the wave-particle resonances inside the plasma cloud which may enhance VLF/ELF wave growth and enhanced energetic electron precipitation.

POINT OF CONTACT:

Morrie Pongratz	SPAN - ESSDP2::PONGRATZ
LANL	PHONE (505) 667-4740
Group SST-7 MS-D466	FAX - (505) 665-7395
Los Alamos, NM 87545	

EXPERIMENTAL ELEMENTS

Release Coordinates: 0.4N 58.1W 33553 km

Canister Type: Large

Chemicals 8A TI 4556 gms B 2056 gms BA 5410 gms

8B TI 4282 gms B 2068 gms BA 5304 gms SR 67 gms; Delay: None

Model Calculations:

Ted Fritz	SPAN-ESSDPI::FRITZ
LANLMS - D438	PHONE (505) 667-9234
Los Alamos, NM 87545	FAX (505) 667-3332

RESULTS:

During the experiment enhanced wave emissions mainly below 100 Hz were observed as well as enhanced auroral precipitation. However, the causal relation of the latter with the injection is still under investigation.

STATIONS COVERING THE RELEASE:

Aircraft -	C 135- 127
Caribbean -	Arecibo, PR; Bonaire, NA; St. Croix, USVI.
North America -	Boston, MA; Greenbelt, MD; Los Alamos, NM; White Sands, NM, Edisto Island, SC
South America -	Cerro Tololo, Chile; El Leoncito, Argentina

RELEASE G-8 OBSERVATIONS

OBSERVATION: Visibility of Chemical Release Clouds

LOCATION: Chincoteague, Virginia

STATION LEADER AND/OR OTHER CONTACT:

Morgan W. McCook
Independent Consultant

TYPE AND DESCRIPTION OF DATA ACQUIRED: Still photography. ASA 1600 color film, 210 mm f 5.6 lens.

FIELD(S) OF VIEW OF INSTRUMENT: 12° - 13°

TIME PERIODS OF DATA: 03:30 UT 2/17/91. Four frames at 1 minute intervals.

FRAME RATE: at intervals of 30, 35, 38, 42 seconds.

ASSESSMENT OF DATA QUALITY (CLOUD COVER, LIGHT CONTAMINATION): Clear. Excellent quality and example of long range of visibility.

INITIAL FINDINGS: Barium streak found and photographed from 33,000 km

ADDITIONAL RESEARCH: Comparison of EL Coqui rocket releases to compare visibility at lower altitudes.

EXPERIMENT G-1

13 July 1991

08:35:25 UT

Title: Diamagnetic Cavity, Unstable Velocity Distributions, Plasma Coupling

Principal Investigator: R. A. Hoffman

Collaborative Investigators: M. Pongratz, D. Papadopoluos, R. Smith, R. Anderson, D. Young, H. Singer, E. Szuszczewicz, J. P. Heppner, R. Hoffman, E. Wescott, H. C. Stenbaek-Nielsen, G. Haerendel, A. Valenzuela.

Location: Over North America

Time: 08:35:25 UT

Coordinates of Release: 17.8N 62.9W 495 km

Canister Type: Small.

Chemicals: BA 1468 gms SR 19 gms

Delay: None

STATIONS COVERING THE RELEASE:

Aircraft - Argentine B707, C135-127, C135-131 (mechanical problems- grounded)]

Caribbean - Arecibo, PR Bonaire, NA Guadeloupe, FR. St. Croix, USVI St. Thomas, USVI

South America - Reconquista, Argentina

POINT OF CONTACT:

Morrie Pongratz

LANL

Group SST-7 MS-D466

Los Alamos, NM 87545

SPAN - ESSDP2::PONGRATZ

PHONE (505) 667-4740

FAX - (505) 665-7395

RESULTS:

Excellent optical data was obtained from several ground and airborne observatories in the Caribbean and South America. Ground stations near the release at St. Croix and Guadeloupe studied the early time effects which caused the initially fast-moving ion cloud to stop and lose momentum and energy. At later times, some of the ions traveled upward along the magnetic field lines and were observed traveling to the southern hemisphere by ground observatories at Aruba, Bonaire, St. Croix, and Guadeloupe and by aircraft observatories in the Caribbean near Venezuela and in South America, south of Buenos. The ion streak traveling along the magnetic field was seen to move westward due to electric fields in the magnetosphere. The experiment was done during a period of moderate to strong geomagnetic activity, and gave good data on the influence of such activity on the magnetosphere and ionosphere.

The effects of the release were seen as well by scientific instruments on the CRRES spacecraft, measuring ionospheric density, magnetic and electric fields, and waves. The Arecibo Incoherent Scatter Radar located in Puerto Rico measured the state of the ionosphere "upstream" of the release point and provided valuable data for correlation with other measurements.

EXPERIMENT G-9

19 July 1991 08:37:07 UT

Title: Field Line Tracing and Equipotentiality, Momentum Coupling Velocity Distribution Relaxation and Field Equipotentiality

Principal Investigators: M. Pongratz and E. Wescott

Collaborative Investigators: D. Simons, D. Papadopolous, R. Smith, S. Mende, R. Hoffman, R. Anderson, W. Swartz, E. Szuszczewicz, G. Haerendel, H. C. Stenbaek-Nielsen, A. Valenzuela, P. A. Bernhardt, J. D. Huba.

Location: Caribbean with Orbital Velocity Perpendicular to Magnetic Field

Time of Day: Dawn

Altitude: CRRES /GTO near Perigee

Chemicals: 40 kg barium (2 large canisters)

OBJECTIVE:

An artificial plasma release at high velocity produces a plasma that is far removed from thermal equilibrium with free energy that can support the growth of electric and magnetic fields. Departures from thermal equilibrium in the form of non-Maxwellian distributions and distributions peaked away from zero velocity lead to kinetic instabilities which create high frequency electric fields. These electric fields provide anomalous collisions allowing momentum, energy, and current transport that would not otherwise exist in the absence of binary collisions. Such processes compete with the polarization fields in slowing down the cross-field directed plasma and lead to very different plasma states at the end of the coupling process. This experiment will investigate what instabilities are active; the instability saturation, or limiting conditions; the resulting electric and magnetic DC and AC fields, and the final velocity distribution of the injected plasma.

EXPERIMENTAL ELEMENTS:

Coordinates of Release: 17.4N 62.8W 441 km

Canister Type: Large

Chemicals: 9A TI 4692 gms B 2118 gms BA 5202 gms LI 11 gms
9B TI 4693 gms B 2118 gms BA 5203 gms LI 11 gms

Delay: None

Point of Contact:

M. Pongratz
LANL MS - D466
Group SST
Los Alamos, NM 87545

SPAN- ESSDP2::PONGRATZ
PHONE (505) 667-4740

STATIONS COVERING THE RELEASE:

Aircraft - Argentina B-707 Aircraft- C 135- 127 Aircraft- C 135- 131
Caribbean - Arecibo, PR Aruba Guadeloupe, FR. St. Croix, USVI St. Thomas, USVI
South America - Reconquista, Argentina

RESULTS:

The G-9 barium release was done on Feb. 19, 1991 at 08:37:07 UTC at 17.4N, 62.8W, altitude 441 km. This location was directly over the island nation of St. Kitts. The release was immediately confirmed by visual sightings, with reports of "very spectacular". The early-time measurements showed that most of the ions skidded to a stop in -10 kilometers, but that some ions de-coupled from the plasma cloud and traveled upward and downward along the magnetic field in single particle trajectories.

Both Caribbean aircraft reported "excellent data," with tracking of the barium ion streaks to the horizons. This confirms that a portion of the ions made the trip along the magnetic field for large distances.

The release was seen and the subsequent ions tracked by ground sites at Arecibo, St. Croix, Guadeloupe, and Aruba. Observations were made as well by the Soviet Committee for Hydrometeorology Research ship "Professor Zubov" located in a favorable position for triangulation with the sites at St. Croix and Guadeloupe.

The ground site at Reconquista, Argentina observed barium ions coming along the magnetic field lines from the northern release point. The position showed that the ions had drifted westward under the influence of a magnetospheric electric field. The magnetic field indices at the release time were $A = 17$ and $K = 04$ (Boulder).

The B-707 aircraft over the South Atlantic observed barium ion streaks beginning at 11 minutes after release until 1 hour, 10 after the release.

This experiment therefore satisfied the dual objectives of studying both early-time momentum coupling (the process that stops the majority of the ions) and the conjugate-point tracing to the opposite end of the magnetic field in the southern hemisphere.

EXPERIMENTS G-11, G-12

Title: Mirror Force, Field Equipotentiality, Unstable Velocity Distributions, Ambipolar Acceleration

Principal Investigator: E. Wescott, University Of Alaska

Collaborative Investigators: R. Hoffman, M. Pongratz, S. Mende, D. Simons, H. C. Stenbaek-Nielsen, D. Papadopolous, A. Valenzuela, G. Haerendel

Location: Caribbean at Points Selected for Conjugate Point Geometry

Time of Day: Dawn

Altitude: CRRES/GTO near Perigee

Chemicals: 10 kg. Barium (2 small canisters) G-11, G-12

OBJECTIVE:

The "mirror force" technique for dispersing visible Barium ion tracers along magnetic field lines provides the only feasible means for measuring the altitude distribution of weak parallel electric fields. The objective is to evaluate the accuracy and time-altitude resolution of this technique and establish the observational and model simulation approaches to extract parallel electric fields from the measured Ba ion motions. By conducting tests at low latitudes the threshold accuracy's and limitations can be defined under conditions of extremely weak parallel electric fields prior to extensive application in future high-latitude missions where highly complex parallel electric field distributions can be anticipated.

One of the fundamental early concepts in space plasma physics was that magnetic field lines are "frozen into" the plasma. This means that parallel electric fields are zero and that field lines are equipotentials. It also means that the transverse electric field should be identical at both ends of the field line at the same magnetic field strength. In one previous experiment using a Ba shaped charge release at low latitude it was observed that the Ba ions in opposite hemispheres did not move identically and hence it was concluded that the field line was not an equipotential. In another case the observations agreed with the "frozen in" concept. These releases will paint entire field lines between the hemispheres, and will be done under varying conditions of magnetic activity. High-resolution optical observations in both hemispheres should permit determination of where and under what conditions a breakdown of the equipotential condition occurs.

It should be remarked that experiments G-8 through G-12 all benefit from the high release altitude of the CRRES/GTO compared to the original baseline of CRRES in LEO at 358 km. The experiments all depend upon launching ions upward along magnetic field lines, and this process is impeded by collisions of the ions with the upper atmosphere. Computer modeling has shown that a significant difference, perhaps an order of magnitude, exists in the number of ions launched upward from initial injection altitudes of 400 versus 358 km.

EXPERIMENT G-11a

22 July 1991

08:38:24 UT

POINT OF CONTACT:

E. Wescott
Geophysical Institute
University of Alaska
Fairbanks, AK 99701

SPAN- UAFGI::ROCKET
PHONE (907) 474-7576
FAX (907)474-7290

EXPERIMENTAL ELEMENTS:

Coordinates of Release: 16.8N 60.3W 411 km

Canister Type: Small

Chemicals: TI 1270 gms B 573 gms BA 1371 gms SR 19 gm

Delay: None

STATIONS COVERING THE RELEASE:

Aircraft - Argentine B707 C135-127 C135-131 Caribbean - Arecibo, PR Aruba Bonaire, NA
Guadeloupe, FR. St. Croix, USVI St. Thomas, USVI. South America - Reconquista, Argentina

RESULTS:

The CRRES G-11a release was completed on July 22, 1991 at 08:38:24 UTC. The release location was 16.8 N, 60.3 W, altitude 411 km, a point northeast of Guadeloupe.

The release was observed and tracked by several ground sites and two aircraft in the Caribbean. The ion streak was observed to initially travel southward, and the slow considerably. In contrast with G-1 and G-9, there was no immediate signature of the barium ions in the southern hemisphere.

Initial reports from the Caribbean sites indicated that the ion cloud did not travel very far up the field and most of the ions remained in a region near the initial release point. The location of the release had been chosen so that the pitch angle (angle between the magnetic field and the spacecraft velocity vector) was as large as possible so that the ions would have a larger velocity component upward along the field line than in previous releases. However, the altitude (411 km) was lower than in previous releases and this may have allowed increased collisions with the neutral atmosphere to impede the ion transportation.

EXPERIMENT G-11b

25 July 1991

08:37:11 UT

POINT OF CONTACT: E. Wescott

EXPERIMENTAL ELEMENTS:

Coordinates of Release: 17.3N 69.5W 478 km

Canister Type: Small

Chemicals: TI 1270 gms B 573 gms BA 1471 gms SR 19 gms

Delay: 5 seconds

STATIONS COVERING THE RELEASE:

Aircraft - Argentine B707 C135-127 C135-131 Caribbean - Arecibo, PR Aruba Guadeloupe, FR.
St. Croix, USVI St. Thomas, USVI South America - Reconquista, Argentina

RESULTS:

The G-11b was unique among the CRRES experiment series. One small barium (1.5 kg) canister was ignited at a point below the UV terminator, and 17 seconds later the expanding neutral cloud crossed the terminator into sunlight. The objectives of this release were to study the contributions of early-time thermal ionization to the barium yield, to study the contribution of charge exchange and collisional ionization to the process, and to study the photoionization and early-time barium plasma processes under the conditions of an initially diffuse neutral cloud. This in contrast to the usual situation of a release in sunlight where the neutral cloud is initially very dense. In other words, this was a test to see if the photo-ions, created from a neutral cloud that had expanded to 50 kilometers diameter, would act more as a single particles and would be less affected by the collective MHD effects that caused significant ion energy loss in the earlier releases.

The release occurred on a point just south of the Dominican Republic. The magnetic conditions were relatively quiet. The estimated A index for the previous 24 hours 07, and the Boulder K index at 0000, 0300, and 0600 was 02, 0900 was 04, at 1200 was 03. At 1800 UTC on July 25 the A index was 12.

The negative factors operating were that the Caribbean stations had a full moon a few degrees above the horizon at the time of the release, and the South American stations had a full moon 10-20 degrees elevation. This, coupled with considerable haze in the Caribbean resulting from the recent passage of a tropical wave, made the viewing conditions less than ideal. On the plus side, however, the three aircraft all had excellent viewing conditions and were placed to view the release in the opposite direction (Caribbean aircraft) or 90 degrees (South American aircraft) to the setting full moon.

Two ground optical sites reported seeing ions at the release point, which were apparently created at the moment of release and became visible as the sun rose through the point. The majority of the ions, formed when the neutral cloud crossed into the sunlight, were seen to stay near the point of formation. However, the St. Croix optical site and the Caribbean aircraft observed an initial fast ion streak going southward up the magnetic field line. The first sighting of the canister ignition was on Aruba, and 17 seconds later the bright glow as the neutral cloud entered sunlight was also visible. At 1006 UTC the communication Center in Buenos Aires reported that B-707 flying at 47.0 S, 60.0 W saw the ion streak at times between T + 35 and T + 44 minutes. In every respect, this experiment is considered a success. The prime objective was to study barium ion plasma formation under a new set of conditions, and as a plus ions reached the conjugate point in the southern hemisphere.

EXPERIMENT G-12

12 August 1991 09:31:20 UT

Title: Mirror Force, Field Equipotentiality, Unstable Velocity Distributions, Ambipolar Acceleration

Principal Investigator: E. Wescott

**Collaborative Investigators: R. Hoffman, M. Pongratz, S. Mende, D. Simons, D. Papadopolous,
A. Valenzuela, G. Haerendel.**

Location: Caribbean at Point Selected for Conjugate Point Geometry

Time: Dawn

POINT OF CONTACT:

E. Wescott	SPAN -UAFGI::ROCKET
Geophysical Institute	PHONE (907) 474-7576
University of Alaska	FAX (907) 474-7290
Fairbanks, AK 99701	

EXPERIMENTAL ELEMENTS

Coordinates of Release: 9.1N 63.5W 507 km

Canister Type: Small

**Chemicals 12A TI 1271 gms B 573 gms BA 1471 gms SR 19 gms 12B TI 1271 gms B 574 gms
BA 1471 gms SR 19 gms**

Delay: 12A: None 12B: 5 sec.

STATIONS COVERING THE RELEASE:

Aircraft - C135-127 N146 Learjet

Caribbean - Arecibo, PR Aruba Bonaire, NA St. Croix, USVI

South America - El Leoncito, Chile Reconquito, Argentina

RESULTS:

The final chemical release from the CRRES spacecraft occurred at 09:31 :20 UT at an altitude of 507 km. The release was located at 9.1 N latitude and 63.5 W longitude about 320 km west of Trinidad. Two small barium canisters were released containing 3.0 kg of barium. Both Arecibo and Bonaire ground sites saw the release and recorded data until background became too bright. Aruba also observed the release and ion streak. The KC-135, located over the Caribbean north of Bonaire, tracked the ion streak as it traveled over the equator and down to the horizon. The ion streak was seen traveling to the conjugate point by both the Learjet and the ground site at Reconquista.

EL COQUI SOUNDING ROCKET CAMPAIGN

EXPERIMENT AA-3 A

Title: HF-Induced Ionospheric Striations

Principal Investigator: L. M Duncan

Collaborative Investigators: E. P. Szuszczewicz, F. T.. Djuth, R. A. Behnke, P.A. Bernhardt,
D. J. Simons

Locations: Arecibo tilted HF beam

Altitude: 230 km, 250 km, 270 km

Time: Launch 19:52, Release 19:54:30

Date: 25 May 1992

Chemicals: Three 5-kg Barium releases

OBJECTIVE:

Using a sounding rocket, three 5 kg releases of barium were to be deployed within the high-power HF modification region. The releases were to be 20 km below, at, and 20 km above the HF reflection height. Barium is intended to act as a tracer of the beam filamentation accompanying the HF self-focusing instability, serving to resolve scale size and geometry issues that cannot be adequately addressed by ground-based measurements. The primary diagnostics will be the Arecibo ISR and ground-based photography and CCD imaging. Ground-based VHF radar also support this experiment. The experiment complements AA-2 by comparing striation dynamics under comparable HF ionospheric modification conditions for a small and large barium releases.

RESULTS:

Arecibo Observatory supported the Experiment AA-3A through the use of its 430 MHz Incoherent Scatter Radar (ISR), as did two optical sites, one located at the observatory and the other at the Ramey Optical Station on the northwest corner of Puerto Rico. A field station on Guadeloupe Island supplied 35 mm still photographs of some of the chemical releases. The rockets injected the chemicals with velocities on the order of 1 km/s, compared to a 7 km/s injection velocity provided by the satellite. This allowed for the study of mechanisms involving velocities greater than those induced by conventional heating experiments.

The idea behind the AA-3A release was to inject a chemical that would be visible in both its neutral and ionized state to optical instruments when illuminated by sunlight. Also, the chemical had to photoionize, so that its interaction with the ionosphere and magnetosphere could be studied. Barium was chosen because it meets both of these requirements. The AA-3A experiment provided for the release of three clouds of barium, each separated by 20 km in altitude, and entered near the height of HF reflection. The yield of each Release was kept to a minimum so that, although each would be visible, the amount of ionization added by each release would not, in itself, modify the ionosphere to an appreciable extent.

Hours prior to the release, the HF heating facility that is used in conjunction with the Arecibo Observatory had been operating in a mode which is known to produce large-scale density

irregularities near the altitude where the HF wave reflects. It was intended that the releases would optically "paint across" the density striations that had been formed by the HF facility. As the releases expanded in the heated region, it was hoped that the scale size and structure of the density striations would be evident from the optical and radar data.

The experimental setup was centered around the heated volume produced by the HF heating facility in Islote, which is 17 km northeast of Arecibo Observatory. The HF facility can operate between the frequencies of 3 and 12 MHz, in any polarization, but was configured for 5.1 MHz, O-mode polarization for this experiment. Around the time of launch (10 minutes before until 20 minutes after) the HF facility went from kW to a 13 s ON / 2 s OFF cycle. The reason for this was to get some natural (unenhanced by the heater) plasma line profiles to see the effect of the barium without the heater on the plasma waves. Also this allowed for a means of determining whether or not any observed disturbances were HF-induced. The enhanced plasma line decay (how quickly it disappears when the HF is turned off) is on the order of 10 ms, so 2 s off would be sufficient to observe this effect. The barium yields were small so that this effect would hopefully be negligible. The heating power is produced by 4 independent generator/transmitters, each rated at 200 kW full power, which drive a $4\lambda \times 8\lambda$ inverted log-periodic antenna array. On the night of the releases, the heater was operated at 4×50 kW to reduce the chance of any arcing in the antenna field, as the weather was quite damp. The longer dimension of the array runs east to west, so the radiation pattern has its longer dimension running north to south.

The rocket range was to launch a Nike-Tomahawk sounding rocket containing the three Barium canisters at dusk with a trajectory which would carry the rocket through the center of the heated volume at 250 km altitude. The 430 MHz ISR was also pointed to the center of the heated volume at 250 km, as was the optical site at Ramey. The dusk launch was a requirement because the ground-based optical diagnostics had to be in darkness while 250 km above in altitude, the barium clouds would still be exposed to direct sunlight. This condition made for a very narrow launch window, and adding to the requirements good visibility during Puerto Rico's rainy season, the mission was scrubbed on the first six attempts. On the seventh night, May 25th, 1992, the rocket launched successfully into an ionosphere that was critical for 5.1 MHz at 273 km. The rocket was a "aim and fire" version, carrying no internal guidance mechanisms. It released the first canister at 251.0, a mere 1 km off of the intended altitude and managed to release the second canister at 270.8 km in altitude. No third cloud was ever observed, so it was inferred that the third canister was never ignited. The fact that the second release was so accurate and that the 430 MHz radar was fortuitously pointed within a few kilometers of the Ba cloud allowed for the acquisition of some very intriguing data.

The ISR results of the AA-3A experiment are in the form of plasma line and ion line profiles, or amplitude versus height plots. The results that were obtained were quite unexpected but very interesting. Before the first release, there was an HF enhanced plasma line at 273 km in altitude, where 5.1 MHz was reflecting. The first barium release gave rise to a density perturbation which was able to satisfy the frequency and wave vector matching conditions and an enhanced plasma line from the first barium cloud appeared ~2 seconds after release at 255 km in altitude. This persisted for ~12 seconds. Then both the barium and the HF induced plasma lines disappeared for ~165 s. The second release occurred ~15 seconds into this time span in which no plasma wave activity was observable. Two plasma lines then reappeared, one at 273 km and one a few km below this. These two lines modulated in amplitude for ~45 seconds, at which point the profiles returned to their pre-release state (single HF enhanced plasma line) and remained this way for the duration of the experiment.

Figure 1 shows the initial 12 seconds of profiles made after the first release. Figures 1 (a)-(d) are plasma line profiles, showing only the altitude range of interest. These show the emergence of a plasma line due to the first barium cloud close to 255 km in altitude, 2 s after release. Taking into consideration the velocity of the injection and the expansion rate of the cloud, this altitude is reasonable (i.e. 5 km higher than release point). Notice that within 3 s after release, the amplitude of the barium plasma line began to dominate the enhanced plasma line. Figures 1 (e)-(h) show the ion line profiles taken after the radar was switched to this mode for 5 s. The broadening of the ion line is due to actual density from the release. Figures 1 (i)-(l) are again plasma line profiles, showing the

plasma line from the barium cloud decreasing in amplitude. The HF enhanced plasma line has disappeared in (i), or seconds after release, and in (l) the barium line is disappearing. The computer simulation of the barium cloud density predicts that the density of the cloud plus the ambient density goes underdense after ~ 8 s. This is in fairly good agreement compared to 12 s observed in the radar data. There are obvious shortcomings in the computer simulation, the most serious being the assumption that the density in the cloud is uniform. Comparing Figures 1 (e)-(h) with (i)-(l), it is evident that the plasma line is coming from the upper edge of the cloud. This would suggest that there is a density gradient in the cloud, with density increasing with height in the cloud.

The 12 seconds shown in Figure 1 was followed by 165 seconds of no observable plasma or ion line activity. This was in turn followed by the reappearance of two plasma lines and their subsequent modulation. Figure 2 shows this, in 4 second intervals. The modulation persisted for ~ 45 seconds, with sporadic disappearances of both lines (see figure 2 (h)) during this time. The plasma lines seems very wide in altitude in these figures, which is misleading. The plasma line is actually from very narrow (~ 1 km) range in altitude, and the discrepancy arises because of Barker coding the correlation time of the medium is shorter than the pulse length, then the plasma wave will change phase while the pulse is in the medium, introducing error in the code. The spectral bandwidth of the plasma line can be upwards of 200 kHz. Thus the correlation time of the plasma line can be as short as $\sim 1/\text{bandwidth} \sim 5 \mu\text{s}$. The pulse length of the barker code is $52 \mu\text{s}$, so the side lobes introduced by the code will be artificially elevated above their ideal level, which is $(1/13)^2 = 1/69$ that of the main lobe.

The following argument is offered as an explanation of the CRRES data. In the early times after ease, the barium cloud was overdense but still spatially small. It was reflecting the HF energy that was incident on it, but enough of the energy passed around it to maintain the Airy pattern and the parametric decay instability. As the cloud grew, it reflected and refracted an increasing portion of the HF energy. After 7 - 8 seconds, the average density of the cloud plus ambient ionization went underdense to 5.1 MHz. The HF energy could once again propagate up to the reflection height, but by this time the ionosphere and hence the Airy pattern had been sufficiently distorted such that plasma waves were no longer being produced. Also, the radar data suggest that the upper edge of the cloud was above average density, so it could still reflect the HF wave. These perturbed conditions only had to last for 26 s after the first release, or until the second release. The second release took place within a few kilometers of reflection height, causing further distortion of the ionosphere.

Figure 3 shows an interpretation of the radar data based on the idea that the Barium cloud from the first release shadowed the natural reflection height above it, effectively halting the enhanced plasma line activity in the region where this had been at a maximum. Some of the HF energy does reach reflection height, illuminating the periphery of the HF volume. If the cloud acts as a divergent lens, then it can be hypothesized that a diffraction pattern would form on the reflection height centered around the shadowed region. This diffraction pattern could then be responsible for the modulation that occurs in the plasma line data as the pattern drifted through the ISR beam.

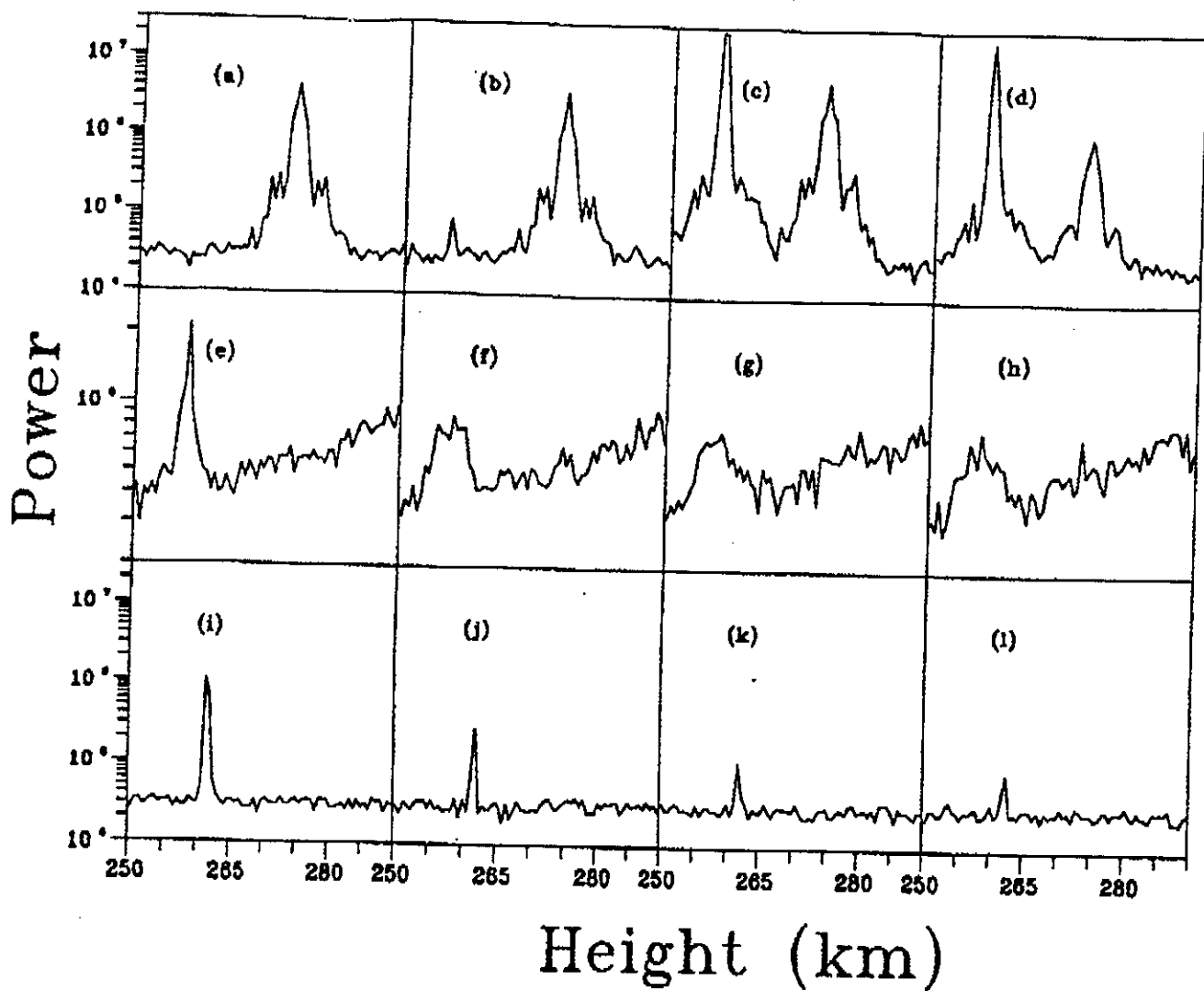


Figure 1. The first 12 seconds after the first barium release. (a)-(d) and (i)-(l) are plasma line profiles and (e)-(h) are ion line profiles.

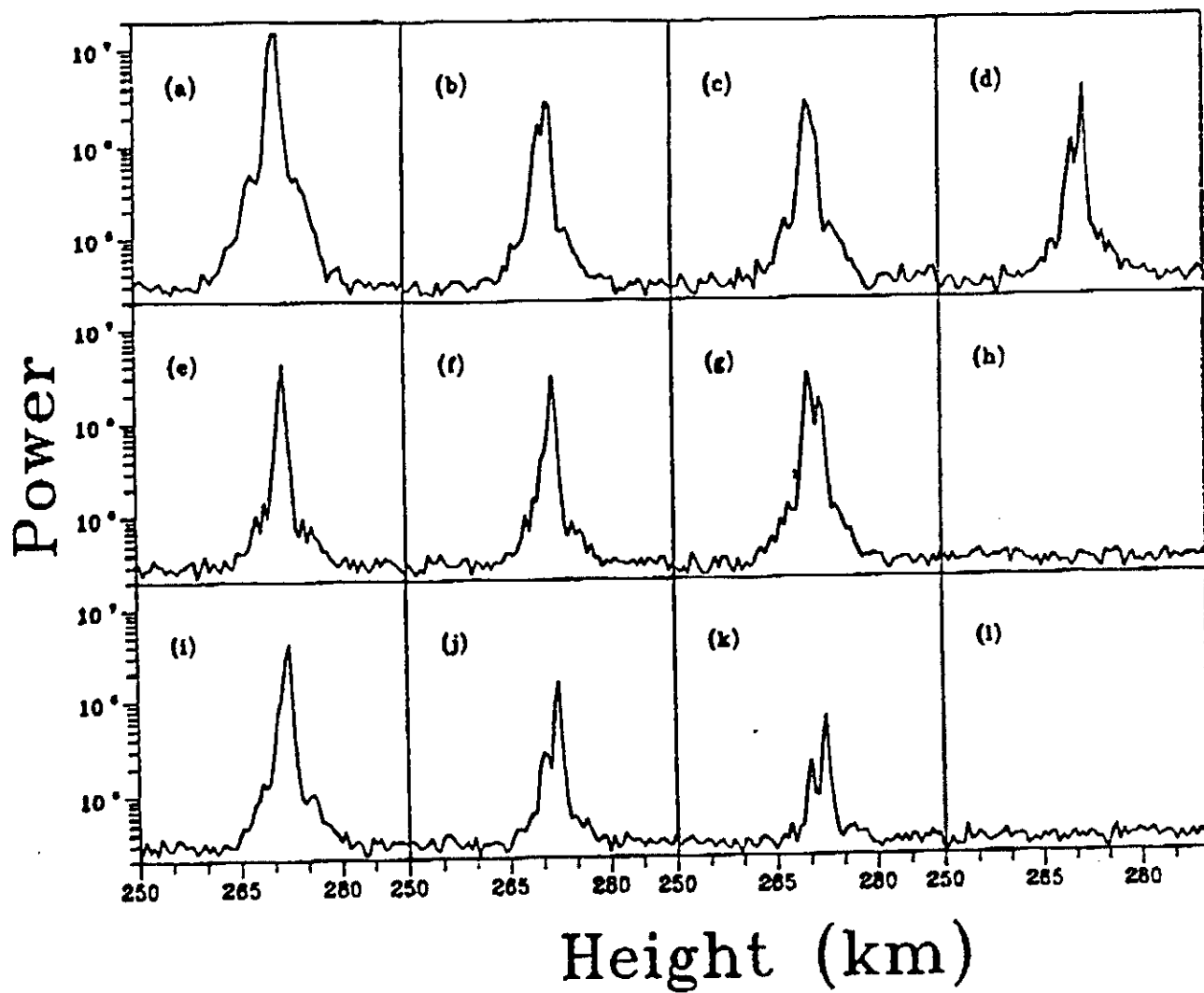


Figure 2. The modulation of the plasma lines ~ 3 minutes after the first release. The frames are 4 seconds apart.

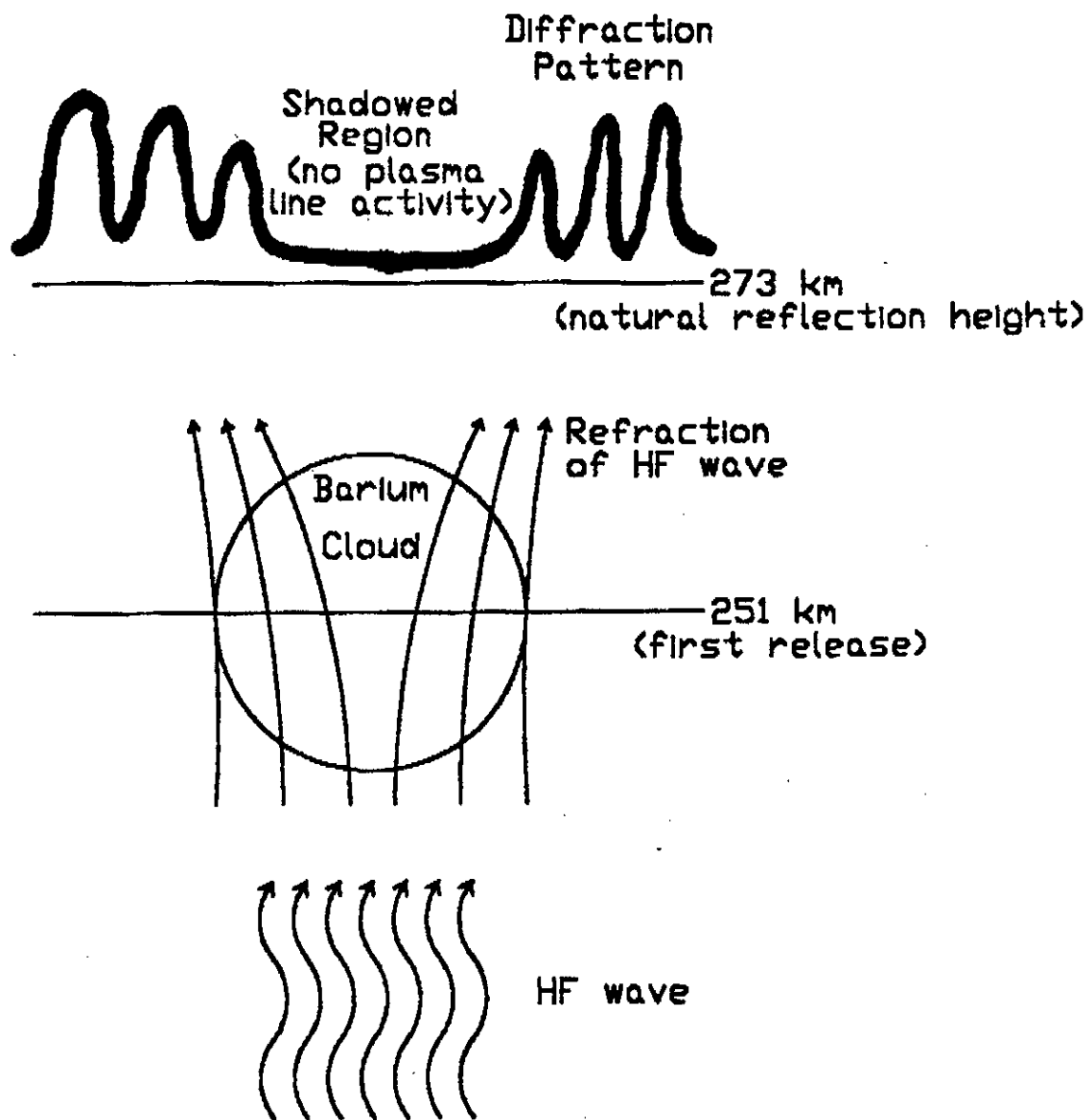


Figure 3. Schematic showing refraction of HF wave by barium cloud resulting in both shadowed and interference regions above the cloud.

EXPERIMENT AA-4

Title: Ionosphere Focused Heating

Principal Investigator: P. A. Bernhardt

Collaborative Investigators: D. E. Hunton, C. Pollack, F. T. Djuth, L. M. Duncan, P. E. Argo, C. Stokes, P. Rodriguez, C. Siefiring, H. Romero, L. Wagner, J. Goldstein.

Location: Arecibo High-Frequency Radio Heater Beam

Altitude: 250 km

Time: Night Launch 04:11 AST, Release 04:14:30

Date: 30 May 1992

Chemicals: 40 kg. CF_3Br (Trifluoromethylbromide)

OBJECTIVE:

The Ionospheric Focused Heating (IFH) experiment was designed to (1) demonstrate the use of chemical releases to enhance the effective radiated power of high-power HF facilities, (2) measure in situ the turbulence in the heated plasma, and (3) determine the relationship for a wide variety of phenomena that simultaneously occur during ionospheric heating experiments. The rocket payload for the IFH experiment consisted of a chemical release and a set of instruments. The IFH payload was launched on 30 May 1993 during the Combined Release and Radiation Effects Satellite (CRRES) program. All of the CRRES Caribbean rockets took off from the north coast of Puerto Rico. The CRRES rocket campaign, called "El Coqui" was organized to take advantage of the ionospheric heating facility, incoherent scatter radar, and other ground support diagnostics located near the Arecibo Observatory in Puerto Rico [Djuth, 1993].

The term "Ionospheric Heating" refers to ionospheric modification by high power radio waves. The transmitted high frequency (HF) electromagnetic wave is called the pump. The effective radiated power (ERP) of the pump for HF facilities typically ranges from 50 MW to greater than 1 GW. The ERP is calculated as the product of the transmitter power and the antenna gain for the facility. The ERP of the Arecibo HF facility was about 50 MW at the 5.1 MHz frequency used during the El Coqui campaign. The HF beam was tilted 12 degrees to the north to allow penetration by the rockets without endangering populated areas. The tilted beam lowered the ERP of the normally vertical beam.

The Arecibo incoherent scatter radar (ISR) is a primary diagnostic for the heated plasma. The transmitted wave ($f_T = 430$ MHz) from the radar is scattered from plasma waves (f_p) yielding scattered electromagnetic waves (f_s) that are received with the 300 meter dish antenna located at Arecibo. Scattering takes place from either electron plasma (Langmuir) waves or ion acoustic waves. The scattering conditions require that the scattering wavelength is equal to one-half the transmitted wavelength ($\lambda = c/f_T = 0.698$ m) of the radar. Consequently, the Arecibo ISR only detects scale sizes of $\lambda/2 = 0.35$ meters.

The components of the ISR spectrum from Arecibo has been described by Showen and Kim [1978]. Without ionospheric heating, ISR received spectrum is mainly composed of the thermal ion line which is scatter by natural ion acoustic waves. When the powerful HF transmitter is turned on, enhanced ion lines may be produced by scatter from HF induced ion acoustic waves. All ion line spectra reside within about 10 kHz of the radar frequency. Upshifted plasma lines are scattered by downgoing electron plasma (DEP) waves. Similarly, downshifted plasma lines are scattered by

upgoing electron plasma (UEP) waves. The frequencies of these lines fall near $f_T \pm f_{HF}$ where f_{HF} is the pump frequency.

The electromagnetic pump may be scattered by plasma waves to yield stimulated electromagnetic emissions (SEE) [Thide et al., 1989]. SEE is often characterized by a downshifted maximum (DM) located about 15 kHz below the pump frequency. When the pump frequency is located near a harmonic of the electron cyclotron frequency ($n f_c$), the DM vanishes and a broad upshifted maximum (BUM) may be found in the spectrum recorded on the ground. Stimulated Raman and two-plasmon decay processes may yield electromagnetic emissions at 1/2 and 3/2 the pump frequency [Bernhardt and Duncan, 1987; Derblom et al., 1989]. During the IFH experiment, both ISR and SEE measurements were made near 1/2, 1 and 3/2 the pump frequency. The SEE observations were conducted with a radio frequency spectrum analyzer connected to a broad band receiving antenna.

The process for conversion of high power radio waves into plasma waves (called anomalous absorption) has been explained by parametric instabilities [Fejer, 1979] or Strong Langmuir Turbulence [Dubois et al., 1990]. With the parametric decay instability (PDI), the pump electromagnetic wave is converted into two plasma waves, an electron plasma wave and an ion acoustic wave propagating in opposite directions. The frequency of the electron plasma waves is offset from the pump frequency by the frequency of the ion acoustic wave. Using another threewave process, the purely growing model can yield upgoing and downgoing electron plasma waves at the pump frequency.

Strong Langmuir Turbulence (SLT) has been developed to explain turbulence arising from more than three wave interactions. The nonlinear evolution of the heated plasma leads to the generation of cavitons that trap electron plasma waves. The size of the cavitons is on the order of 0.5 meter for ionospheric plasmas. In general, SLT yields a wider spectrum of Langmuir waves than the PDI.

High power radio waves simultaneously produce large scale (>10 km) cavities, medium scale irregularities (~ 1 km), and small scale Langmuir turbulence (~ 1 m). Often, these scales are located in the same region of heated plasma. At Arecibo, large scale cavities produced by thermal expansion of the plasma have been observed near the reflection point of the HF beam [Duncan et al., 1988; Hansen et al., 1990]. Inside these cavities the ISR often detects enhanced ion lines from trapped ion acoustic waves [Duncan et al., 1988; Bernhardt et al., 1989].

The effects of electron acceleration are seen as airglow clouds near the HF wave reflection point. Suprathermal electrons result from electron plasma waves acting on the thermal population in the F-layer. They may also be generated during the collapse of cavitons. Fluxes of energetic electrons can collisionally excite the red-line (630 nm) and green-line (557.7 nm) emissions from atomic oxygen in the upper atmosphere. The electron energies required to measurably excite the two lines are 3.5 and 6.0 eV, respectively. The measured intensities of 630.0 and 557.7 emissions have been analyzed to yield estimates of the suprathermal electron energy spectra [Bernhardt et al., 1989]. Images of the 630 nm airglow enhancements produced by the Arecibo HF facility have been obtained with low-light-level cameras by Bernhardt et al., 1989. The shape of the airglow clouds matches the cross-section of the HF antenna beam. The motion of the airglow results from the plasma drift of the large-scale cavities that capture the radio wave beam.

BACKGROUND:

For decades scientists have conducted experiments with chemical releases from rockets, high power radio wave injections and satellite releases of barium and lithium into the ionosphere. In October 1989 and August 1990, the Negative-Ion, Cation Release Experiment (NICARE-1 and -2) were carried out using chemicals such as SF_6 , $Ni(CO)_4$, and CF_3Br to attach electrons in the ionosphere and yield negative ions. From 1985 optical measurements of accelerated electrons during heating experiments were conducted using imagers in Puerto Rico and in Russia. Experimental experience combined with simulations and theory have provided a basis for the new IFH experiment.

ACCOMPLISHMENTS:

The IFH experiment demonstrated that (1) the release of a chemical with a large electron affinity can produce a large, 30 km hole in the F-region and (2) that this hole acts like a convergent lens to focus the HF pump waves. Using a 1200 km baseline, the NRL Channel Probe demonstrated that communications channels can be influenced by simultaneous action of chemical releases and radio wave heating. With in situ Langmuir probes, ion probe, and plasma wave receivers, the experimenters obtained unique observations of the electron densities and plasma waves inside the chemically modified region. Small scale structures, on the order of 1 - 100 meters in size, were detected using the high resolution instrumentation. The thermal energy capped hemisphere spectrograph (-IECHS) instrument detected a strong burst of particles only just after the release. Broadening of the frequency spectrum around the electromagnetic pump wave indicated nonlinear interactions between electrostatic turbulence produced by the chemical release and the HF beam. Based on numerical simulations of wave propagation through the modified ionosphere, NRL scientist have shown that the artificial hole acts like a thick lens to focus the HF beam onto a reflection point in the ionosphere. The focusing increases the power density of the electromagnetic wave by more than a factor of 50 and, through nonlinear processes, enhances in the ion-acoustic and electron acceleration and enhanced airglow has recorded during periods of strong Langmuir turbulence. However, during the IFH experiment no evidence of electron acceleration was recorded.

The IFH rocket carried an instrument and chemical payload along a trajectory that crossed the intersection of the beams from the 430 MHz incoherent scatter radar and the 5.1 MHz high power facility near Arecibo. The release of 30 kg of CF_3Br into the F-region at 285 km altitude produced an ionospheric hole that acted like a convergent lens to focus the HF transmissions. The equivalent radiated power inside the radio beam was raised from 50 MW to over 5000 MW by the action of the 30 km diameter lens. Surprisingly, no enhancements in optical emissions were observed that could be attributed to the focusing inside the chemically produced cavity. Instead, a wide range of new processes were recorded by in situ and ground based instruments. These include smallscale micro-cavities (< 1 meter) and down shifted electron-plasma (Langmuir) waves inside the artificial cavity, electron density spikes at the edge of the cavity, and Langmuir waves trapped in ion-gyro-radius (6 meter) cavities near the radio wave reflection altitude. The Ionospheric Focused Heating experiment verified some the preflight predictions but, after a preliminary look at the measurements, more questions were raised than were answered.

Experiment Concept - Chemically Produced Cavity

At Arecibo, large-scale cavities and enhanced ion-acoustic waves have been found to be coincident with electron acceleration that produces airglow [Bernhardt et al, 1989]. The processes that couple these phenomena are not understood so an experiment was devised to control the cavity formation and then see the response of the enhanced ion lines and the optical emissions. The active experiment used a chemical to form a large electron scale cavity in the HF beam. The effects of the artificial cavity on the heated ionosphere were recorded with in situ and ground based instruments. This experiment was called the Ionospheric Focused Heating (IFH) experiment because it was thought that the chemically produced cavity would focus the HF yielding substantially larger field strengths for the HF waves.

The ionospheric hole was produced by the release of CF_3Br which removed electrons by dissociative attachment. The effectiveness of this chemical was demonstrated in the F-region during the NASA sponsored NICARE 1 experiment [Bernhardt et al., 1991]. The dissociative attachment reaction is:



With a 30 kg release of this material, the electron population is depleted within 10 km of the release point [Bernhardt et al., 1991]. The negative and positive ions are mutually neutralized by the reaction



Measurements of airglow are complicated by the presence of excited atomic oxygen that may yield green-line (557.7 nm) or red-line (630.0 nm) emissions. Care must be taken to distinguish between airglow excited by suprathermal electron fluxes and by chemical reactions in the negative ion plasma.

The plasma waves measured in situ during the IFH experiment were expected to be strongly influenced by the presence of the negative ions. During the NICARE 1 and 2 experiments, new wave modes are excited inside the negative ion cloud even without the presence of a high power radio wave [Ganguli et al., 1993]. Enhanced electric field fluctuations come from lower hybrid waves, ion plasma waves, and ion cyclotron waves excited by the presence of Br and O⁺ in the chemically modified plasma [Scales et al., 1993]. With the IFH experiment, the addition of an electromagnetic pump field added to the complexity of plasma wave structures in the negative ion cloud.

The magnitude of the focusing by the chemically produced cavity was estimated in the theoretical paper by Bernhardt and Duncan [1987]. This paper showed that an ionospheric hole on the bottomside of the F-layer would yield a 20 dB increase in the HF pump near the focal region. The heating at the focus yielded channeling of the HF beam.

In situ instruments were delivered by Naval Research Laboratory, Phillips Lab, and Marshall Space Flight Center for integration into the payload in 1990. The launch of AA-4 occurred on 30 May 1992 at 0411 Atlantic Standard Time (0811 Universal Time) from the launcher located near Vega Baja in Puerto Rico. The release of 30 kg of CF₃Br occurred at 08:13:49.8 UT within 5 km of the center of the Arecibo HF beam. Figure 1 illustrates the locations of the flight trajectory, heater beam, ISR scan projected onto the ground plane containing the island of Puerto Rico. The CF₃Br release occurred slightly to the east of the HF beam center. The ISR beam positioned at the release point based on post launch extrapolations for the rocket trajectory and commanded release. After the ionospheric hole was well developed, the ISR was scanned in azimuth to keep track of the westward convection of the ionospheric hole. The IFH rocket was fully instrumented to measure the plasma densities, electric fields, plasma waves, and suprathermal electrons expected to be detected in the modified plasma (Table I). The placement of the sensors is shown in Figure 2.

Both electron and ion densities were measured using probes on the IFH rocket. The Naval Research Laboratory provided a double Langmuir probe that was biased at a fixed voltage (+6 V) to collect electrons. The separation between the two probes was 1.26 meters. Two disk probes biased to collect ions were mounted on the payload skin just aft of the E-Field Booms. The disk probes, one small (1.5") and one large (3"), were provided by the Phillips Laboratory.

Multiple electric field and plasma wave receivers were provided by the Naval Research Laboratory covering the 0 to 10 MHz frequency range. The electric fields were detected with booms deployed from the payload after launch. The spacings between sensors on the booms varied from 0.3 to 3.4 meters. Plasma waves near the HF pump frequency of 5.1 MHz were detected with four radio frequency sensors with spacings of 5.5 and 11 cm.

The energy spectrum of suprathermal electrons between 2 and 100 eV was to be detected with the Thermal Electron Capped Hemispherical Spectrometer (TECHS) instrument provided by Marshall Space Flight Center. The TECHS was mounted on the opposite side of the EF-5 and EF-6 booms. Unfortunately, after launch the voltage sweep was lost on the instrument and the energies of the detected electrons has not been determined.

In Situ Measurements

The data from the flight instruments can be divided into 5 phases (Figure 3). In Phase 0, before the release, the electron density measurements contain both spin modulation and fine scale irregularities from the heater (Figure 3a). For the first 9 seconds (Phase 1) after the CF₃Br release, the depressed plasma is pitted with narrow micro cavities with sizes of 1 meter or less (see Figure 3b). A high

resolution sample of this data is given in Figure 4a. The micro cavities were recorded by both Langmuir probes. Usually the features smaller than the distance between the two probes were detected only at one of the probes. The micro cavities larger than 2 meters were usually measured with both probes simultaneously.

During Phase 2, the IFH payload entered the negative-ion cloud boundary layer where the electron density is 1 to 10 % of ambient (Figures 3b and c). The density fluctuations were dominated by spikes with widths of about seven meters. A detailed sample of these micro spikes is illustrated in Figure 4b. These enhancements are interpreted to be regions where electrons neutralize the regions of negative-ion micro-cavities in a relatively uniform positive ion background. Further investigation of the data from the Phillips Laboratory positive-ion, disk probe is required to verify this speculation.

The amplitude of density fluctuations decreased until the rocket payload approached the 5.1 MHz reflection region. Between 311 and 316 km altitude at times 21 through 30 seconds after release, the fluctuation level increased until, near the critical density of $3.23 \times 10^5 \text{ cm}^{-3}$, large (up to 40%) density reductions were found (Figures 3d and 4c). Note that the irregularities must have been newly formed by the HF wave because this reflection level at the top of the ionospheric hole did not exist ten seconds earlier. The scale sizes of the cavities in this region were on the order to an ion cyclotron radius (6 meters). Similar size structures have been reported by M.C. Kelley and coworkers [private communication, 1993] during a rocket flight through the Arecibo heater beam on 9 June 1993. After passing through the reflection level, the rocket entered the unheated plasma labeled phase 4 in figure 3d. Here, the electron density fluctuations decreased to values of $\Delta n/n$ less than one percent.

The sudden effects of chemical release were recorded by the in situ measurements of the 5.1 MHz pump wave using the NRL downconverters (Figure 5). Before the CF_3Br release (Phase o), the payload traveled through the ambient ionosphere heated with 5.1 MHz HF beam. Quasi periodic variations in the amplitude of the 5.1 MHz pump were produced as the payload passed through the standing-wave (or Airy) pattern of the reflected HF signal. The measured spacing between the nulls in this pattern was 71.5 meters, slightly larger than the free space wavelength $\lambda = 58.8$ meters (Figures 6 a,b,c). After the release, the electric field amplitude increased by more than a factor of three and the periods between nulls was as short as 22 meters less than a free space wavelength (Figures 5 c,d,e).

The frequency spectrum from the 5.1 MHz downconverter on the IFH rocket is shown in Figure 6. While the rocket payload was inside the ionospheric hole, the 5.1 MHz pump was broadened into a downshifted spectrum with a width of 1.3 kHz. This broadening started at the time of the release (169.3 seconds after launch). The intensities of the downshifted waves were more than 10 dB above the pre-release level. The width and intensity of the waves returned to the prerelease level 14 seconds after release when the rocket had passed through the Phase 2 irregularities. A localized burst of broad band HF noise ($\Delta f \leq 8 \text{ kHz}$) was next recorded when the payload transited the critical region of the ionosphere during Phase 3.

A plot of the electron density irregularities and the spectral deviations from 5.1 MHz show evidence of Langmuir waves coincident with the density cavities near the reflection level (Figure 7). This data is consistent with formation of field aligned irregularities that trap Langmuir waves generated by parametric decay instabilities. For Strong Langmuir Turbulence, one would expect to observe smaller cavities (< 1 meter) and a broader plasma wave spectrum ($> 25 \text{ kHz}$) [DuBois, 1990]. The absence of these effects suggests that SLT was not present when the IFH rocket passed through the HF reflection point. The measured irregularities are more consistent with the field-aligned ducts described by Muldrew [1978 and 1988] that trap Langmuir waves.

Figure 8 illustrates the spectrum of electric fields obtained with sensors spaced by 3.4 meters on the E-field booms. Immediately after release, the E-field spectrum saturated resulting in a absence of data for the first 7 seconds after release (170 through 177 seconds after launch). While in the modified plasma, strong enhancements in electric fields were recorded below 500 Hz until the rocket passes through the critical region 29 seconds after release (199 seconds after launch). Between 180

and 190 seconds, a VLF noise band appeared in the range 3.0-5.5 kHz. The amplitude of these waves are modulated by the spin of the rocket yielding vertical stripes in the spectra. These bands are located in the region of intense electron density spikes at the negative ion boundary layer illustrated in Figure 3c. An intensification of the low frequency electric field spectrum occurred when the payload passes through the reflection region for the HF waves in the time period 25 to 29 seconds after release (between 195 and 199 seconds in Figure 8). The spectral features seem to be the result of polarization electric fields in the structures composed of the 6-meter cavities.

Incoherent Scatter Radar Measurements

Even though the 5.1 MHz HF transmitter was in operation continuously, no enhanced ion lines were recorded before or up to 450 seconds after the launch of the IFH rocket. The trajectory of the rocket was measured by the sidelobes of the Arecibo radar. Backscatter by the thermal ion line showed the reduction in electron density following the chemical release. Both of these effects are shown by the left half of Figure 9. The azimuth of the radar was fixed at 13 degrees until 300 seconds after launch. After which, the azimuth was scanned from one edge of the ionospheric hole to the other.

The right half of Figure 9 shows the effects of focusing through the artificial hole. Because of a westward drift, the azimuth of the hole center was found to be located at an azimuth of ~5 degrees, 500 seconds after release. Around this time, a strongly enhanced ion line (EIL) was observed where the HF wave reflected at the critical density region. This region occurred where the pump frequency equals the electron plasma frequency across the top of the artificial hole. The intensity of this EIL was the largest recorded during the May-July period of the El Coqui rocket campaign. This unusual intensification of the EIL was the result of focusing by the chemically produced hole in the F-region.

The radar plasma line (PL) went through a number of changes during the IFH experiment (Figure 10). Before the chemical release, a weak PL was recorded near the HF reflection height of 290 km in the F-region. During the first ten seconds following the release, the plasma line was recorded at multiple altitudes between 285 and 300 km. The intensity increased by 10 dB in a path aligned with the rocket trajectory between 295 and 300 km. After this initial enhancement, the PL vanished only to reappear at the top of the chemically produced cavity with an intensity comparable to the prerelease value. The strongest enhancements in the PL occurred between 280 and 430 seconds after release. This is the same time when the strongest enhanced ion lines were observed. At 480 seconds after launch (310 seconds after release) the azimuth scan reversed directions. Both the plasma line and enhanced ion line show mirror image symmetry around this time. This indicates that long-lived turbulence was excited at the HF reflection layer.

The spectra of the plasma lines were obtained during the data gaps shown as white vertical bars in Figure 10. The downshifted plasma line spectrum taken 504 seconds after launch is illustrated in Figure 11. This plasma line shows all of the characteristic features (i.e., growing mode, decay line, cascade bump) of an unfocused plasma line at Arecibo.

Based on raytracing through a model ionosphere, the source of the enhanced turbulence has been attributed to focusing by the chemically produced cavity. Without the chemical release, the pump beam reflects near 300 km independent of ray launch angle (Figure 12a). In the early phase of the release, the strong electron density gradients form a focal point inside the ionospheric hole. Using an electron density model that matches the ISR electron density profile 10 seconds after the CF₃Br release, the focus is 8 km from the center of the hole whereas the upper reflection boundary of the hole is 15 km from the center (Figure 12b). The hole evolves by the action of chemistry and plasma transport. At some point in the evolution, the HF focal point and the reflection boundary coalesce yielding a region of large electric fields. This condition occurs at about 300 seconds after release. Figure 12c shows a tube of rays focused on the upper boundary of the ionospheric hole 293 seconds after release. This is the time period when the unusual enhancements of ion acoustic and electron plasma waves were observed in the ISR data.

Other Ground-Based Observations

A complete set of optical instruments were operated at the Arecibo Observatory during the IFH experiment. Photometers with 5 degree fields of view were pointed at the release location and recorded the 557.7 and 630.0 nm emissions. A low-light-level CCD camera with a 60 degree field of view recorded 630 nm emissions from the release and HF focusing regions. A description of these instruments is given by Bernhardt et al. [1988]. The only enhancement of airglow during the IFH experiment occurred immediately after the CF₃Br release. A 20 Rayleigh increase in 557.7 nm came from the excited atomic oxygen that was a product mutual neutralization reaction (2). No enhancements in the airglow were recorded by the photometers or imager at the time of the strongly enhanced ion line. This is surprising because previous experiments at Arecibo have suggested that extremely strong enhanced ion lines are accompanied by measurable increases in redline airglow [Bernhardt et al., 1988; 1989].

Observations of stimulated electromagnetic emissions (SEE) were attempted at Arecibo, PR and Providenciales, Caicos. No SEE was detected during the entire El Coqui campaign. This is not totally unexpected because previous experiments have demonstrated that SEE is more often observed at higher latitude heating facilities [Thide et al, 1989].

Finally, bistatic HF propagation links were set up between Dominica and Providenciales, Caicos during the IFH release, as well as others. Propagation frequencies were chosen to reflect near the release points for chemicals. The CF₃Br release produced a large Doppler shift in the HF wave passing through the disturbed regions.

Conclusions

The IFH chemical release produced a large (> 30 km) hole in the F-layer centered within 6 km of the 5.1 MHz HF beam. The reactions between CF₃Br and the ambient electrons yielded a turbulent negative-ion plasma. The action of the high power radio wave on the negative-ions, positive ions, and electrons produced micro-cavities with diameters of 1 meter or less and factors of 10 or greater reductions in the already depressed plasma density. In the boundary layer between the negative-ion and electron dominated regions, electron density spikes are recorded with the in situ Langmuir probes. These spikes have been interpreted as cavities in the negative ions that are filled by electrons to maintain charge neutrality.

The in situ measurements of the electron density near the HF reflection region at the top of the ionospheric hole shows electron plasma waves trapped in cavities the size of the positive-ion gyro-radius. The frequency spread of these Langmuir waves is 8 kHz or less. The characteristics of the cavities region are not consistent with cavitons described by Strong Langmuir Turbulence (SLT) theory. Instead, the structure observed at the reflection region is probably associated with field aligned cavities trapping Langmuir waves generated by the parametric decay instability (PDI) as described by Muldrew [1978, 1992].

The artificial ionospheric hole yielded 10 to 20 dB enhancements in the pump wave by focusing, consistent with the predictions by Bernhardt and Duncan [1987]. The strongest focusing lasted for 150 seconds after the ionospheric hole had evolved so that the focal point was located on the reflection level at the top of the hole. The amplitude of the ion acoustic waves and electron plasma oscillations were increased by more than 20 dB during the period of the strongest focusing. The absence of airglow enhancements during this time is difficult to explain. Heated induced airglow usually comes from suprathermal electrons colliding with ambient atomic oxygen. The negative ions trapped on the magnetic field lines below the HF reflection level may have scattered the suprathermal electrons before they could excite the oxygen. The IFH experiment has demonstrated that the release of an electron attachment chemical will form an artificial lens in the F-region that may be used to increase the power density of any HF facility. The effective radiated power of these facilities will be increased by about 20 dB for periods of time longer than 2 minutes.

Table I

INSTRUMENTATION FOR THE IFH ROCKET

Experiment	Group	Sensor Parameter	Specifications	Sample Rate (/s)
Langmuir Probes				
LP1	NRL	20 cm Probe Electron	26 to $4 \times 10^6 \text{ cm}^{-3}$	5556
LP2	NRL	20 cm Probe Density	3 to $4 \times 10^5 \text{ cm}^{-3}$	5556
(n/n)1	NRL	20 cm Probe Relative	0 to 3	11 kHz
(-n/n)2	NRL	20 cm Probe Density	0 to 3	11 kHz
DP1	PL	3.0" Disk	Ion	0 to $>10^6 \text{ cm}^{-3}$
DP2	PL	1.5" Disk	Density	0 to $>10^6 \text{ cm}^{-3}$
Electric Fields				
DC,LF,AC 14	NRL	4.3 m Dipole	DC and	0 to 5.6kHz
DC,LF,AC 12	NRL	0.3 m Dipole	Low Freq.	0 to 5.6 kHz
kSamp/s				11.2
DC,LF,AC 34	NRL	0.3 m Dipole	E-Fields	0 to 5.6 kHz
DC,LF,AC 56	NRL	0.3 m Dipole		0 to 5.6 kHz
DownConv. 1	NRL	1.5 m RF	Langmuir	2.5 to 12MHz
Down Conv. 2	NRL	1.5 m RF	and Pump	2.5 to 12MHz
Down Conv. 3	NRL	5.5 cm RF	Waves	5.050+75kHz
Down Conv. 4	NRL	11.0 cm RF		5.075 +75 kHz
Energy Spectra				
TECHS	MSFC	Cylinder	Thermal	.2to 30eV (32)
Electrons	45° x 15°	(8)	32x8 spectrum	320 msec for

Figure Captions

Figure 1. Ground projection of the IFH rocket trajectory relative to the island of Puerto Rico. The location of the 5.1 MHz HF heater and the 430 MHz UHF radar beams are also indicated. The CF3Br release occurred along the trajectory slightly to the east of the center of the HF beam.

Figure 2. Sensors and instruments on the IFH rocket. The chemical canister was located between the instrument section and the rocket motor.

Figure 3. Electron density on the IFH rocket in four ten second periods. The values are derived assuming that electron density is proportional to the measured current from the NRL Langmuir probe LP2. In regions of very low density, such as phase 1 and the early part of phase 2, the negative ions may provide a substantial portion of the Langmuir probe current. Density fluctuations are evidence of (a) rocket spin, (b) micro cavities, (c) spikes, and (d) heater induced cavities. The rocket speed and altitude at the beginning of each period is indicated along with the initial time after launch.

Figure 4. Details of several regions of Figure 3. The time, speed, and altitude of each segment is given along the top of each data sample.

Figure 5. In situ measurements of the electric fields near the 5.1 MHz pump wave. A large increase in wave amplitude follows the CF3Br release.

Figure 6. Spectrogram of the pump fields and associated Langmuir waves. The spectra is naturally divided into (1) a prerelease narrow line, (2) downshifted broadening after release, (3) a burst when passing through the HF reflection level 196 to 199 second after launch, and (4) a disappearance of the pump thereafter.

Figure 7. Detail of the electron density and Langmuir waves around 5.1 MHz near the HF reflection level. The Langmuir waves seem to be trapped inside the density cavities.

Figure 8. Spectra of electric fields measured between sensors EF1 and EF4 of Figure 2. The low frequency fields are enhanced inside the negative ion cloud and when the rocket passes through the HF reflection region.

Figure 9. Incoherent scatter ion line obtained by the Arecibo radar during the IFH experiment. The radar backscatter is affected by (1) reduction of electron density in the F-layer, (2) side-lobe scatter from the rocket body, and (3) enhanced ion acoustic waves at the top of the F-layer hole. The radar was operated in a spectral mode during the times of data gaps in the figure.

Figure 10. Incoherent scatter measurement of the plasma line at 430 - 5.1 MHz. The plasma line shows (1) the HF reflection layer before the release, (2) a brief focusing after release, (3) a new reflection height at the top of the ionospheric hole, and (4) 20 dB increase in the plasma line after focusing occurs.

Figure 11. Spectrum of the downshifted plasma line during the time of intense HF focusing.

Figure 12. Rays from the 5.1 MHz HF transmitters propagating through (a) the unmodified Flayer, (b) the ionospheric hole 10 seconds after release, and (c) the hole at a later time when the focal point is at the HF reflection level. The electron density contours are derived from a spherical release model adjusted to fit density measurements obtained from the ISR radar.

70



71

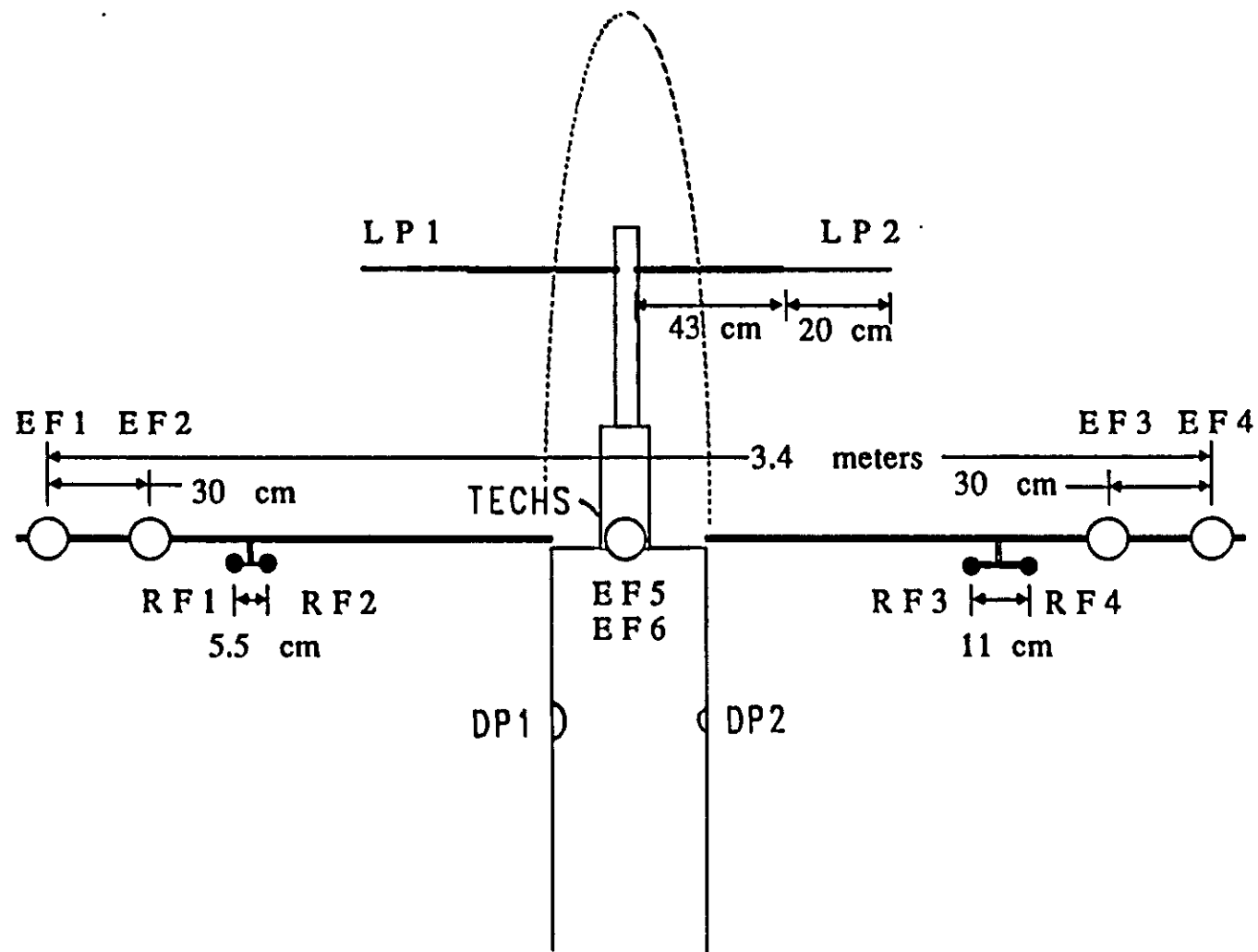


Figure 2.

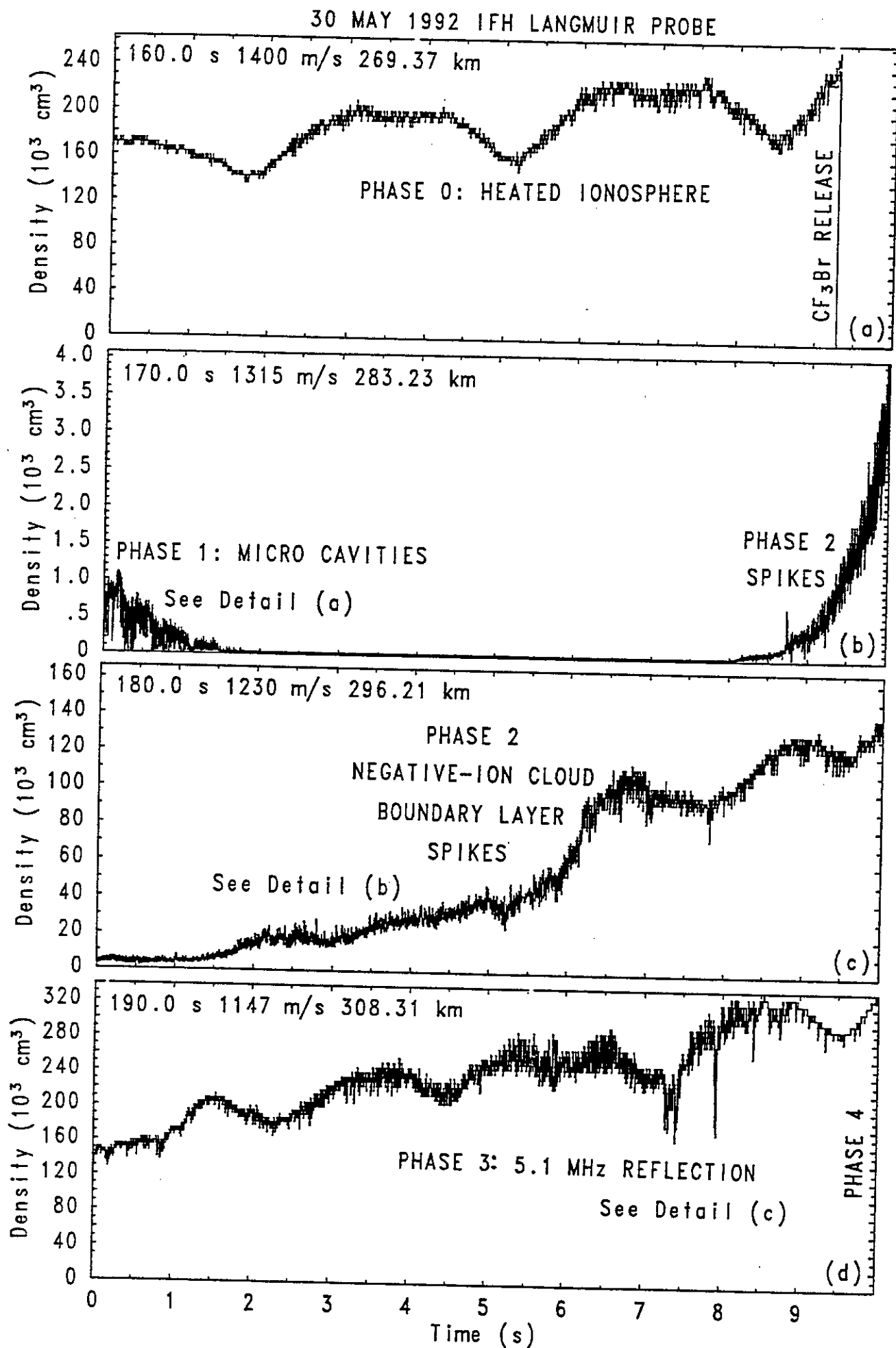


Figure 3.

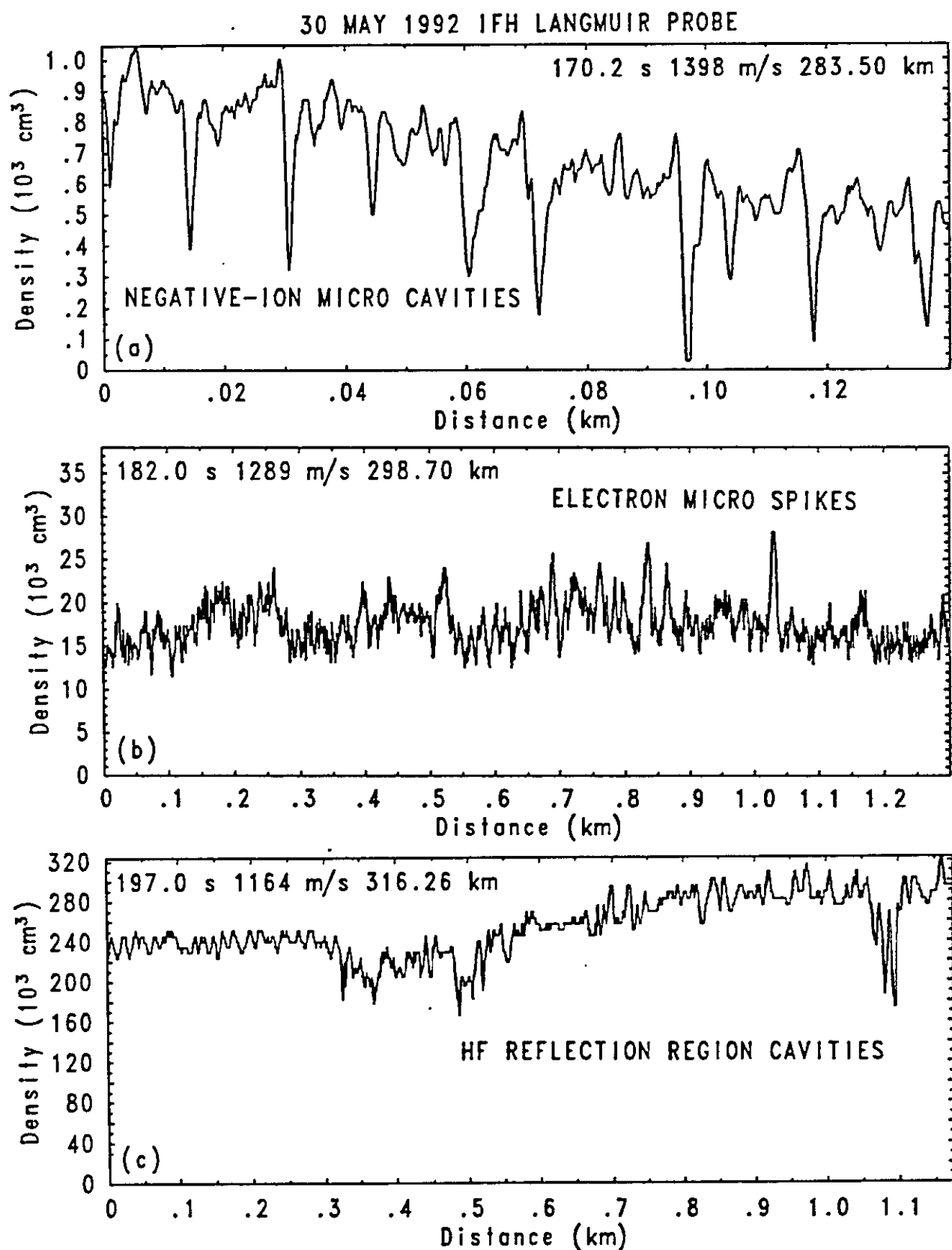


Figure 4.

WAVE MEASUREMENTS NEAR 5.1 MHz

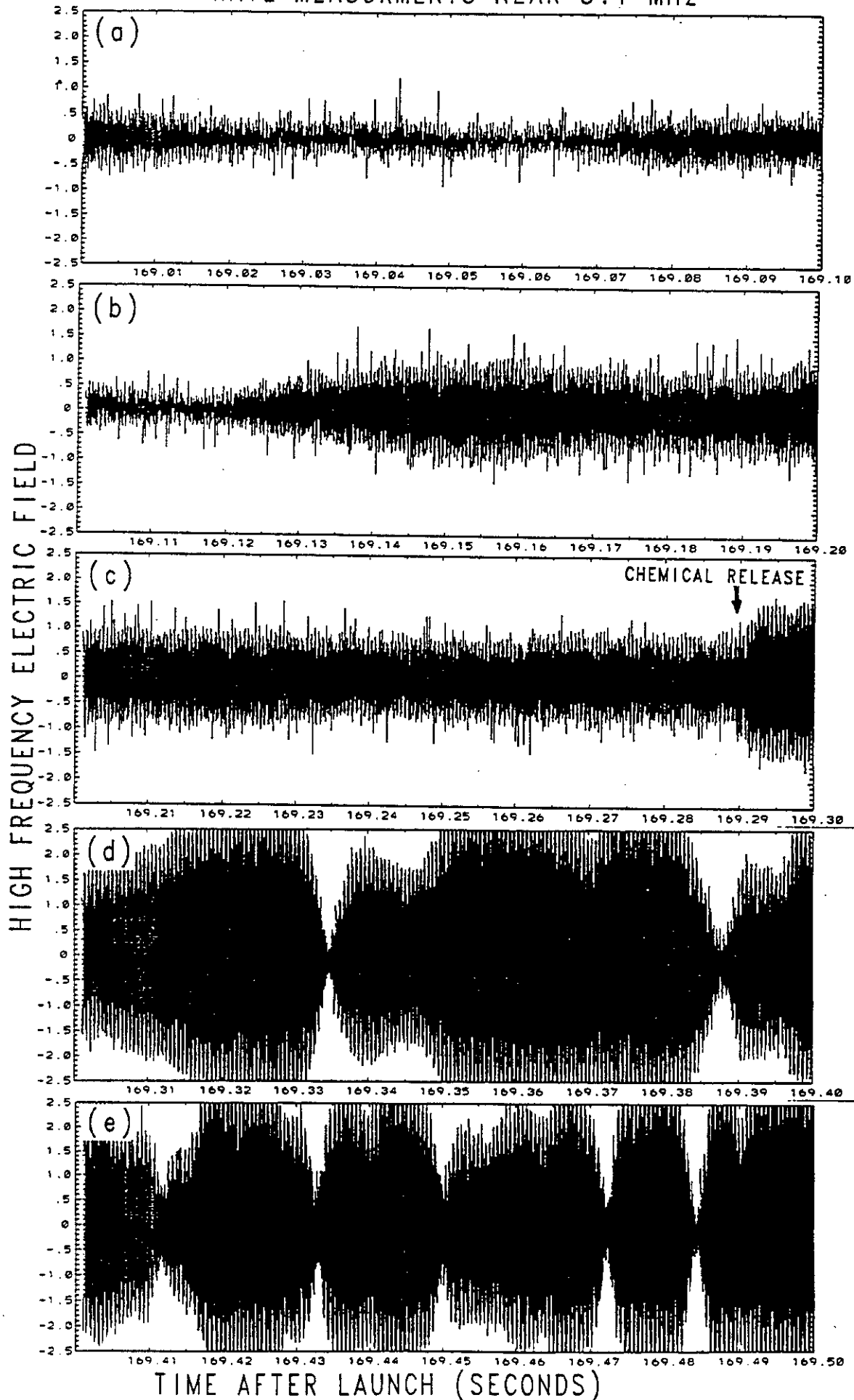


Figure 5.

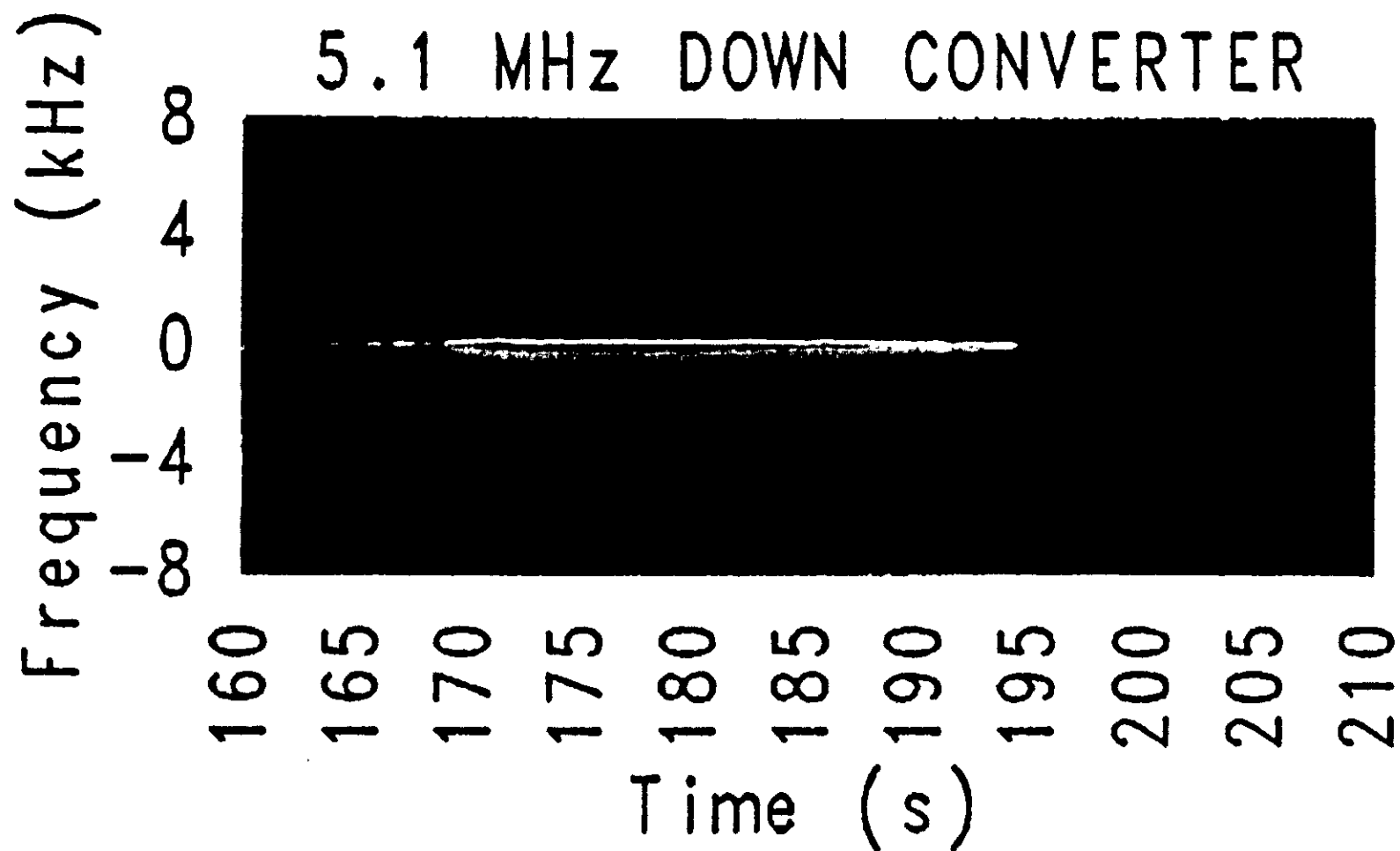


Figure 6.

194 s 1130 m/s 312.90 km

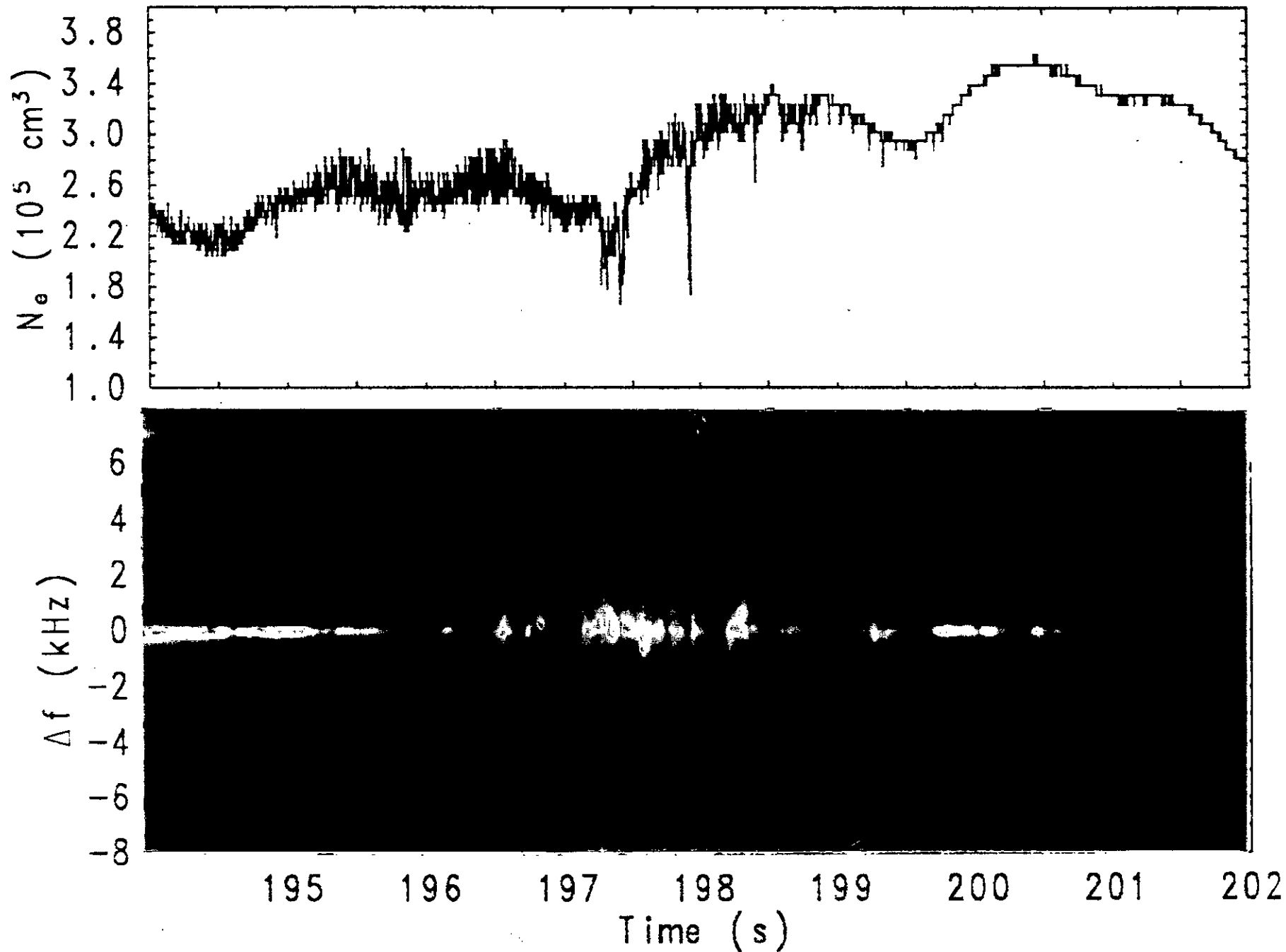
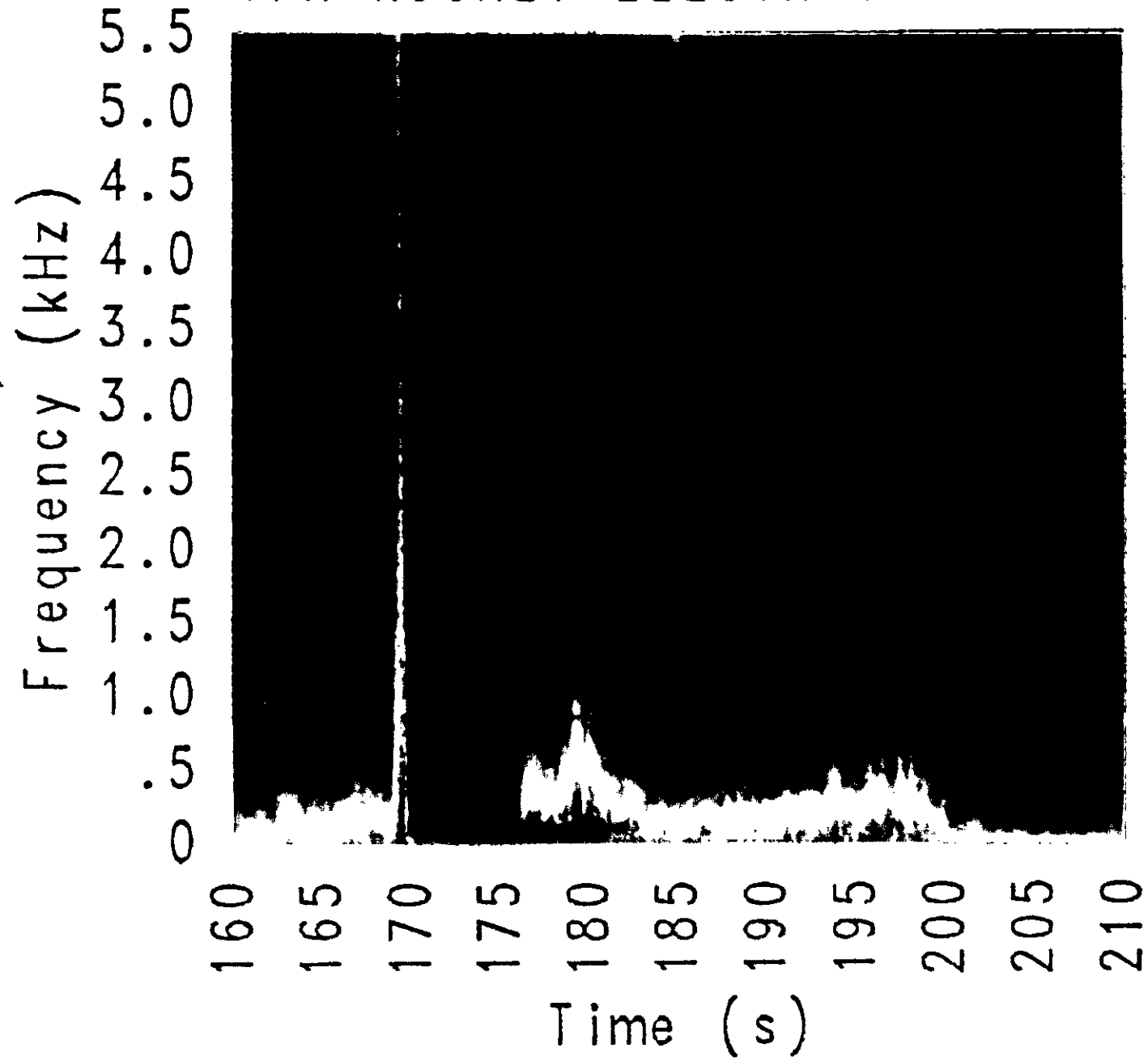


Figure 7.

IFH ROCKET ELECTRIC FIELDS



Ion Line, 30 May 1992, 04:11:00

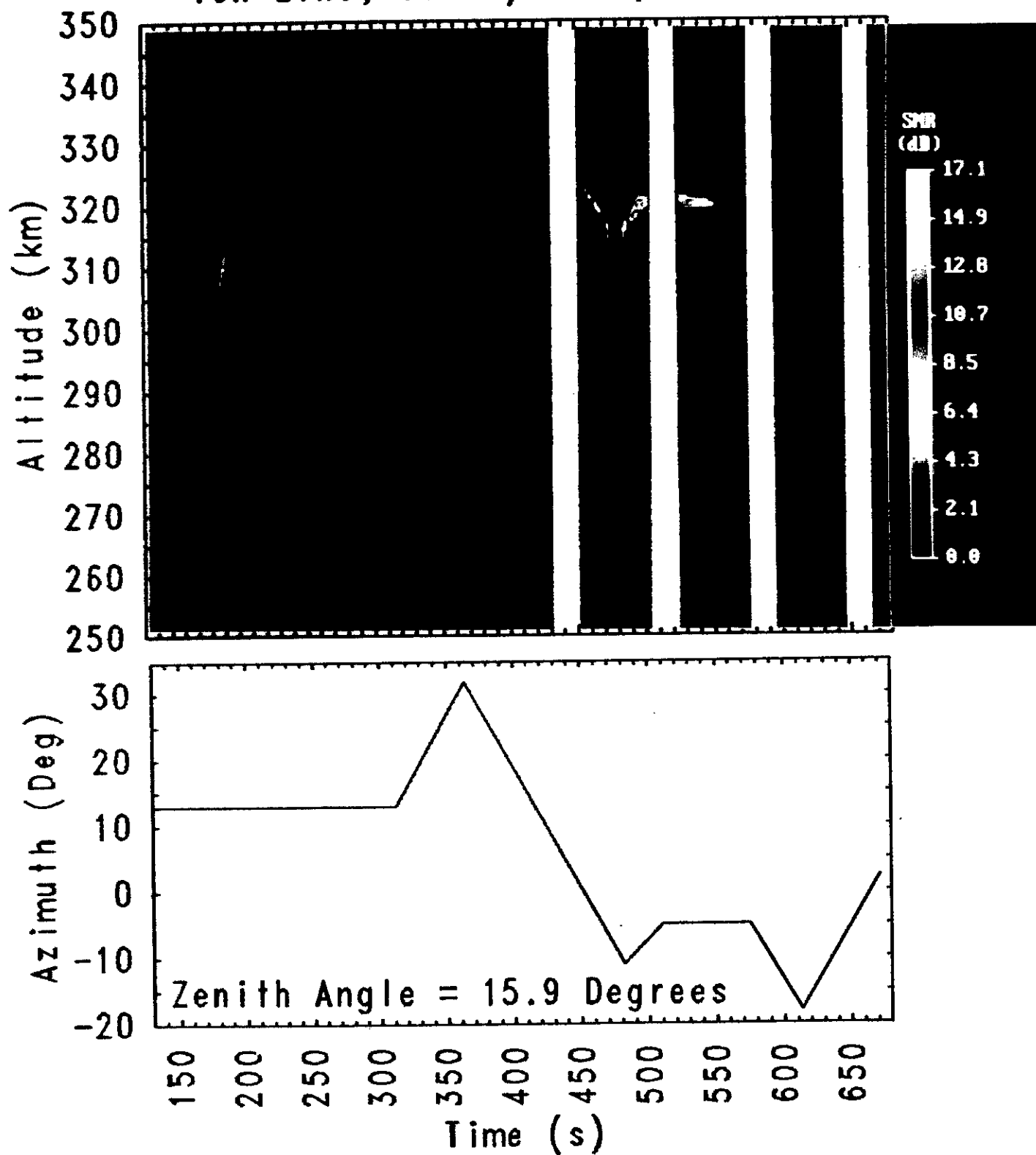


Figure 9.

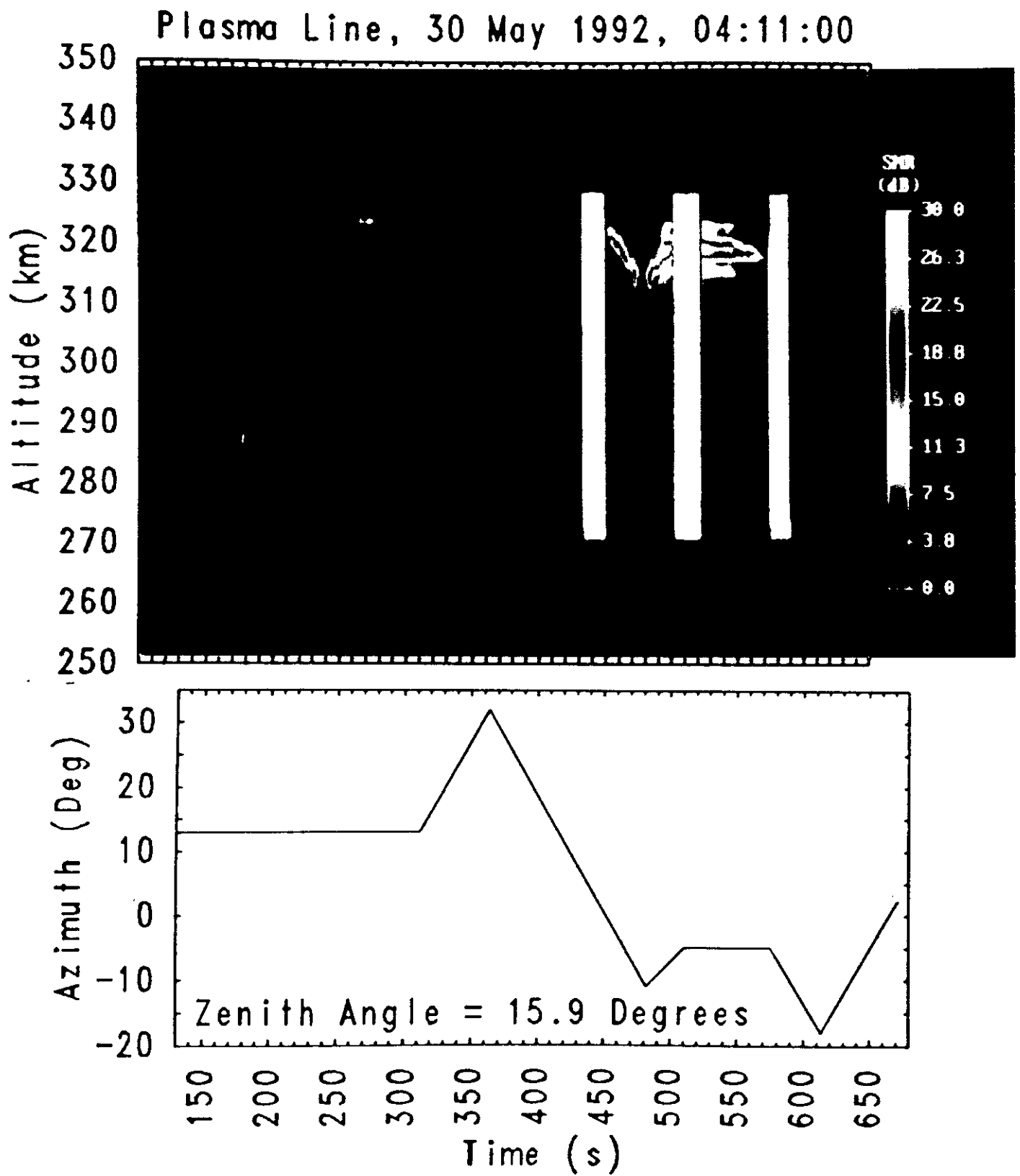


Figure 10.

30 MAY 1992 IFH DOWNSHIFTED PLASMA LINE

08

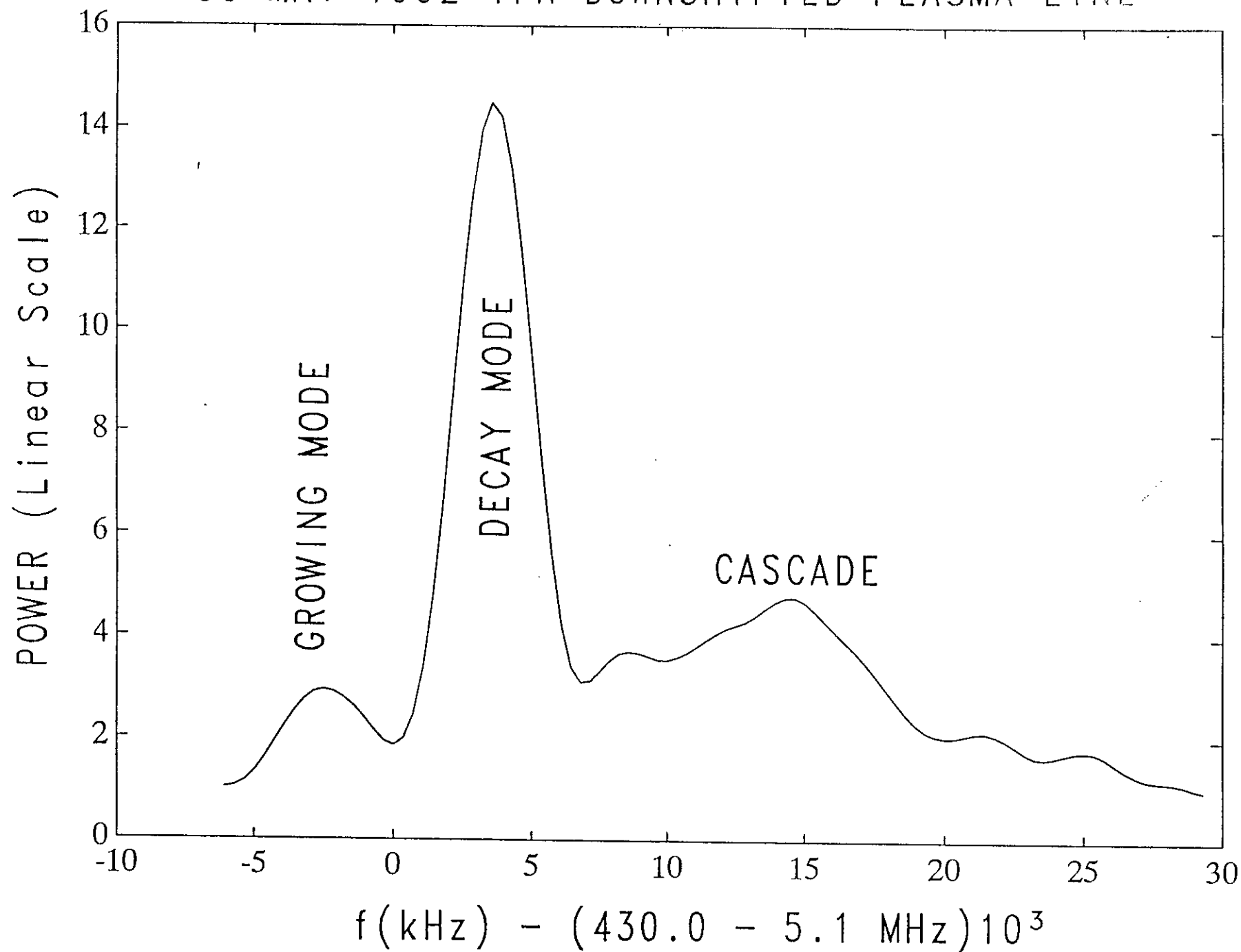


Figure 11.

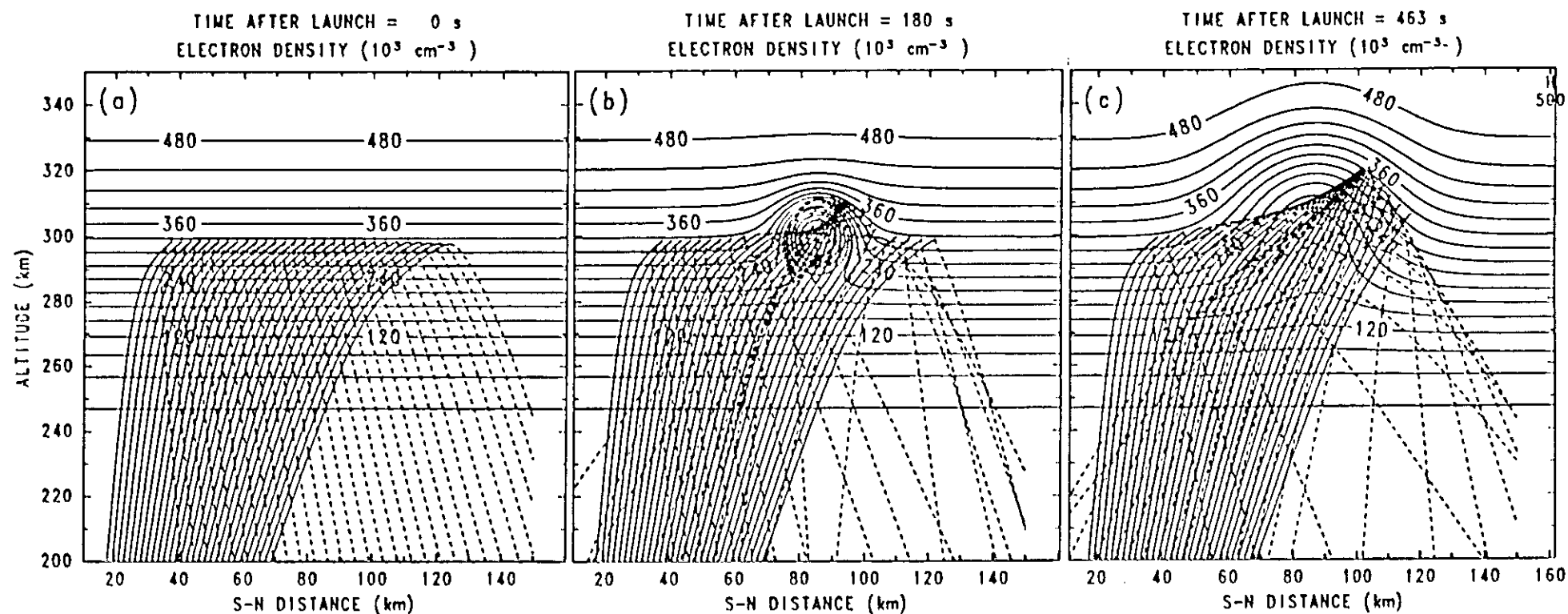


Figure 12.

EXPERIMENT AA-3 B

Title: Early-time Multi-ion Expansion Processes, Simulation of Interhemispheric Ion Flows, and HF-induced Ionospheric Striations

Principal Investigator: E. P. Szuszczewicz

Collaborative Investigators: F. T. Djuth, L. M. Duncan, F. Herrero, G. Earle, Z. Klos, M. Pongratz, P. A. Bernhardt, D. Papadopoulos

Location: Arecibo HF Heater Beam, Puerto Rico

Altitude: 250 - 350 km

Launch: Dawn, 8:37:31 UT

Date: 6 June 1991

Chemicals: Four 2.25 kg. Barium releases; 3 with lithium doping. (Ba/ 51% by mole Lithium, Ba/ 51% by mole Lithium, Ba/ 2% by mole % Lithium)

OBJECTIVE:

Using an instrumented sounding rocket, four small barium releases with chemical dopants were released in the Arecibo vicinity and the ensuing expansion processes diagnosed. The primary science objective was to study early-time multi-ion processes with applications to the simulation and testing of models for solar wind and inter-hemispheric ionospheric-magnetospheric flows. The experiment was also designed to investigate fundamental mechanisms of plasma expansions parallel and perpendicular to a magnetic field, and to study momentum and energy coupling of expanding plasmas to the background geoplasma environment. The principal diagnostics for this experiment were in-situ observations, ground based optics, and multi-frequency radars, supported by background ionospheric measurements using the Arecibo ISR and the Ramey digisonde. The experimental plan also involved an element synergistic with AA-3A, since the AA-3B trajectory provided the possibility for an upleg penetration of the HF heater beam yielding in-situ particle and yield measurements in the perturbed ionospheric domain.

Abstract

With a B-field sensitive attitude control system we were able to execute an experiment scenario which separately studied the parallel- and perpendicular-to-B expansion mechanisms. Our emphasis is on heavy/light ion mixtures using controlled amounts of Ba^+ and Li^+ to mimic the O^+ to H^+ mass ratio in the polar wind. We emphasize the very-early-time expansion phase (i.e., $t \leq 0.5$ sec), as the cloud evolves from continuum, through transitional, to collisionless flow regimes and we focus on the mass sensitive aspects of the expansion process as they are manifested in B-field controls, snowplow effects, and charged-particle acceleration mechanisms. We consider kinetic and electrodynamic mechanisms, Saha and photo-ionization processes, and the limited role of UV radiation in the very earliest phases of the expansion. In this working paper we concentrate only on the first two releases done near apogee which explore gyro-kinetics and quasi-parallel-to-B expansion mechanisms. We also concentrate on the pulsed plasma probe results and the corresponding measurements of the temporal evolution of the cloud as manifested in its characteristics in total density and ion discriminatory effects. Preliminary findings show: 1) clear evidence of gyro-kinetic effects on a Saha-like ionization source (i.e., an ionization process that operates at the very earliest phases of the cloud's evolution), 2) manifestations of snowplowed O^+ , 3) substantial quantities of Ti^+ in what otherwise should have been primarily Ba^+ and Li^+ in the expanding cloud, and 4) the need for a nonlinear ionization source at $t < 50$ msec to quantitatively match the observed cloud densities.

Introduction

The rocket payload was launched on day 158 (June 6, 1992) at 8:37:31 UT (4:37:31 L.T.) to an apogee approaching 370 km. The F-region ionosphere had been well behaved in the hours prior to launch with the F₂ peak nominally around 300 km and f_oF₂ nominally at 8.5 MHz. The time of launch was scheduled to guarantee that each of three chemical releases would be in the sunlit F₂ region, with the Earth's shadow height still high enough to minimize influences on ground-based optical diagnostics designed to remotely study the expansion processes as the rocket payload executed detailed "in-situ" measurements of particle and field distributions of the expanding cloud in the background ionosphere.

Figure 1 illustrates the experiment scenario which involved three release events. The first two involved Li-doped Ba (releases A and B) and the third involved the simultaneous release of two canisters containing Ba with no dopants. In all cases the canisters were thermite releases at an approximate ignition temperature of 2600 °K. Here we concentrate on releases A and B with details of the scenarios and the chemical constituents in the canisters presented in Table 1.

The payload was equipped with an attitude control system which allowed each of the canisters to be separated from the parent plasma diagnostic platform in a prescribed and controlled fashion. In cases A and B the canisters were jettisoned upwards along the magnetic field so that at the time of detonation the expanding cloud ions would be directly fluxtube-coupled to the diagnostics payload. Timers were set so that releases A and B occurred with canister-payload separations of 186 and 684 meters, respectively. In the case of the third event, the simultaneous release of canisters C and D, the separation process took place to guarantee that the expansion of the cloud ions in the direction of the diagnostic payload was perfectly perpendicular to B.

The instrument complement and diagnostic capabilities are summarized in Table 2.

Overview of Measurement Results

A synoptic view of the pulse plasma probe and wave detector results for releases A and B are presented in Figures 2 and 3 respectively. Those figures show the time histories of relative cloud ion-densities. I_e is the electron saturation current measured by the probe, and is directly proportional to the plasma density N_e . I_i is the ion saturation current measured by the probe which in zero-order is directly proportional to $N_j (m_i)^{-1/2}$. The ratio $(I_i/I_e)^2$ provides a high-time-resolved measurement of the mean-ion-mass. This is seen in Figure 4 which plots the theoretical dependence of the $(I_e/I_i)^2$ measurement on ion mass.

The probe measurements in both releases show a small increased density plateau on the leading edge which will be demonstrated as primarily composed of snowplowed O⁺ ions. The figures also show a significant difference in the time histories of relative densities. Release A shows multiple peaks while release B shows only one major peak. The analysis which follows will demonstrate that the differences are attributable to the experiment geometries. In release A the cloud and the diagnostic payload are moving across the magnetic field at an angle of 35°, while in release B both the cloud and the payload are moving in a direction parallel to B. The end result is manifested by gyro-kinetic motion of the cloud ions produced by Saha-like ionization.

Modeling Aspects of the Clouds Evolution

We note that the aspects of the cloud dynamics measured in this experiment are all within an approximate time of 0.5 seconds from initiation of the cloud release. This introduces attention to aspects of collision kinetics that might control the expansion process, and the cloud's optical thickness which might preclude contributions from solar UV photo-ionization. Figure 5 attempts to address both these issues. The left hand panel shows the dependence of the O⁺ mean-free-path as the ambient ionospheric ion interacts in time and in space with the expanding cloud neutrals. The neutrals themselves are modeled using a simple spherical diffusion approach with an effective 40%

vaporization applied to all canister chemicals (i.e., Ti, B, Li, and Ba). That left hand figure suggests that kinetic snowplow effects, if present at all, are there only at distances within 200 meters from the cloud center and at times shorter than 50 ms. We therefore conclude that any observations of O^+ density characteristics resulting in enhancements on the leading edge of the expanding cloud are more likely the effects of electrostatic processes and not collision kinetics.

The right-hand panel attempts to address the issue focused on the potential role of photo-ionization at the very earliest times studied in this experiment. That panel plots the neutral cloud column density (the number of cloud neutrals in a column one meter squared, extending from the cloud center to its edge). We compare this with the column density of the natural thermosphere from 100 km to free space (the horizontal line at 3×10^{18} atoms/m²). This number is used to represent the column density which effectively absorbs the bulk of photo-ionizing UV radiation from the Sun. While a more rigorous approach might be in order, the results here suggest that the cloud is optically thick for the first 200 ms of its expansion process. One should therefore conclude (or at least anticipate) that early-time ion observations will be dominated by an "instantaneous" Saha-like production process and accordingly represent a point plasma source. We note in advance that Saha-ionization at 2600 °K is insufficient to show quantitative agreement with measured density levels in the cloud, and there is the need for another "instantaneous" ionization source to quantitatively explain the results. One such candidate is a collision-induced streaming instability at times less than 50 ms.

The question of relative roles of ionization sources are taken one step further in Figure 6 which shows the time histories of Saha and photo-ionization characteristics in the clouds at the payload's position of 186 meters and 684 meters, in releases A (left hand panels) and B (right hand panels), respectively. It is clear from the temporal characteristics that the Saha process gives rise to a pulse-like density response at the position of the diagnostics payload, while the photo-ionization process provides a longer-term near-constant characteristic. The Saha profile, while more similar to the observations than the photo-ionization mechanism, are still a poor representation for the multi-peak characteristics demonstrated by the P^3 measurements. We investigate this further by imposing B-field controlled gyro-kinetic dynamics on the Saha ions and discuss those results below.

First we look at the geometry of the cloud in the release A configuration. This is shown in Figure 7. The rectangular coordinate system has its origin at the cloud center. The x-direction defines the axis parallel to B and +x is the direction toward the diagnostics payload. The y-direction is in the plane of the magnetic field vector and the canisters bulk velocity vector and it defines the direction perpendicular to B. At the release-A site the canister's center of mass velocity is moving at 1.23 km/sec. To consider the gyro-kinetic motion we add the cloud's radial expansion velocity to its center-of-mass velocity and consider gyro-orbits as a function of spherical coordinates θ and ϕ , and time. An important consideration involves the 3-dimensional aspects of the gyro-orbits and their intersection with the VB plane (i.e., the plane containing the cloud's bulk velocity vector and the geomagnetic field) since this is the plane that contains the diagnostics payload, and the P^3 sensors will only see the orbiting particles when they intersect that plane.

A quick overview of Larmor radii for each of the chemical constituents in the cloud under release A conditions is depicted in Figure 8. We make only two major comments about the information in that viewgraph: 1) Li^+ and B^+ , because of their light masses have small Larmor radii, of the order of 4 and 6 meters respectively for θ and ϕ both near 90°; 2) the heavier ions Ti^+ and Ba^+ have maximum Larmor radii of 30 and 90 meters, respectively. This suggests improved P^3 space-time diagnostics capabilities for the Ti^+ and Ba^+ ions. We show this is indeed the case.

We now return to the P^3 data for release A to revisit the structure and the temporal framework of the observations. This data is shown in a different format in Figure 9 where the left and center panels are measurements of electron-saturation and ion-saturation currents, respectively, while the right panel represents P^3 measurements of mean-ion-mass. We draw attention to the major peaks and the smaller peaks between them, arguing that in the numerical simulation results to be shown in the next figure

we identify the first peak with Ti^+ and the second major peak with Ba^+ . The small peaks between them are Larmor-period multiples of Ti^+ . In all cases these peaks will be shown to be uniquely attributable to the mass-dependent gyro-kinetics of the species and their space-time dependency as they intersect the plane containing the diagnostics payload.

Figure 10 shows particle orbit intersections with the VB plane for Ti^+ on the left and Ba^+ on the right. Each of the panels left-to-right are at exactly the same times and the panels increase by 25 ms increments from top to bottom. The top panel shows the integration of intersecting particle orbits with the VB plane in the 275 - 300 ms time frame relative to the release initiation. The line to the right in each of the panels identifies the location of the diagnostics payload relative to the center of the release located at the coordinates (0,0). When these particle orbits cross the line designating the payload location, the associated currents will be collected by the P^3 instrumentation. The panels start at the 300 ms region because at all prior times there were no particle-payload intercepts. The first intercept occurs at 325 ms and only for Ti^+ ions (see the second panel). At this point in the simulation P^3 instruments would be measuring currents due only to Ti^+ and no currents due to Ba^+ . The Ti^+ currents last about 50 ms, then are undetectable in the 350-375 ms time frame, and reappear for P^3 measurements again for about 50 ms between 350 and 425 ms.

We now look to the right hand set of panels which are focused on Ba^+ orbits. There were no Ba^+ currents at the time of the first Ti^+ intersection with the payload. There were no Ba^+ current at the time of the second Ti^+ intersection with the payload. But there were strong Ba^+ currents (observed for the first time by P^3) during the fourth Ti^+ intersection. In terms of current measurements the numerical simulation suggests Ti^+ currents as a pulse near 350, 375 and 400 ms, and a Ba^+ pulse (masking a fourth Ti^+ peak) in the 425-475 ms time frame. This is in good agreement with the observations, considering the assumptions in the model. The current peaks and associated ion masses are identified in the data shown in Figure 9.

In Figure 9, we draw additional attention to the leading edge of the cloud which shows a plateau of increased densities (see characteristics in the I_e and I_j plots, the left and center panels, respectively). We maintain that this plateau is largely O^+ , resulting from electrostatic snowplow effects. Associating this leading-edge plateau with O^+ is supported by the P^3 measurements of mean-ion-mass reflected in the right-hand panel in Figure 9, which shows little-to no change in the mean-ion-mass measurement as the temporal characteristics move from the background environment of the O^+ -dominated F-region into the cloud. More quantitatively and more convincingly we point to the absolute values of the $(I_e/I_j)^2$ measurement in the third panel. We draw attention to the small plateau region at the cloud's leading edge with an $(I_e/I_j)^2$ value near 10,000 to the region of the first observed peak, with a value near 40,000 and the region of the second major peak, with a value near 90,000. We identify those with O^+ , Ti^+ , and Ba^+ , respectively, and confirm those with the theoretical foundations for the analysis procedure presented earlier in Figure 4. Figure 4 shows that 10,000, 40,000, and 90,000 are the $(I_e/I_j)^2$ measurement domains for mean-ion-masses at 16, 48 and 137 amu, respectively; that is O^+ , Ti^+ , and Ba^+ .

Summary

This rocket experiment provided a unique laboratory-like experiment to diagnose the very-early-time characteristics of an expanding cloud and its interaction with the background ionosphere. The preliminary findings point to the dominance of Saha-like ionization (or some other "instantaneous" ionization process) and gyro-kinetic single particle orbits as the controlling terms for the initial phenomenological and morphological characteristics of the expanding plasma. The "discovery" of Ti^+ was unexpected, suggesting an incomplete understanding of the burning process in the canister, including the prevailing temperatures. At 2600 °K, Saha supports and justifies the kinetic calculations and qualitative features of P^3 measurements in the measured density profiles, but suggests density levels substantially lower than those observed.

EL COQUI/CRRES ROCKET CAMPAIGN SZUSZ36.064CE

A CONTROLLED ROCKET-BORNE INVESTIGATION OF MULTI-ION EXPANSION PROCESSES

E. Szuszczewicz, G. Earle, T. Bateman, Z. Klos, A. Kiraga, F. Herrero,
F. Djuth, M. Pongratz, P. Bernhardt and K. Bibl

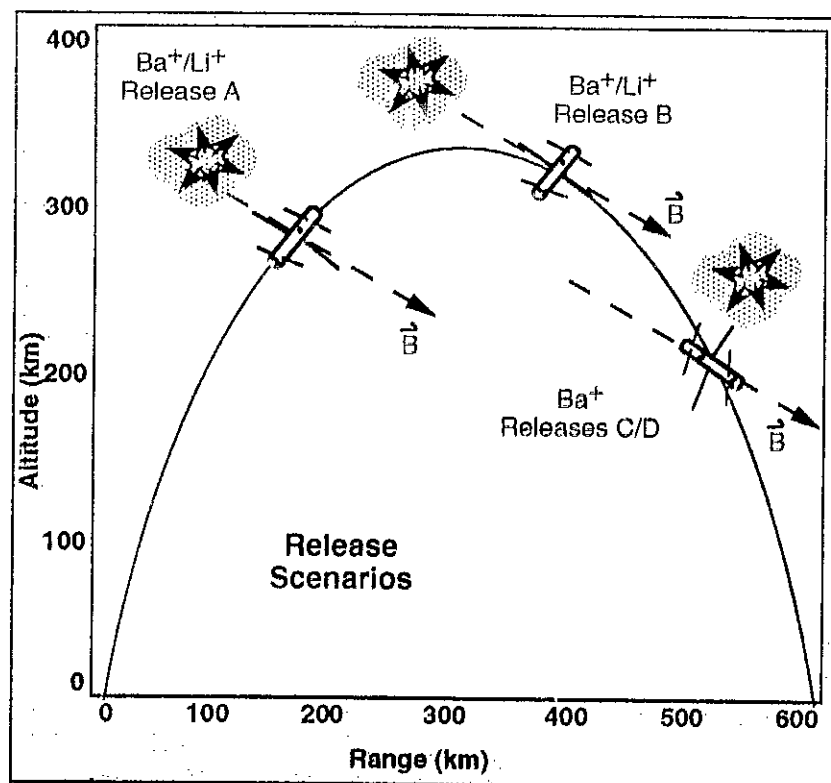
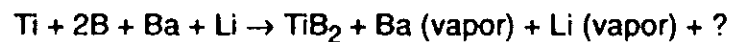


Figure 1

CHEMICAL CONSTITUENTS AND ASPECTS OF THE PARALLEL-TO-B SCENARIOS

- Thermite Release ... 3.4 kg Total Chemicals ... 2600°K "Ignition" Temperature



<u>Element</u>	<u>amu</u>	<u>V_i[v]</u>	<u>τ_i[s]</u>	<u>%wt</u>	<u>$N_0 \times 0.4$</u>	<u>τ_i[ms]</u>
Lithium	6.94	5.39	3450	1.38	$1.62(10^{24})$	12.2
Boron	10.82	8.3		22.64	$1.7 (10^{25})$	19.1
Titanium	47.9	6.33		50.18	$8.52(10^{24})$	84.7
Barium	137.36	5.21	28	25.8	$1.53(10^{24})$	243

	<u>Release A</u>	<u>Release B</u>
Payload Motion	— — — — — Across \vec{B}	Along \vec{B}
Release Time (MET)	— — — — — 180 sec	365 sec
Release Altitude	— — — — — 290 km	359 km
Ionospheric Domain	— — — — — F_2/O^+ dominant Dawn/Sun-Lit	F_2/O^+ dominant Dawn/Sun-Lit
Payload Canister Separation	— — — 186 meters	684 meters

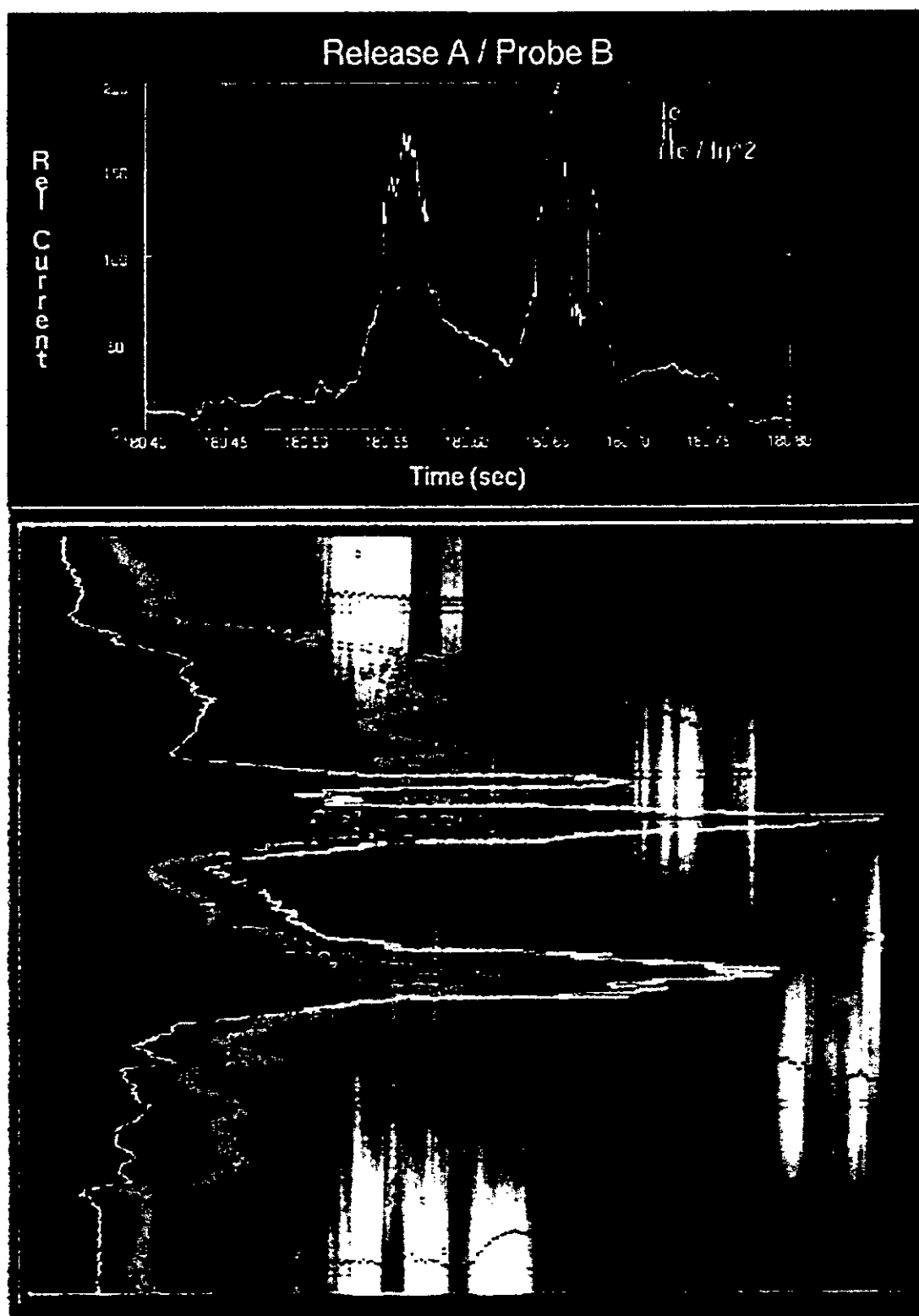
INSTRUMENTS AND MEASURED PARAMETERS

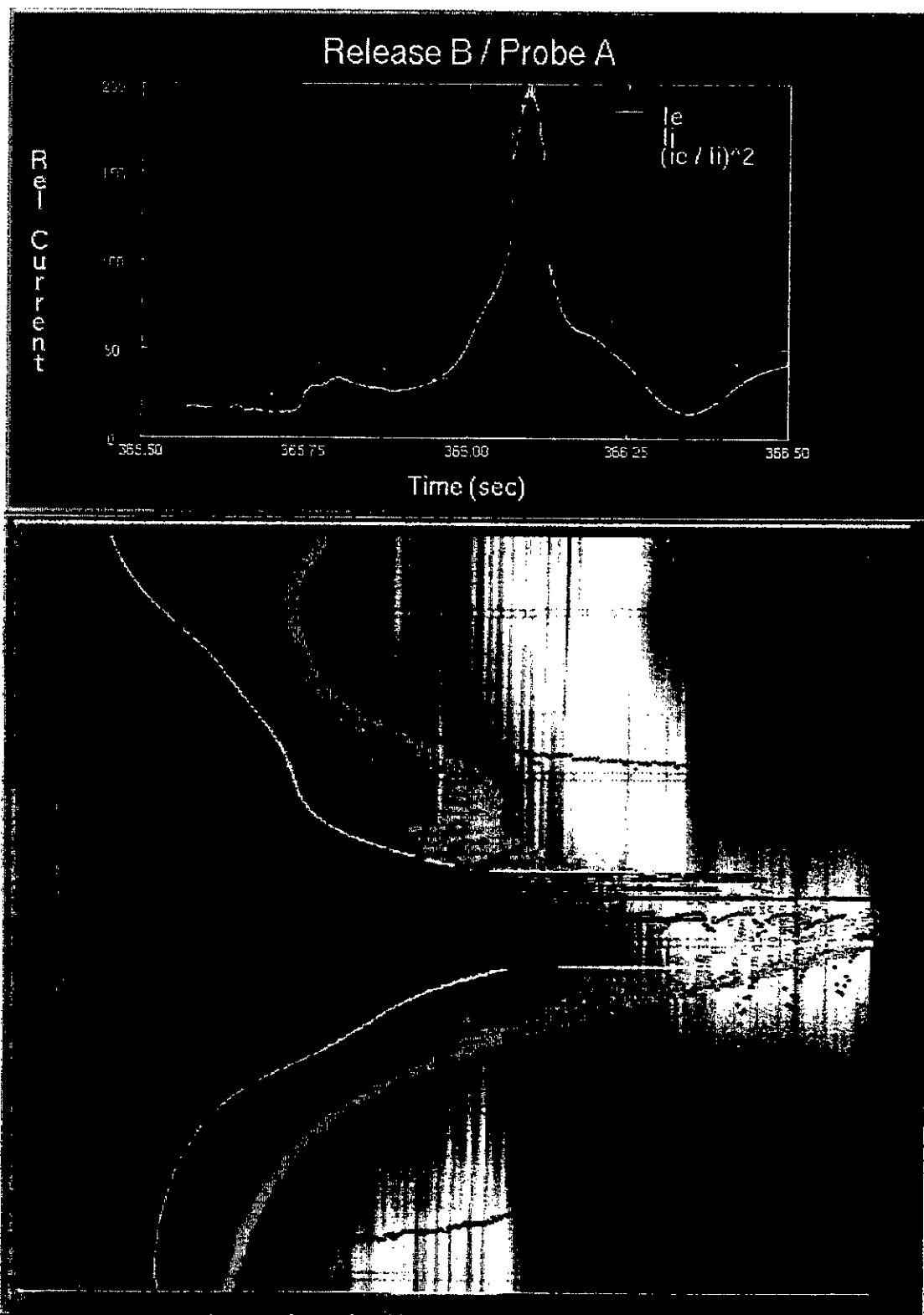
Instrument	Parameter	Dynamic Range	Time (Space) Resolution	
P ³	N _e , N _i	10 ³ -5 x 10 ¹⁰ /cm ³	a) 250-300ms	(250 m)
			b) 250 μs	(25 cm)
	δN _e /N _e	> 0.5%	250 μs	(25 cm)
	T _e (hot & cold)	0.1 - 20 eV	250-300 ms	(250 m)
	<M _i >, δM _i	16 - 180 amu	a) 250-300 ms	(250 m)
			b) 250 μs	(25 cm)

RMS/TAWRS	M _i , \vec{V}_n	O ⁺ , N ₂ ⁺ , NO ⁺ , O ⁺ , H ₂ O ⁺ , Li ⁺ , Ba ⁺ , S _R ⁺	30 ms	(30 m)
		50 m/s \lesssim V _n \lesssim 10 ³ m/s		

E-Field (Waves)	\vec{E}	0.1 - 400 mV/m	100 ms	(3 m)
		100 kHz $\leq f \leq$ 10 MHz		

B-Field	\vec{B}	60 - 60,000 nT	2 ms	(2 m)
		0 $\leq f \leq$ 500 Hz		





P³ MEASUREMENTS OF MEAN-ION-MASS

$$(I_e/I_i)^2 = \frac{T_e}{T_i} \left(1.67 (10^{-27}) \frac{M}{m} \right) \frac{1 + \frac{V_e}{KT_e}}{1.67 (10^{-27}) w^2 \frac{(\sin[\theta_0])^2}{2KT_e} M + \frac{V_i}{KT_i}}$$

V_e = e-saturation bias potential

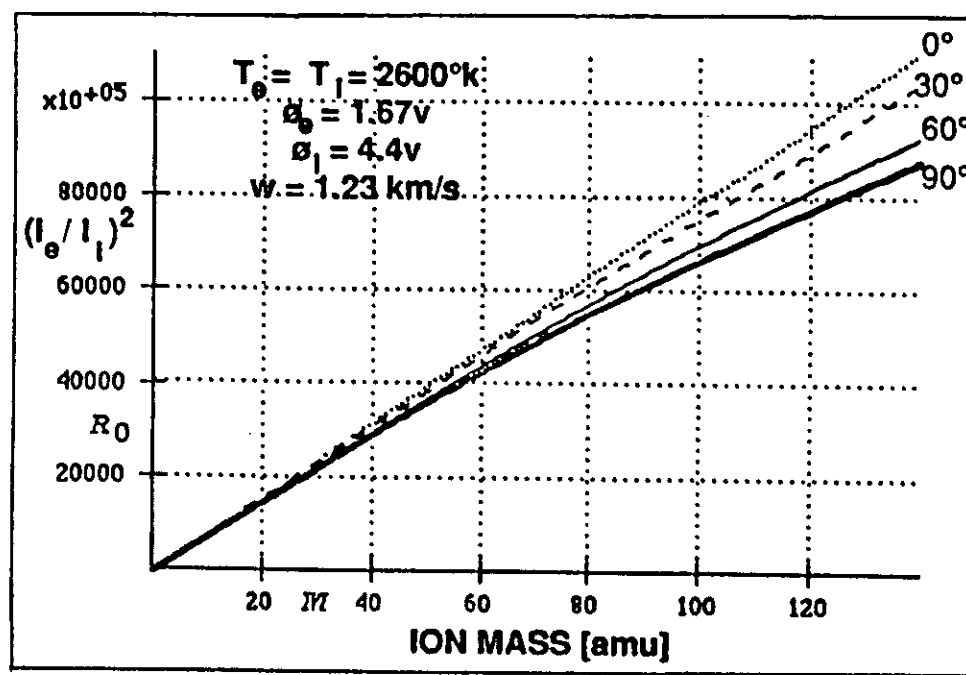
V_i = i-saturation bias potential

w = bulk ion (expansion) velocity

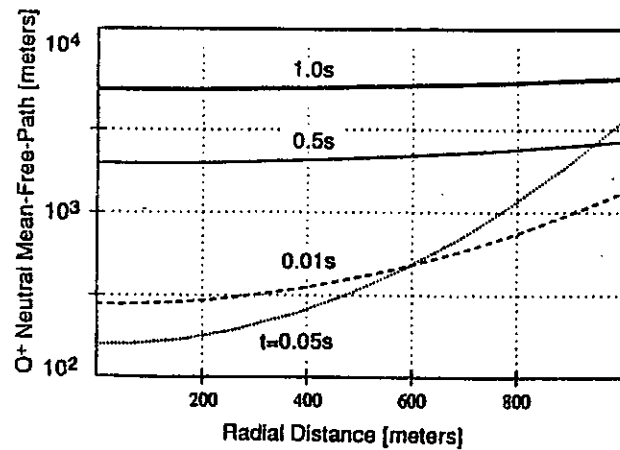
M = ion mass

m = electron mass

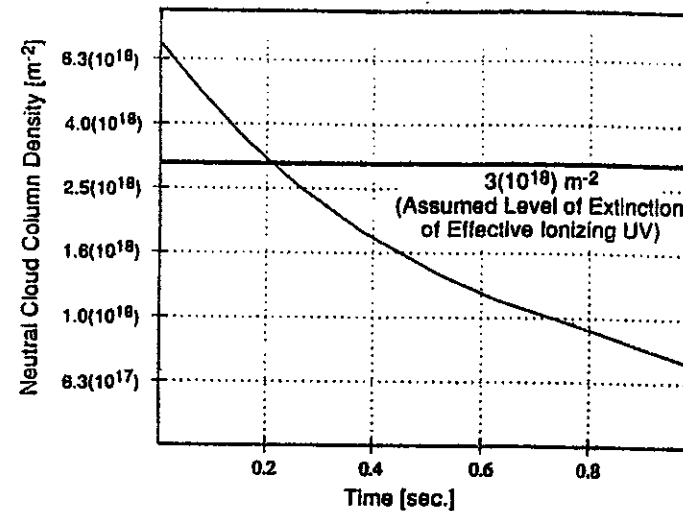
θ_0 = angle between w and P3 axis



NEUTRAL/O⁺ COLLISIONALITY AND UV OPTICAL THICKNESS



Collision Mean-Free-Path in Gaseous Cloud of Ba, Li, B, and Ti atoms.



Neutral Cloud Column-Density as a Function of Time, Illustrating Temporal Domain ($t \geq 0.2s$) in which UV Radiation Effectively Penetrates and Creates Photo-ionization Products.

SPHERICAL DIFFUSION MODEL SAHA vs PHOTO-IONIZATION CHARACTERISTICS

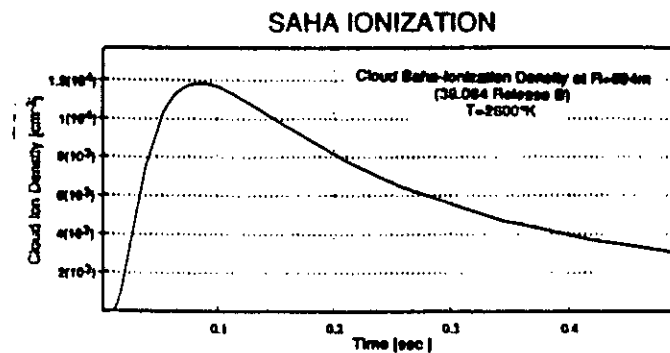
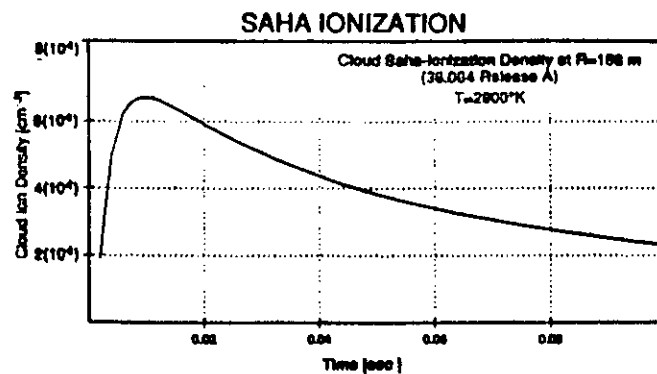
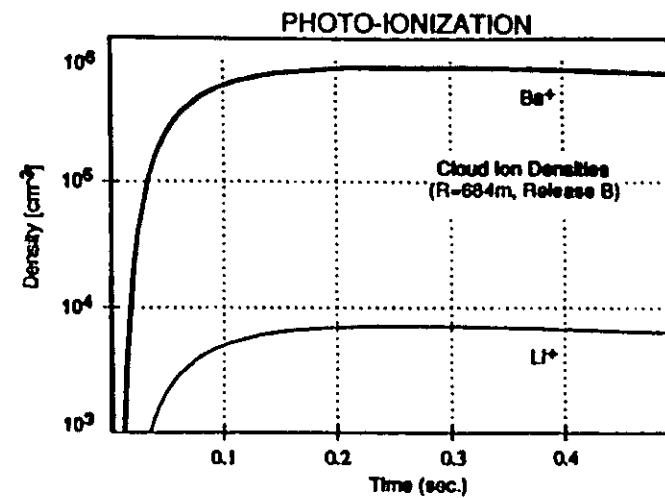
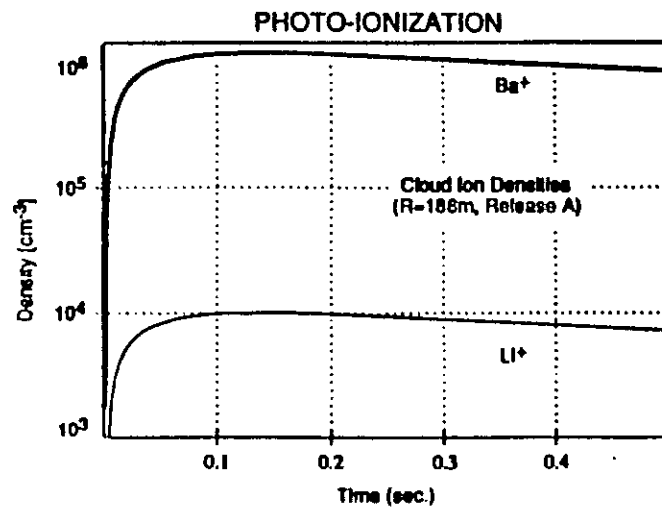


Figure 6

RELEASE "A" GEOMETRY

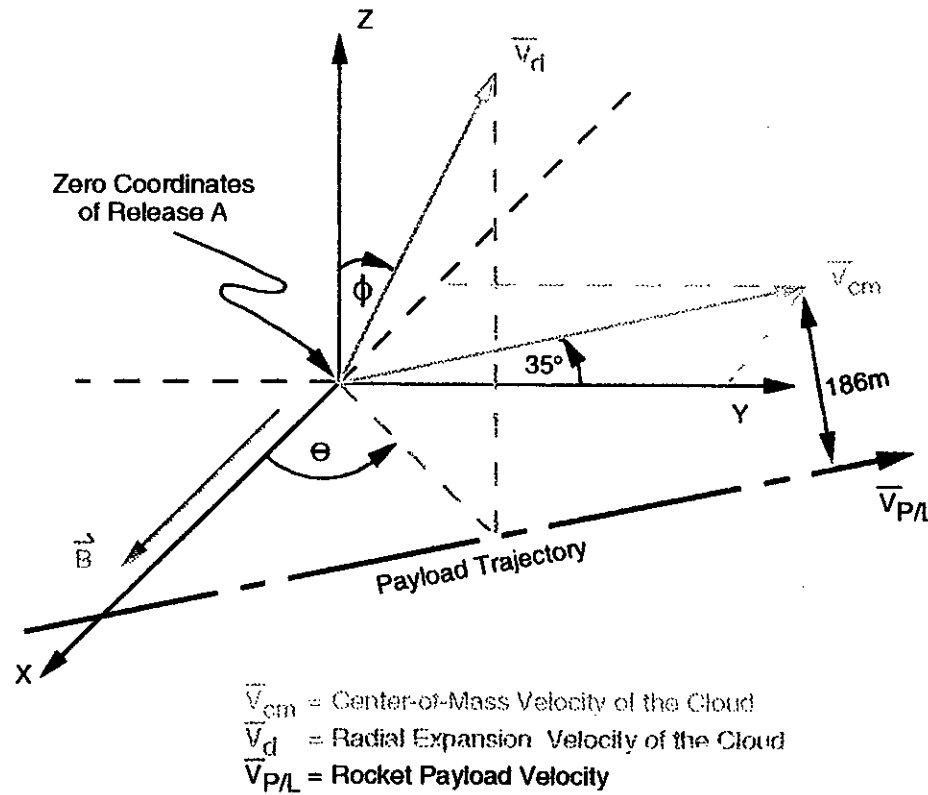


Figure 7

DISTRIBUTION OF LARMOR RADII FOR RELEASE A IONS

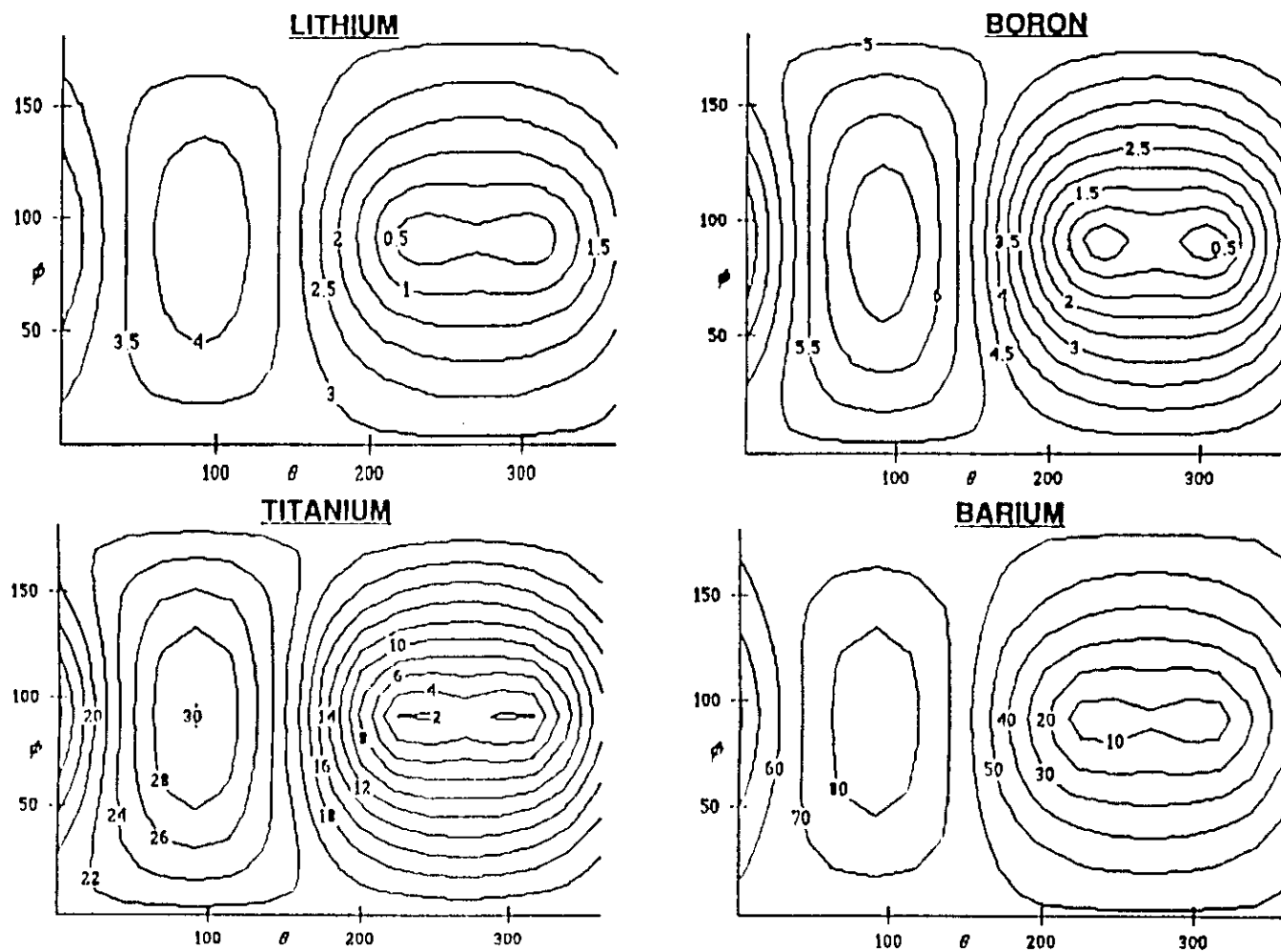


Figure 8

P³ RELEASE "A" MEASUREMENTS TEMPORAL CHARACTERISTICS OF RELATIVE DENSITY AND MEAN-ION-MASS

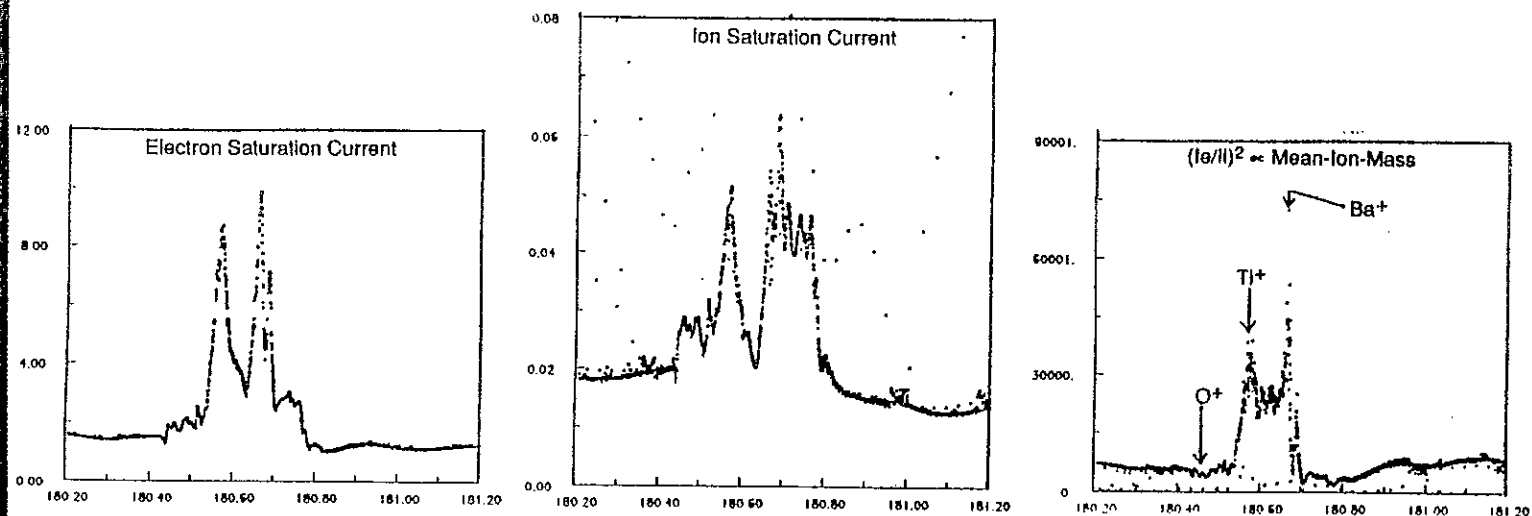
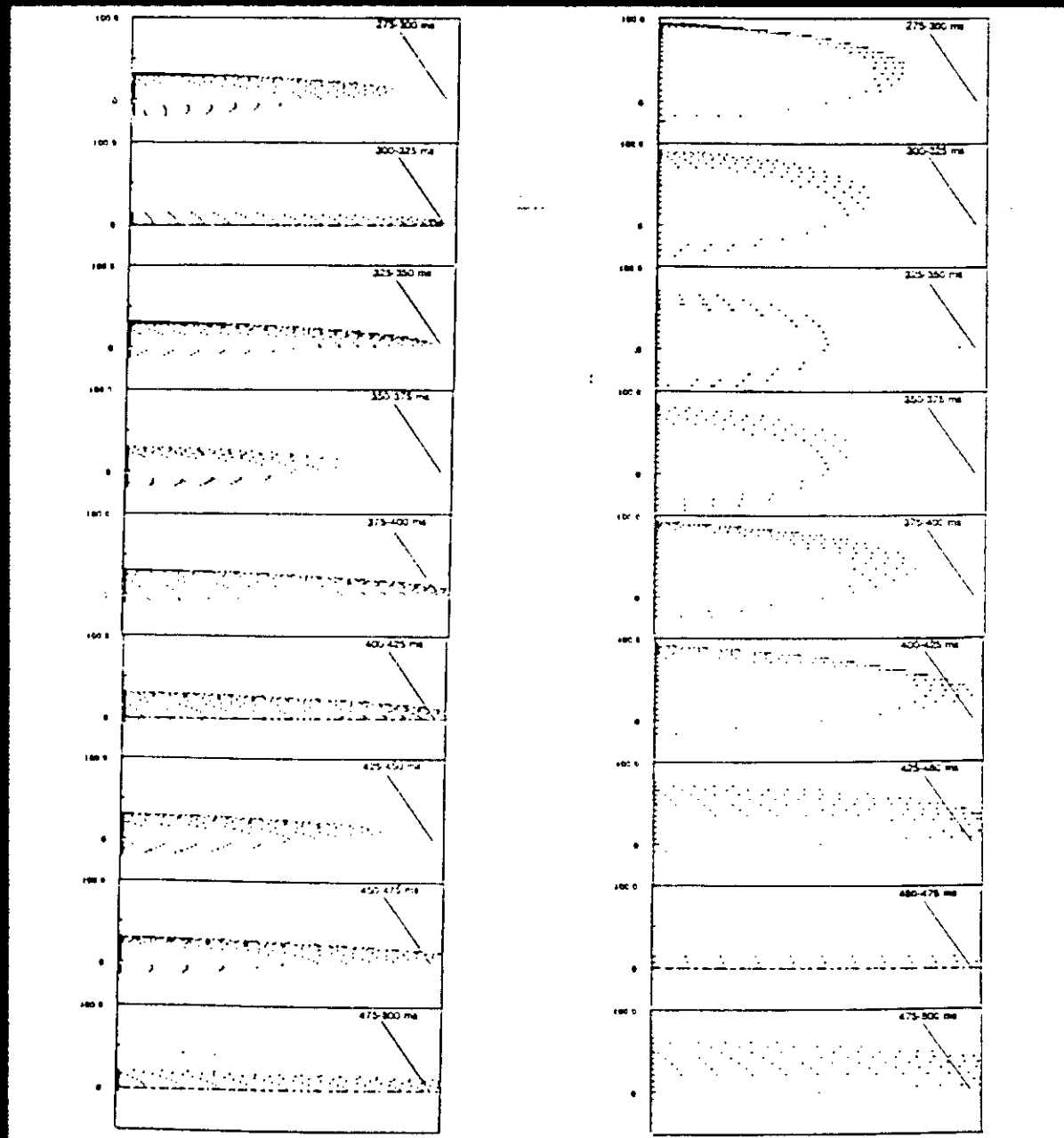


Figure 9

LARMOR ORBIT PARTICLE CURRENTS IN THE V.B PAYLOAD DETECTION PLANE



AGU CRRES-9

EXPERIMENT AA-1

Title: F-Region Irregularity Evolution

Principal Investigators: E. C. Weber and F. T. Djuth,

Collaborative Investigators: K. Groves, M.. Kelley, K. Vickery, L. Linson

Location: Arecibo Incoherent Scatter Radar (ISR) Beam, Puerto Rico

Altitude: 250 km

Time: Dawn, Launch 05:01:15 AST, Release ~05:03:45 AST

Date: 2 July 1992

Chemicals: 22.5 kg. Barium/2 % by mole Strontium

OBJECTIVE:

The earth's ionosphere normally reflects high-frequency (HF) radio waves. This radio wave reflection off a smooth conducting ionosphere allows reception of AM radio, long range HF communications, and over-the-horizon surveillance radar. When stressed, this smooth layer fractures and somewhat like a fractured pane of glass obscures transmission in some directions and gives blinding glints in other directions. The ionosphere is electrically charged, and these fractures line up along the direction of the magnetic field and act like a picket fence to scatter radio waves.

Understanding this plasma fracturing process is a great challenge, both at the level of basic physics and at a practical level of anticipating when the worldwide network of HF and satellite communications will experience degraded performance in certain regions of the world. This experiment and a companion experiment AA-7 will stimulate this plasma fracturing process with large barium releases in the F and E regions of the ionosphere over the Arecibo radar. The radar will diagnose the details of the structuring, and at the same time receivers on aircraft will monitor fading and disruption of satellite radio signals. Comparison of observation with theoretical predictions will be the acid test of present understanding of principles of plasma physics with far reaching implications.

RESULTS:

Figures 1 through 5 depict the electron density as recorded.

TORTUGERO, PUERTO RICO

STATION LEADER AND/OR OTHER CONTACT:

Morgan W. McCook
Consultant

TYPE AND DESCRIPTION OF DATA ACQUIRED: Still photography. ASA 1600 color film, 210 mm f 5.6 lens.

FIELD(S) OF VIEW OF INSTRUMENTS: 12° - 13°

TIME PERIODS OF DATA: 05:02 AST. Sequence of 11 frames ~ 1 minute intervals.

FRAME RATE: at intervals of 30 seconds.

ASSESSMENT OF DATA QUALITY (CLOUD COVER, LIGHT CONTAMINATION): Clear. Excellent quality and examples of short range visibility from launch area.

INITIAL FINDINGS: Barium found and photographed clearly.

ADDITIONAL RESEARCH: Comparison of G-8 High Altitude release to compare visibility at widely different altitudes.

ST. CROIX, USVI (CARIBBEAN)

STATION LEADER AND/OR OTHER CONTACT:

Wesley E. Swartz SPAN - wes@magneto.ee.cornell.edu
Engineering Theory Center PHONE (607) 255-7120
Cornell University
Ithaca, NY 14863

TYPE AND DESCRIPTION OF DATA: 50 MHz coherent backscatter radar data

FIELD(S) OF VIEW: 5 degree beam, site location 17.65 N, 64.89 W. Beam azimuth fixed at 290.3 degrees. Zero aspect angle at upper E region heights (130 - 150 km altitudes).

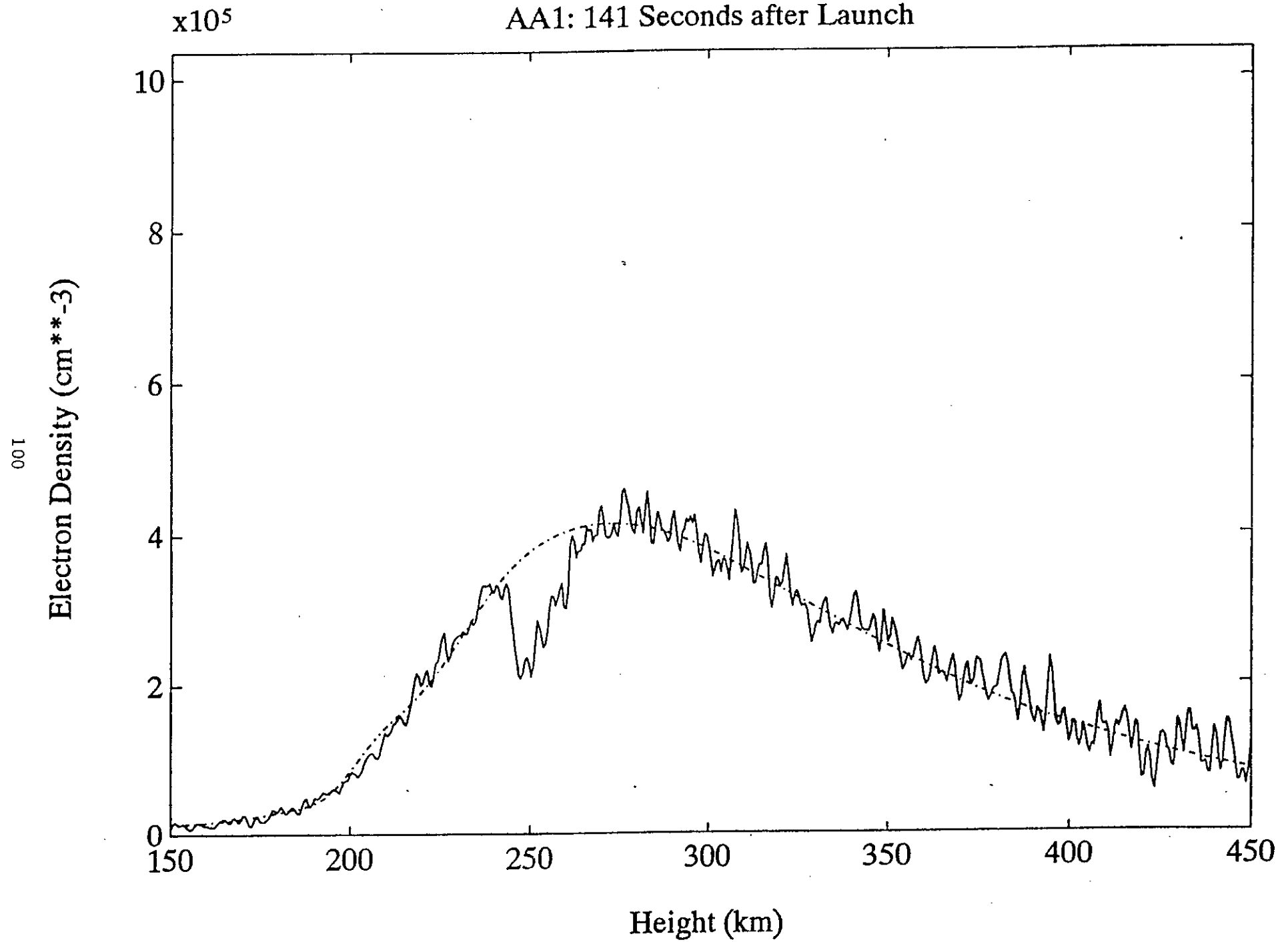
TIME PERIODS OF DATA: all night runs: 0000 to 1100 hours, July 2 - July 11, 1992

SAMPLING RATES:

11 ms IPP usually, 4 ms IPP during possible/actual launch times with 30 minute window

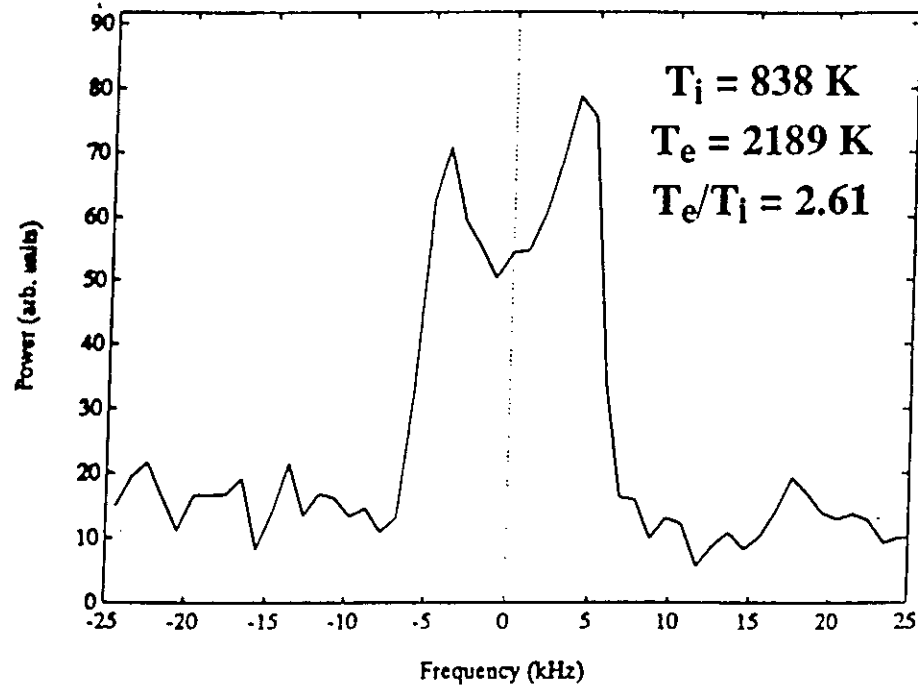
ASSESSMENT OF DATA QUALITY (CLOUD COVER; LIGHT CONTAMINATION): Radar detection of releases was minimal to none detectable. Possible detection of rockets and release events are confused with ongoing meteoric activity.

AA1: 141 Seconds after Launch

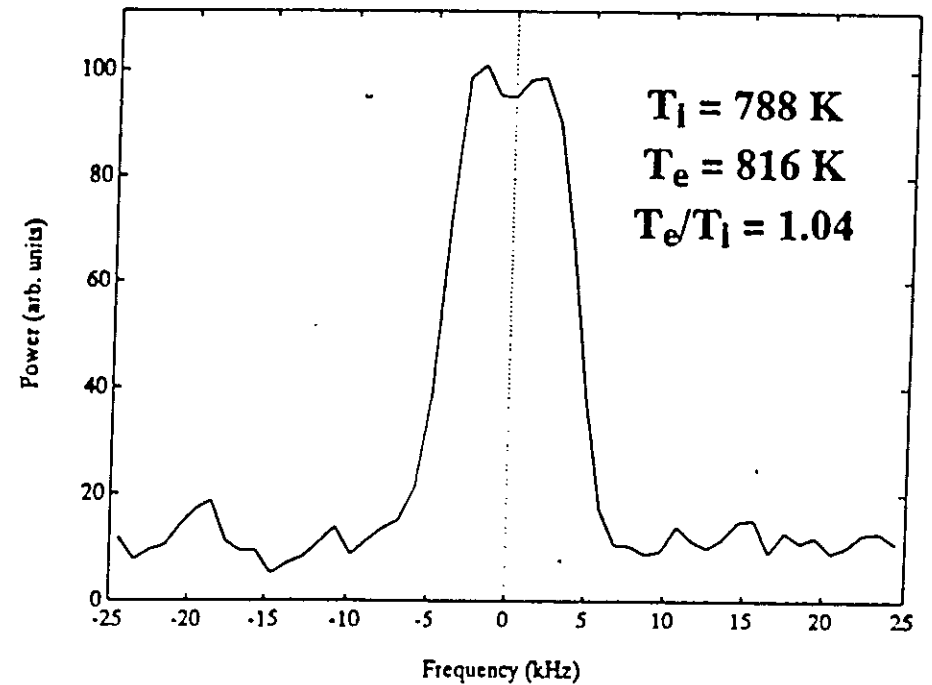


142.8 - 148.2 s after launch

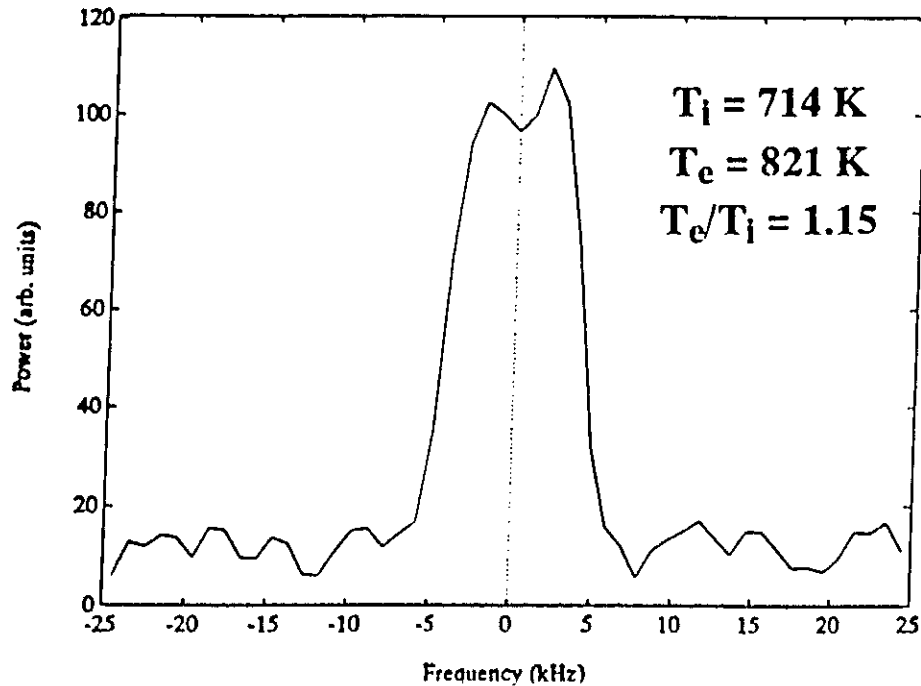
AA1: 245 - 261 km



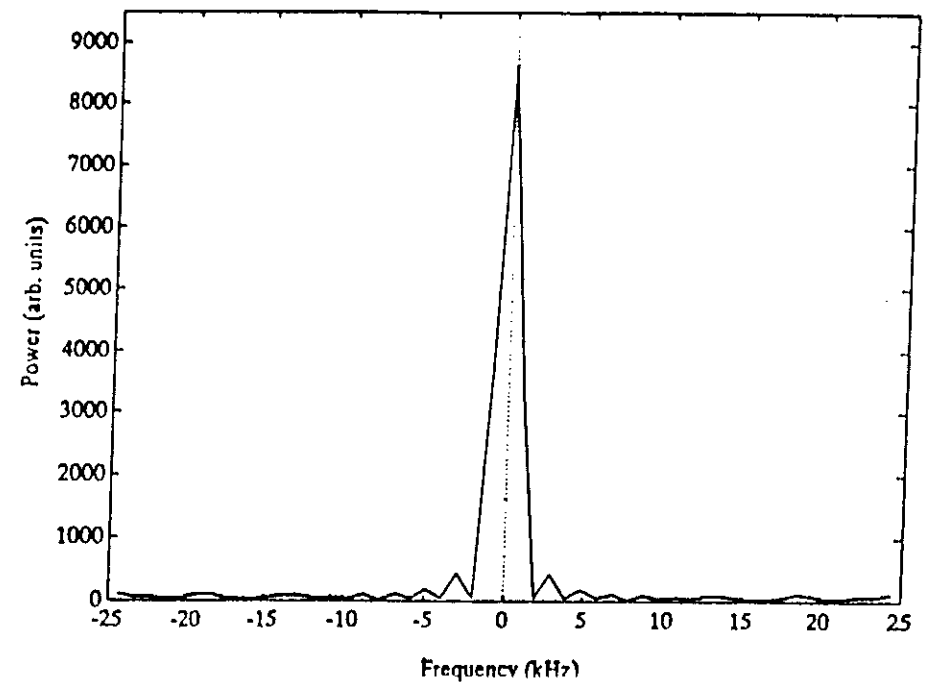
AA1: 272 - 300 km



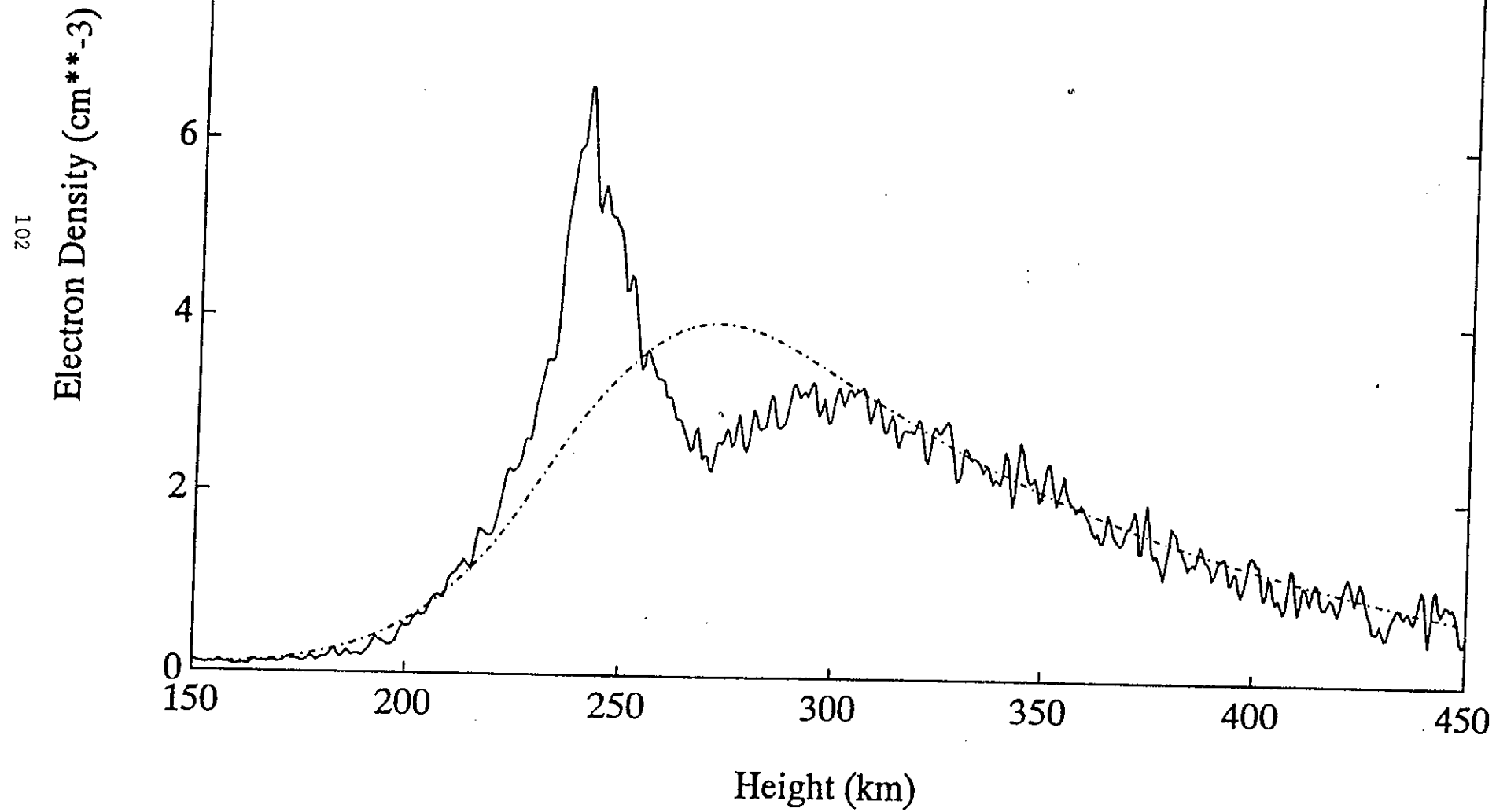
AA1: 225 - 243 km



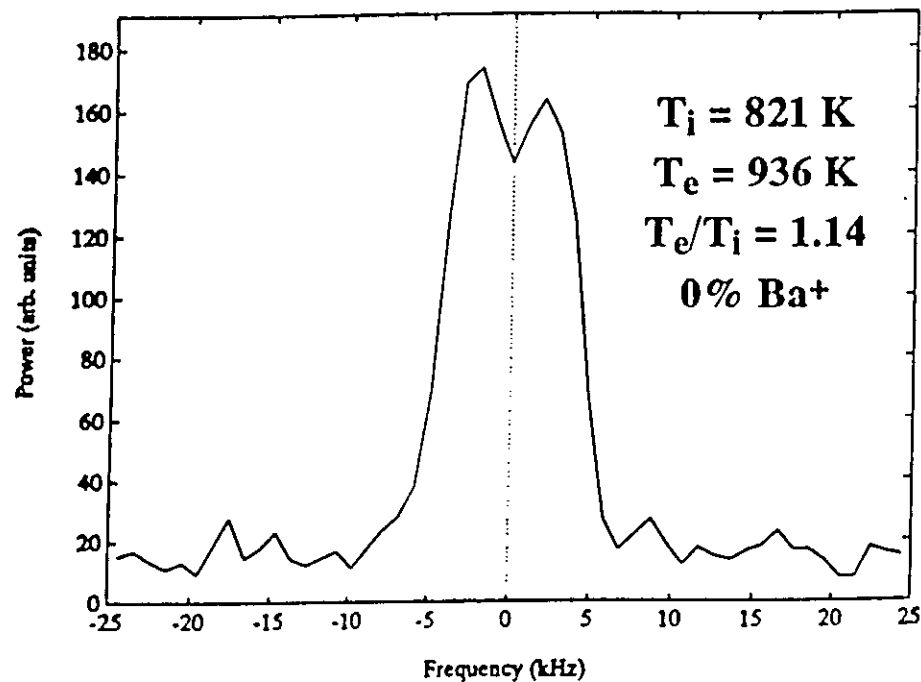
AA1: Tx Pulse



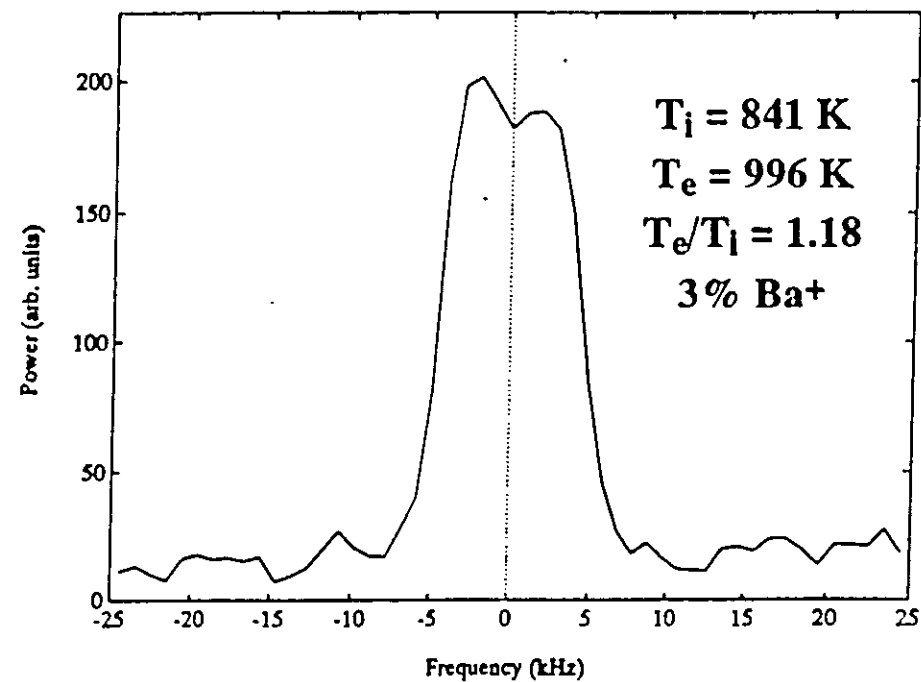
AA1: 1041 Seconds after Launch



AA1: 300 - 320 km

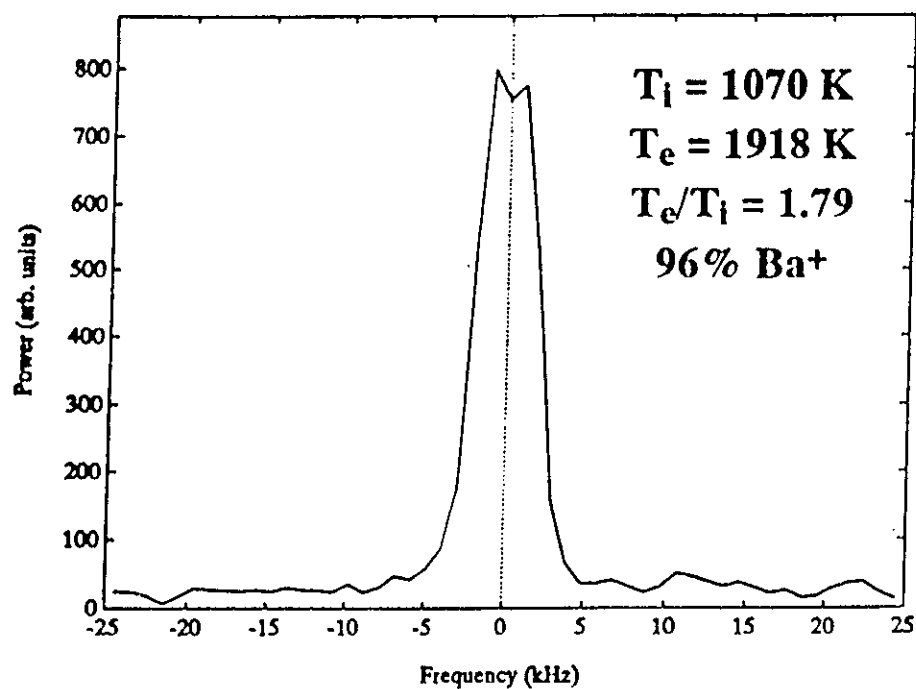


AA1: 279 - 300 km

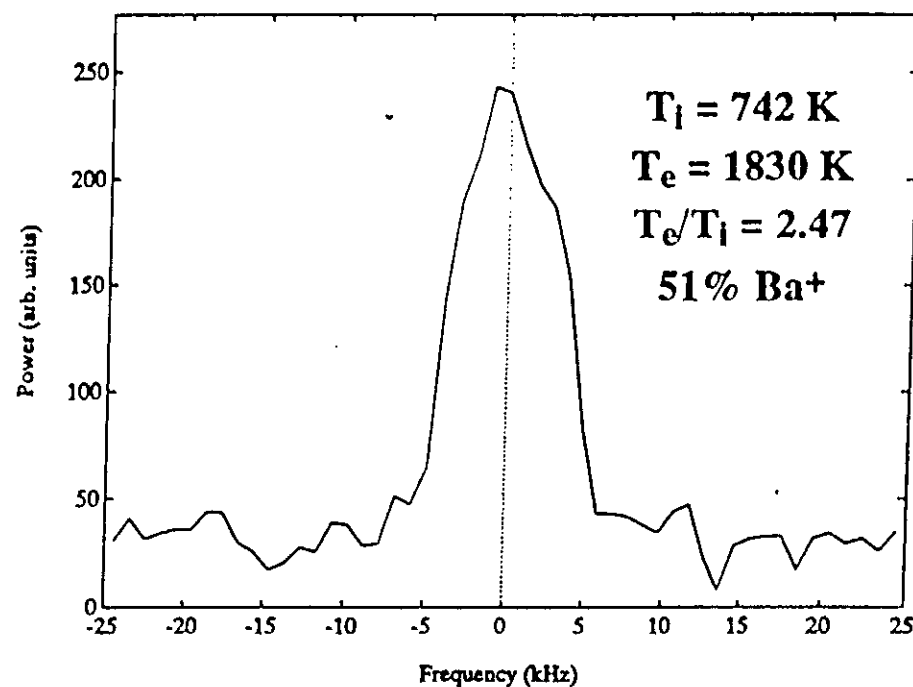


103

AA1: 240 - 250 km



AA1: 264 - 271 km



EXPERIMENT A-7

Title: E-Region Image Formation

Principal Investigator: E. C. Weber

Collaborative Investigators: K. Groves, F. T. Djuth, M. Kelley, J. Huba

Location: 40 km north of Arecibo

Altitude: 250 km

Time: Dawn; Launch 04:58 AST, Release ~04:59:40

Date July 4, 1992

Chemicals: 22.5 Kg. Barium/2% by mole Strontium

OBJECTIVE:

The layers of the ionosphere, the D, E and G regions, are connected by magnetic field lines. In this experiment a large barium release in the F-region will be placed so that the connected E region is directly over the Arecibo radar. This experiment is the companion to AA-1 discussed earlier.

ST. CROIX, USVI (CARIBBEAN)

STATION LEADER And/or OTHER CONTACT:

Wesley E. Swartz
Engineering ~c Theory Center
Cornell University
Ithaca, NY 14863

SPAN - wes@magneto.ee.comell.edu
PHONE (607) 255-7120

TYPE AND DESCRIPTION OF DATA: 50 MHz coherent backscatter radar data

FIELD(S) OF VIEW: 5 degree beam, site location 17.65 N, 64.89 W. Beam azimuth fixed at 290.3 degrees. Zero aspect angle at upper E region heights (130 - 150 km altitudes).

TIME PERIODS OF DATA: all night runs: 0000 to 1100 hours, July 2 - July 11, 1992

SAMPLING RATES:

11 ms IPP usually, 4 ms IPP during possible/actual launch times with 30 minute window

ASSESSMENT OF DATA QUALITY (CLOUD COVER; LIGHT CONTAMINATION); Radar detection of releases was minimal to none detectable. Possible detection of rockets and release events are confused with ongoing meteoric activity.

TORTUGERO, PUERTO RICO

STATION LEADER AND/OR OTHER CONTACT:

Morgan W. McCook
Consultant

TYPE AND DESCRIPTION OF DATA ACQUIRED: Still photography. ASA 1600 color film, 210 mm f 5.6 lens.

FIELD(S) OF VIEW OF INSTRUMENTS: 12° - 13°

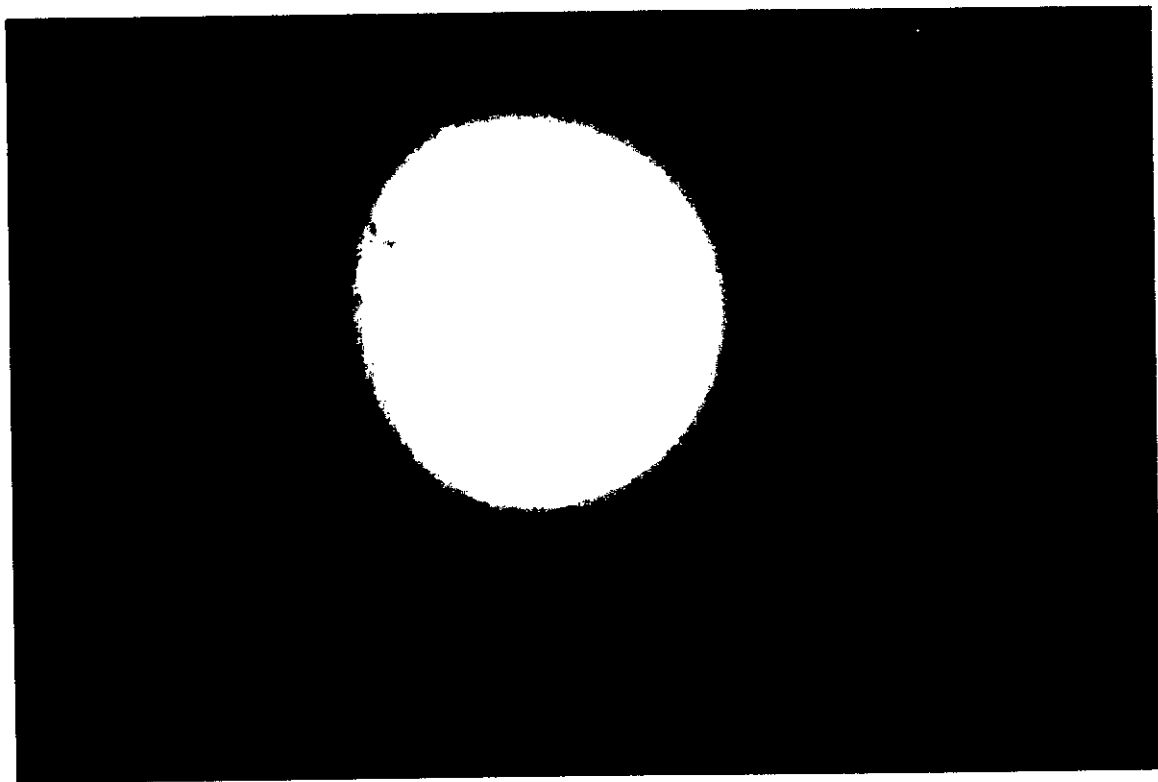
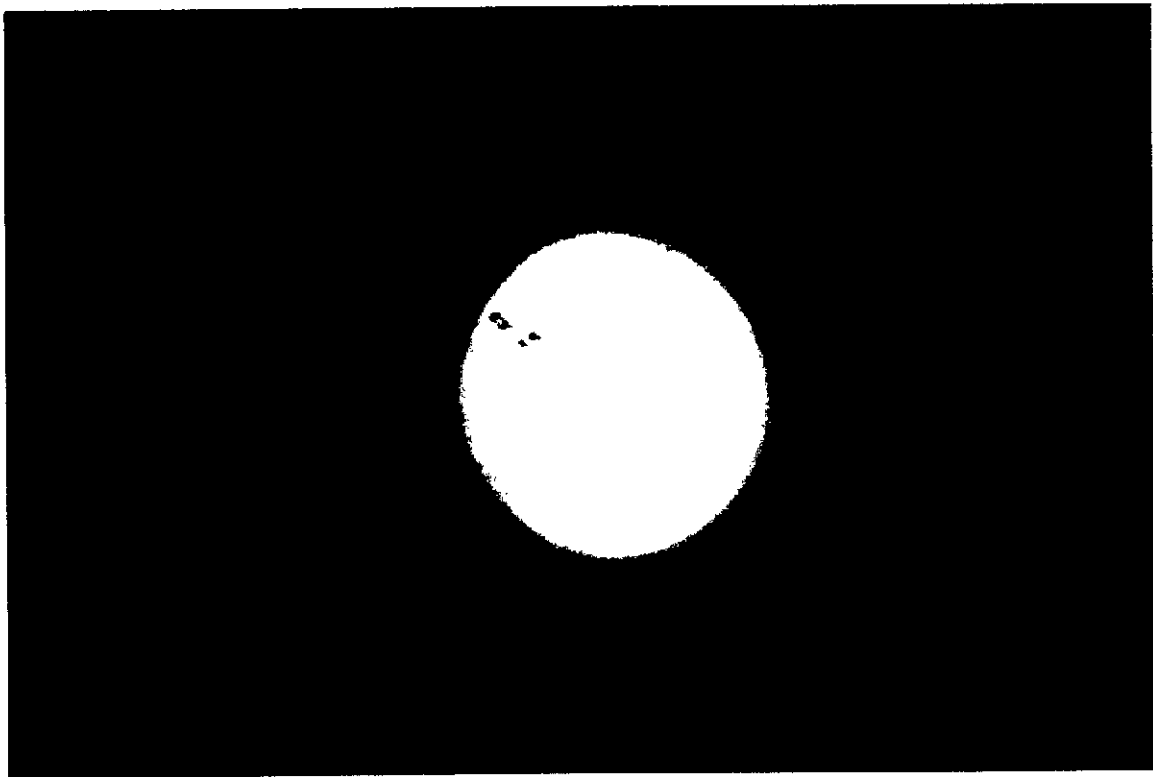
TIME PERIODS OF DATA: Sequence of 15 frames @ 1 minute intervals from 7/4 4:59 AST.

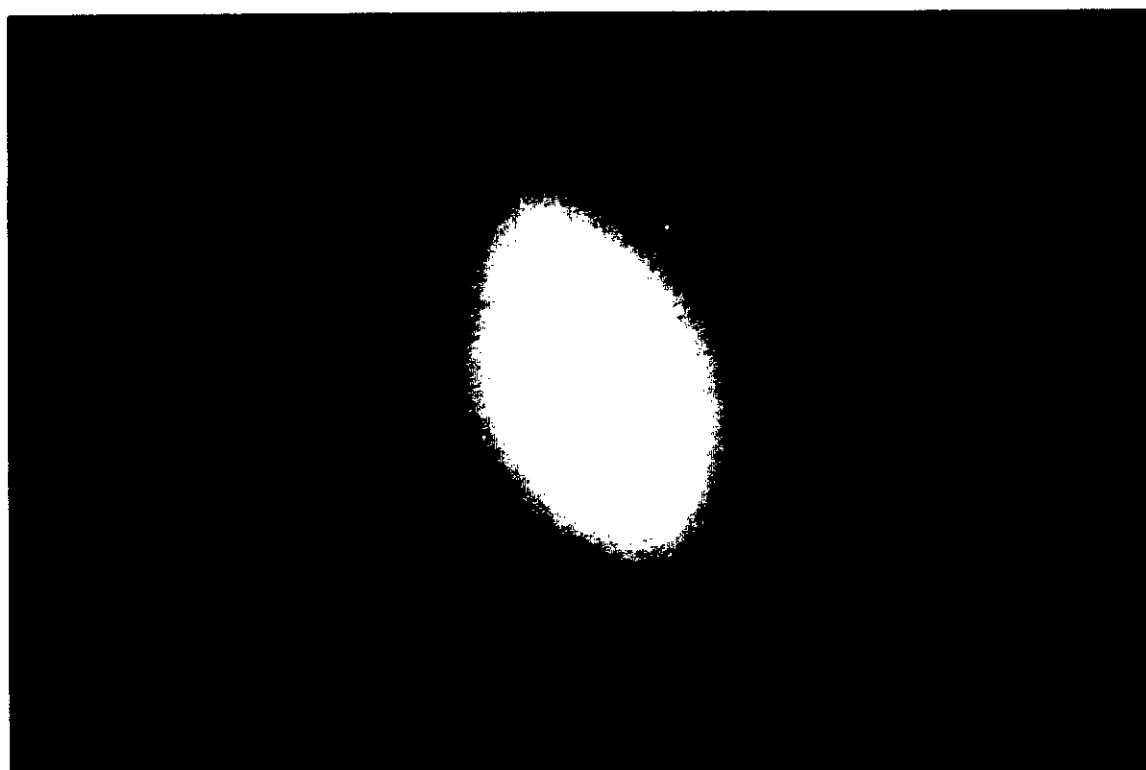
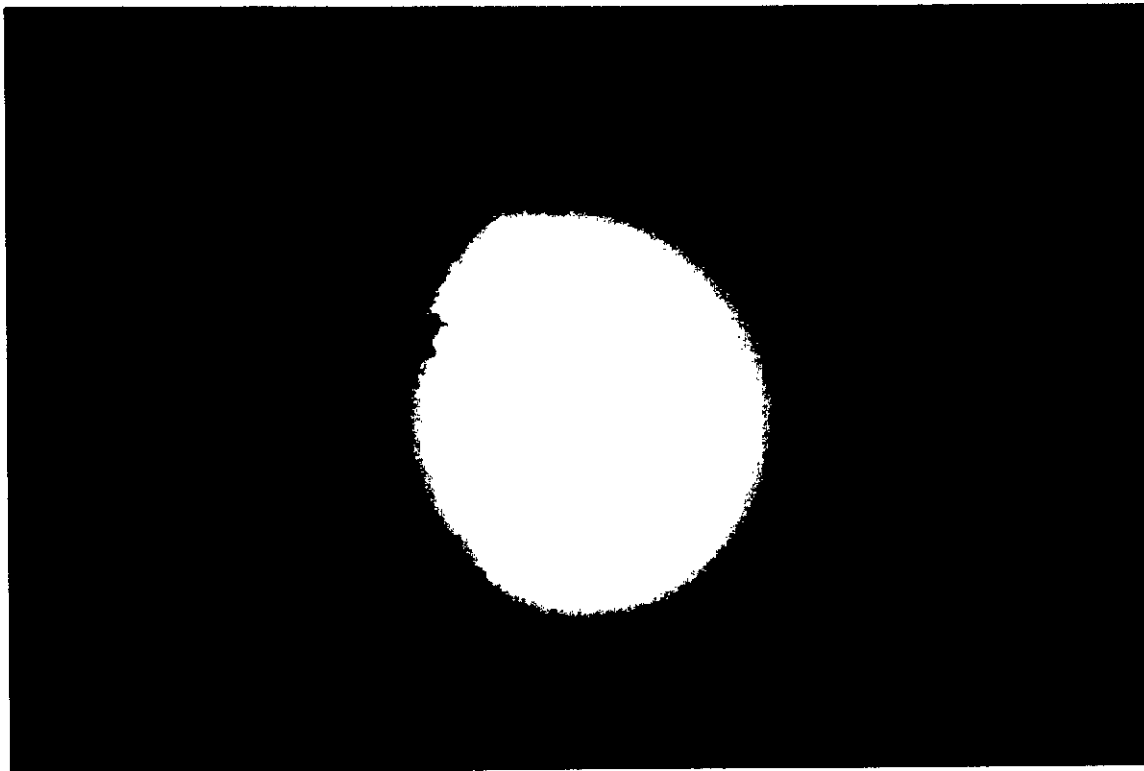
FRAME RATE: at intervals of 30 seconds.

ASSESSMENT OF DATA QUALITY (CLOUD COVER, LIGHT CONTAMINATION): Clear. Excellent quality and examples of short range visibility from launch area.

INITIAL FINDINGS: Barium found and photographed clearly. This is demonstrated in still photographs which follow of the Barium streak as visible from Tortugero, Puerto Rico.

ADDITIONAL RESEARCH: Comparison of G~ High Altitude release to compare visibility at widely different altitudes.





EXPERIMENT AA-2

Title: HF Ionospheric Modification of a Barium Plasma

Principal Investigators: F. T. Djuth and L. M. Duncan

Collaborative Investigators: Edward C. Weber, M. C. Kelley, P.A. Bernhardt, J. Huba

Location: Arecibo High-Frequency Radio Heater Beam, Puerto Rico

Altitude: 250 km

Time: Dawn, Launch 05:02 AST; Release ~05:04:30 AST

Date 12 July 1992

Chemicals: 36 kg. Barium (Ba/2% by mole, Strontium), (Ba/2% by mole, Europium), (Ba/4% by mole, Lithium)

OBJECTIVE:

The Arecibo High-Frequency Radio Ionospheric Heater is a facility that is capable of beaming powerful radio waves upward into the ionosphere. These radio waves, millions of watts effective power, are capable of "pushing the ionosphere around" and creating significant perturbations and structures. In this experiment a heavy barium plasma will replace the natural light ionosphere plasma in the beam of the radio wave heater (Here "heavy" and "light" refer to the weight of the ions. Hydrogen and oxygen, the natural ions, have masses of 1 and 16 atomic mass units. while barium is "heavy" with 137 mass units). The heater beam will then be turned onto the new heavy plasma and for the first time scientists will be able to see how this plasma responds to the perturbations, and to compare the results to known results from previous heater experiments with the natural ionosphere.

ST. CROIX, USVI (Caribbean)

STATION LEADER AND/OR OTHER CONTACT:

Wesley E. Swartz
Engineering ~ Theory Center
Cornell University
Ithaca, NY 14863

SPAN - wes@magneto.ee.cornell.edu
PHONE (607) 255-7120

TYPE AND DESCRIPTION OF DATA: 50 MHz coherent backscatter radar data

FIELD(S) OF VIEW: S degree beam, site location 17.65 N, 64.89 W. Beam azimuth fixed at 290.3 degrees. Zero aspect angle at upper E region heights (130 - 150 km altitudes).

TIME PERIODS OF DATA: all night runs: 0000 to 1100 hours, July 2 - July 11, 1992

SAMPLING RATES: 11 ms IPP usually, 4 ms IPP during possible/actual launch times with 30 minute window

ASSESSMENT OF DATA QUALITY (CLOUD COVER; LIGHT CONTAMINATION); Radar detection of releases was minimal to none detectable. Possible detection of rockets and

Abstract

An ionospheric chemical release, designated AA-2, was performed on July 12, 1992 as part of the NASA Combined Release and Radiation Satellite (CRRES) El Coqui rocket campaign. The purpose of the AA-2 experiment was to study the interaction between a powerful radio wave and a high ion mass (Ba^+), "collisionless" plasma. Approximately 35 kg of Ba were explosively released near the center of the Arecibo high-frequency (HF) beam at 252 km altitude. This was the largest Ba release of the CRRES experiments; it yielded a distinctive ionospheric layer having a maximum plasma frequency of 11 MHz. At early times (less than one minute after the release), the high-power HF beam produced the strongest Langmuir waves ever detected with the Arecibo 430 MHz radar. Initially, resonantly enhanced Langmuir waves were observed only at the upshifted plasma line (i.e., near $430 \text{ MHz} + f_{HF}$, where f_{HF} is the frequency of the modifying HF wave); no HF-excited waves were apparent at the downshifted plasma line ($430 \text{ MHz} - f_{HF}$). At the time of maximum upshifted plasma line backscatter, the power asymmetry between the upshifted and downshifted lines was greater than 10^7 . The upshifted plasma line was accompanied by strong HF-enhanced ion acoustic waves that were present only at the downshifted acoustic sideband. After geomagnetic field-aligned irregularities formed in the plasma, the amplitude of the upshifted and downshifted plasma lines were approximately equal. The experimental results seem to indicate that the so-called parametric decay instability can be excited in an extremely asymmetric manner; that is, the counterstreaming of induced Langmuir waves may not be symmetric relative to the HF wave electric field. In contrast, the parametric decay instability is by definition symmetric in a stationary homogeneous plasma. New theoretical approaches aimed at resolving this dilemma are needed with particular attention paid to the role played by relatively steep plasma gradients.

Introduction

The Puerto Rico, or El Coqui, rocket campaign consisted of rocket experiments launched from Tortuguero, Puerto Rico during the period May 18 through July 13, 1992. Six rocket launches involved the release of chemicals in the ionosphere north of Arecibo Observatory, Puerto Rico. Of these, two entailed the modification of a Ba^+ plasma by transmissions from the Arecibo high-power, high-frequency (HF) facility, located 17 km northeast of Arecibo Observatory. Initial results from the largest of these two chemical releases, designated AA-2, are presented below.

The objective of the AA-2 experiment was to explore the interaction between a high-power HF beam and a high ion mass (Ba^+ , 137 amu) plasma under conditions of low electron collisions. In addition, a moderate plasma scale length $H = n_0/[dn_e(z)/dz]$ was highly desirable, where $n_e(z)$ is electron density as a function of altitude z and n_0 is the electron density at the point of reflection of the HF wave. Scale lengths of the order of 2 - 20 km were anticipated on the bottomside of the B^+ plasma cloud. The experiment design focused principally on the development of microinstabilities in the plasma. Originally, it was believed that it might be possible to suppress the parametric decay instability [e.g., Fejer, 1979] in a Ba^+ plasma and permit preferential growth of the oscillating two-stream instability. Such conjectures were made prior to the application of the strong Langmuir turbulence theory [DuBois et al., 1990; DuBois et al., 1991; Hanssen et al., 1992] to HF ionospheric modification experiments in the natural ionosphere at Arecibo. Subsequent experiments at Arecibo confirmed certain elements of the strong turbulence approximation [e.g., Fejer et al., 1991]. In light of a rapidly changing understanding of the HF modification process, the predicted outcome of the Ba^+ modification experiment became far less certain.

Prior to the AA-2 release, HF modification experiments had been performed in natural sporadic E regions [Gordon and Carlson, 1976; Djuth, 1984; Schlegel et al., 1987; Djuth and Gonzales, 1988]. In mid-latitude sporadic E, Fe^+ ions having relatively high mass (56 amu) often dominate the plasma. However, unlike the AA-2 experiment, electron collision frequencies are quite high (10-30 kHz), and vertical and horizontal electron density scale lengths are extremely small ($H = 100 - 500 \text{ m}$). Indeed,

the plasma parameters of sporadic E give rise to HF waveplasma processes that are significantly different than those encountered at higher F-region altitudes [Djuth and Gonzales, 1988]. In general, the AA-2 experiment has no real analog in the natural environment; it provides a unique view of wave-plasma interactions in a previously unexplored plasma medium.

Experiment Description

The AA-2 chemical release occurred on July 12, 1992 at 05:04:32 AST. At this time, the solar depression angle was 12.2° at the release altitude (252 km); this permitted rapid ionization of the neutral barium cloud while preserving dark viewing conditions at ground level for optical observations. AA-2 entailed the explosive release of approximately 35 kg of Ba, doped with 148 gm of Sr, 260 gm of Eu, and 24 gm of Li to facilitate ground-based diagnostic measurements. This was the largest chemical release of the CRRES program. The chemicals were carried in six, rocket-borne canisters which were simultaneously discharged. An estimated 6×10^{25} atoms of Ba vapor were injected into the ionosphere near the center of the Arecibo HF beam. An overview of the release geometry is provided in Figure 1. The Arecibo HF beam was tilted 12° from vertical in the direction of geographical north to accommodate restrictions placed on rocket flight trajectories. Because the tilted beam was achieved through time-delay phasing, the HF facility could be operated only at a single frequency. A frequency of 5.1 MHz was selected for all El Coqui HF experiments. The AA-2 release occurred approximately 10 km south-southwest of the center of the HF beam. This was well within the 3-dB power points of the beam in the ionosphere.

The AA-2 release, like many of El Coqui campaign chemical releases, was positioned well inside the viewing limits of the Arecibo 430 MHz radar (i.e. within 20° of the zenith). The 430 MHz radar was the principal diagnostic for the AA-2 microphysics. Additional AA-2 measurements were made with a wide variety of optical instrumentation, HF bistatic links that penetrated the release volume, and with a VHF radar-interferometer positioned on the island of Antigua. The VHF radar was tuned to 49.92 MHz, and was used to detect HF-induced geomagnetic field-aligned irregularities. The current work focuses primarily on results from the 430 MHz radar.

Special efforts were made with AA-2 to fully exploit the information available with the Arecibo incoherent scatter radar. Three types of phase-coded radar pulses were employed. These included a 13-baud Barker-coded pulse (BKR) having a baud length of 4 μ s; a three-baud Barker-coded pulse (1- μ s bauds), referred to as a coded short pulse (CSP); and a 512-baud, pseudo-random phase-coded pulse (1- μ s bauds), generically termed a coded long-pulse (CLP). The three pulses were cyclically transmitted within a "frame time" of 30 ms. A frame consisted of three 10 ms interpulse periods (IPPs), one for each type of pulse. Throughout the experimental period, ionospheric backscatter from each radar pulse was simultaneously sampled at the radar center (ion line) frequency and across both "plasma line" sidebands. The plasma line bandpasses were centered at $430 \text{ MHz} + 5 \text{ MHz}$. In general, baseband filters were selected to optimize measurements made with a particular type of pulse. The spectral bandwidths of the data channels ranged from 250 kHz on the BKR ion line to 4 MHz on the CLP plasma lines. The three pulse types were used to extract different kinds of information about the processes occurring the Ba^+ plasma. Power profile (i.e. power versus range) measurements made with the BKR pulse had the best detection sensitivity with moderately good altitude resolution (600 m). On the other hand, good altitude resolution (150 m) and wideband spectral information was achieved with the CLP with some loss of sensitivity. The CSP yielded power profile measurements with good range and temporal resolution when strong HF-enhanced plasma (ion) lines were present near $430 \text{ MHz} + f_{\text{HF}}$ (430 MHz), where f_{HF} is the frequency of the HF transmissions (5.1 MHz).

An important feature of the AA-2 radar data-taking was that raw, unintegrated voltage samples were preserved on all data channels throughout the experiment period (45 min.). This made it possible to optimize temporal integration periods after the fact, change digital processing techniques as desired, and examine radar returns on a pulse-by-pulse basis to explore interesting events.

Observations

The background F-region just prior to the AA-2 release had a peak plasma frequency of ~ 8 MHz at a height of 340 km. As noted earlier, the release occurred at ~ 253 km altitude at 05:04:32 AST on July 12, 1992. The Arecibo HF beam was turned on continuously for 30 min. prior to the release; it was operated at an effective radiated power (ERP) of ~ 60 MW and tuned to a frequency (f_{HF}) of 5.1 MHz. The height of the HF-excited Langmuir waves and ion waves provided a convenient and continuous calibration of the electron density profile. From the time of the rocket launch to the release 152 s later, the altitude of the HF-enhanced waves as determined with the Arecibo 430 MHz radar, was $271 \text{ km} \pm 0.5 \text{ km}$. This altitude closely corresponds to the critical point in the plasma (i.e., the altitude where $f_{pe} = f_{HF}$, where f_{pe} is the electron plasma frequency). With $f_{HF} = 5.1$ MHz, the critical layer has an electron density of $3.2 \times 10^5 \text{ cm}^{-3}$. One of the go/no-go launch criteria required that the critical layer in the natural ionosphere be located above the projected release altitude. This was done to ensure that the HF beam would undergo total reflection in a predominantly Ba^+ plasma. At the time of release, the background electron density at the discharge height was $1.3 \times 10^5 \text{ cm}^{-3}$.

Ba^+ Cloud Formation

In Figure 2, the AA-2 release event is illustrated with BKR data acquired at the ion line. Time is shown relative to launch at 05:02:00 AST. The range-corrected backscatter power is proportional to $n_e/[1 + T_e/T_i]$, where n_e is electron density, and T_e and T_i are electron temperature and ion temperature, respectively. This plot has not been corrected for T_e/T_i as would be required to convert the measurements into absolute electron density. An accurate determination of T_e/T_i is extremely difficult in a plasma containing multiple ions of different mass and significant vertical electron density gradients. A limited effort has been made to determine T_e/T_i near the peak of the Ba cloud at 300 s relative to launch (L) and in the background plasma at 100s L. This necessitated the use of CLP data to obtain ion line spectra. The CLP measurements are severely clutter limited in this particular case. Initial studies indicate that T_e/T_i was 1.2 prior to the release but increases to about 2 at 300s L. If this is the case, then 10 dB signal-to-noise ratio in the barium cloud at 300 s in Figure 2 corresponds to $n_e = 1.5 \times 10^6$.

In Figure 2, the light vertical streak/speckles seen near 150 s L is the rocket as viewed through a high order sidelobe of the radar beam. The pink speckles at the very bottom of the Ba cloud at 190 s L are produced by HF-enhanced ion waves that are resonantly excited over a very narrow altitude interval. This will be discussed in greater detail below. Temporal changes in the structure of the Ba cloud are caused primarily by changes in the pointing of the 430 MHz radar. For the first 228 s L (or 76 s relative to the release) and at all times prior to launch, the 430 MHz beam was pointed at the center of the HF beam at a nominal altitude of 250 km (see Figure 1). The radar beam was then moved across the Ba cloud in an effort to adjust for the ~ 10 km horizontal displacement between the projected release point and the actual one, and concurrent efforts were made to spatially map out the locations of resonantly-excited Langmuir and ion waves. In addition, continuous pointing adjustments were made to keep the radar beam on a critical surface in the Ba cloud as the cloud drifted toward the perimeter of the HF beam. Optical data indicated that the cloud drifted toward the northwest at an average speed of $\sim 50 \pm 5 \text{ m/s}$.

The location of the radar beam versus time after launch is shown in Figure 3. An altitude of 240 km was selected for the horizontal projection of position because the strongest resonantly enhanced Langmuir ion waves were detected near this height. Once the beam motion is initiated, beam locations are indicated with the symbol (+) at 12-s intervals. Temporal integrations (12 s in duration) centered on these times were used to construct the temporal evolution of the electron density profile shown in Figure 4. Forty profiles are shown beginning with the launch of the rocket. For presentation purposes, each profile is displaced from preceding one by $0.4 \times 10^6 \text{ cm}^{-3}$. In this data display, strong HF-enhanced ion lines are evident near 271 km prior to the release. A rocket echo is

evident in the integration period just before the release. The Ba plasma initially expands over a 30-km altitude interval. Once the cloud is fully formed it slowly sinks in altitude at the rate of $\sim 25\text{m/s}$.

The radar data of Figure 4 can be used to determine the temporal history of the critical altitude, its rate of change in the vertical direction, and the ionospheric scale length H at the critical layer. These results are presented in Figure 5. Prior to the release at 152 s L, the critical height and its rate of change was determined using the HF-enhanced ion line height and its height difference between consecutive integration periods. After the release, changes in $3.2 \times 10^5 \text{ cm}^{-3}$ electron density contour were used. Each electron density profile was least-squares-fit to a fifth order polynomial so that the critical height could be accurately determined. The scale length H was determined from the first derivative of the fitted electron density profile at the critical height. Within 30 s of the release, a "stable" 5.1 MHz critical altitude develops near 240 km; over the next 4-5 min. the critical altitude rises slightly, then slowly declines in altitude to 235 km. The apparent vertical velocity of the critical layer prior to release is caused mostly by the movement of large-scale HF-induced irregularities across the radar beam. In effect, the radar maps out the critical contour in the horizontal dimension as electron density irregularities drift through the beam. The vertical velocity of the critical layer immediately after the release is determined primarily by the expansion of the Ba cloud downwards in altitude. This expansion comes to a gradual halt approximately 80 s after the release. The scale length H at the critical layer ranges between 3 and 5 km in the Ba cloud following the release.

In Figure 6, the altitude and temporal scales of the data of Figure 2 are greatly expanded to show HF-enhanced ion line echoes that were excited on the bottomside of the Ba cloud. These echoes are not evident in Figure 4 because of the long (12 s) temporal integrations used in the presentation. During a 12 s period, the enhanced ion line backscatter is smeared across many range cells, and as a result, sharp peaks cannot be discerned in the profiles of Figure 4. The enhanced ion lines of Figure 6 provide a clear indication of the location of the critical layer as the Ba^+ cloud is forming and expanding downwards in altitude.

HF-Induced Plasma Turbulence

Extremely strong HF-enhanced plasma lines were detected at the upshifted plasma ($430 \text{ MHz} + f_{\text{HF}}$) during the AA-2 release. The largest echoes occurred during two periods: 175-230 s L (23 - 78 s after release, period P1) and 278 - 291 s L (126 - 139 s after release, period P2). Indeed, in terms of absolute signal strength in the spectral domain, these were the strongest enhanced plasma line echoes ever recorded at Arecibo. During P1 no echoes were detected at the downshifted plasma line ($430 \text{ MHz} - f_{\text{HF}}$). During the second period, an enhancement at the downshifted plasma line was observed for the first time. However, the power levels of the downshifted plasma line enhancements were approximately 20 times less than those at the upshifted line. Strongly enhanced ion lines were evident throughout P1 when the largest amplitude upshifted plasma lines were present; no enhanced ion lines were detected during P2.

Figure 7 summarizes the resonant plasma line measurements made prior to and during the AA-2 release. Also shown is the ionospherically-reflected HF wave received at Arecibo Observatory. The signal-to-noise ratios are measured across a 2-MHz bandpass. Prior to the release at 152 s L, the upshifted and downshifted plasma line power levels in the natural ionosphere are approximately the same. Following the release, it is clear that a large asymmetry develops between the upshifted and downshifted plasma line power. At the time of the strongest upshifted plasma line echo during P1, no downshifted plasma backscatter is detected, even in the more sensitive frequency domain discussed below. The estimated power asymmetry between the two signals at this point is greater than a factor of 107. Resonantly-enhanced downshifted plasma lines were first observed at 280 s L (128 s after the release). The appearance of the downshifted plasma line coincided with the first detection of HF-induced, geomagnetically field aligned irregularities in the Ba cloud. A VHF radar-interferometer sensitive to irregularities having a spatial scale of 3-m across geomagnetic field lines was used to make this measurement. The VHF radar was deployed on the island of Antigua, where it had an optimum viewing geometry for detection of field-aligned irregularities near the 5.1 MHz

critical layer in the Ba cloud. The formation of such irregularities may in fact be responsible for the equalization of the upshifted and downshifted plasma line power after 340 s L (188 s after release).

Spectra of the enhanced upshifted plasma line and ion line recorded during P1 are shown in Figures 8 and 9. The plasma line spectrum consists of a narrow "decay line" peak [see, e.g. Showen and Kim, 1978], where the frequency offset of this peak from $430 \text{ MHz} + f_{\text{HF}}$ is approximately the ion-acoustic frequency in the Ba plasma. In a similar manner, the HF-enhanced ion line spectrum contains of a single peak downshifted from 430 MHz by a Ba ionacoustic frequency. Overall, these spectra are representative of many others obtained during P1. However, during a brief period when strong enhancements were first detected in the Ba plasma, plasma line/ion line spectra with dominant frequency components at exactly $430 \text{ MHz} + f_{\text{HF}}$ and 430 MHz were also observed. Examples of these *atypical* spectra are presented in Figures 10 and 11.

Downshifted plasma line spectra are available during time period P2 and at later times. Examples of these spectra are provided in Figures 10-12. The downshifted plasma line spectra contain time varying features not evident in the P1 upshifted plasma line spectrum. As noted above, the downshifted plasma lines were excited in a presence of geomagnetic field-aligned irregularities, and this may have influenced the spectral features detected with the 430 MHz radar.

Discussion

The observations of Section 3 indicate that HF-excited Langmuir waves measured in the Ba^+ cloud with the Arecibo 430 MHz radar exhibit a large power asymmetry in the backscatter return from wavevectors \mathbf{k} ($|\mathbf{k}| = 18 \text{ m}^{-1}$) directed toward the radar (upshifted plasma line) versus those directed away from the radar (downshifted plasma line). This asymmetry is most evident at early times following the release. The observed ratio of upshifted plasma line power to down shifted plasma line power is very large ($>10^7$). Because no enhanced echo is detected at the downshifted plasma line, the magnitude of the asymmetry is determined by the combination of scattered power at the upshifted plasma line and the noise statistics at the downshifted plasma line. Typically, the upshifted plasma line spectrum exhibits a single dominant "decay line peak" [Showen and Kim, 1978] located at $430 \text{ MHz} + f_{\text{HF}} - \delta$, where δ is of the order of the ion acoustic frequency, f_{ia} , in the Ba plasma. Experimentally measured value for δ are typically $1.5 \pm 0.2 \text{ kHz}$. The only exception to this is the atypical case presented in Figure 10, where $\delta = 0$. The calculated value of f_{ia} in a Ba plasma with $T_e = 2000 \text{ K}$ and $T_i = 1000 \text{ K}$ is 1.5 kHz, which is consistent with the observations. When a strong upshifted plasma line is present in the data, it is accompanied by an HF-enhanced ion line consisting of a single spectral line located at a frequency displacement of $-\delta$ from 430 MHz, where δ matches the offset of the upshifted plasma line peak from $430 \text{ MHz} + f_{\text{HF}}$.

In general, the radar observations indicate that strongly excited Langmuir waves with \mathbf{k} directed toward the radar are coupled to large-amplitude ion-acoustic waves having oppositely directed wavevectors. Absent in the data are Langmuir waves with wavevectors direct away from the radar and ion-acoustic waves with \mathbf{k} directed toward the radar. The observations seem to indicate that only half of the counterstreaming waves expected for a parametric decay instability [e.g., Fejer, 1979] are present in the plasma. In a homogeneous plasma, for example, the parametric decay instability is by definition symmetric; Langmuir waves and ion waves stream in both directions. The question arises as to what plasma process can give rise to a 10^7 power asymmetry between oppositely directed Langmuir waves.

Observations made in the past in natural ionosphere at Arecibo have yielded no large, systematic asymmetries between the power at the downshifted and upshifted plasma lines. At F-region altitudes, the time-averaged power measured at the upshifted and downshifted plasma lines are roughly comparable. In sporadic E, either the upshifted plasma line or the downshifted plasma line may be dominant. The ratio of power at the upshifted plasma line to power at the downshifted plasma line ranges from 10^{-1} to 10^2 , with very few cases encountered near the extrema of this range.

Although there are several processes that may contribute to the observed Langmuir wave asymmetry in the Ba plasma, few appear capable of generating the magnitude of asymmetry observed. Standard parametric instability theory applied to an inhomogeneous plasma can give rise to wave asymmetries because of Langmuir wave propagation. However, it is unlikely that propagation alone can give rise to 10^7 power asymmetries. In sporadic E, for example, plasma inhomogeneities containing very large vertical gradients are present, yet plasma line power asymmetries are at most a factor of 10^2 . One might argue that the Arecibo radar is detecting waves initially excited near the critical layer as a result of linear conversion or other processes, and that these waves propagate into the field-of-view of the radar. However, this explanation cannot easily account for the fact that "decay line" frequency offsets are found in the upshifted plasma line spectrum. In addition, it is difficult to explain the observed counterstreaming of the ion waves within this scenario.

Other efforts to link effects observed shortly after the release to unusual plasma conditions have not met with success. For example, immediately following the release, large downward flows of Ba ions are present, and the critical layer rapidly descends to lower heights. However, the plasma/ion line properties do not appear to be dependent on the magnitude of the downward velocity of either effect. Indeed, the large power asymmetry is still evident even after the downward motion comes to a halt. Moreover, supersonic speeds of potential interest to instability processes are never approached by the downward ion flow or by rate of decline of the critical layer.

The late-time development of the plasma line echo in the Ba cloud is far easier to understand within the context of our current knowledge of HF ionospheric modification processes. Once HF-induced, geomagnetic field-aligned irregularities develop in the Ba plasma, the magnitude of the enhancement at the upshifted plasma line declines, and the ratio of upshifted plasma line power to downshifted plasma line power approaches unity. This is similar to the situation encountered in the natural ionosphere where propagation in HF-induced ionospheric ducts is important [e.g., Muldrew, 1978]. While many of the properties of the plasma lines observed in the late-time environment are in need of further study, ducted propagation of Langmuir waves offers an attractive mechanism for explaining complex spectral features observed at the downshifted plasma line.

Conclusions

HF radio wave modification of the AA-2 barium release yielded the strongest plasma turbulence ever detected with the Arecibo 430 MHz radar. At early times following the release strong upshifted plasma lines near $430 \text{ MHz} + f_{\text{HF}} - \delta$ were observed, where $\delta = 1.5 \pm 0.2 \text{ kHz}$. These echoes are caused by HF-excited Langmuir waves with wavevectors pointed toward the radar. The greatly enhanced Langmuir waves were accompanied by counterstreaming ion waves. No Langmuir waves having wavevectors directed away from the radar were observed in the early-time release environment. Currently, no acceptable explanations exist for the large ($>10^7$) power asymmetry observed between the radar echoes at the upshifted plasma line and the downshifted plasma line. Without question, interpretation of these observations pose a significant challenge for all existing theoretical treatments of Langmuir/ion turbulence. The late-time features of the plasma turbulence excited in the Ba cloud appear to be understandable within the context of ducted propagation of Langmuir waves in geomagnetic field-aligned irregularities. Additional work is needed to specify the way in which field-aligned irregularities are generated in the plasma and the extent to which Langmuir waves impact their development.

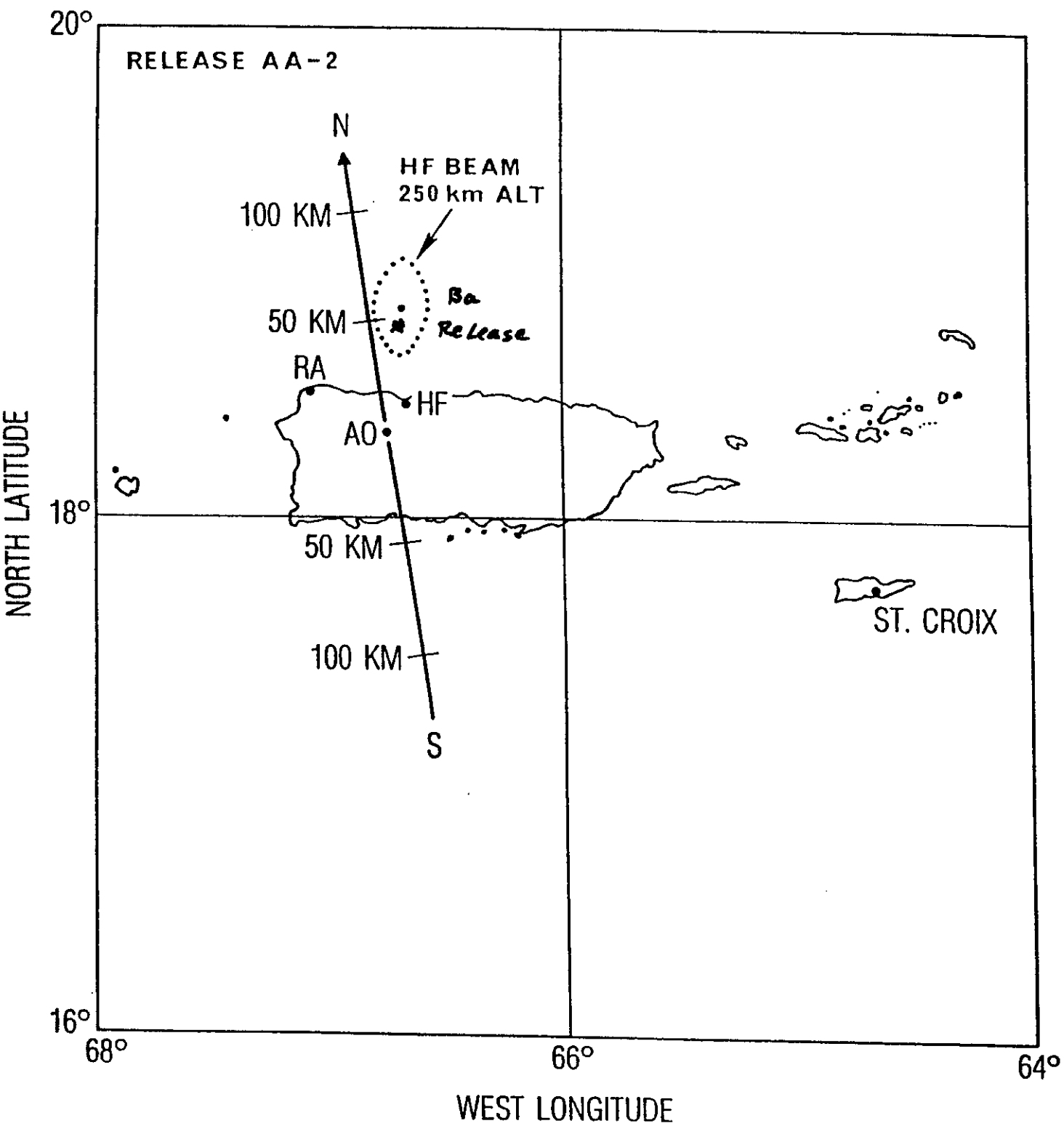
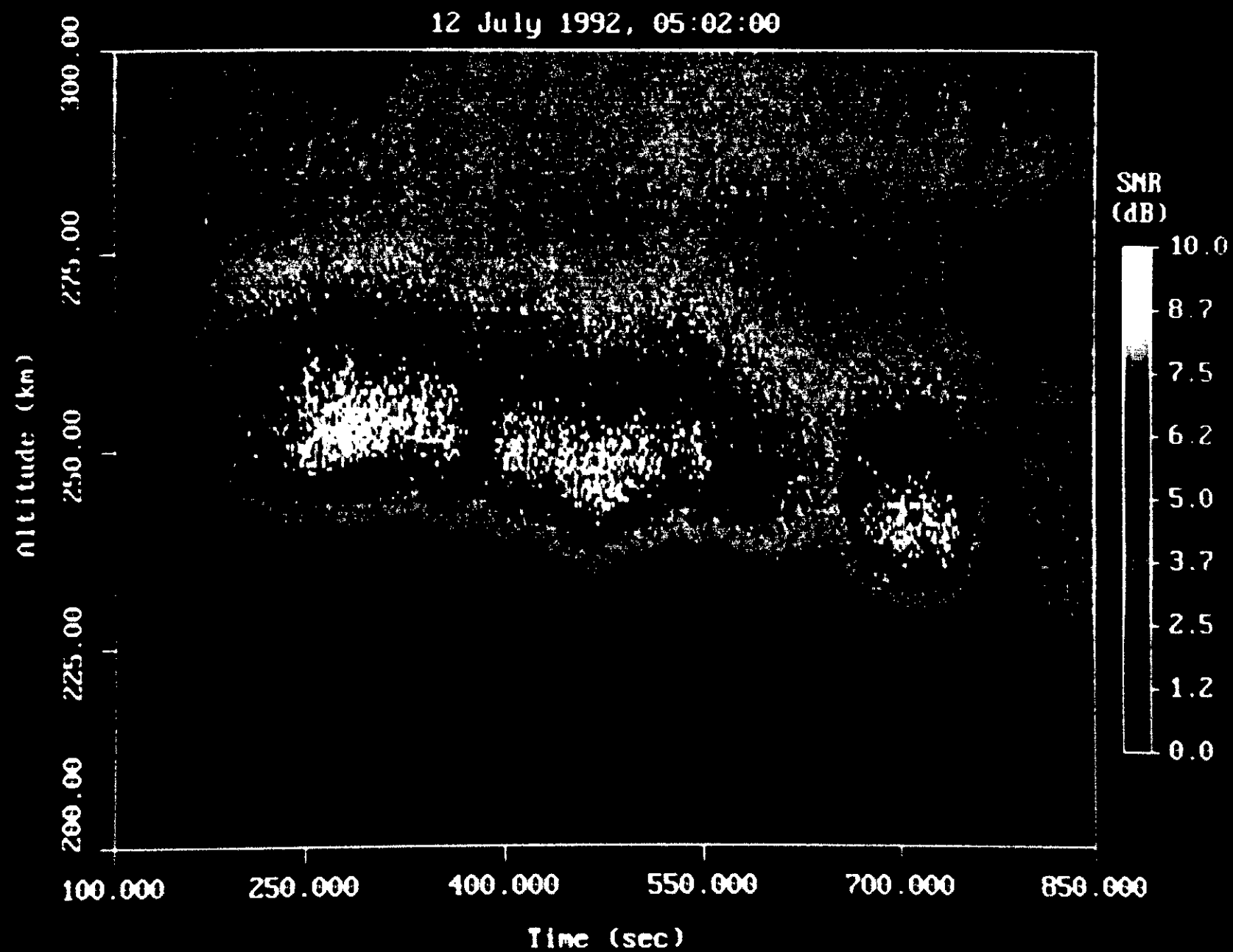


Figure 1



Location of 430 MHz Beam at 240 km Altitude

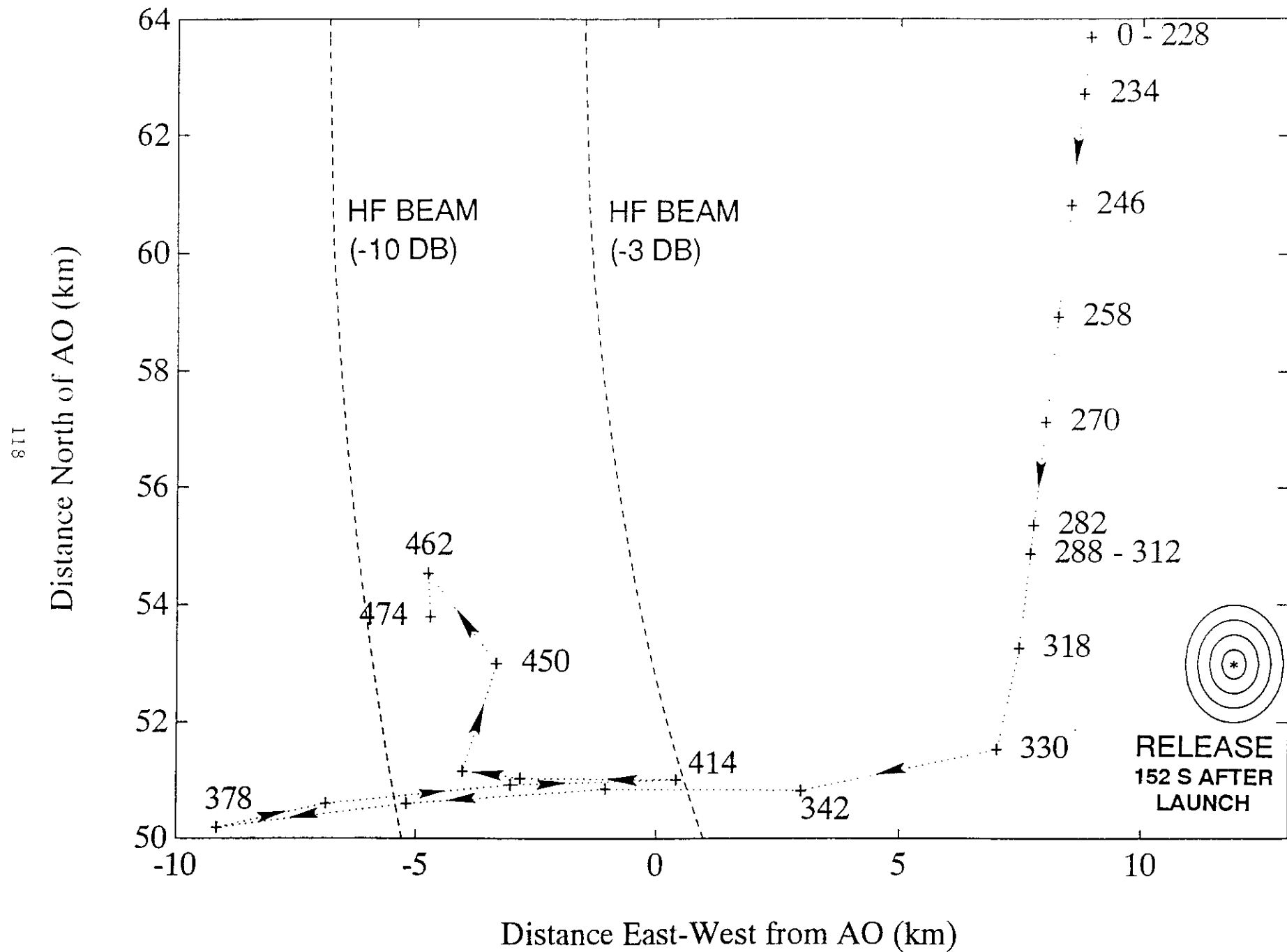


Figure 3

CRRES AA2 Barium Release

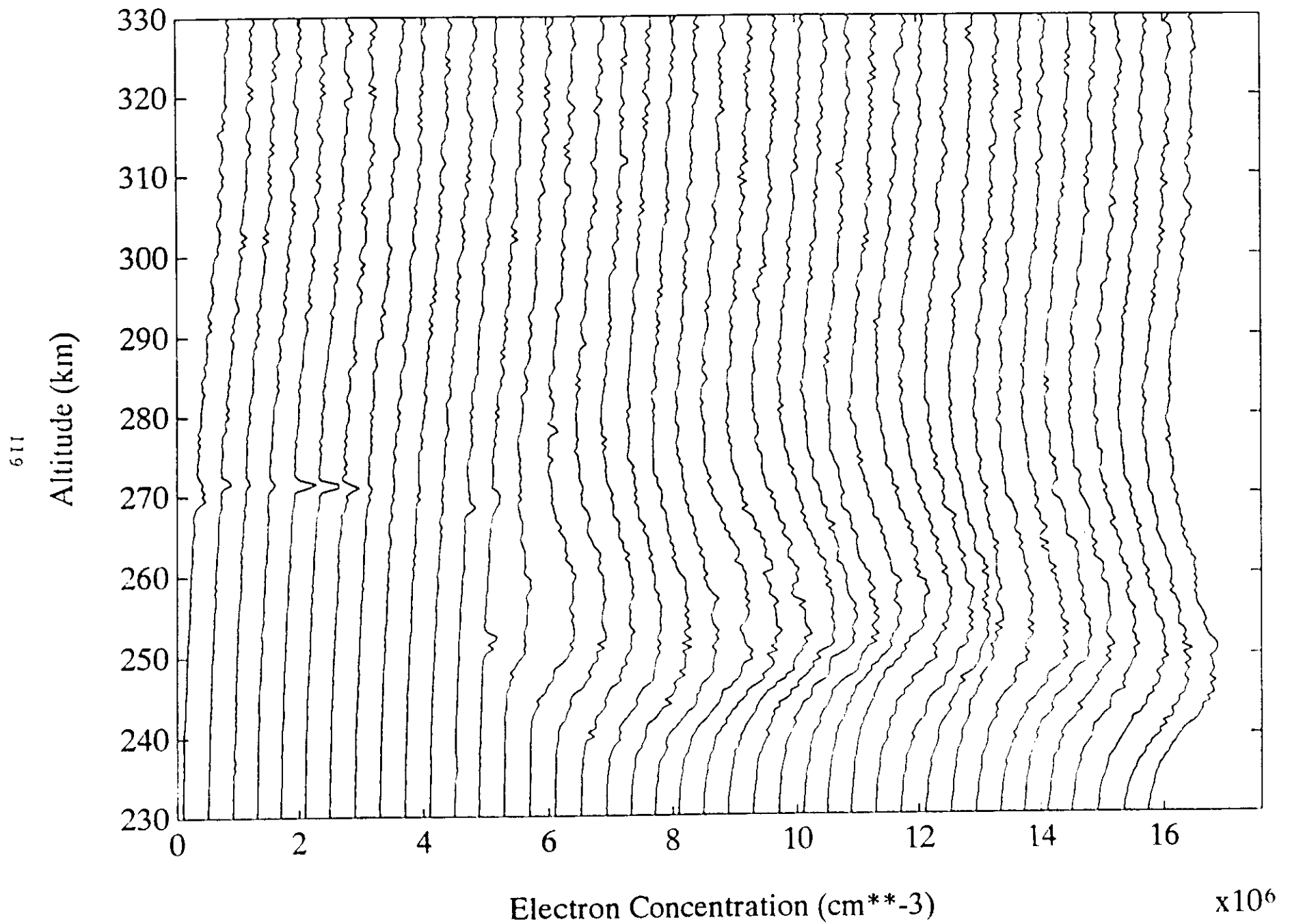


Figure 4

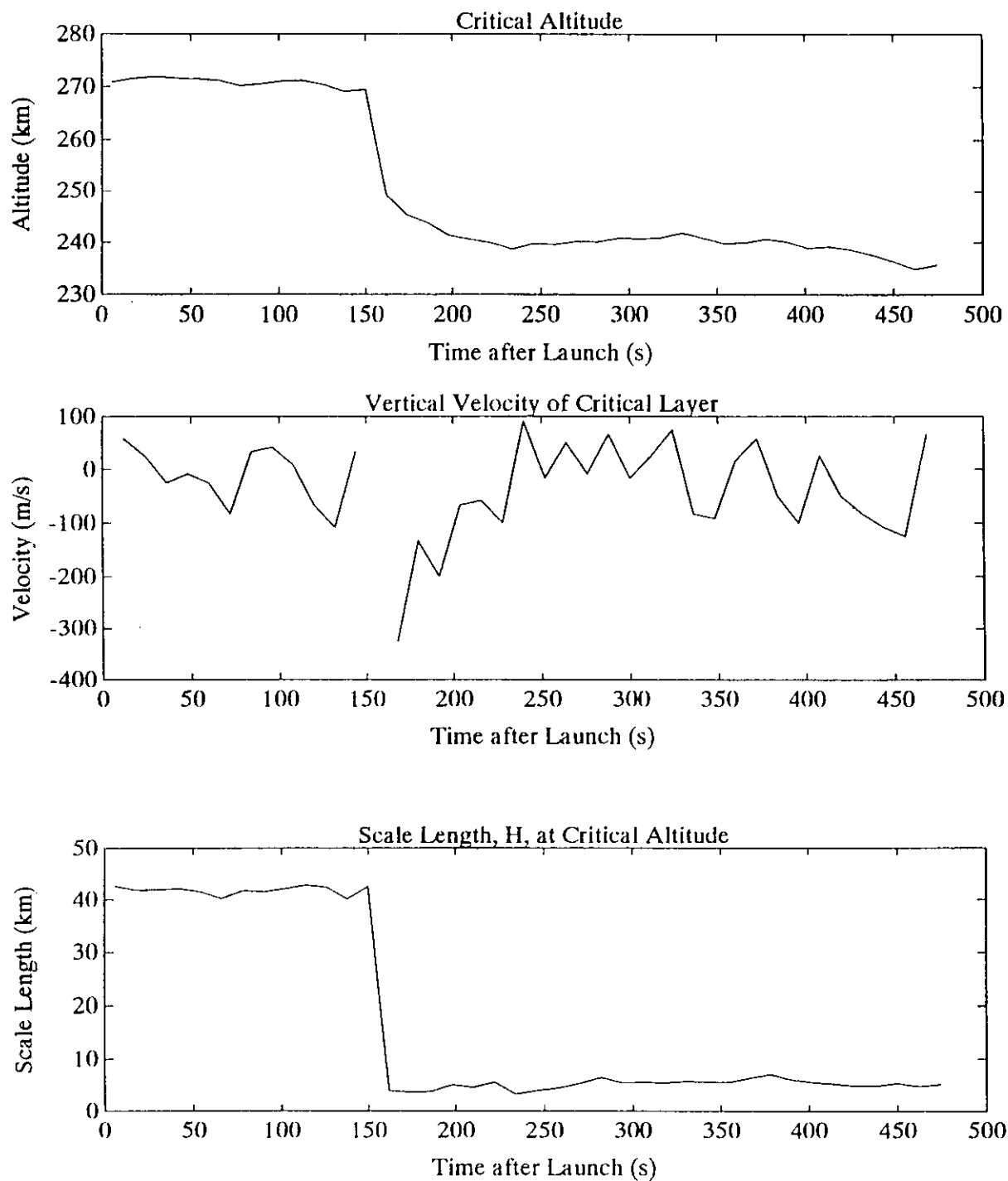
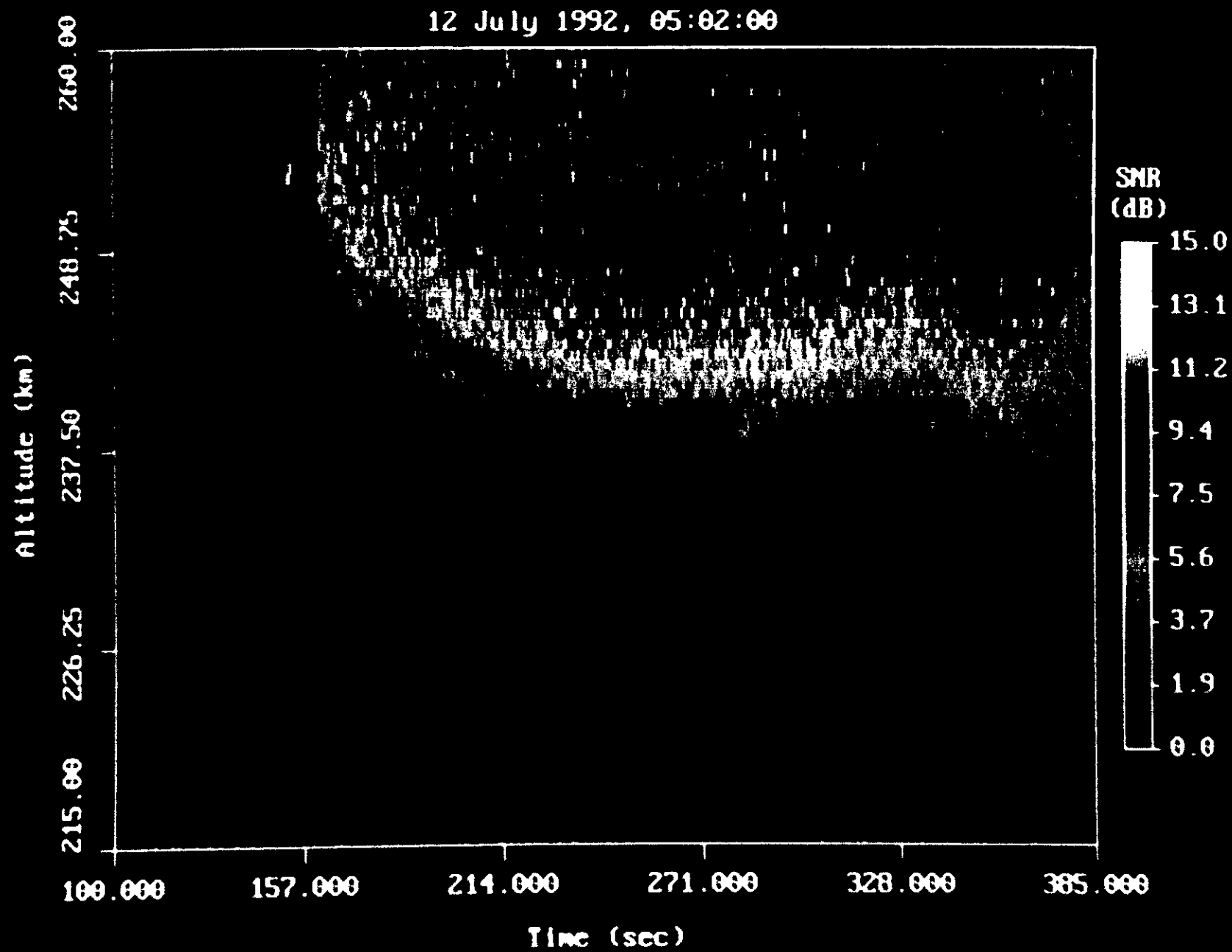


Figure 5



AA2: Plasma Lines

122

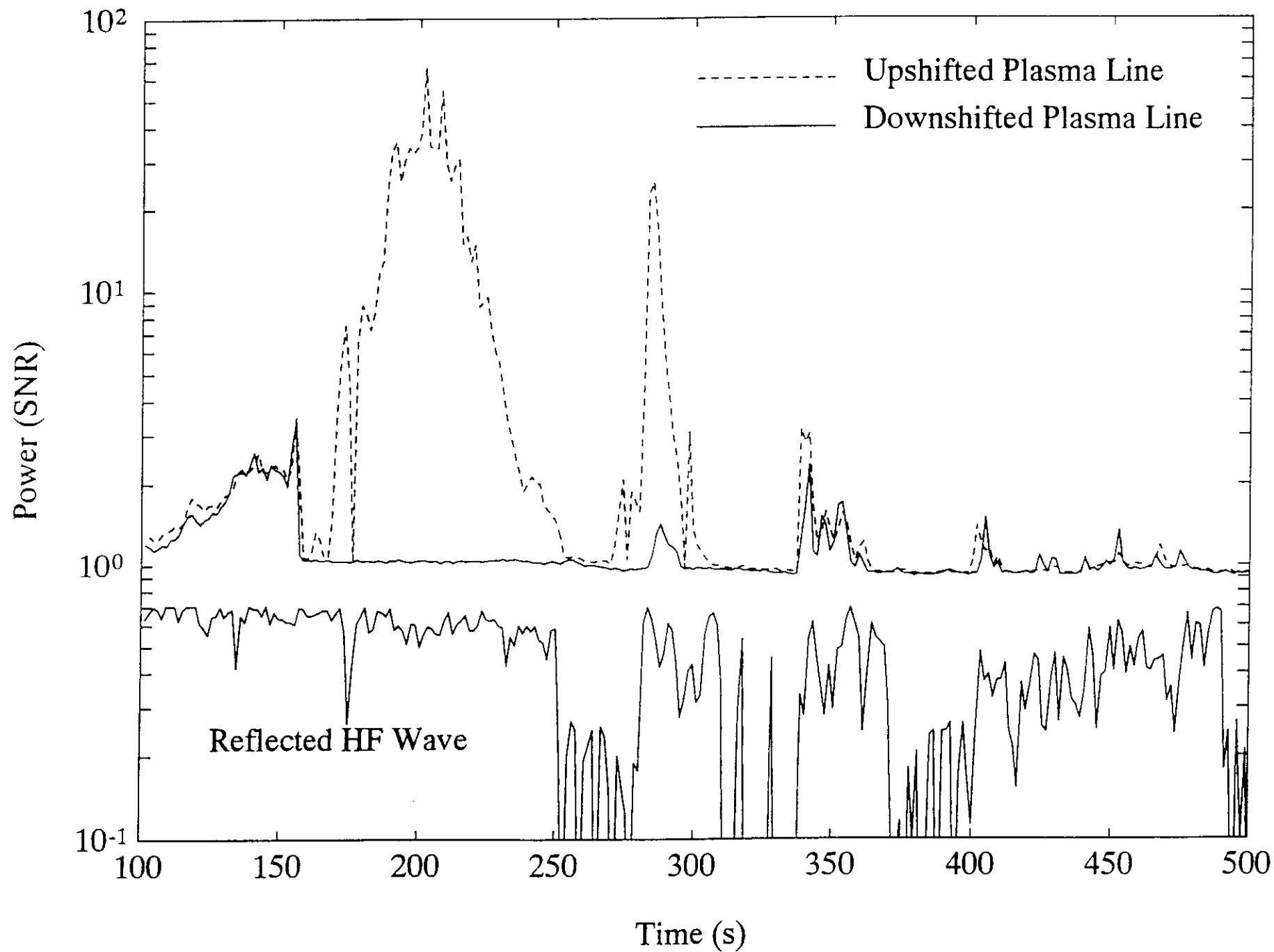
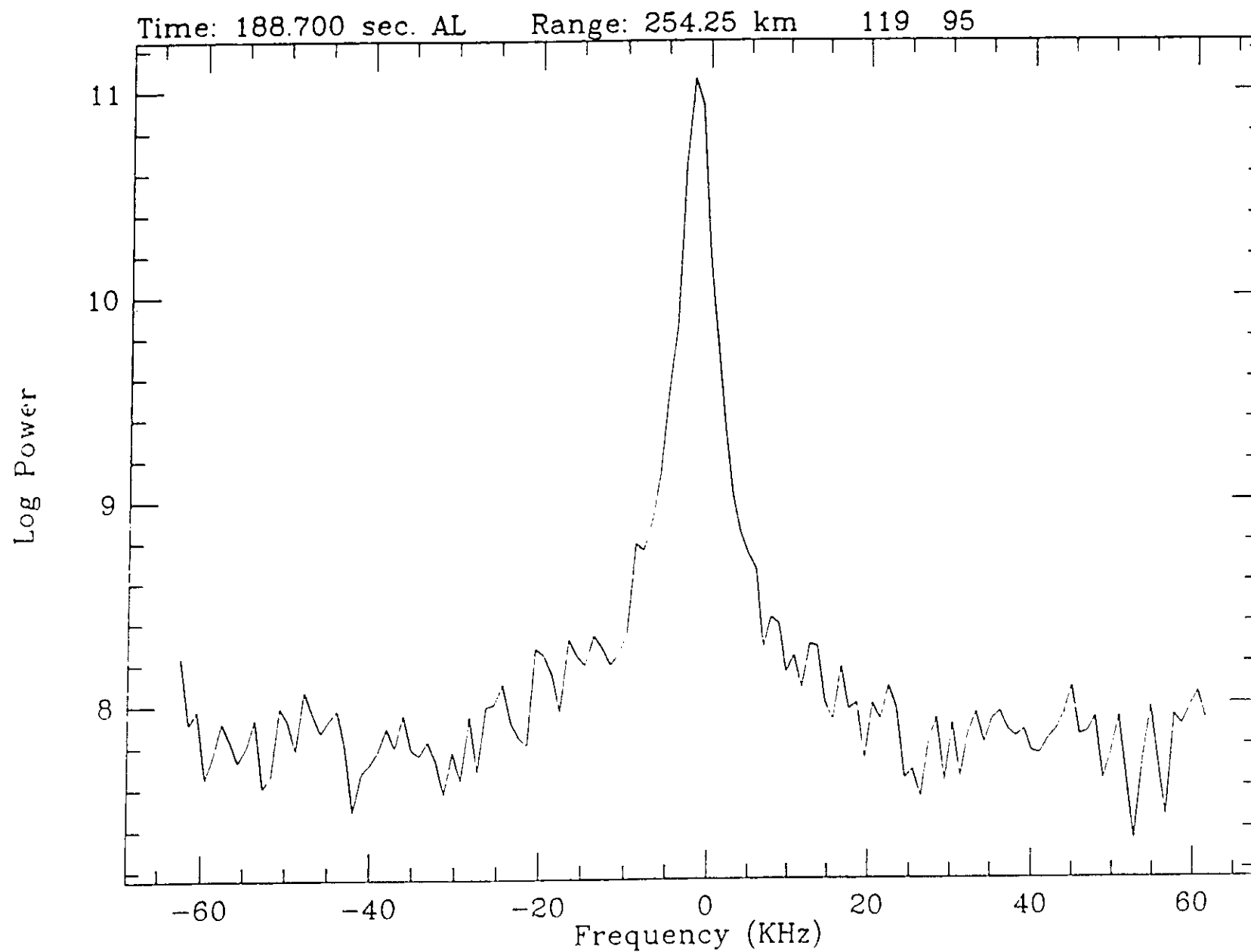
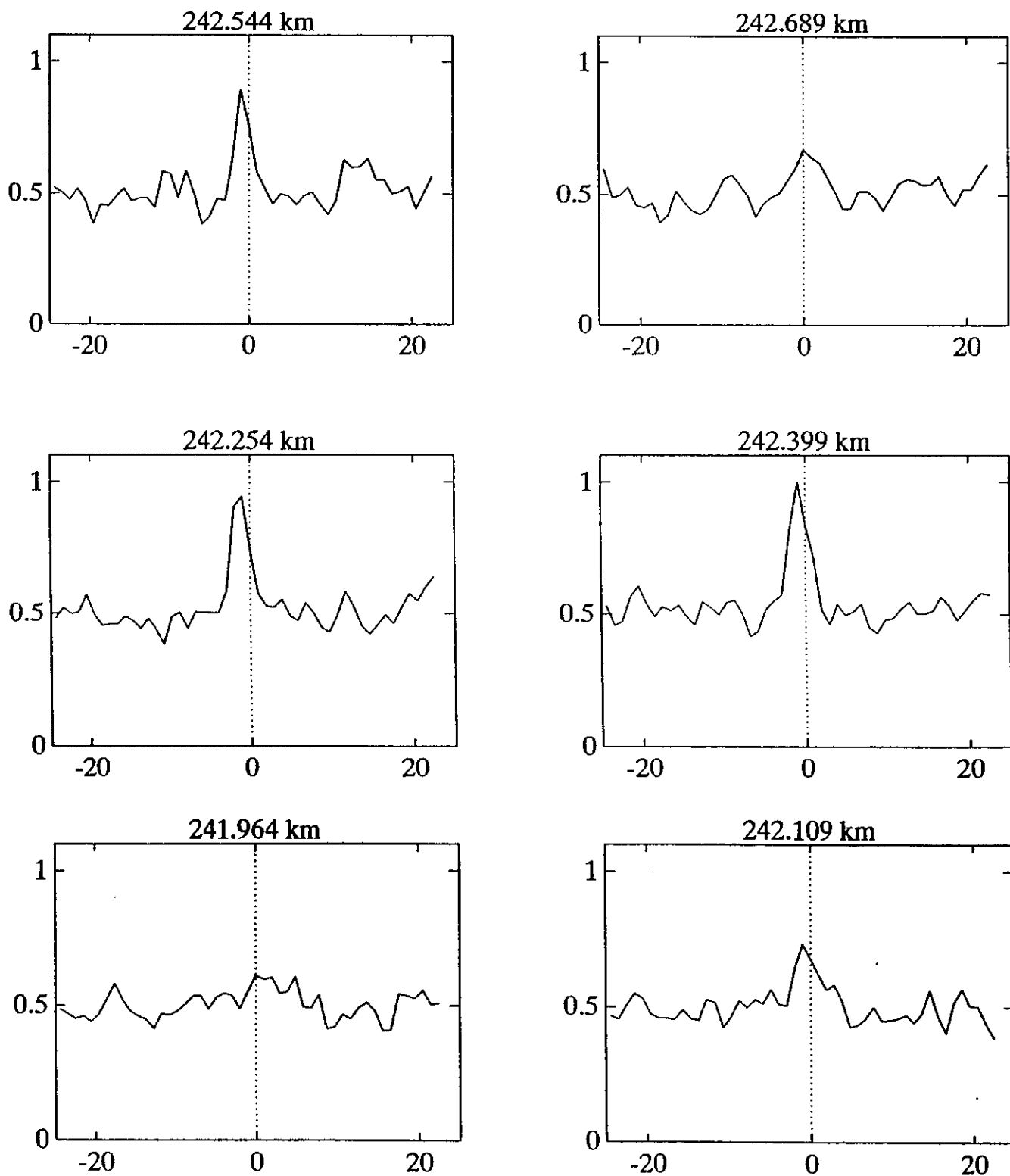


Figure 7



Frequency offset from (430 MHz + f_{HF})

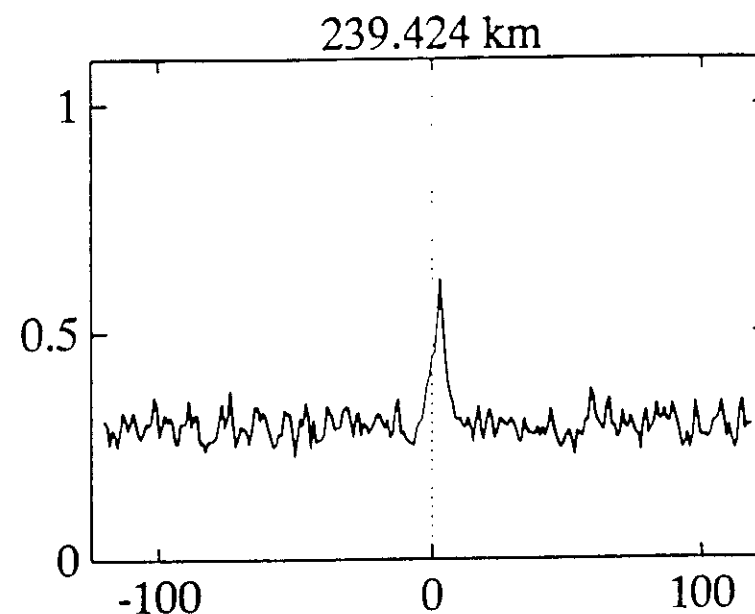
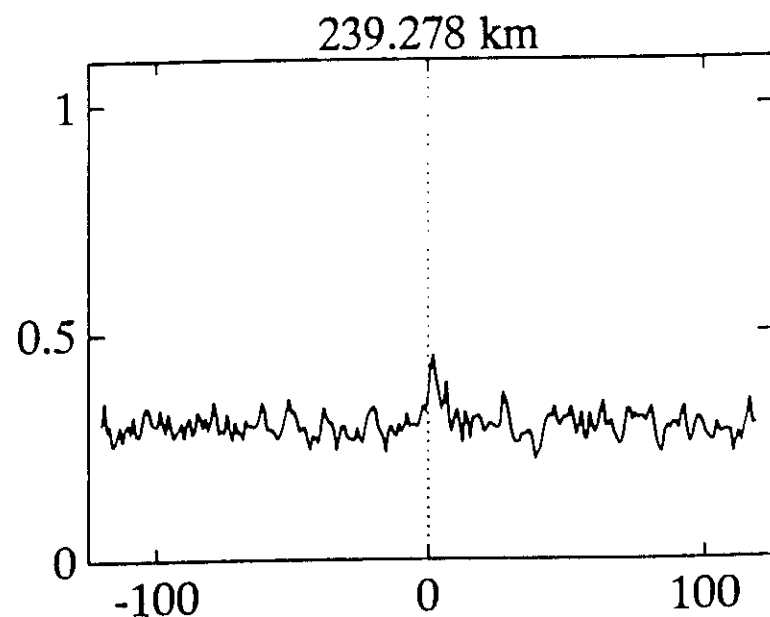
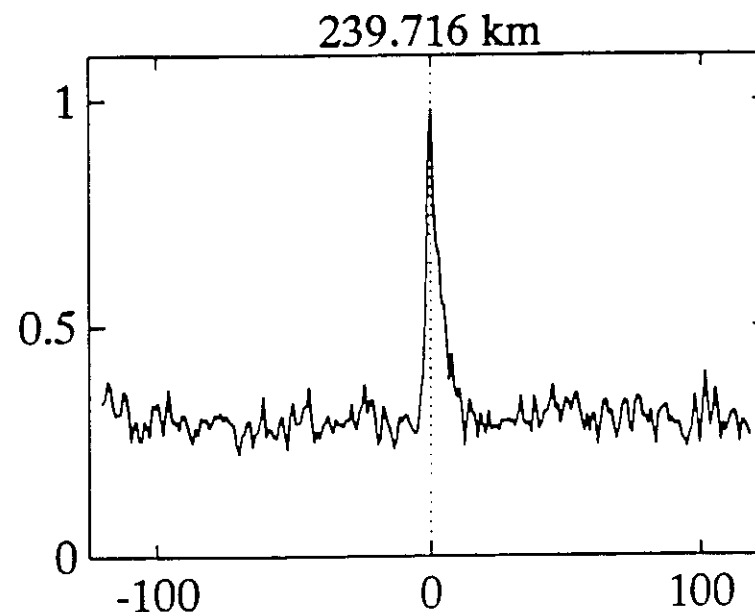
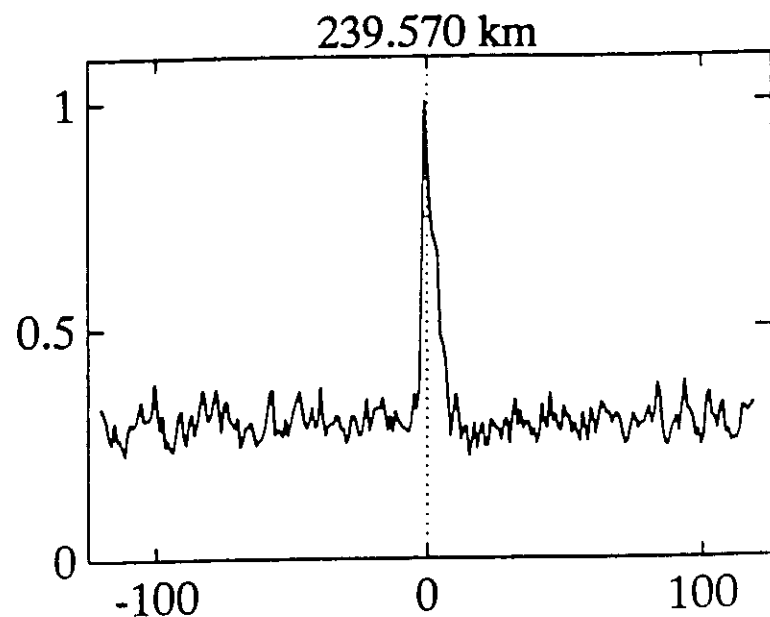
Figure 8



Frequency offset (kHz) from 430 MHz

12 July 1992, 05:02:00 AST, 188 seconds, 100 IPPs, Peak SNR = 0.602

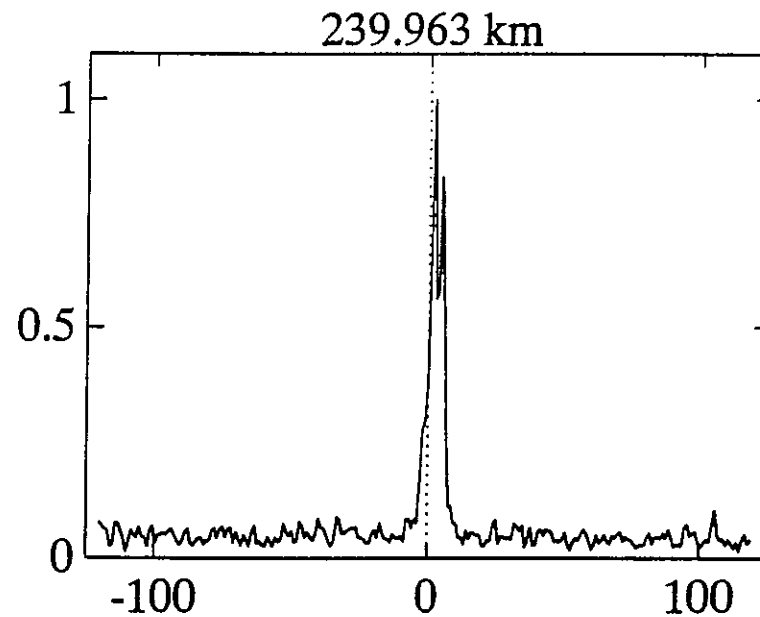
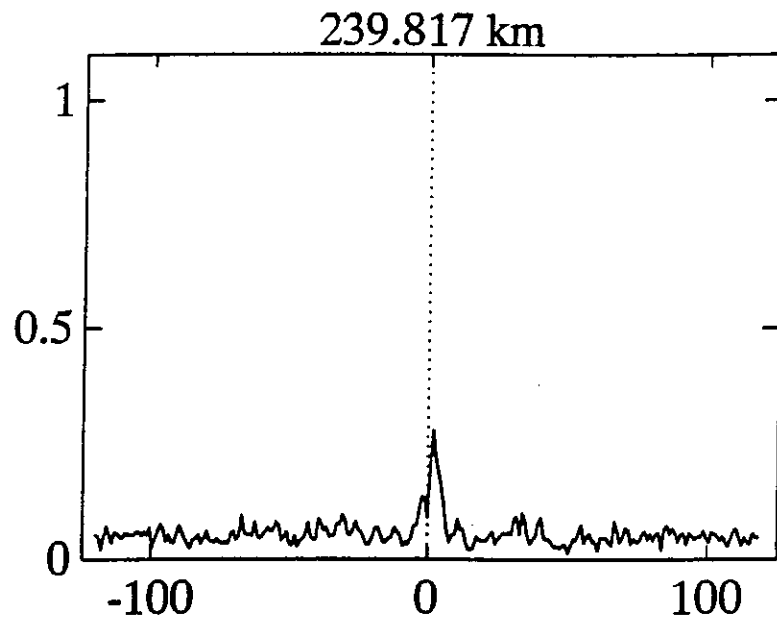
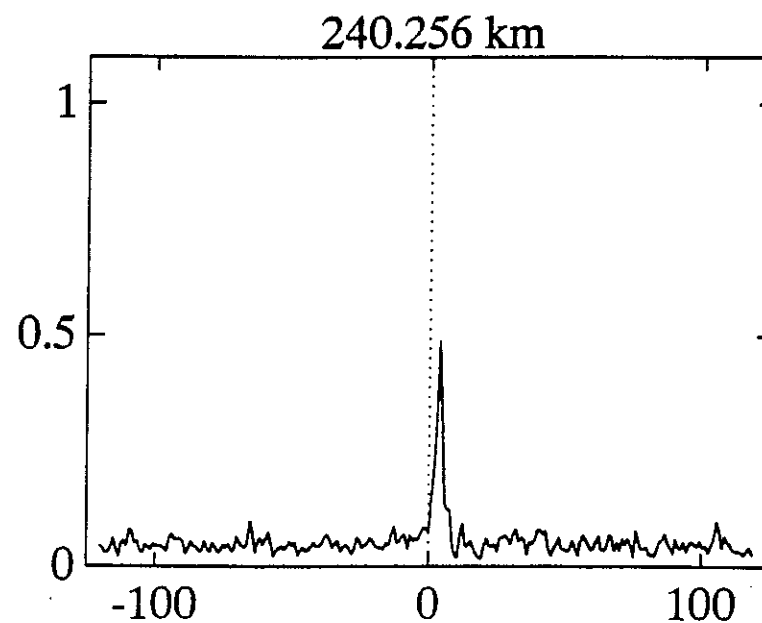
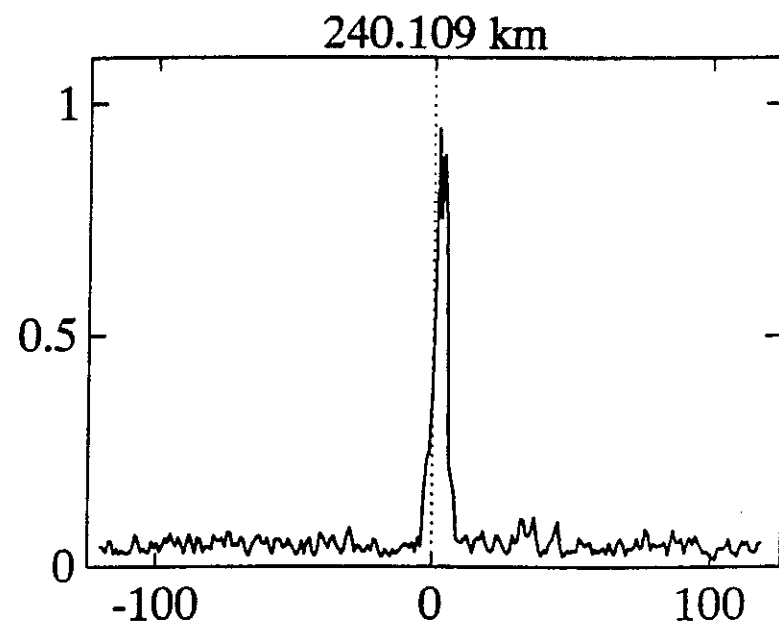
Figure 9



12 July 1992, 05:02:00 AST, 279.8 seconds, 100 IPPs, Peak SNR = 4.293, ZA = 13.13 deg

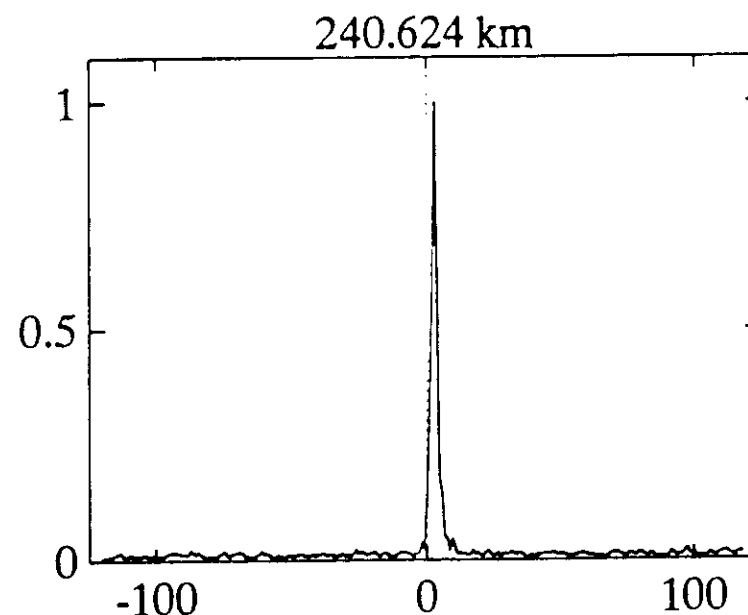
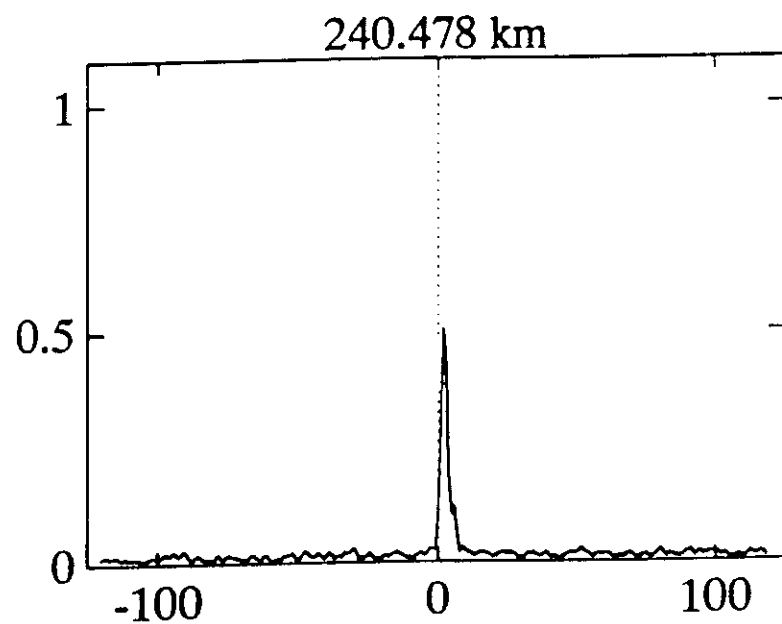
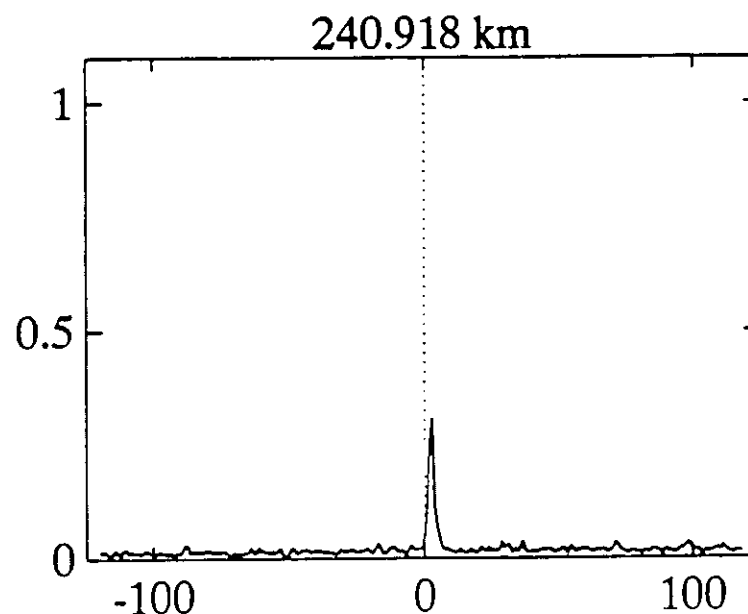
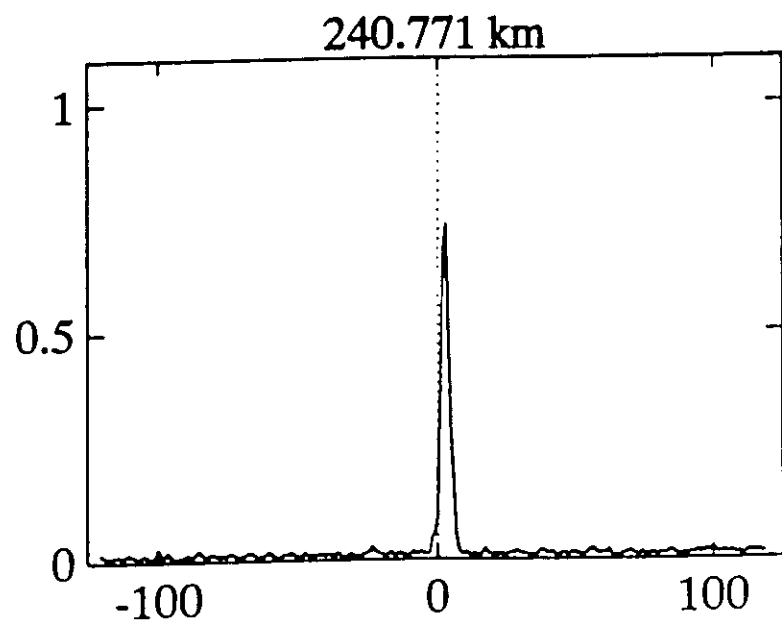
Frequency offset from (430 MHz - f_{HF})

Figure 10



12 July 1992, 05:02:00 AST, 284 seconds, 10 IPPs, Peak SNR = 34.2, ZA = 13.02 deg

Frequency offset from (430 MHz - f_{HF})



12 July 1992, 05:02:00 AST, 340.8 seconds, 10 IPPs, Peak SNR = 336.1, ZA = 12 deg

Frequency offset from (430 MHz - f_{HF})

Figure 12.

APPENDIX A. RUSSIAN STATIONS

Principal Investigator: G. P. Milinevsky

ABSTRACT

In two barium releases made over the Caribbean during the summer of 1991, the ion cloud was observed to last more than 10 hours. Observations were made with a low light level TV imager and a TV spectrograph operated onboard a Russian research vessel conducting ionospheric research and participating in the NASA-CRRES mission. The two clouds were observed near the release region for 15 to 25 minutes during the twilight following the initial release. One of the releases was made during evening twilight and the ion cloud reappeared the next morning, while the other was a morning release and the late-time observations made the next evening. The observations are highly surprising since, generally, it has been assumed that the ion cloud would dissipate within a few hours. However, the long life time appears consistent with current knowledge about dissipative processes. The long lifetime of barium ion clouds may provide for the most sensitive experimental testing of ionospheric convection models, a possibility with clear implications for future barium release experiments.

OPTICAL EQUIPMENT:

Gran-Piedro Mountain (Cuba)

TV camera with the intensifier of a sensitivity $10^{-3}-5 \cdot 10^4$ lx with recording information Panasonic with $F = 50$ mm.

One guidance system with the intensifier which has a resolution of 0.6 nm and spectrum recording.

The neon spectrum from a self-contained source was used to identify the spectrum in a frame.

A two channel photometer with a field of view of each channel 6, centered in the lines of ionized Ba and principle atmospheric emissions has also been used.

Two cameras with 35 mm and 60 mm films were mounted on a separate holder.

Airplane- YaK-40

Two B/W cameras with the intensifier, one of which was paired with a high-sensitive spectrograph.

Equipment characteristics were similar to those in Gran-Piedro. In addition, to obtain images in several spectral ranges, the interference filters set before the input lens were used.

Video cameras F-10 and M7 (Panasonic) with 8 transfocaters were used to obtain a colored image of a barium cloud at the initial phase of its formation.

The splitless spectrograph with the grating of 600 slits/mm was used.

To obtain the formation images applied were also the wide-frame camera AFA-BA-21C ($F = 210$ mm, aspect ratio of frame size 130 x 180 mm) and 35 mm camera.

HYDROMET RESEARCH VESSEL - "PROF. ZUBOV"

Four tele systems produced on a basis of TV cameras WV-1410, WV-1850, F10 (Panasonic) which were supplied with the image intensifier, TV units transmitting tubes of image isocon (sensitivity of 10^{-6} - $5 \cdot 10^{-7}$ lx) and isocon (sensitivity of 10^{-5} - $5 \cdot 10^{-6}$ lx) types.

The lens of different types with different focal lengths were used as the entrance optics.

The sensitivity of guaranteed recording cloud formation at all stages.

Temporal resolution specified by frame frequency was 0.02 sec.

For photographic recording space formation structure used were a well-known 35 mm camera and two RFK-5 cameras with high-sensitive lens of the focal length of 80 mm and 58 mm, one of which with an electron-optical intensifier.

The formations were recorded on a high-sensitive 35 mm film with 10 frames per second.

Wide-frame cameras MK-25 (F = 250 mm), AFA-BA-21C (F = 210 mm) and UA-47 (F = 100 mm) provided for recording images on a high-sensitive film of 19 and 8 cm, respectively, with exposure 1 - 10 sec.

Filming was carried out with light color filters.

To study spectral radiation composition applied was CP-48 spectrograph equipped with the image intensifier (the operating spectral region of 400-800 nm; resolution 0,5-1 nm; field of view 10 x 12 deg.; time of spectrum exposure 0,5-Ss), as well as splitless, tele and photo high-sensitive spectrographs similar to those installed on the airplane and Gran-Piedro mountain.

Photometric equipment involved four photometers, two of which are similar on Gran-Piedro mountain but one is equipped with a vertical scanning device.

The third and the fourth photometers are designed for recording radiation in separate spectral regions specified by narrow-band interference filters (4-10A).

Principle characteristics: measured luminance threshold 10-9W/sr m; field of view 0,5-6 deg.

Photometer data were entered to computers.

It should be noted that after a part of data has been photochemically treated, found was the decrease in their speed due to meteorological conditions, therefore only the initial cloud formation phases were registered.

HYDROMET RESEARCH VESSEL - "PROF. ZUBOV"

EQUIPMENT	MEASURED PARAMETERS STUDIED EVENTS	PRINCIPLE TECHNICAL DATA
Ion probe "Basis ionosounder.	Electron density distribution in ionosphere, including its modification. Artificial spread F event when modifying ionosphere in active experiments.	Frequency band 0.3-20 MHz Pulse duration 100 ms. Repetition frequency 50 (100)Hz. Pulse power 15 kW. Delta-antenna.
Multi-frequency complex of Doppler sounding.	Dynamic processes in ionosphere. Fine structure dynamics of modified ionosphere. Plasma distribution in modified ionosphere with high resolution. Artificial spread F.	Sounding at 8 frequencies in the 2-20 MHz range. Pulse duration 50-500 ms. Repetition frequency 100 or 200 Hz. Radiation intensity 1.5 kW. Rubidium frequency standard, instability not less than 10^{-10} . Spectral treatment with resolution 1/32 Hz at the complete analyzing band to 16 Hz 16-channel recording of measurement data, calculating dynamic spectra and secondary processing with PC IBM.
Receiving-recording equipment of Doppler radio set signals.	Radio-wave propagation in undisturbed and modified ionosphere in inclined paths. Diagnostic of spread F.	Receiving complement of broadcasting radiostations in the 2-32 MHz range. Recording of Doppler. Spectra of broadcasting radio stations in the band up to 200 Hz with resolution not less than 0.1 Hz. Two antennas of the "incident beam" type.
A set for recording satellite radio beacon signals.	Diagnostics of ionospheric structure and its disturbances.	Recording ionospheric. Doppler shift component of two coherent radio waves emitted by navigation satellites. Working frequencies 150 MHz and 400 MHz

APPENDIX B. INSTRUMENTATION

Title: CRRES Plasma Wave Experiment

Principal Investigator: Roger R. Anderson

The Passive Plasma Sounder (AFGL 701-15) and Search Coil Magnetometer (AFGL 701-13-2) Experiments on the SPACERAD portion of CRRES are collectively known as the Plasma Wave Experiment (PWE). The CRRES SPACERAD Plasma Wave Experiment instrumentation was designed to measure the plasma wave environment in the earth's radiation belts with emphasis on high frequency and time resolution, a large dynamic range, and sufficient frequency response to cover throughout nearly all of the CRRES orbit the characteristic frequencies of the plasma. The experiment makes measurements of electric fields from 5.6 Hz to 400 kHz and magnetic fields from 5.6 Hz to 10 kHz with a dynamic range of at least 100 dB (five orders of magnitude in amplitude) beginning at the respective receiver's noise level. The basic CRRES Plasma Wave Experiment includes two receivers (1) a 1218-channel sweep frequency receiver for high-frequency-resolution spectrum measurements from 100 Hz to 400 kHz, and (2) a 14-channel spectrum analyzer to provide high-time-resolution spectra from 5.6 Hz to 10 kHz.

The SPACERAD Plasma Wave Experiment instrumentation not only measures and characterizes the plasma wave environment but also measures the electron number density up to $2,000 \text{ cm}^{-3}$. From the identification of the upper hybrid resonance frequency and/or the electron plasma frequency in the data, the PWE is able to obtain the total plasma density near the spacecraft down to low densities and without regard to spacecraft charging. The CRRES Plasma Wave Experiment provides electron number density measurements continuously over the range from about 10^{-6} cm^{-3} to $2 \times 10^3 \text{ cm}^{-3}$ using passive sounding techniques that are free from spacecraft charging effects. The electron number density, N_e , is determined from $F_{pe} = 8.98 \text{ kHz} \times (N_e)^{1/2}$ where N_e is in units of electrons per cm^{-3} .

Double-spherical probe electric field and electrostatic dN/N measurements from 5.6 Hz up to 400 kHz are also possible via signals from the antennas and preamps of the Langmuir Probe experiment whose instrument scientist is Dr. John R. Wygant from the University of California, Berkeley.

The Plasma Wave Experiment measures the electromagnetic and/or electrostatic fields detected by three sensors: (1) a 100-meter tip-to-tip extendible fine wire long electric dipole antenna, (2) a search coil magnetometer mounted at the end of a 6-meter boom, and (3) a 100-meter tip-to-tip spherical double probe electric antenna. The first two sensors are the primary sensors for the Plasma Wave Experiment while the third sensor is the primary sensor for the Langmuir Probe Experiment. High-input-impedance preamplifiers are located on the spacecraft near the base of each half of the extendible fine wire long electric dipole antenna. The search coil magnetometer contains a high permeability mu-metal core 0.41 meter long wound with 10,000 turns of #42 wire, and a preamplifier. Signals from the sensors, after buffering and processing by appropriate preamplifiers and differential amplifiers, are routed via antenna selection switches to the Sweep Frequency Receiver and the Multichannel Spectrum Analyzer.

The Sweep Frequency Receiver (SFR) covers the frequency range from 100 Hz to 400 kHz in four bands with 32 steps per band. The fractional step separation of the SFR, df/f , is about 6.7% across the entire frequency range. Band 1 (100 Hz to 810 Hz) is sampled one step per second or 32 seconds per sweep, Band 2 (810 Hz to 6.4 kHz) is sampled two steps per second or 16 seconds per sweep, and Band 3 (6.4 kHz to 51.7 kHz) and Band 4 (51.7 to 400 kHz) are each sampled four steps per second or 8 seconds per sweep. The nominal bandwidths of the four bands are 7 Hz, 56 Hz, 448 Hz, and 3.6 kHz, respectively. The four bands each have a logarithmic compressor which measures the signal amplitude over about a 100 dB dynamic range beginning at the noise level of the receiver and produces a 0.0 to 5.10 Volt DC analog output proportional to the logarithm of the input amplitude.

The Multichannel Spectrum Analyzer consists of 14 narrow band filters logarithmically spaced in frequency (4 filters per decade in frequency) from 5.6 Hz to 10 kHz followed by 14 logarithmic compressors each having a dynamic range of about 110 dB. The nominal 3 dB sine wave bandwidth of each narrow band filter is $\pm 15\%$ of the center frequency except for the two highest frequency channels (5.62 kHz and 10.0 kHz) whose bandwidths are $\pm 7.5\%$ of the center frequency. The 14 0.0 to 5.10 Volt DC analog outputs are sampled simultaneously 8 times per second to produce high time resolution spectra.

The Spacecraft Telemetry Data System provides the clock and command lines for controlling the receivers and the sampling and the analog to digital conversions of the receivers' 0.0 to 5.10 Volt DC analog outputs. The CRRES PWE has two high-level relay commands and one 16 bit serial command. The high-level relay commands turn the experiment power on and off. The serial command determines which sensor is connected to which receiver and whether or not the receivers are locked onto a single sensor or cycle through all of the sensors. Throughout the majority of the CRRES lifetime and throughout the high altitude chemical release campaign, the CRRES PWE was operated with the SFR locked onto the long-wire electric antenna and the Multichannel Spectrum Analyzer cycling through all three sensors: 4 seconds B, 4 seconds E, 4 seconds B, and 4 seconds LANG. B is the search coil magnetometer, E is the long electric dipole antenna, and LANG is the input from the Langmuir Probe Experiment.



LRRES SFR/SA

dBV/m/√Hz -166.0

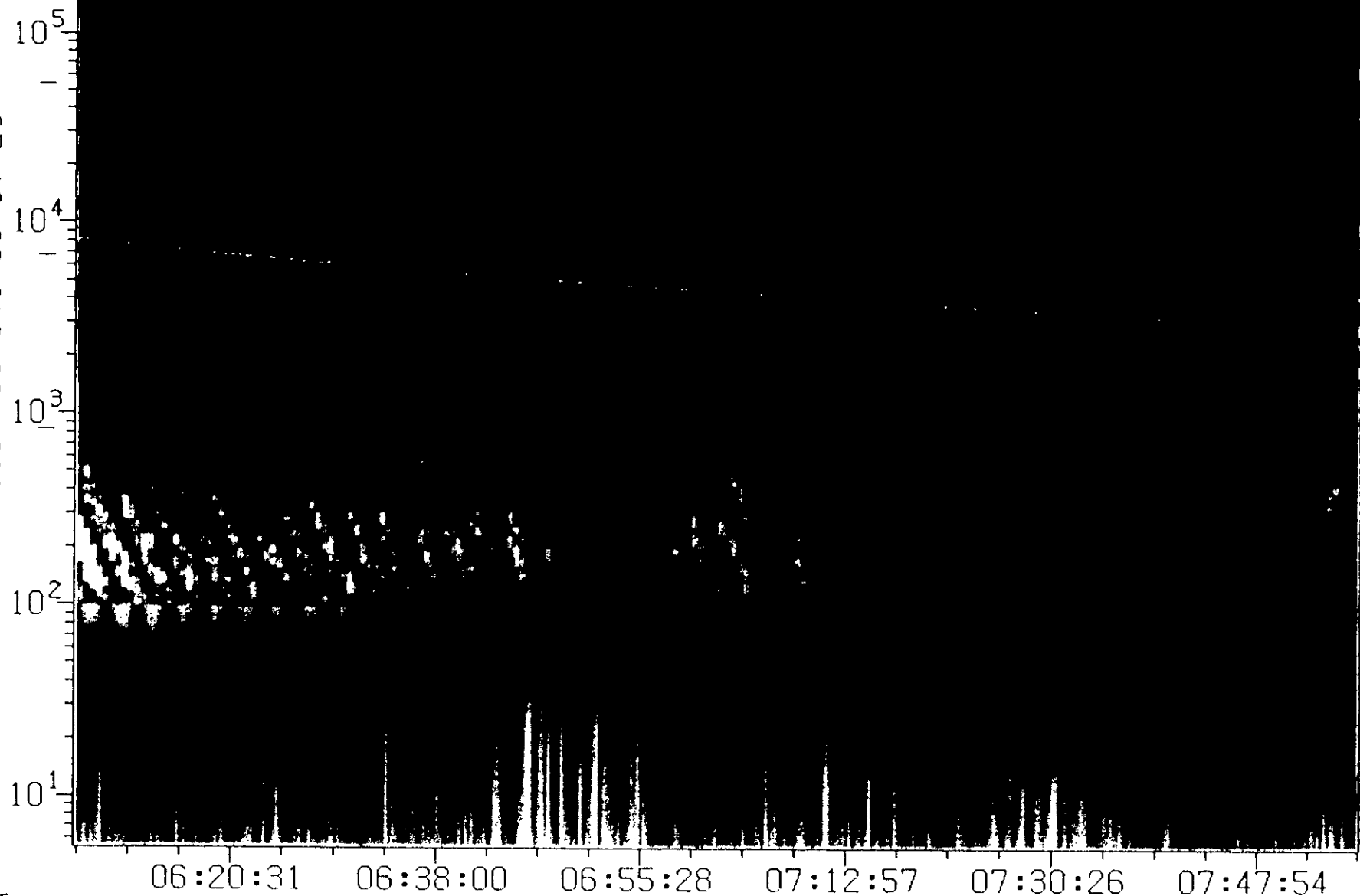
LMSC P-0357

AFGL

-66.0

135
VTCW 085BA800 91-049 06:07:25

ANTENNA
L B E



858C000

858E000

85C0000

85C2000

85C4000

85C6000

Figure A8b

THE UNIVERSITY OF IOWA/AFGL 701-15

SFR200 V2.3

PROCESSED 11-AUG-91 19:33 /S= 3



LRRES SFR/SA

dBV/m/√Hz -166.0

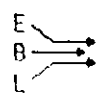
-66.0

LMSC P-035

AFGL

136
VTCW 085C7000 91-049 07:56:38

ANTENNA



08:05:23 08:22:51 08:40:20 08:57:48 09:15:17 09:32:46

85C8000

85CA000

85CC000

85CE000

85D0000

85D2000

Figure A8c

THE UNIVERSITY OF IOWA/AFGL 701-15

SFR200 V2.3

PROCESSED 11-AUG-91 19:33 /S= 3



LRRES SFR/SA

dBV/m/√Hz -166.0

LMSU F-033366

AFGL

-66.0

VTCW 08503800 91-049 09:45:52

ANTENNA

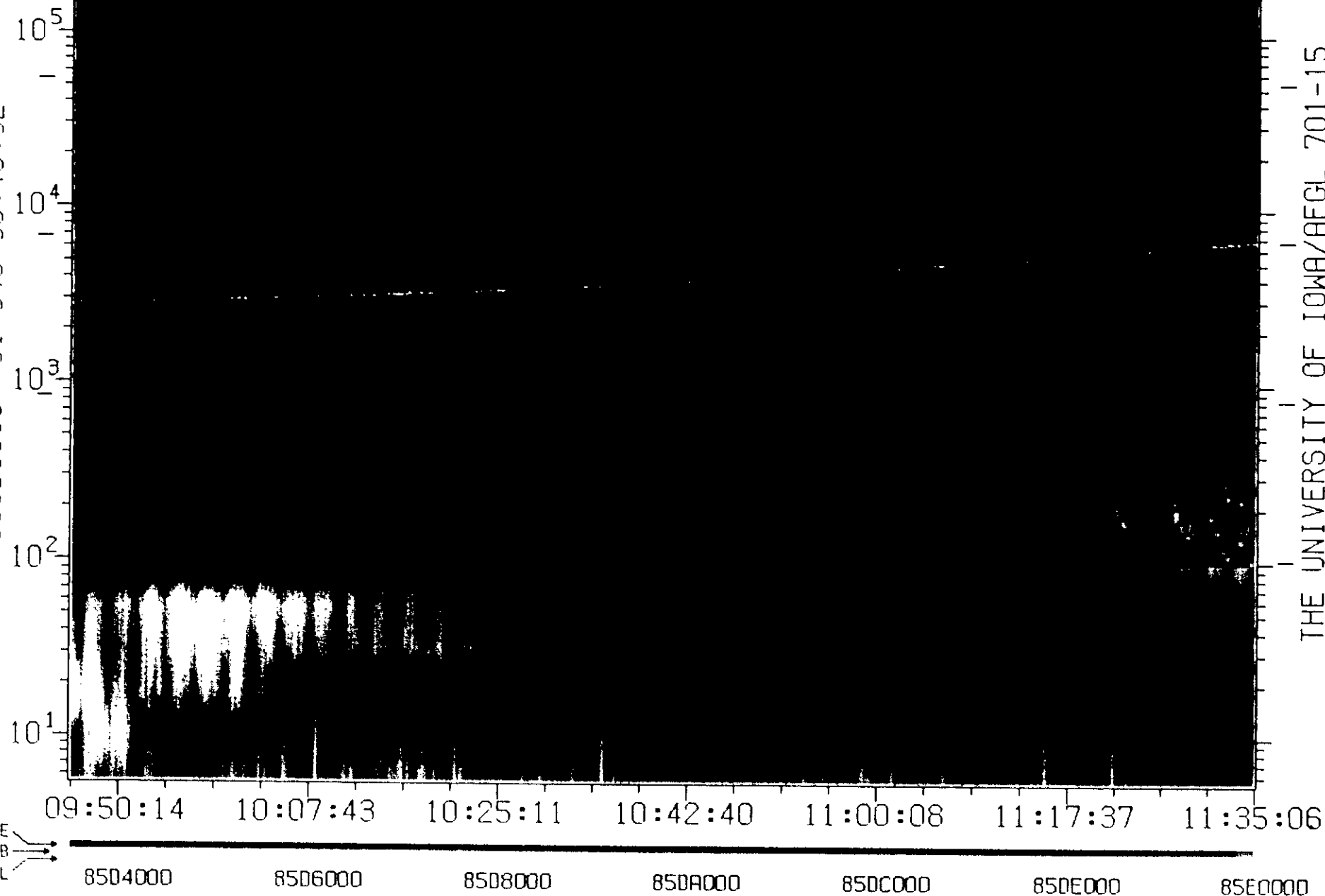


Figure A8d

THE UNIVERSITY OF IOWA/AFGL 701-15

SFR200 V2.3 PROCESSED 11-AUG-91 19:33 /S: 3



CRRES SFR/SA

dBV/m/√Hz -166.0

LMSU R-035

AFGL

-66.0

VTCW 085E0000 91-049 11:35:06

ANTENNA

11:35:06

11:52:34

12:10:03

12:27:31

12:45:00

13:02:28

13:19:57

85E0000

85E2000

85E4000

85E6000

85E8000

85EA000

85EC000

Figure A2

THE UNIVERSITY OF IOWA/AFGL 701-15

SFR200 V2.3

PROCESSED 11-AUG-91 19:33 /S= 3

APPENDIX C. THEORY AND COMPUTATIONS

Title: Theoretical and Computational Studies of the CRRES Barium Releases

Principal Investigator: Joseph D. Huba

INTRODUCTION:

A series of high-altitude ($h \sim 350 - 33,600$ km) barium releases were conducted in the ionosphere and magnetosphere during the NASA/DOD sponsored Combined Release and Radiation Effects Satellite (CRRES) Mission. The scientific objectives of the mission included the study of the formation of diamagnetic cavities, the coupling of the barium plasma to the ambient plasma and geomagnetic field, and the stability of the barium plasma. A number of theoretical and computational studies were performed at NRL to accomplish these objectives. In particular, we have developed a detailed kinetic theory of the early time microinstabilities associated with the high-altitude releases (G-4 and G-10; $h \sim 33,000$ km), and have performed numerical simulations using a 2D Hall MHD code of these releases; we have performed 3D kinetic simulation studies to investigate early time structuring of transition-altitude releases (G-2; $h \sim 6,000$ km); and have performed 2D electrostatic fluid simulations of the low-altitude CRRES releases (G-9; $h \sim 450$ km) to study cloud 'skidding'.

Background

The Combined Release and Radiation Effects Satellite (CRRES) program used the scientific resources of NASA and DOD to (1) perform chemical release experiments in the ionosphere and magnetosphere, (2) study the natural radiation environment and its effects on electronic circuit components, and (3) probe naturally occurring ionospheric irregularities. The CRRES spacecraft was launched on 25 July 1990 at 1921 Universal Time. Eight small and eight large barium-thermite canisters were located in injection tubes on two sides of the satellite. The canister eject mechanisms permitted releases as singles or pairs. The chemical release experiments were designated by G-1 through G-14 where G signified the geosynchronous transfer orbit with apogee and perigee of 33,600 and 350 km, respectively. Releases occurred at low altitudes ($h \sim 350$ to 500 km), transition altitudes ($h \sim 6,000$ to 25,000 km), and near-geosynchronous altitude ($h \sim 33,000$ km). Ground-based optical and *in situ* instruments recorded the effects of the chemical releases.

The released materials were chosen for the properties of (1) low ionization potential, and (2) fluorescence of its neutral or ion component in sunlight. The substances were vaporized from CRRES canisters heated internally with a mixture of titanium-boron thermite. The vaporization process determines the initial velocity distribution for the injected neutrals. The neutral cloud expands as a shell centered on the CRRES satellite. Barium was used for most of the CRRES releases because (1) atomic Ba is rapidly photoionized ($\tau_i = 28$ s), and (2) both Ba and Ba^+ glow in the visible spectrum. For barium, the characteristics of the shell are a radial speed $V_R = 1.38$ km/s and a shell thickness $V_T = 0.26$ km/s. For other species, these velocities tend to be inversely proportional to the square root of the atomic mass. A more complete overview of the chemical release experiments from the CRRES satellite is given by Bernhardt [1992].

Diamagnetic cavities are formed if the ambient magnetic field is canceled by a magnetic field from a current loop. For an expanding ion cloud, this current loop is driven by radial electric fields set up as unmagnetized ions try to out-run magnetized electrons on the surface of the cloud. If the dynamic pressure of an expanding ion cloud greatly exceeds the ambient magnetic pressure in the ionosphere, a well defined diamagnetic cavity will be produced. The maximum cavity radius (R_B) may be estimated by solving the energy balance equation $M_0 V_0^2/2 = (B^2/8\pi)4\pi R_B^3/3$ where M_0 is ion mass, V_0 is expansion velocity, and B is the strength of the unperturbed magnetic field. This process is relevant for sub-Alfvenic expansions, i.e., $V_0 < V_A$ where $V_A = B/(4\pi n_i m_i)^{1/2}$ is the Alfven velocity. *In situ* magnetometer measurements confirm the development diamagnetic cavities [Singer et al., 1991]. The background magnetic field was totally excluded for the two largest releases, G-8 and G-10, in the 125 nT magnetic field. The other high altitude barium releases produced less pronounced cavities.

Plasma microinstabilities can be generated by the diamagnetic current in the expanding barium shell. These instabilities are important because they can seed large scale instabilities, and can provide a mechanism for rapid diffusion of plasma and magnetic field across the boundary layer. A comprehensive theory of the linear stability of sub-Alfvenic plasma expansions has been developed at NRL [Huba et al., 1990]. The calculation is based upon Vlasov theory and includes finite β effects (i.e., electromagnetic coupling and electron ∇B drift-wave resonances), collisional effects, and neutral gas flow effects. Instability is found to occur in both the strong drift ($V_d > v_i$) and weak drift ($V_d < v_i$) regimes, where V_d is the crossfield drift velocity and v_i is the ion thermal velocity. *In situ* plasma wave measurements found that high frequency electrostatic and electromagnetic wave turbulence occurred in and near the expanding barium shell [R.R. Anderson, private communication, 1992].

Optical observations of sub-Alfvenic plasma expansions [Bernhardt et al., 1987] resulting from the AMPTE magnetotail barium releases showed the formation of large-scale plasma irregularities on their surfaces (Figure 1). Similar field aligned irregularities have been observed with diamagnetic cavities generated in the laboratory [Ripin et al., 1987]. The structuring has been attributed to the unmagnetized ion Rayleigh-Taylor instability [Huba and Hassam, 1987; Huba et al., 1990]. A 2D magnetohydrodynamic (MHD) simulation of the G-10 release [Huba et al., 1992a] has demonstrated that the Hall term is crucial to development of instability on time scales $t < \Omega_i^{-1}$ where Ω_i is the ion cyclotron frequency. This is dramatically shown in Figure 2 which contrasts the G-10 expansion with and without the Hall term. When the Hall term is absent (top panel of Figure 2), the barium plasma uniformly expands to a radius $\sim R_B$ and recollapses; however, when the Hall term is present (bottom panel of Figure 2), the plasma rapidly structures and develops large plasma flutes which 'jet' across the magnetic field lines. These results are consistent with optical observations of the G-10 barium release [P.B. Pongratz, private communication, 1992].

The simulation results of G-10 can also be compared to *in situ* magnetometer data. In Figure 3a the magnitude of the magnetic field $|B|$ versus time is plotted using magnetometer measurements on the CRRES spacecraft [Singer, 1992]. For times UT < 5:30:05 the satellite is in the ambient field and plasma. Then, at time UT \sim 5:30:05, the diamagnetic cavity envelops the satellite and the magnetic field goes to zero. From UT \sim 5:30:05 - 5:30:40 the satellite is in the diamagnetic cavity. Finally, for UT > 5:30:40 the satellite begins to exit the diamagnetic cavity and eventually returns to the ambient plasma and field conditions after undergoing several oscillations. The satellite data is compared to the simulation results by 'flying' the satellite through the simulation data at $t = 46$ sec; the simulation results are shown in Figure 3b. The scaling is chosen to be consistent with the length of time the satellite is in the magnetic cavity ($B \sim 0$). The important aspect of this comparison is the similarity between the large-scale oscillations of the magnetic field; this is interpreted as a manifestation of the unstable nature of the plasma expansion. There is not an exact match between the time scale of the oscillations because the relative velocity between the satellite and magnetic cavity is more complex than assumed. In general, the Hall MHD code results agree reasonably well with

observational data: a diamagnetic cavity forms and eventually collapses, the plasma structures during the expansion phase and seems to free-stream across the field, and finally, the time and length scales associated with these processes are appropriate.

Transition Altitude Release Studies

A high resolution telescope filtered at the 455.4 nm barium ion-line recorded curved irregularities 25 seconds after the CRRES G-2 release (see Figure 4a). These irregularities, unlike those associated with the high-altitude releases, were not aligned with the magnetic field but they conformed to the contour of the expanding barium cloud shell. Figure 5 illustrates the 'cycloid bunching' mechanism for generation of these irregularities. Consider a small barium cloud moving along a trajectory with velocity V_e which lies in the x-z coordinate plane. After photoionization, the ions will move with a constant speed along z-axis in the direction of the background magnetic field if polarization electric fields are neglected. The ion cyclotron motion around the magnetic field lines has a period of $T_2 = 2\pi/\Omega_i$ where $\Omega_i = eB/m_i c$ is the ion cyclotron frequency. For an impulse source of neutrals, the ion orbits form into a cycloid which has a spatial period of $V_{Cx}T_2$. The density of the ions are larger at the cusps of the cycloid. For an extended neutral cloud, the cycloid bunching is effective if the center of mass velocity perpendicular to B (V_{Cx}) is much larger than the characteristic speeds (V_R and V_T) of the release distribution.

The CRRES G-2 cloud was injected with velocity components $V_e = (5.8, 0.0, -2.1)$ km/s. In the ambient 5000 nT magnetic field, the gyro period was 1.7 s. The spatial period of the cycloid is calculated to be 10 km, closely matching the distance between the irregularities illustrated in Figure 4a. We have used a three dimensional simulation of the Vlasov equation without electric fields to study the cycloid bunching [Bernhardt et al., 1992]; the results are shown in Figure 4b. The computer model includes effects of radiative transfer and Doppler shifts of the barium ions relative to the sun's absorption line near 455.5 nm. The computer simulations of cycloid bunching yield an excellent match to the observed structures.

Low Altitude Release Studies

The CRRES chemical releases were designed to study the braking of ion clouds injected perpendicular to B. The question of motion of artificial ion clouds in the magnetosphere is over twenty years old [Scholer, 1970]. In a low- β plasma, ions created moving perpendicular to the ambient magnetic field will polarize to set up an electric field to keep the ion cloud moving in the same direction. This process has been labeled 'skidding'. Braking of the cloud occurs as the polarization electric field transfers momentum to the background plasma contained in the magnetic flux tube through the cloud [Mitchell et al., 1985]. The electric field may propagate along magnetic field lines to be dissipated by the high conductivity in the E-region ionosphere [Nalesso et al., 1988]. Thus, parameters which control the braking of the injected ion cloud are (1) the mass and perpendicular velocity of the cloud, (2) the content of the flux tube, and (3) the Pedersen conductivity of the E-region.

The braking or 'skidding' experiments were conducted with the CRRES G-1, G-9, and G-11a releases which occurred between 400 and 500 km altitude. All releases occurred at dawn when the E-region conductivity was at a minimum. The CRRES canisters were moving at 9 km/s within 20 degrees of perpendicularity to the magnetic field. Figure 6 is a composite of two images for the G-9 barium release. The 10 km distance between the initial burst and the edge of the second image is evidence of 'skidding'.

A simulation study based on a two dimensional electrostatic code yields good agreement with this distance [Huba et al., 1992b]. The plasma dynamics is modeled using a two-layer, field-line integrated set of equations. A novel aspect of the model is that the coupling to the background ionosphere is time dependent; the coupling distance is based upon the propagation time for an Alfvén wave. This is crucial to accurately modeling the braking distance of the barium cloud. The position of the maximum field-line integrated neutral density (N_n) and barium ion density (N_e), potential (ϕ),

and cloud velocity (V_c) at maximum ion density versus time (t) are shown in Figure 7. The ion and neutral clouds are initially co-located moving at the orbital velocity V_{n0} ; the polarization field is initially $E_{pol} \approx V_n \times B/c$. The maximum N_c falls behind the maximum N_n and the barium cloud skids ~ 15 km in ~ 3 sec. These results are consistent with observational evidence.

Conclusion

Theoretical and computational studies of the CRRES barium releases performed at NRL have provided the scientific community with a clearer understanding of the physical processes associated with chemical releases in space. In particular, studies of the rapid structuring of the high-altitude barium releases caused by the Hall term, the curved irregularities observed in the transition altitude releases caused by cycloid bunching, and the 'skidding' of barium across the magnetic field have provided new insights into space phenomena.

Figure Captions

Fig. 1) CCD image showing irregularities on the surface of the AMPTE barium ion cloud in the magnetotail. The release occurred on March 21 1985. The scale size of the irregularities is smaller than the ion Larmor radius p_i . Inside the cloud is a diamagnetic cavity.

Fig. 2) Color-coded contours of the density versus spatial position for the G-10 barium release at times $t = 6, 16, 32$, and 46 s. These results are based upon a 2D MHD simulation code. The top panel shows the expansion without the Hall term, while the bottom panel shows the expansion with the Hall term. It is clear that the Hall term is crucial to the structuring of the plasma.

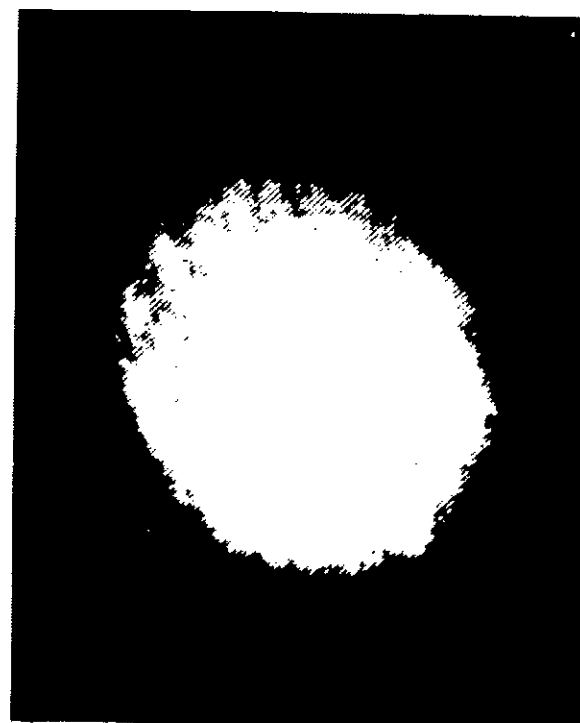
Fig. 3) The magnitude of the magnetic field $|B|$ (nT) versus time t (s). (a) Magnetometer data [Singer, 1992]. (b) Simulation results.

Fig. 4) (a) High resolution image of the G-2 barium ions obtained with a two second exposure using an intensified CCD camera filtered at 455.4 nm. The release occurred at 20:17:00 UT on 13 January 1991 at 6180 km altitude. The injection velocity was 6.136 km/s. The ion cloud evolved into curved irregularities within 25 seconds after release. (b) Computer simulation of the G-2 release based upon a 3D kinetic model.

Fig. 5) Diagram of the cycloid produced by photoionization of a point source of barium neutrals. The emissions from this cycloid have a temporal period of $T_2 = 2\pi/\Omega_i$ and a spatial period of $V_{Cx}T_2$

Fig. 6) Superimposed images of the G-9 barium cloud at times 0 and 21 seconds after the release. The separation of the two images is the result of ion 'skidding'.

Fig. 7) The positions of maximum field-lined integrated barium ion (N_c) and neutral (N_n) densities, the electrostatic potential (ϕ), and the ion cloud velocity (V_c) versus time t (s). These results are based upon 2D electrostatic simulation code and show that the barium cloud skids ~ 15 km in ~ 3 sec consistent with observational results.



09:24:01

AMPTE BARIUM RELEASE IN THE MAGNETOTAIL
MARCH 21, 1985 GMT

Figure 1

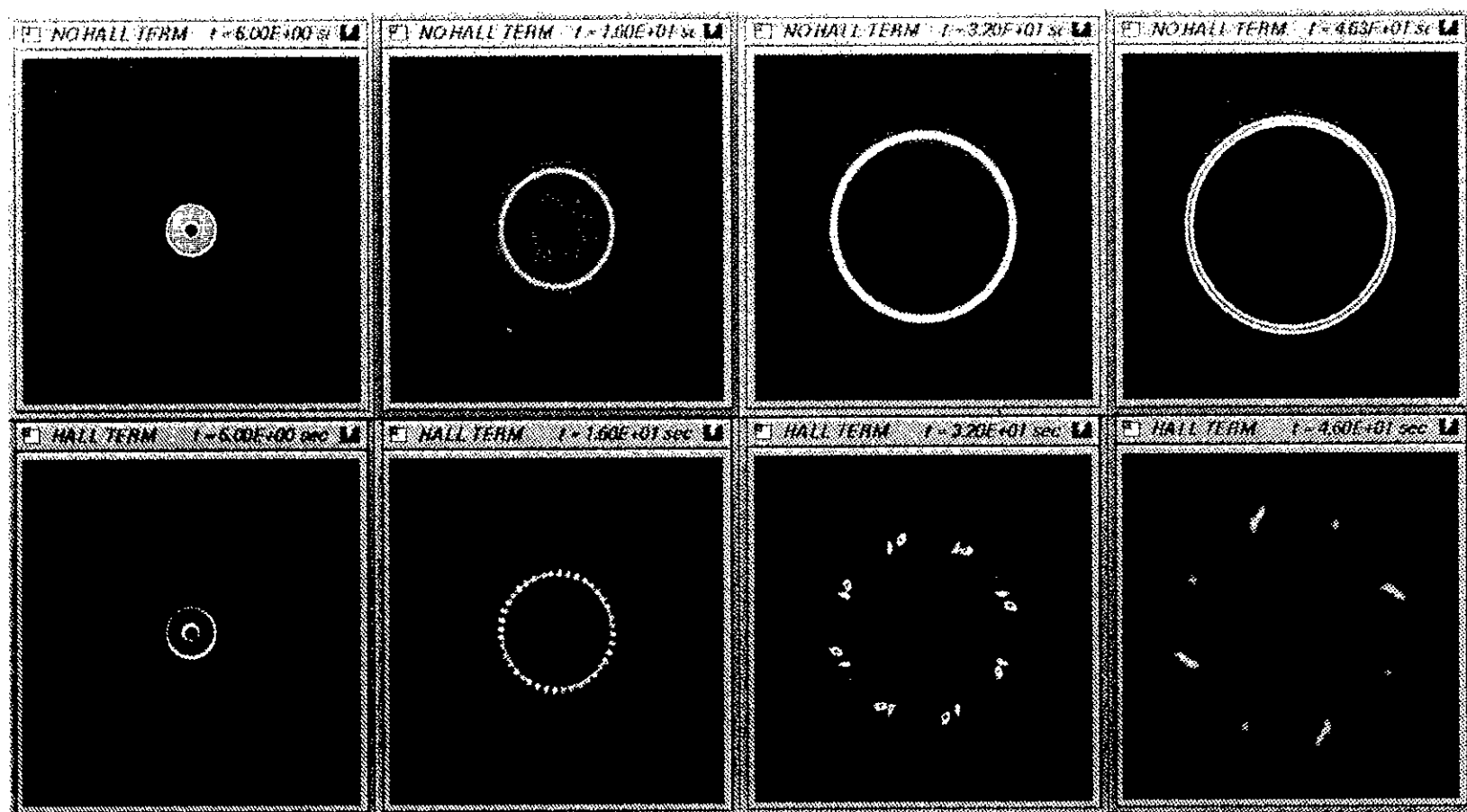
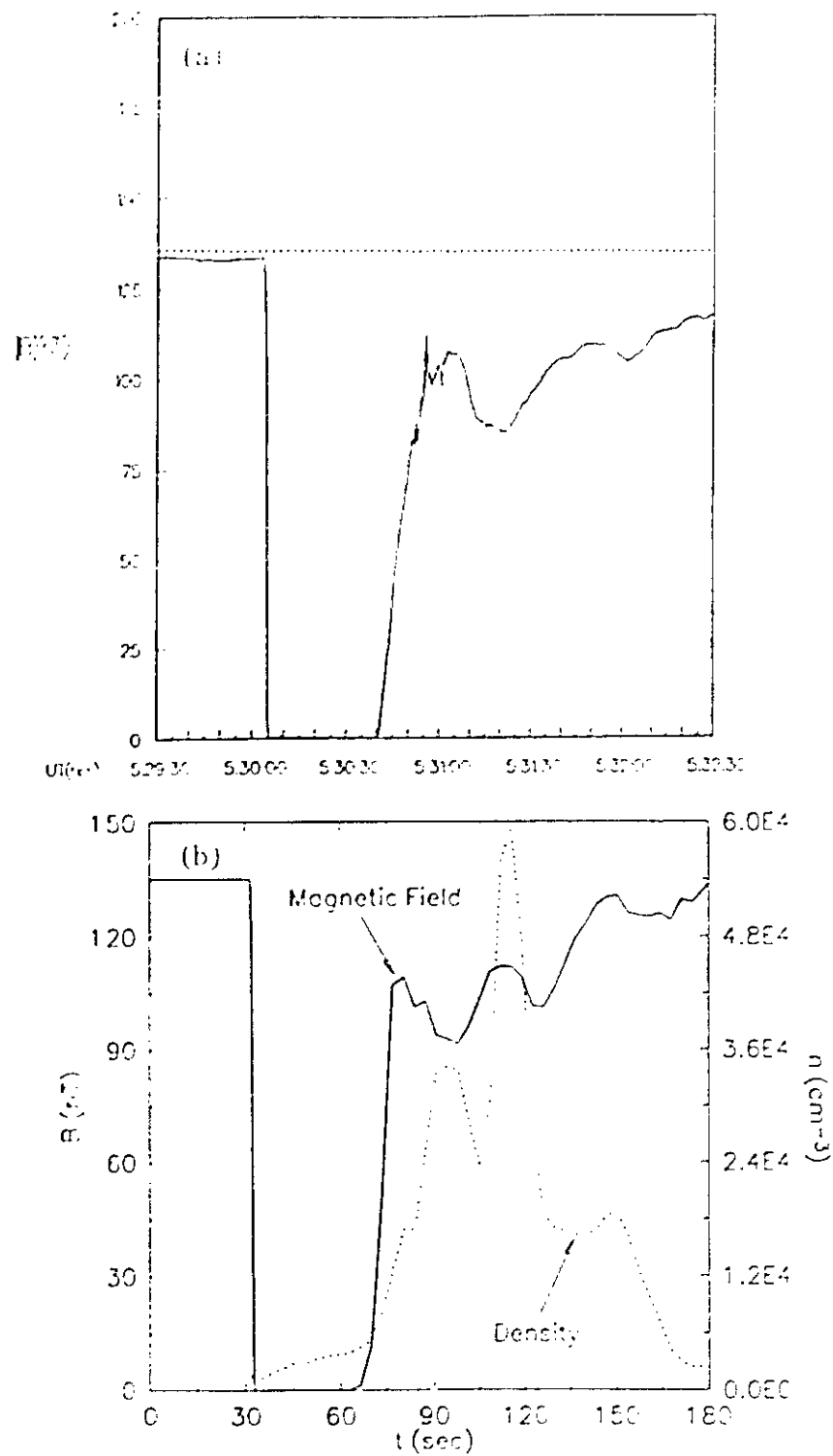


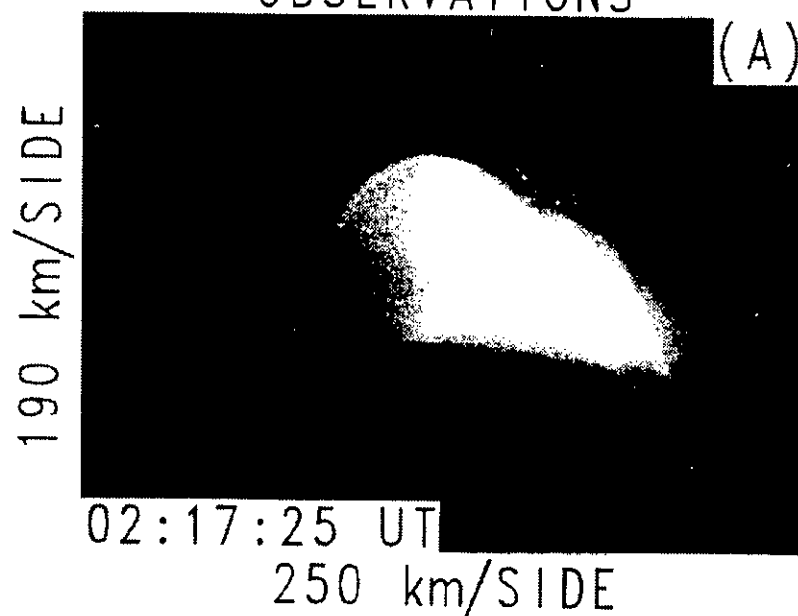
Figure 2



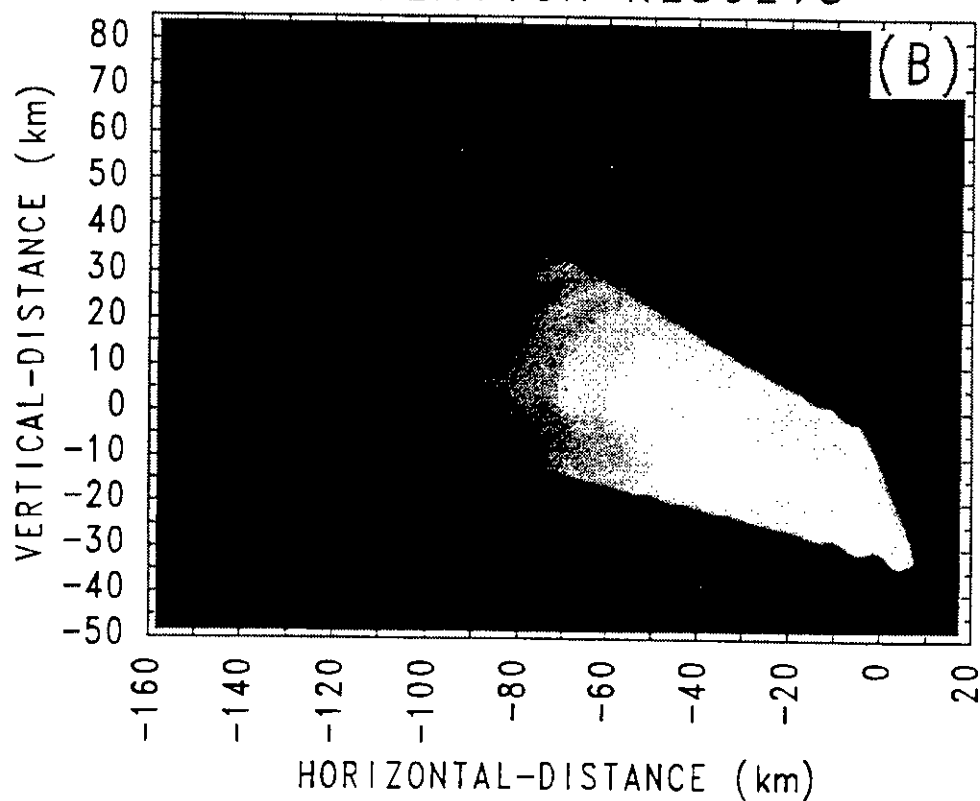
CRRES G-2 BARIUM ION CLOUD

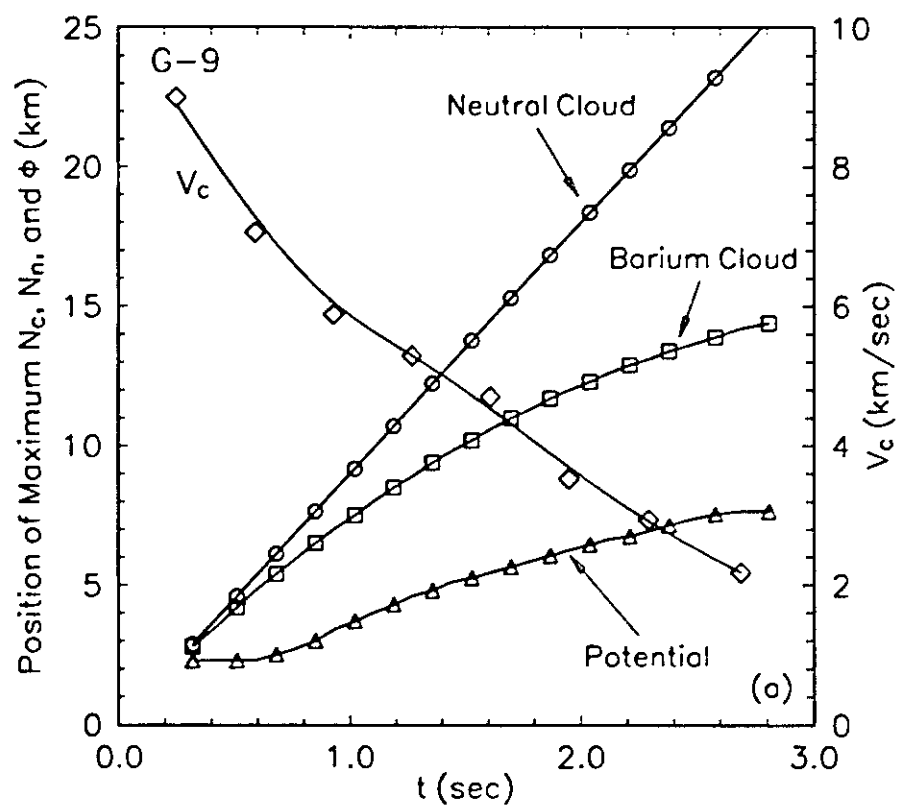
13 JAN 1991 02:17:00 UT

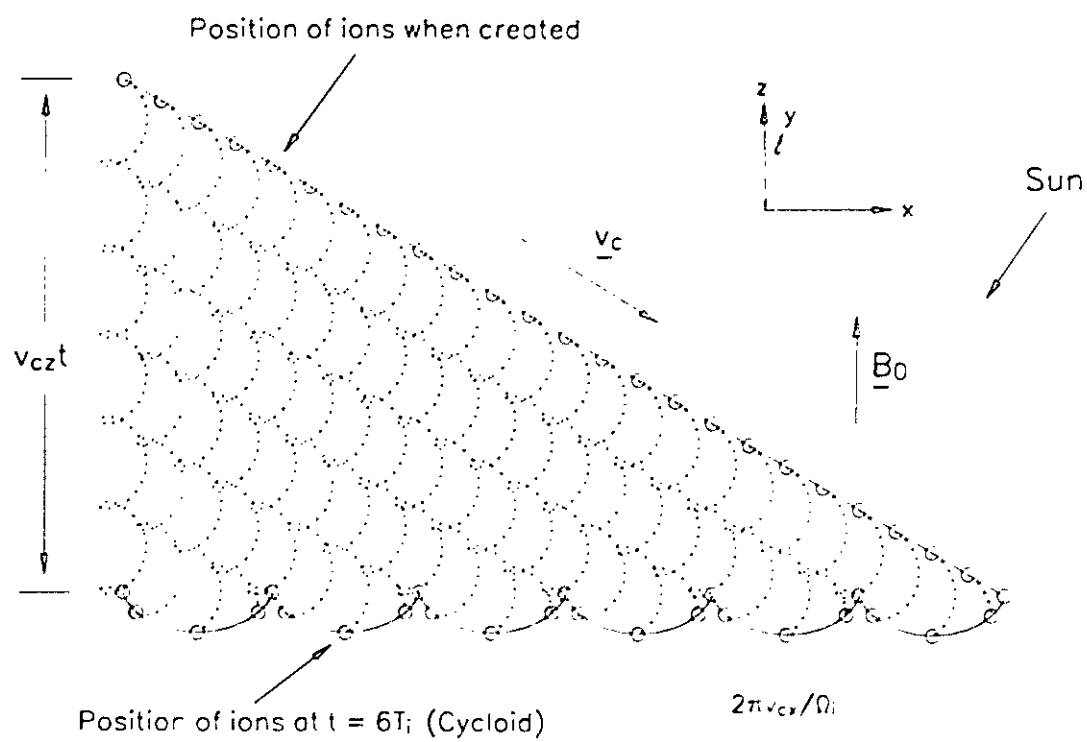
OBSERVATIONS



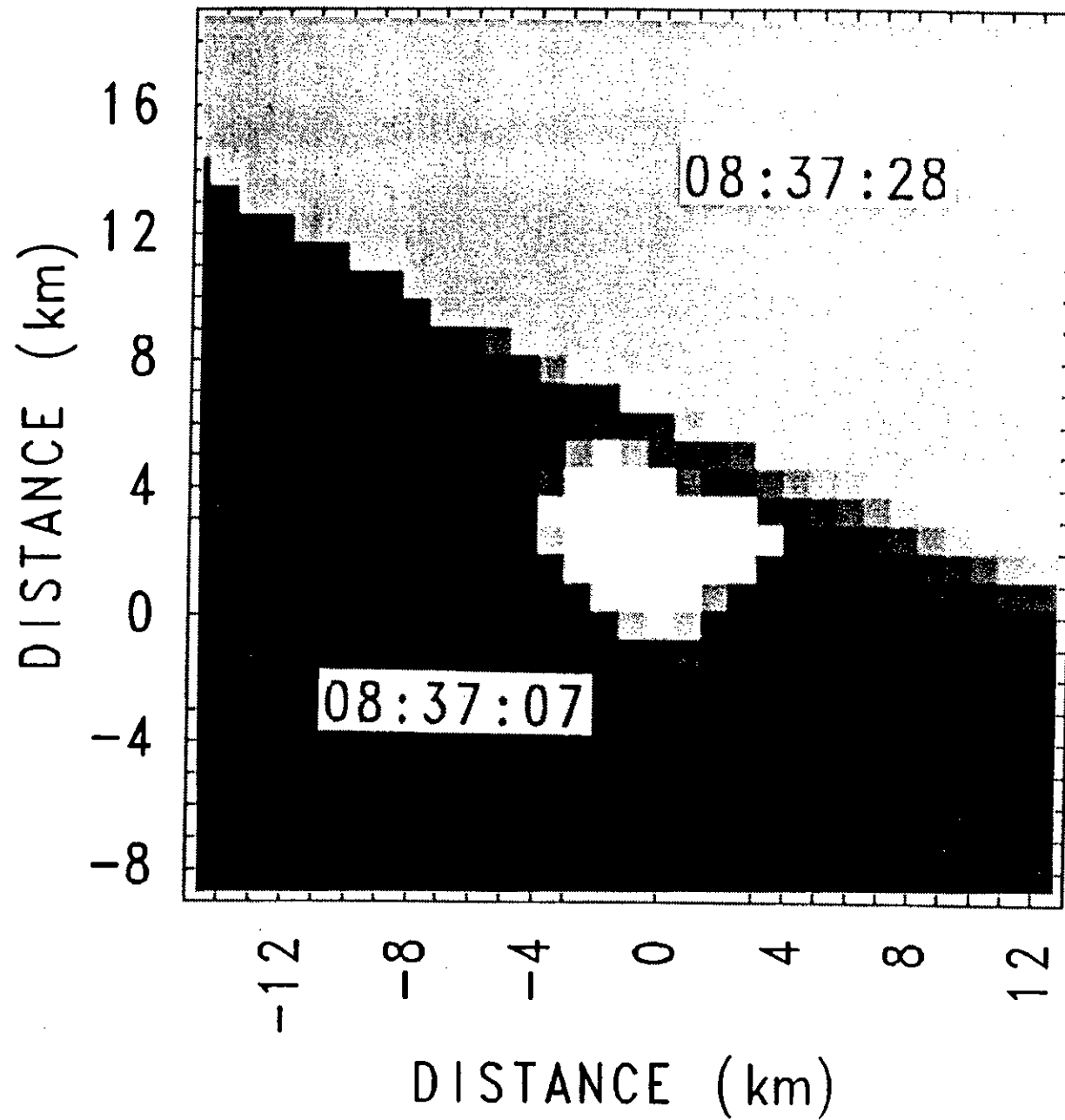
SIMULATION RESULTS







CRRES G-9, 19 JULY 1991



APPENDIX D. CRRES PUBLICATIONS BY MAIN AUTHOR

Anderson, Roger R.—University of Iowa

CRRES Plasma Wave Observations at the Plasmapause *American Geophysical Union (AGU)—1992 Spring Meeting—Oral Presentation* No Specific Campaign

Anderson, Roger R.—University of Iowa

CRRES Plasma Wave Experiment *Journal of Spacecraft and Rockets—Vol. 29, No. 4, 1992—Publication* No Specific Campaign

Author Unlisted—

The CRRES El Coqui Caribbean Campaign *The Cedar Post—9-93—Publication* Sounding Rocket Campaign

Bass, J. N.—Radex Inc.

Energetic Electron and Magnetic Field Variations Observed by CRRES During the Magnetic Storm of 26 August, 1990 *American Geophysical Union (AGW)—1991 Spring Meeting—Poster Session* No Specific Campaign

Baumback, Mark M.—Naval Research Laboratory

LASSII Pulsed Plasma Probe on CRRES *Journal of Spacecraft and Rockets—Vol. 29, No. 4, 1992—Publication* No Specific Campaign

Bernhardt, P. A.—Naval Research Laboratory

In Situ and Radar Observations During the Ionospheric Focussed Heating (IFH) Experiment *AGU Meeting—Fall 1993—Oral Presentation* CRRES Sounding Rocket Campaign

Bernhardt, P. A.—Naval Research Laboratory

Plasma Irregularities Caused by Cycloid Bunching of the CRRES G-2 Barium Release *American Geophysical Union—2-1-93—Publication* High Altitude Campaign

Bernhardt, P. A.—Naval Research Laboratory

Probing the Magnetosphere Using Chemical Releases from the Combined Release and Radiation Effects Satellite *American Institute of Physics—12-93—Publication* Multiple Campaigns

Bernhardt, Paul—Naval Research Laboratory

Development of Irregularities in Artificial Plasma Clouds by Initial Velocity Distributions *National Radio Science Meeting—7-11 January 1992—Oral Presentation* Multiple Campaigns

Bernhardt, Paul—Naval Research Laboratory

Observation and Theory of the Barium Releases from the CRRES Satellite *AIAA Aerospace Sciences Meeting* January 6-9, 1992 Oral Presentation Multiple Campaigns

Bernhardt, Paul—Naval Research Laboratory

Probing the Magnetosphere Using Chemical Releases from the CRRES Satellite *American Physical Society Division of Plasma Physics Meeting—8 November 1991—Oral Presentation* Multiple Campaigns

Bernhardt, Paul—Naval Research Laboratory

The Role of Initial Stage Distributions to Develop Irregularities in Artificial Plasma Clouds *AGU Campaign Conference—17-21 February 1992—Oral Presentation* Multiple Campaigns

Bernhardt, Paul—Naval Research Laboratory

Physical Properties of Luminous Vapor Releases During CRRES *American Geophysical Union (AGU)—1991 Spring Meeting—Oral Presentation* Multiple Campaigns

Bernhardt, Paul—Naval Research Laboratory

Preliminary Results from the Ionospheric Focussed Heating Experiment During the CRRES Rocket Campaign at Arecibo *National Radio Science Meeting—January 5 - 8, 1993—Oral Presentation* No Specific Campaign

Bernhardt, Paul—Naval Research Laboratory

Remote Diagnostics During the Ionospheric Focused Heating (IFH) Experiment over Arecibo *American Geophysical Union (AGW)—1993 Spring Meeting—Oral Presentation* El Coqui Campaign

Bernhardt, Paul—Naval Research Laboratory

Plasma Irregularities Caused by Cycloid Bunching of the CRRES G-2 Barium Release *J. Geophys. Res.*—1992—
Publication High Altitude Campaign

Bernhardt, Paul—Naval Research Laboratory

Probing the Magnetosphere Using Chemical Releases from the CRRES Satellite *Physics of Fluids*—22 November
1992—Publication Multiple Campaigns

Bernhardt, Paul—Naval Research Laboratory

Probing the Magnetosphere Using Chemical Releases from the Combined Release and Radiation Effects Satellite *Phys. Fluids B*—4 (7) July 1992—Publication Multiple Campaigns

Blake, J. Bernard—The Aerospace Corporation

Energetic Ion and Electron Observations Made Aboard CRRES—21 March To 9 April *American Geophysical Union (AGU)*—1991 Fall Meeting—Oral Presentation No Specific Campaign

Brautigam, D. H.—Geophysics Directorate/Phillips Lab

Omnidirectional Outer Zone Electron Statistical Model *American Geophysical Union (AGU)*—1991 Spring Meeting—
Poster Session No Specific Campaign

Chiu, Yam T.—Lockheed Palo Alto Research Laboratory

Outer Magnetosphere and Radiation Belt Particles Dynamics in the Storm of August 26, 1990 *American Geophysical Union (AGU)*—1991 Spring Meeting—Oral Presentation No Specific Campaign

Cladis, John B.—Lockheed Palo Alto Research Laboratory

Storm-Time Dynamics Implied by CRRES Measurements of Ring-Current Ions *American Geophysical Union (AGU)*—1991 Spring Meeting—Oral Presentation No Specific Campaign

Clodius, W. B.—Los Alamos National Laboratory

The Modelling of Chemical Releases Using a Monte Carlo Code *American Geophysical Union (AGU)*—1991 Fall Meeting—Oral Presentation PEGSAT Campaign

Collin, Henry L.—Lockheed Palo Alto Research Laboratory

Low Energy Ring Current Ions During the Storm of 26 August 1990: Observations by IMS-LO on CRRES *American Geophysical Union (AGU)*—1991 Spring Meeting—Poster Session No Specific Campaign

Collin, Henry L.—Lockheed Palo Alto Research Laboratory

Low-Energy Ion Mass Spectrometer on CRRES *Journal of Spacecraft and Rockets*—Vol. 29, No. 4, 1992—
Publication No Specific Campaign

Fennell, Joseph F.—The Aerospace Corporation

Composition Changes in Association with Energetic Particle Flux Dropouts: Preliminary CRRES Results *American Geophysical Union (AGU)*—1991 Spring Meeting—Poster Session No Specific Campaign

Frederickson, A. R.—Geophysics Directorate/Phillips Lab

Radiation-Induced Insulator Discharge Pulses in the CRRES IDM Satellite Experiment *American Geophysical Union (AGU)*—1991 Spring Meeting—Poster Session No Specific Campaign

Gussenhoven, M. Susan—Geophysics Directorate/Phillips Lab

Response of the Inner Magnetosphere to the 24 March 1991 Sudden Commencement *American Geophysical Union (AGU)*—1991 Fall Meeting—Oral Presentation No Specific Campaign

Gussenhoven, M. Susan—Geophysics Directorate/Phillips Lab

Preliminary Static Radiation Belt Models for the Quiet Magnetosphere *American Geophysical Union (AGU)*—1991 Spring Meeting—Poster Session No Specific Campaign

Gussenhoven, M. Susan—Geophysics Directorate/Phillips Lab

CRRES Spacerad Experiment Descriptions *Rept. AFGL-TR-85-0017*—January 1985—Publication No Specific Campaign

Haerendel, Gerhard—Max Planck Institut

Stabilization of the Rayleigh-Taylor Instability in Trans-equatorial Plasma Clouds *American Geophysical Union (AGU)—1991 Fall Meeting—Oral Presentation* Caribbean Campaign

Huba, Joseph D.—Naval Research Laboratory

Modelling of the CRRES Magnetospheric Barium Releases *Cambridge Workshop—24-28 June 1991—Oral Presentation* High Altitude Campaign

Huba, Joseph D.—Naval Research Laboratory

Waves and Irregularities Excited by the CRRES Magnetospheric Barium Releases *National Radio Science Meeting—7-11 January 1992—Oral Presentation* High Altitude Campaign

Huba, Joseph D.—Naval Research Laboratory

Hall Magnetohydrodynamics in Space Plasmas *AGU Chapman Conference—17-21 February 1992—Oral Presentation* High Altitude Campaign

Huba, Joseph D.—Naval Research Laboratory

Modelling of the CRRES Magnetospheric Barium Releases *American Geophysical Union (AGU)—1991 Spring Meeting—Oral Presentation* High Altitude Campaign

Huba, Joseph D.—Naval Research Laboratory

Modelling the Dynamics of the CRRES Barium Releases *World Space Congress—August 28 - September 5, 1992—Oral Presentation* Multiple Campaigns

Huba, Joseph D.—Naval Research Laboratory

Modelling of the CRRES Ionospheric Barium Releases *American Geophysical Union (AGU)—1991 Fall Meeting—Oral Presentation* Caribbean Campaign

Huba, Joseph D.—Naval Research Laboratory

Theory and Simulation of a High Frequency Electromagnetic Drift Wave *Physics of Fluids B: Plasma Physics—Publication* High Altitude Campaign

Huba, Joseph D.—Naval Research Laboratory

Preliminary Study of the CRRES Magnetospheric Barium Releases *Journal of Geophysical Research: Space Physics—Vol. 97, No. 11, 1992—Publication* High Altitude Campaign

Huba, Joseph D.—Naval Research Laboratory

'Skidding' of the CRRES G-9 Barium Release *Geophysical Research Letters—Vol. 19, No. 11, 6-2-1992—Publication* Caribbean Campaign

Hunton, D. E.—Geophysics Directorate/Phillips Lab

CRRES Low Altitude Chemical Releases: In-situ Ion Composition Measurements with the LASSII/QIMS Quadrupole Ion Mass Spectrometer *American Geophysical Union (AGU)—1991 Fall Meeting—Oral Presentation* Caribbean Campaign

Johnson, M. H.—

Combined Release and Radiation Effects Satellite *Journal of Spacecraft and Rockets—Vol. 29, No. 4, 1992—Publication* No Specific Campaign

Johnstone, Alan D.—Mullard Space Science Laboratory

Pitch Angle Diffusion of Low Energy Electrons by Whistler Mode Waves *American Geophysical Union (AGU)—1991 Spring Meeting—Oral Presentation* No Specific Campaign

Jordan, C E—Radex Inc.

Various Magnetic Field Model Representations of the 26 August 1990 Storm *American Geophysical Union (AGU)—1991 Spring Meeting—Poster Session* No Specific Campaign

Jordan, C E—Radex Inc.

Comparison of Magnetospheric Magnetic Field Models with CRRES Observations During the August 26, 1990 Storm *Journal of Geophysical Research—Vol. 97, No. 16, 1992—Publication* No Specific Campaign

Kems, K. J.—Geophysics Directorate/Phillips Lab

Inner Magnetosphere Morphology During the 26 August 1990 Geomagnetic Storm *American Geophysical Union (AGU)—1991 Spring Meeting—Oral Presentation* No Specific Campaign

Koons, Harry C.—The Aerospace Corporation

Observations of Waves Generated by the Low-Altitude CRRES Chemical Releases *American Geophysical Union (AGU)—1991 Fall Meeting—Oral Presentation* Critical Velocity Experiment

Korth, Axel—Max Planck Institut

Electron and Proton Wide-Angle Spectrometer (EPAS) on the CRRES Spacecraft *Journal of Spacecraft and Rockets—Vol. 29, No. 4, 1992—Publication* No Specific Campaign

Ludlow, G. R.—Boston University

CRRES Observations of ULF Waves During the Magnetic Storm of August 26, 1990 *American Geophysical Union (AGU)—1991 Spring Meeting—Poster Session* No Specific Campaign

Mende, Stephen B.—Lockheed Palo Alto Research Laboratory

Real Time Monitoring of the Geophysical Parameters in Support of the CRRES Chemical Releases *American Geophysical Union (AGU)—1991 Spring Meeting—Oral Presentation* High Altitude Campaign

Mendillo, Michael—Boston University

The CRRES-at-Kwajalein Sounding Rocket Experiments *American Geophysical Union (AGU)—1991 Spring Meeting—Oral Presentation* Kwajalein Campaign

Milnevsky, G. P.—Kiev University

Long-Lived Artificial Ion Clouds in the Earth's Ionosphere *American Geophysical Union—6-7-93—Publication* High Altitude Campaign

Mullen, Edward G.—Geophysics Directorate/Phillips Lab

The Solar Proton Event on 2-26 August 1990 *American Geophysical Union (AGU)—1991 Spring Meeting—Oral Presentation* No Specific Campaign

Nightingale, Richard W.—Lockheed Palo Alto Research Laboratory

The Energetic Particle Environment as Observed by the Spectrometer for Electrons and Protons on CRRES During the Geomagnetic Storm of August 26, 1990 *American Geophysical Union (AGU)—1991 Spring Meeting—Poster Session* No Specific Campaign

Nightingale, Richard W.—Lockheed Palo Alto Research Laboratory

CRRES Spectrometer for Electrons and Protons *Journal of Spacecraft and Rockets—Vol. 29, No. 4, 1992—Publication* No Specific Campaign

Papadopoulos, K Dennis—University of Maryland

CIV Triggering in Ba Injection Experiments *American Geophysical Union (AGU)—1991 Spring Meeting—Oral Presentation* Multiple Campaigns

Papadopoulos, K Dennis—University of Maryland

Critical Ionization Velocity in Space *AIAA 30th Aerospace Sciences Meeting—January 6-9, 1992—Oral Presentation* Critical Velocity Campaign

Paranicas, C.—Boston University

Banded Electrostatic Emissions Observed by the CRRES Plasma Wave Experiment *Journal of Geophysical Research—Vol. 97, No. 13, 1992—Publication* No Specific Campaign

Pfitzer, Carl A.—McDonnell Douglas

Models and Model Uses in the Inner Magnetosphere *American Geophysical Union (AGU)—1991 Spring Meeting—Oral Presentation* No Specific Campaign

Pongratz, Morris B.—Los Alamos National Laboratory

Effect of Ion-Neutral Collisions on Dynamics of CRRES Barium Ions *American Geophysical Union (AGU)—1991 Fall Meeting—Oral Presentation* Caribbean Campaign

Pongratz, Morris B.—Los Alamos National Laboratory

Velocity Distribution of Post-coupled Plasmoid Ions: Remote Observations of CRRES Barium Ions *American Geophysical Union (AGU)—1991 Fall Meeting—Oral Presentation* Multiple Campaigns

Pongratz, Morris B.—Los Alamos National Laboratory

Non-Equilibrium Plasmas in Space: Active Experiments Using CRRES Barium Releases *American Geophysical Union (AGU)—1991 Fall Meeting—Oral Presentation* Caribbean Campaign

Pritchett, Phillip L.—University of California, Los Angeles

Simulation of Whistler Waves Excited in the Presence of a Cold Plasma Cloud: Implications for the CRRES Mission *Journal of Geophysical Research—Vol. 96, No. 19, 1992—Publication* No Specific Campaign

Rairden, Richard L.—Lockheed Palo Alto Research Laboratory

Barium Ion Doppler Velocity Distributions Observed in Fabry-Perot Images of the CRRES Caribbean Releases *American Geophysical Union (AGU)—1991 Fall Meeting—Oral Presentation* Caribbean Campaign

Ray, K P.—Geophysics Directorate/Phillips Lab

The Effects of the March 1991 Storm on Microelectronic Performance *American Geophysical Union (AGU)—1991 Fall Meeting—Oral Presentation* No Specific Campaign

Ray, K P.—Geophysics Directorate/Phillips Lab

Microelectronic Performance in Space: New Measurements from the CRRES Satellite *American Geophysical Union (AGU)—1991 Spring Meeting—Poster Session* No Specific Campaign

Reasoner, David L.—Marshall Space Flight Center

The First CRRES Chemical Release Campaigns—Kwajalein, South Pacific, and High-Altitude Magnetosphere *American Geophysical Union (AGU)—1991 Spring Meeting—Oral Presentation* High Altitude Campaign

Reasoner, David L.—Marshall Space Flight Center

The Chemical Release Mission on CRRES *Journal of Spacecraft and Rockets—Vol. 28, No. 1, 1991—Publication* No Specific Campaign

Reasoner, David L.—Marshall Space Flight Center

Chemical-Release Mission of CRRES *Journal of Spacecraft and Rockets—Vol. 29, No. 4, 1992—Publication* No Specific Campaign

Robinson, Robert L.—National Science Foundation

CRRES Energetic Particles and Ion Composition Measurements During the March 1991 Storm *American Geophysical Union (AGU)—1991 Fall Meeting—Oral Presentation* No Specific Campaign

Rodriguez, P.—Naval Research Laboratory

In-Situ Evidence of Parametric Decay Instability in the Ionosphere *American Geophysical Union —1993 Fall Meeting—Oral Presentation* CRRES Sounding Rocket Campaign

Rodriguez, Paul—Naval Research Laboratory

An Overview of LASSII Measurements in CRRES Chemical Release *American Geophysical Union (AGU)—1991 Fall Meeting—Oral Presentation* Multiple Campaigns

Rodriguez, Paul—Naval Research Laboratory

In-Situ Measurements of Small Scale Structure with the CRRES Ionospheric Focused Heating (IFH) Experiment *American Geophysical Union (AGU)—1993 Spring Meeting—Oral Presentation* El Coqui Campaign

Rodriguez, Paul—Naval Research Laboratory

An Overview of the LASSII Experiment on CRRES *Journal of Spacecraft and Rockets—Vol. 29, No. 4, 1992—Unknown* No Specific Campaign

Roeder, James L.—The Aerospace Corporation

Ion Composition Changes in the Magnetosphere During the March 1991 Solar Particle Event *American Geophysical Union (AGU)—1991 Fall Meeting—Oral Presentation* No Specific Campaign

Romero, H.—Naval Research Laboratory

Linear Mode Coupling During Ionospheric Heating in a Chemically Modified Ionosphere *American Geophysical Union (AGU)—1993 Spring Meeting—Oral Presentation* El Coqui Campaign

Scales, Wayne A.—Naval Research Laboratory

Simulation of High-Speed (Orbital) Releases of Electron Attachment Materials in the Ionosphere *Journal of Geophysical Research—Vol. 96, No. A8, 8-1-1991—Publication* Mission theory Description

Schriver, David—University of California, Los Angeles

Stimulated Auroral Precipitation by Wave-Particle Interactions: Implications for the CRRES Satellite Mission *Journal of Geophysical Research—Vol. 96, No. 11, 1991—Publication* No Specific Campaign

Schulz, Michael—The Aerospace Corporation

Opportunities for Radiation-Belt Modeling: Empirical and Theoretical *American Geophysical Union (AGU)—1991 Spring Meeting—Oral Presentation* No Specific Campaign

Schunk, Robert W.—Utah State University

Plasma Expansion characteristics of Ionized Clouds in the Ionosphere: Macroscopic Formulation *American Geophysical Union—2-1-91—Publication* High Altitude Campaign

Schunk, Robert W.—Utah State University

Plasma Expansion Characteristics of Ionized Clouds in the Ionosphere *J. Geophys. Res.—Vol. 96, 1337 (1991)—Publication* Caribbean Campaign

Schunlc, Robert W.—Utah State University

Early-Time Plasma Expansion Characteristics of Ionized Clouds in the Ionosphere *J. Geophys. Res.—Vol. 93, No. 12, 1988—Publication* Caribbean Campaign

Schunk, Robert W.—Utah State University

Early-Time Plasma Expansion Characteristics of Ionized Clouds in the Ionosphere *Journal of Geophysical Research—Vol. 93, No. A11, 11-1-1988—Publication* Mission Theory Description

Siefring, Carl L.—Naval Research Laboratory

Ionospheric Focused Heating (IFH): In-situ HF Heater Characteristics in the Electron Depleted/Negative Ion Region *American Geophysical Union (AGU)—1993 Spring Meeting—Oral Presentation* El Coqui Campaign

Simons, David—Los Alamos National Laboratory

Observations of Structuring in the CRRES Barium Ion Clouds *American Geophysical Union (AGU)—1991 Fall Meeting—Oral Presentation* Multiple Campaigns

Singer, Howard J.—Geophysics Directorate/Phillips Lab

Diamagnetic Cavities Formed by the CRRES High Altitude Chemical Release Experiments *American Geophysical Union (AGU)—1991 Spring Meeting—Oral Presentation* High Altitude Campaign

Singer, Howard J.—Geophysics Directorate/Phillips Lab

Fluxgate Magnetometer Instrument on the CRRES *Journal of Spacecraft and Rockets—Vol. 29, No. 4, 1992—Publication* No Specific Campaign

Stenbaek-Nielsen, H. C.—University of Alaska

Observed and Calculated Barium Emission Rates *American Geophysical Union (AGU)—1991 Fall Meeting—Oral Presentation* Caribbean Campaign

Straus, P. R.—The Aerospace Corporation

Observations of the High-Altitude Chemical Releases by the Photometer Aboard the CRRES Satellite *American Geophysical Union (AGU)—1991 Spring Meeting—Poster Session* Multiple Campaigns

Swenson, Gary R.—Lockheed Palo Alto Research Laboratory

Late Time Measurements of High Altitude Barium Clouds *American Geophysical Union (AGU)—1991 Spring Meeting—Oral Presentation* High Altitude Campaign

Szuszcwicz, E. P.—SAIC

Observations and Model Comparisons of Early-Time Expansion Characteristics of a Satellite-Born Barium-Lithium Release at F-Region Altitudes *Geophysical Research Letters*—1993—Publication High Altitude Campaign

Szuszcwicz, E. P.—SAIC

Observations and Model Comparisons of Early-Time Expansion Characteristics of a Satellite-Borne Barium-Lithium Release At F-Region Altitudes *American Geophysical Union*—10-8-93—Publication High Altitude Campaign

Szuszcwicz, Edward P.—Science Applications International Corporation

Observations and Model Comparisons of Early-Time Expansion Characteristics of a Barium-Lithium Release at F-Region Altitudes *Geophysical Research Letters*—April 1993—Publication High Altitude Campaign

Torr, Marsha R.—Marshall Space Flight Center

Optical Observations of a Lithium Release from the CRRES Spacecraft *American Geophysical Union (AGU)*—1991 Spring Meeting—Oral Presentation High Altitude Campaign

Trzcinski, E.—Geophysics Directorate/Phillips Lab

NRL-701 LASSII/QIMS Quadrupole Ion Mass Spectrometer on CRRES *Journal of Spacecraft and Rockets*—Vol. 29, No. 4, 1992—Publication No Specific Campaign

Valenzuela, Arnoldo—Max Planck Institut

Observations of Ba-Ions Sedimenting in the Southern Ionosphere *American Geophysical Union (AGU)*—1991 Fall Meeting—Oral Presentation Caribbean Campaign

Vampola, Alfred L.—University of Michigan

Magnetospheric Electron and Proton Response to the 26 August 1990 Storm *American Geophysical Union (AGU)*—1991 Spring Meeting—Oral Presentation No Specific Campaign

Vampola, Alfred L.—University of Michigan

Outer Zone Energetic Electron Response to the GTO CRRES Chemical Releases *American Geophysical Union (AGU)*—1991 Spring Meeting—Oral Presentation High Altitude Campaign

Vampola, Alfred L.—University of Michigan

Effects of the March 1991 Magnetic Storm on Outer Zone Energetic Particles *American Geophysical Union (AGU)*—1991 Fall Meeting—Oral Presentation No Specific Campaign

Vampola, Alfred L.—University of Michigan

Combined Release and Radiation Effects Satellite *Journal of Spacecraft and Rockets*—Vol. 29, No. 4, 1992—Publication No Specific Campaign

Violet, M. D.—Geophysics Directorate/Phillips Lab

Magnetospheric Response to the 26 August 1990 Sudden Commencement *American Geophysical Union (AGU)*—1991 Spring Meeting—Oral Presentation No Specific Campaign

Voss, Hank D.—Lockheed Palo Alto Research Laboratory

CRRES IMS-HI Energetic Ion Composition Measurements During the August 1990 and March 1991 Storms *American Geophysical Union (AGU)*—1991 Fall Meeting—Oral Presentation No Specific Campaign

Voss, Hank D.—Lockheed Palo Alto Research Laboratory

The Medium Energy Ion Mass and Neutral Atom Spectrometer on the CRRES Satellite *American Geophysical Union (AGU)*—1991 Spring Meeting—Poster Session No Specific Campaign

Walton, D. M.—Mullard Space Science Laboratory

Observations by the Low Energy Plasma Analyzer of the Storm of 2-27 August, 1990 *American Geophysical Union (AGU)*—1991 Spring Meeting—Oral Presentation No Specific Campaign

Wescott, Eugene M.—University of Alaska

Results From the CRRES Ba, Sr, and Ca Critical Velocity Experiments *American Geophysical Union (AGU)*—1991 Spring Meeting—Oral Presentation Critical Velocity Experiment

Wescott, Eugene M.—University of Alaska

CRRES Caribbean Barium Releases: Conjugate Electric Fields and Non-Solar Illuminated Release Physics *American Geophysical Union (AGU)—1991 Fall Meeting—Oral Presentation* Caribbean Campaign

Wescott, Eugene M.—University of Alaska

Auroral Activity Observed Following Two Large Barium Releases From the CRRES Satellite Near 32,000 km Altitude in the Midnight Sector *American Geophysical Union (AGU)—1991 Spring Meeting—Poster Session* High Altitude Campaign

Wilken, Berend—Max Planck Institut

Magnetospheric Ion Composition Spectrometer Onboard the CRRES Spacecraft *Journal of Spacecraft and Rockets—Vol. 29, No. 4, 1992—Publication* No Specific Campaign

Wygant, John R.—University of California, Berkeley

Observations of Whistler Wave Packets Embedded in 1~100 Millisecond Density Depletions From The UCB/AFGL Langmuir Probe/Electric Field Experiment on CRRES *American Geophysical Union (AGU)—1991 Spring Meeting—Oral Presentation* No Specific Campaign

Wygant, John R.—University of California, Berkeley

Electric and Magnetic Field Measurements During the CRRES Ionospheric and Magnetospheric Chemical Releases *American Geophysical Union (AGU)—1991 Fall Meeting—Oral Presentation* Multiple Campaigns

Wygant, John R.—University of California, Berkeley

CRRES Electric Field/Langmuir Probe Instrument *Journal of Spacecraft and Rockets—Vol. 29, No. 4, 1992—Publication* No Specific Campaign

Young, David T.—Southwest Research Institute

CRRES Low-Energy Magnetosphere Ion Composition Sensor *Journal of Spacecraft and Rockets—Vol. 29, No. 4, 1992—Publication* No Specific Campaign


APPROVAL

**CRRES COMBINED RADIATION AND RELEASE
EFFECTS SATELLITE PROGRAM**

By

M. A. McCook, M. W. McCook, and G. P. Miller

This report has been reviewed for technical accuracy and contains no information concerning national security or nuclear energy activities or programs. The report, in its entirety, is unclassified.



Gregory S. Wilson
Director, Space Sciences Laboratory

REPORT DOCUMENTATION PAGE

Form Approved
OMB No. 0704-0188

Public reporting burden for this collection of information is estimated to average 1 hour per response, including the time for reviewing instructions, searching existing data sources, gathering and maintaining the data needed, and completing and reviewing the collection of information. Send comments regarding this burden estimate or any other aspect of this collection of information, including suggestions for reducing this burden, to Washington Headquarters Services, Directorate for Information Operations and Reports, 1215 Jefferson Davis Highway, Suite 1204, Arlington, Va 22202-4302, and to the Office of Management and Budget, Paperwork Reduction Project (0704-0188), Washington, DC 20503.

1. AGENCY USE ONLY (Leave Blank)		2. REPORT DATE June 1995	3. REPORT TYPE AND DATES COVERED Technical Memorandum	
4. TITLE AND SUBTITLE CRRES Combined Radiation and Release Effects Satellite Program			5. FUNDING NUMBERS	
6. AUTHOR(S) B. L. Giles, M.A. McCook*, M.W. McCook*, and G.P. Miller*, Compilers				
7. PERFORMING ORGANIZATION NAME(S) AND ADDRESS(ES) George C. Marshall Space Flight Center Marshall Space Flight Center, Alabama 35812			8. PERFORMING ORGANIZATION REPORT NUMBERS	
9. SPONSORING/MONITORING AGENCY NAME(S) AND ADDRESS(ES) National Aeronautics and Space Administration Washington, DC 20546			10. SPONSORING/MONITORING AGENCY REPORT NUMBER NASA TM-108494	
11. SUPPLEMENTARY NOTES Prepared by the Space Sciences Laboratory, Science and Engineering Directorate *The University of Alabama in Huntsville, Huntsville, Alabama				
12a. DISTRIBUTION/AVAILABILITY STATEMENT Unclassified-Unlimited Subject Category: 46			12b. DISTRIBUTION CODE	
13. ABSTRACT (Maximum 200 words) The various regions of the magnetosphere-ionosphere system are coupled by flows of charged particle beams and electromagnetic waves. This coupling gives rise to processes that affect both technical and non-technical aspects of life on Earth. The CRRES Program sponsored experiments which were designed to produce controlled and known input to the space environment and the effects were measured with arrays of diagnostic instruments. Large amounts of material were used to modify and perturb the environment in a controlled manner, and response to this was studied. The CRRES and PEGSAT satellites were dual-mission spacecraft with a NASA mission to perform active chemical-release experiments, grouped into categories of tracer, modification, and simulation experiments. Two sounding rocket chemical release campaigns completed the study.				
14. SUBJECT TERMS Plasma, Aurora, Magnetosphere, Ionosphere, Barium, Lithium, Active Experiment			15. NUMBER OF PAGES 165	
			16. PRICE CODE NTIS	
17. SECURITY CLASSIFICATION Unclassified	18. SECURITY CLASSIFICATION OF THIS PAGE Unclassified	19. SECURITY CLASSIFICATION OF ABSTRACT Unclassified	20. LIMITATION OF ABSTRACT Unclassified	

National Aeronautics and
Space Administration
Code JTT
Washington, DC
20546-0001

*Official Business
Penalty for Private Use, \$300*

Postmaster: If Undeliverable (Section 158 Postal Manual), Do Not Return
